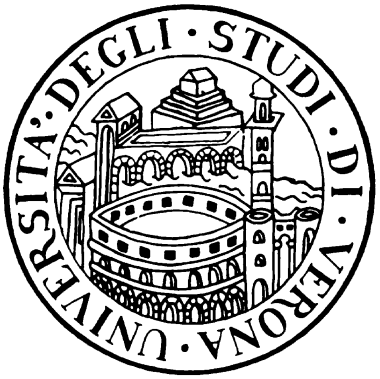

UNIVERSITA' DEGLI STUDI DI VERONA

DEPARTMENT OF BIOTECNOLOGY

PhD School of natural sciences and engineering

PhD in Nanoscience and Advance Technologies

XXX Cycle

LUMINESCENT COMPLEXES OF LANTHANIDE IONS FOR SENSING AND TECNOLOGICAL APPLICATIONS

S.S.D. CHIM/03

Coordinator: Prof.re Franco Tagliaro

Tutor: Prof.re Fabio Piccinelli

PhD Candidate: Marco Leonzio

LUMINESCENT COMPLEXES OF LANTHANIDE IONS FOR SENSING AND TECNOLOGICAL APPLICATIONS

Leonzio Marco

PhD Thesis

Verona, 30 November 2017

ISBN

Abstract

The discovery of the unique emission properties of trivalent lanthanide complexes has contributed to their broad employment in many applications. For example, the almost monochromatic metal-centered emission stemming from f-f transitions, or fluorescence or phosphorescence of the ligand are suitable features for OLED application. In addition, the long luminescence lifetime and large energy difference between the absorbing and emissive states allow to mitigate the interference of background fluorescence originating from the biological sample and to remove self-absorption issues, respectively. Thanks to the lack of self-absorption, the luminescence signal intensity of the complexes is proportional to their concentration over a wide range of values. With this in mind, lanthanide-based molecular probes have been employed for the detection of several important analytes in biological environments. High emission quantum yield and high values of the overall luminosity (brightness) are strongly required for optical applications, in particular in the biosensing and the biomedical fields. These two characteristic can be ensured by a proper choice of the ligand which must be capable to transfer efficiently its excitation energy to the metal ion and to hamper the coordination of solvent molecules (i.e. water). These entities are able to quench non-radiatively the excited states of the lanthanide ions through the multiphonon relaxation processes. Finally a chiral ligand around the metal ion can produce a metal-centered emission of circularly polarized (CP) light which has been found to be very useful for the detection of biomolecules in solution and for the fabrication of OLED emitting CP light (CP-OLED).

In the present work, new chiral ligands based on the chiral fragment 1,2-diaminecyclohexane (DACH) and their Ln(III) complexes, soluble in different solvents, have been synthetized and characterized from a structural point of view, in solution and, when possible, in the solid state. Also a deep spectroscopic characterization has been performed. Several experiments have been carried out in order to investigate the optical responsivity in solution towards several anions and therefore the possible applications in the field of (bio)sensing. As far as the applications in the field of OLED (also CP-OLED) are concerned, the spectroscopy of several complexes has been studied in the solid state.

Table of Contents

General introduction

In the proper environment and under a variety of stimuli, Ln(III) ions display strong luminescence, as measured by the luminescence quantum yield (φ) or the brightness (B= ε·φ , with ε molar absorption coefficient). Owing to their low intrinsic value of ε , they are most conveniently excited by means of a ligand-to-metal energy transfer, involving the excitation of the organic ligand to a singlet state followed by the relaxation to a lower lying, long-lived triplet state and eventually by the transfer of the excitation to the Ln(III) ion through an exchange (Dexter) or a multipolar (Förster, etc.) mechanism. The Ln(III) luminescence is composed of sharp lines and for this reason it finds important applications, for example in the phosphors and solid state lasers technologies, in the labelling of banknotes, documents and goods, etc. Of particular importance are the applications in diagnostics: in fact, the fingerprint spectrum of a lanthanide lends itself to the development of sensitive and specific analytical and biomedical assays[1]. When the environment around Ln(III) is chiral, the metal may display circularly polarized luminescence (CPL), a chiroptical phenomenon, which is rapidly gaining interest in the literature, thanks to its biomedical and technological applications[2]. Lanthanide CPL can be extremely efficient and free of common fluorescence artifacts. Emission dissymmetry factors, $g_{lum} = 2(I_L - I_R)/(I_L + I_R)$, of up to about 1.4 (with 2 maximum possible value) have been reported, the highest of any system in solution or in polymer dispersion[3]. Indeed, the chiroptical behavior of strongly emissive Ln(III) complexes has dominated CPL probe development. Optical sensors based on Ln(III) complexes are ideal candidates for the detection of specific analytes in complex microenvironments such as cells, tissues or living animals since, compared with the short emission lifetimes of most organic dyes (on the scale of nanoseconds), the long emission lifetimes of Ln(III) ions (μs-ms) are suitable for minimizing interference from light scattering or autofluorescence via time-gated detection[4]. For the development of (bio)probes the designed ligand should:

- provide a stable Ln(III) coordination, hampering the intrusion on the inner coordination sphere of solvent molecules, which would reduce the non-

radiative quenching of the Ln(III) excited state by the multiphonon relaxation process;

- have a triplet excited state suited to maximize energy transfer (ET), while preventing the back-energy transfer (BT) from the metal to the ligand.

Ligands bearing heteroaromatic rings can be good sensitizer (good antennae) for the Ln(III) luminescence[5], also thanks to their strong absorption (ε). A further ligand feature is to modulate the Ln(III) environment, in response to the presence of an analyte, thus triggering a spectroscopic signal (luminescence or CPL on/off or change, i.e. optical or chiroptical switches). Induced CPL upon binding to Ln chiral bioanalytes is of particular use to signal selectively the presence of chiral species in solution, such as certain proteins[6] or chiral ions e.g. lactate or sialic acid[7].
Luminescent lanthanides are largely used in technological applications. In the first place, in the production of organic light-emitting devices (OLEDs), but also in information and communication technologies (ICT) and biomedical applications. In these field not only the visible-emitting Eu and Tb are popular, but also Er, Nd and to a lesser extent Yb because of their near-IR luminescence. Although solution processed Ln-based OLEDs are a quite well-established technology[7], the chiral electroluminescence of these emitters is only in its infancy (g_{EL} = 0.79 for an Eu(III) complex)[8]. One may conceive to replace standard emitting species with chiral ones and to this end a precise knowledge and mastering of the luminophores, their geometrical and electronic structure, and of their compatibility with the devices' active layers plays a fundamental role[9].
In this increasing demand of material having specific properties, the present PhD thesis tries to explore the photo-physical and sensing properties of new lanthanide complexes with 1,2-cyclohexandiamine derivatives as ligand. The chiral 1,2-cyclohexandiamine (DACH) molecule offers two main advantages: i) it can be easily functionalized and ii) it is relatively cheap.
The work is divided into two section. One section is devoted to luminescence and concern the investigation of photo-physical properties (CPL included) of new lanthanide complexes. The other section is devoted to sensing properties of trivalent europium and terbium complexes toward inorganic and organic. All the chapters contain materials which are either published or submitted to publication.

Each chapter has an own introduction with theoretical concepts necessary properly understand the successive results.

Section devoted to luminescence:

- Chapter 1. Photo-physical investigation of lanthanide complexes with DACH-based pyridine and quinoline derivatives[10,11]
- Chapter 2. CPL investigation of two kind of complexes: i) with potential as materials for CP-OLED and ii) Eu(III) and Tb(III) complexes with potential as chiroptical probes[12].

Section devoted to sensing

- Chapter 3: The sensing properties of DACH-based pyridine derivatives of Eu(III) have been tested in acetonitrile toward inorganic anion such as, nitrate, chloride, etc.[13,14]
- Chapter 4: The sensing properties of DACH-based complexes of Eu(III) and Tb(III) toward chiral organic anion (l-lactate) by using total luminescence (TL) and circularly polarized luminescence (CPL).

Bibliography

(1) Bünzli, J.-C. G. *Chem. Rev.* **2010**, *110* (5), 2729–2755.

(2) Zinna, F.; Di Bari, L. *Chirality* **2015**, *27* (1), 1–13.

(3) Lunkley, J. L.; Shirotani, D.; Yamanari, K.; Kaizaki, S.; Muller, G. *Inorg. Chem.* **2011**, *50* (24), 12724–12732.

(4) Montgomery, C. P.; Murray, B. S.; New, E. J.; Pal, R.; Parker, D. *Acc. Chem. Res.* **2009**, *42* (7), 925–937.

(5) de Bettencourt-Dias, A.; Barber, P. S.; Viswanathan, S. *Coord. Chem. Rev.* **2014**, *273–274*, 165–200.

(6) Carr, R.; Di Bari, L.; Lo Piano, S.; Parker, D.; Peacock, R. D.; Sanderson, J. M. *Dalt. Trans.* **2012**, *41* (42), 13154.

(7) Carr, R.; Evans, N. H.; Parker, D. *Chem. Soc. Rev.* **2012**, *41* (23), 7673.

(8) Zinna, F.; Giovanella, U.; Bari, L. Di. *Adv. Mater.* **2015**, *27* (10), 1791–1795.

(9) de Bettencourt-Dias, A. *Dalt. Trans.* **2007**, No. 22, 2229.

(10) Mihorianu, M.; Leonzio, M.; Bettinelli, M.; Piccinelli, F. *Inorganica Chim. Acta* **2015**, *438*, 10–13.

(11) Mihorianu, M.; Leonzio, M.; Monari, M.; Ravotto, L.; Ceroni, P.; Bettinelli, M.; Piccinelli, F. *ChemistrySelect* **2016**, *1* (9), 1996–2003.

(12) Leonzio, M.; Melchior, A.; Faura, G.; Tolazzi, M.; Zinna, F.; Di Bari, L.; Piccinelli, F. *Inorg. Chem.* **2017**, *56* (8), 4413–4421.

(13) Piccinelli, F.; Leonzio, M.; Bettinelli, M.; Monari, M.; Grazioli, C.; Melchior, A.; Tolazzi, M. *Dalt. Trans.* **2016**, *45* (8), 3310–3318.

(14) Piccinelli, F.; Leonzio, M.; Bettinelli, M.; Melchior, A.; Faura, G.; Tolazzi, M. *Inorganica Chim. Acta* **2016**, *453*, 751–756.

Section 1: Luminescence

CHAPTER ONE: Lanthanide luminescence

Introduction

Lanthanides are a series of chemical elements in the periodic table from lanthanum to lutetium and they can generate a unique luminescence that has always roused the curiosity of many researchers. Their most stable oxidation state is +3, although +2 and +4 valences are possible for some lanthanide in particular conditions. The electronic configuration of trivalent lanthanides ions is constituted starting from Xenon electronic configuration by adding a variable number of *f* electrons along the lanthanide series. The *f*-orbitals do not lie in the outer part of electronic shell, but in the inner one, completely shielded by the outer and filled *5s* and *5p* orbitals. The filling of *f*-orbitals implies the existence of many different electronic configuration levels of $[Xe]4f^N$, whose number is given by: 14!/N!(14-N)!. Due to the shield of the filled $5s^2$ and $5p^6$ subshells, the ligand and/or crystal field have only a weak influence on the *f*-electrons (*f*-orbitals) and for this reason that their electronics levels are in practice unperturbed upon change of the environment surrounding the metal. So this feature permits the construction of the energy diagram for each trivalent lanthanides that apllies in different compounds (Diecke diagram, Figure 1).

The states originated from different electronic configuration (f^N) can be described under the Russell Saunders Coupling scheme by the multiplet $^{2S+1}L_J$ that is composed of (2S+1)(2L+1) state , where S and L denote the total electron spin and orbital angular moment and J denote the total angular moment. The state having lowest energy (ground state) can be easily determined through the Hund's rules.[1]

The f-f transition

The light absorption of matter is very a complex phenomenon that in general is simplified by the odd parity electric dipole (ED) transition. However, the electron can be promoted to higher levels through magnetic dipole (MD) and electric quadrupole (EQ) transition, although they are less strong than ED. The symmetry

selection rule (Laporte's rules) states that levels with same parity cannot be connected by electric dipole transition. So *f-f* transitions are forbidden by the ED mechanism but are allowed by the MD and EQ. However, the small ligand or/and crystal field cause a partial mixing of *f*-orbitals with *d*-orbitals with a consequent relaxation of the selection rules.[2]

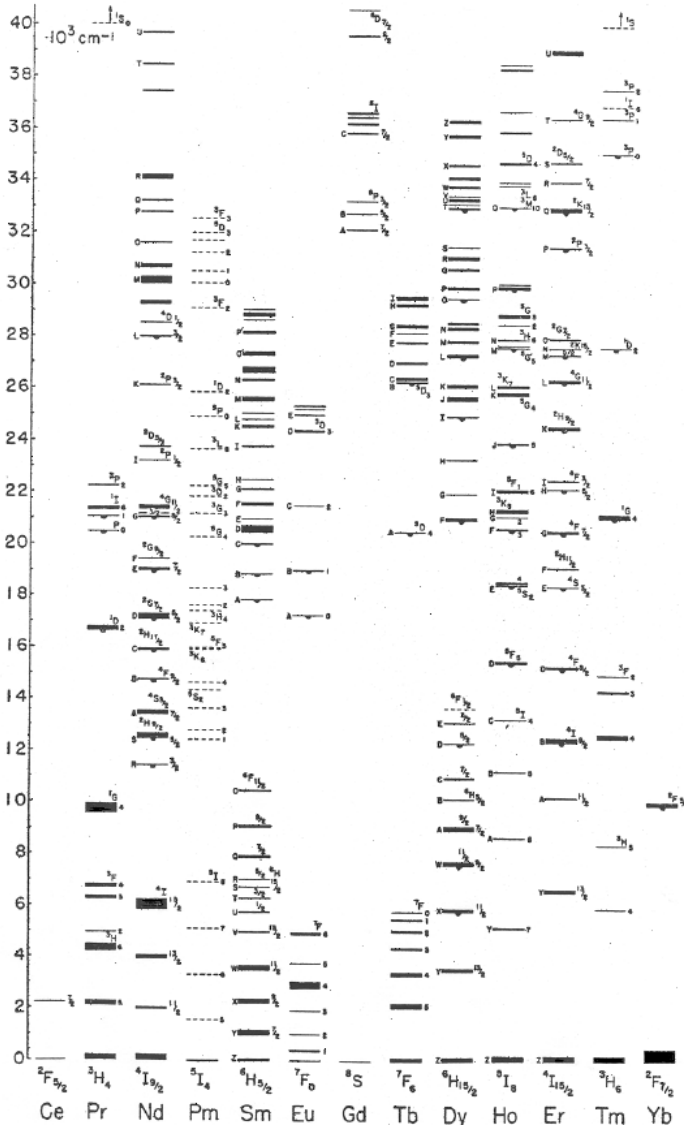

Figure 1 Energy-level diagrams of trivalent Lanthanide ions in doped in low-symmetry crystal LaF_3.

In this way, the ED transitions become partially allowed (they are called induced (or forced) electric dipole transition). The oscillator strength of such *f-f* transition (forced ED transition) is roughly about 10^{-4} time that of a fully allowed ED transition. However, the same ED selection rules can be applied to such transitions due to the presence of interconfiguration state admixture. Judd and Ofelt give a

simplification of all the selection rules for f-f transition which are reported in Table 1.[3]

Table 1 Selection rules and approximate relative I_{rel} for f-f transition

Transition	Parity	ΔS	|ΔL|	|ΔJ|	I_{rel}
ED *4f-5d*	Opposite	0	≤1[a]	≤1[c]	0.01-1
Forced ED, *f-f*	Same	0	≤6[a] (2,4,6 if L'=0)	≤6[c] (2,4,6 if L'=0)	10^{-4}
MD, *f-f*	Same	0	0	≤1[c]	10^{-6}
EQ	Same	0	≤2[b]	≤2[d]	10^{-10}
ED vibr, *f-f*	Same	0	≤6[a] (2,4,6 if L'=0)	≤6[c] (2,4,6 if L'=0)	10^{-7}-10^{-10}

[a]L=0↔L'= 0 forbidden.
[b]L=0↔L'= 0,1 forbidden.
[c]J=0↔J'= 0 forbidden.
[d]J=0↔J'= 0,1 forbidden.

The Sensitisation Mechanism

The forbidden condition of *f-f* transitions limits the access to the excited state of lanthanide. Source with very high intensity(i.e. lasers) are necessary for an efficient direct excitation of the lanthanide ions, a not suitable condition for many applications. For this reason, it is preferable an indirect excitation route, for example upon excitation of an organic chromophore (sensitizer or antenna) and the transfer of the excitation energy to the lanthanide ion. A representation of whole process is given in the Figure 2.

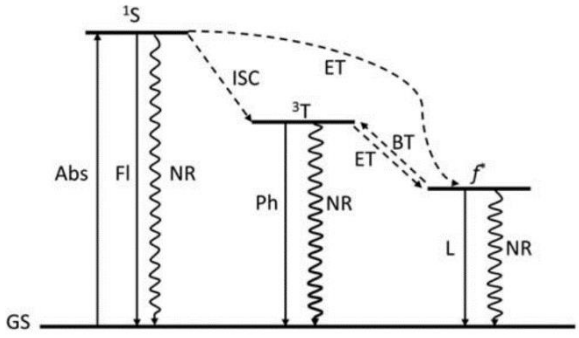

Figure 2 Modified Jablonski diagram illustrating the antenna effect. Abs – absorption, Fl – fluorescence, Ph – phosphorescence, L – luminescence, ISC – intersystem crossing, ET – energy transfer, BT – back energy transfer, NR – non-radiative deactivation, ^1S – first excited singlet state, ^3T – lowest excited triplet state, GS – ground state, f – emissive f excited state*

The sensitizer or antenna harvests energy through the absorption of photons that leads the population of the excited state ^{1}S state. After that, the triplet state ^{3}T can be populated by InterSystem Crossing process which is facilitated by the presence of heavy atom. The long-living of such state permits the Energy Transfer (ET) to one lanthanide ion's excited state (*f**). If the triplet state (^{3}T) of the antenna is very close in energy to emissive state of lanthanide ions a reverse energy transfer is possible and a Back Energy Transfer (BT) processes is possible. This process belongs to the family of deleterious processes, such as fluorescence, phosphorescence and etc., that reduce the overall quantum efficiency,:

$$\phi_{Ln}^{L} = \eta_{ISC} * \eta_{ET} * \phi_{Ln} = \phi_{sens} \quad \textbf{(1)}$$

Although it is usually assumed that the energy transfer occurs from the triplet state, there are evidences that same process can occur from the singlet excited state of sensitizer or antenna.[4,5]

The intensive studies focused on better understanding of Antenna process, highlighted the importance of relative energy position of singlet and triplet states. In fact, they can strongly influence the efficiency of intersystem crossing as well as the energy transfer (ET), more precisely the magnitude of back energy transfer (BT). Latva et al.[6] have found, through the use different ligands, that a good energy transfer happens when the triplet state of the antenna is located between 2000-4000 cm^{-1} above to *f** excited state. More precisely, they observed that at a lower value of 2000 $^{cm-1}$ (lower limit of energy gap) the back energy transfer (BT) became more significant with consequent reduction of overall quantum yield.

The energy transfer between a Donor (D) and Acceptor (A), that in the lanthanide complexes are respectively the Antenna and the Lanthanide, can occur in two different mechanisms:

- **Dexter** energy transfer, involve a double electron transfer[7]
- **Foster** energy transfer, involve a dipole-dipole interaction.[8]

The main condition that must be satisfied for the Dexter energy transfer is the orbital overlap between Donor and Acceptor. So, the main accepted energy transfer mechanism in the lanthanide complexes is that involve a dipole-dipole interaction

(Foster mechanism)[9]. The mechanism can occur between Donor and Acceptor placed relatively far from each other as well, and it depends on R^{-6} (where R is the distance between the Donor and Accepter). Nevertheless, it requires the overlap of the emission spectrum of the donor and the absorption spectrum of the acceptor to occur.

Although the efficiency of the energy transfer process contributes largely on the final emission of lanthanide complexes, a little contribute is also given by the efficiency of intersystem crossing. This process is influenced by the relative energy of Singlet and Triplet levels of sensitizenr or Antenna, and also by the presence of spin-orbit coupling promoted by heavy atoms. Moreover, the Yuster and Weissmen investigation's made on debenzoylmethanide lanthanide complexes (Ln = La, Gd and Lu) highlighted also the positive influence of the magnetic moment of the lanthanide ion on Intersystem Crossing process.[10]

The no-radiative phenomena are also usually present in whole process of sensitization of lanthanide ions. The most significant way is the non-radiative quenching through vibrational modes, which is called the multiphonon relaxation process (MRP). The europium case is one of the most emblematic and its graphical representation is shown in Figure 3.

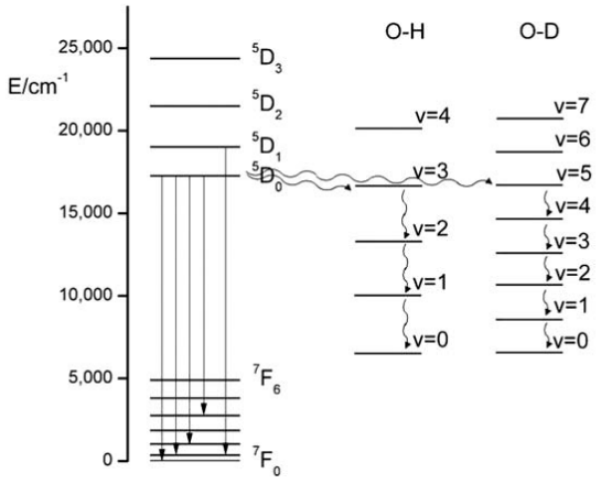

Figure 3 Radiative transitions of Eu(III) and non-radiative quenching through O-H and O-D bonds

The MRP depends on the energy gap between of the emitting level and the one below. It is important if the gap is bridged by less than four vibrational quanta.The emitting state of europium is usaually $^5D_0$ and it is placed at 12000 cm^{-1} above the

highest ^7F_J level and this energy gap could be bridged by three O-H vibrational quanta (vibrational energy 3600 cm^{-1}). Since five vibration quanta of O-D vibration (2200 cm^{-1}) are necessary to fill the aforementioned energy gap of europium, the MPR play an important role only in the case of O-H vibrations. In addition to O-H, other vibrations, such as N-H (3300 cm^{-1}) and C-H (2900 cm^{-1}), also significantly contribute to vibrational quenching of Ln(III)-centered emission.[11] Obviously, for all the applications in aqueous media, the MRP process plays an important role.

Luminescent Lanthanide Complexes

The starting point of research and development of luminescent lanthanide complexes can be placed between the 1930s and the beginning of 1940s thanks to two important studies. The first one by Freed et al.[12], that shown the intensity variation of the absorption lines band for Eu(III) in different solvents. The second one by Weissamn who discovered that some Eu(III) complexes are able to give the characteristic lanthanide emission under UV excitation[13]. Nevertheless, the photochemistry waited roughly 20 years before to take into consideration these compounds. Only at the beginning of 1990s, the luminescent lanthanide complexes solicited the curiosity of scientific community, after the successful application of these materials in medical diagnostic[14].

Nowadays, it's possible counting numerous papers regarding luminescent lanthanide complexes for different applications. All these contributions underline the crucial role of the ligand: it is able to give specific properties to their final lanthanide complexes. In this context, the exploration of different properties of lanthanide complexes having specific ligands is of primary importance for the correct design of new complexes or materials with specific properties or for specific applications.

Aim of Study

The use of organic ligands permit to bypass the problem of low molar extinction coefficients of *f-f* transitions and succeed to access at the characteristic emission of lanthanides. All the photo-physical processes involved in the luminescence of lanthanide complexes are completely understood and a correct design of ligands lead to have compounds with high brightness and quantum yield. However, the function of ligands can be double, in fact, they can provide to complexes other important properties, as in the recognition of ions and biomolecules. This property can be strongly influenced by the geometry of the complexes and a better understanding of this relation is necessary to design new probes[15].

The 1,2-substituted cyclohexanes represents a special chelating backbone since their different enantiomeric forms generate complexes with different geometries[16]. Among the 1,2-substituted cyclohexanes, the 1,2-diamine cyclohexane derivatives are one the most used ligand family for the formation of complexes thanks to the coordinative ability of nitrogen. Also, they can be easily functionalized in different ways permitting the introduction of other chelating group or antennas (chromophores) necessary to increase the luminescence of the final lanthanide ions or increase the stability of whole complex. By using these knowledge, we have synthesized a new ligands containing both DACH and the pyridine or quinoline rings as antennas. (Figure 4)

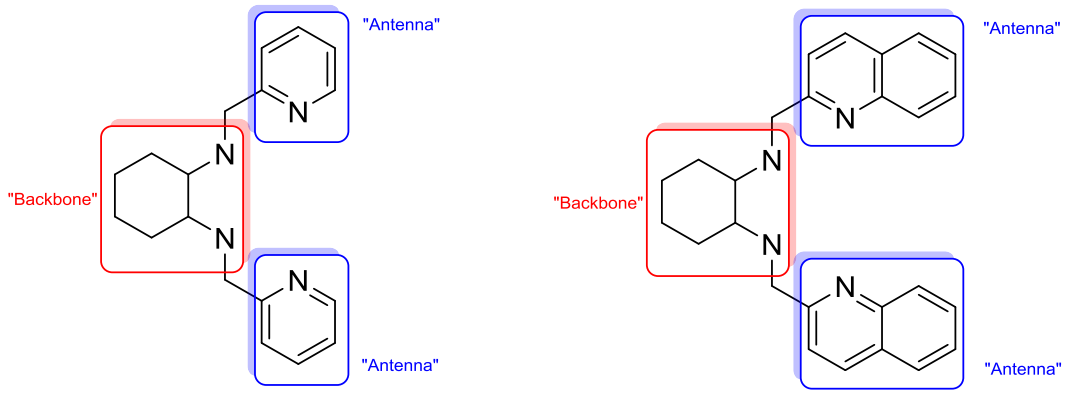

Figure 4 Scheme of ligand used

The geometry of complexes is also strongly influenced by the flexibility of ligand so we have synthesized two main ligand families, in the first family, an imine group

joins the backbone and the antennas, in the second family, is the amine groups that carry out this task. Their properties and their ability to generate luminescent lanthanide complexes have been investigated.

Results

Synthesis and Photo-Characterization N,N'-(cyclohexane-1,2-diyl)bis(1-(pyridin-2-yl)methanimine) and N^1,N^2-bis(pyridin-2-ylmethyl)cyclohexane-1,2-diamine Lanthanide complexes

To investigate the abilities of the ligands to generate luminescent complexes with lanthanide we have synthesized lanthanide nitrate complexes (Figure 5 and 6).

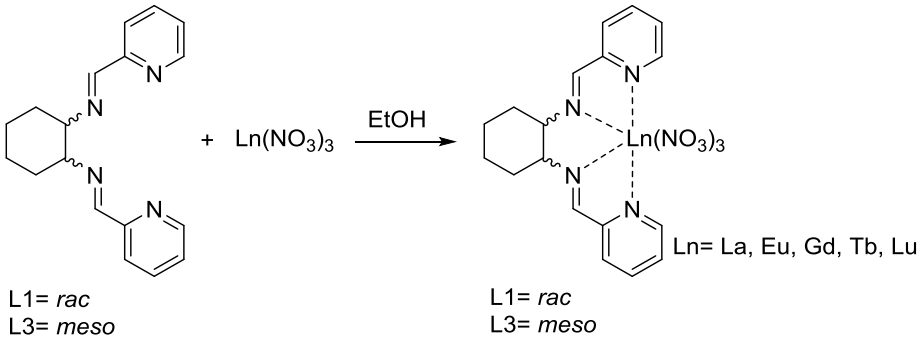

Figure 5 Synthesis of Lanthanide complexes with imine pyridine ligand

The nitrate anions are able to saturate the number of coordination, so reducing the number of solvent molecules directly coordinated to metal center, increasing the luminescence of whole complexes.

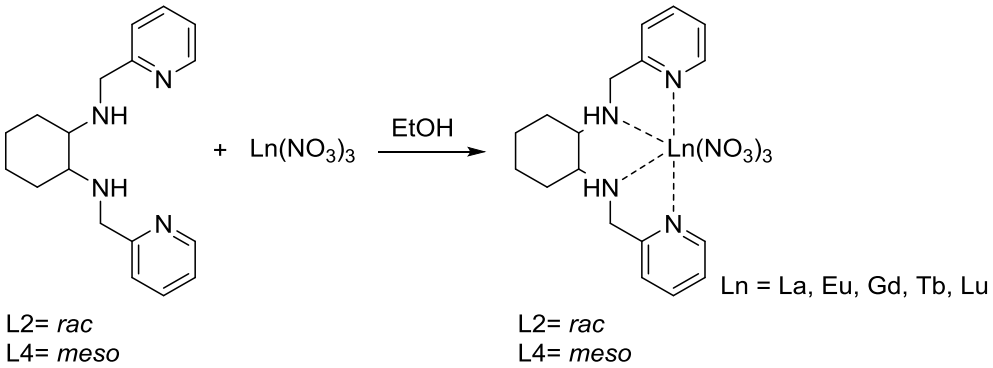

Figure 6 Synthesis of Lanthanide complexes with amine pyridine ligand

Structural studies of lanthanide complexes

The europium complex with the ligand **L1** crystallizes in the centric space group $P2_1/c$ and therefore the racemic mixture is present. The Eu(III) ion has a 10-fold

coordination, being coordinated by one tetradentate ligand **L1** and three bidentate nitrates. The observed coordination polyhedron is a distorted sphenocorona. The XRPD patterns of the Gd(III) and Eu(III) complexes with the ligand **L1** are superimposable (Figure 7). The pattern of the Eu(III) complex has been collected on a powdered sample obtained by grinding crystals of known structure.

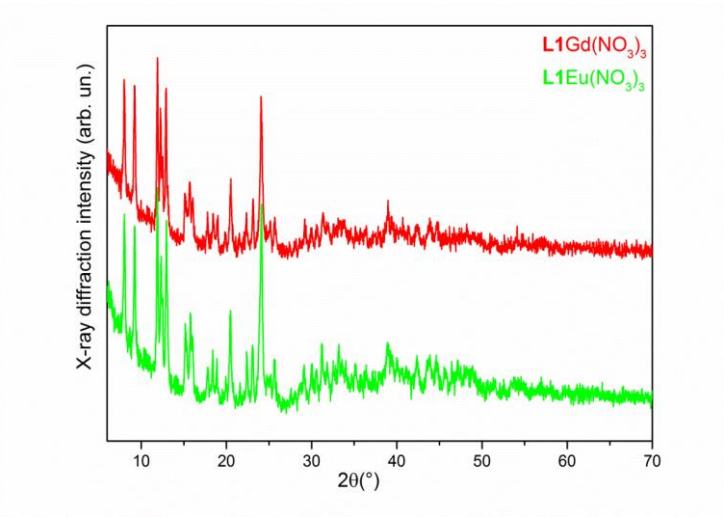

*Figure 7 Overlapping XRD pattern of **L1**Gd(NO3)3 and **L1**Eu(NO3)3*

Complex **L3**Eu(NO3)3 crystallizes in the centric triclinic space group $P\bar{1}$. In the asymmetric unit of the crystal two independent molecules of **L3**Eu(NO3)3 and four fifths of one crystallization acetone molecule (occupation factor (OF) 0.80) are present. This is due to a partial loss of solvent by the crystal, which however does not deteriorate the quality of the structural data. In both molecules the Eu(III) ion has a 10-fold coordination, being coordinated by one tetradentate ligand **L3** and three bidentate nitrates. Even if the two complexes exhibit a similar arrangement of the ligands (nitrate anions and **L3**) around Eu(III), they are not superimposable as they differ slightly by the Eu–O bond distances, the N–Eu–N bond angles (Table 3 Appendix) and by the orientation of the cyclohexyl rings. Actually, one of the two complexes shows a disorder over two positions of the cyclohexyl ring (Figure 8). The main orientation of the cyclohexyl moiety (purple carbon atoms, OF 0.60) is converted into the second one (grey carbon atoms) by the well-known chair–boat–chair conformational interconversion, typical of the 6-membered cyclohexane rings. As a consequence of this process, the equatorial N(8) substituent in the dominant conformational isomer (conformer 1, OF 0.60) is converted into the axial

substituent in the conformer 2 (OF 0.40). At the same time, the axial N(9) atoms (conformer 1) are in the equatorial position in the conformer 2 (Figure 8). The small imbalance of the occupation factors of the two conformers (0.6/0.4 instead of the expected 0.5/0.5) should be ascribed to small packing effects.

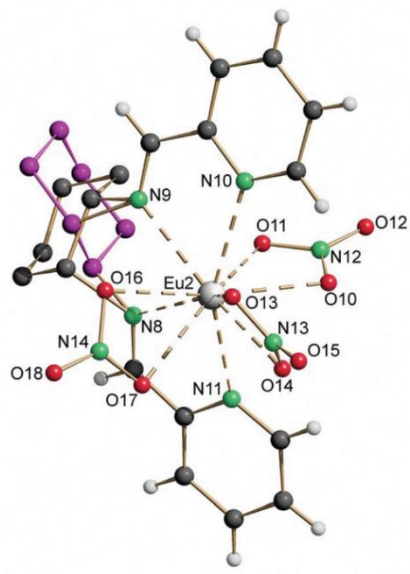

*Figure 8 Crystal Structure **L3**Eu(NO₃)₃*

From a close inspection of Table 3 Appendix, reporting the selected bond lengths and angles of the **L1**Eu$(NO_3)_3$ and **L3**Eu$(NO_3)_3$ crystal structures, we can conclude that the stereochemistry of the ligand [R,R+(S,S)(**L1**)or R,S (**L3**)] does not seem to play a relevant role on its coordination geometry. The main structural difference between the Eu(III) complexes of **L1** and **L3** ligands is the relative orientation of the cyclohexyl unit and the coordinating N4 square plane. In the case of the **L1** racemic(trans) ligand, the cyclohexyl and the N4 units lie on the same plane; on the contrary, in the case of the **L3** meso(cis) ligand, the N4 plane and the cyclohexyl unit are perpendicular to each other (Figure 3 Appendix). The conclusions drawn from the crystal structure determination, in particular the almost identical coordination geometry of the ligands in **L1**Eu$(NO_3)_3$ and **L3**Eu$(NO_3)_3$ complexes, can be strongly related to the similar values of their stability constants calculated in the acetonitrile solution (see the sections below).

The Europium complex with the ligand **L2** crystallizes in the centric space group P*bca* and therefore the racemic mixture is present. The Eu(III) ion is coordinated by one tetradentate ligand **L2** and analogously to complex with **L1**, three chelating

nitrates give rise to 10-fold coordination at the metal ion (Figure 4 in Appendix). Two out of the three coordinated nitrates show disorder thus generating two conformational isomers characterized by different occupation factors and generating different coordination polyhedral. In particular, it's possible observe a sphenocorona and a bicapped square antiprism polyhedra, for the major and the minor conformational isomers, respectively. In both cases, due to the very low site symmetry (C_1) of the Eu(III) ion, the polyhedra are significantly distorted compared with the ideal geometry. It is worth to mention the presence of an axial distorsion in the metal coordination environment of the major isomer of complex with **L2**. A close inspection of the Eu–O and Eu–N bond lengths as well as of the N–Eu–N bite angles for **L1**Eu$(NO_3)_3$ and the dominant conformer of **L2**Eu$(NO_3)_3$, reveals that for the former the two Eu–N(py) bond lengths are almost identical and the distribution of both the Eu–O bond lengths and N–Eu–N bite angles fall in a narrower range (Table 1 and 4 in Appendix). Also in the case of the minor conformer observed in the crystal of **L2**Eu$(NO_3)_3$ we observe a narrower range of Eu–O bond lengths than that in the main con- former. From these evidences we can conclude that the more distorted (less symmetric) environment around the Eu(III) ion was observed in the main conformer of **L2**Eu$(NO_3)_3$.

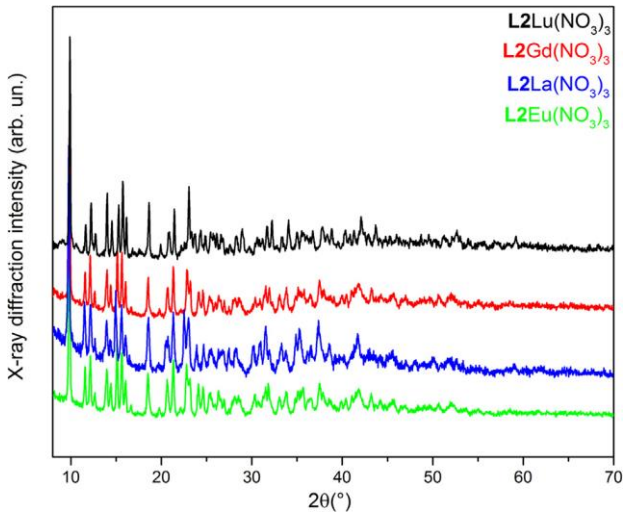

*Figure 9 Overlapping XRD pattern of **L2**Ln$(NO_3)_3$ complexes*

This fact is in agreement with the major conformational flexibility of the amine ligand **L2** that generates a less symmetric (or more distorted) coordination environment. From a close inspection of the Figure 9, we can observe the close

similarity between the XRDP patterns of all the investigated complexes with the ligand **L2** and the one of the **L2**$Eu(NO_3)_3$. Also in this case, the powder of the latter compound has been obtained by grinding crystals whose structure has been previously reported. As the La(III), Gd(III), Lu(III) and Eu(III) complexes with **L2** are isostructural they must possess the same molecular crystal structures. The same argument can be used to claim that the Gd(III) and Eu(III) complexes with the ligand **L1** have the same molecular crystal structure.

As far as the structures of the **L1** complexes with Eu(III) and Gd (III) and of the **L2** complexes with Eu(III), La(III), Gd(III) and Lu(III) are concerned, in all cases the metal center is bound to three bidentate nitrate anion and one tetradentate ligand molecule and the crowded Ln(III) environments are characterized by a 10-fold coordination, as observed for the Eu(III) complex.

Spectroscopy in the solid state

Reflectance spectra

The absorption spectra of the complexes with the **L1** and **L2** ligands are reported in Figure 10 and 11. In the case of imine-based complexes (**L1**$La(NO_3)_3$, **L1**$Gd(NO_3)_3$, **L1**$Lu(NO_3)_3$, Figure 10) the main absorption band is located around 290 nm. Two other absorption features are present at around 210 and 235 nm. All these absorptions are ascribable to electronic transitions involving both the pyridine ring and the conjugated C=N group (i. e. $\pi \rightarrow \pi^*$, $n \rightarrow \pi^*$).

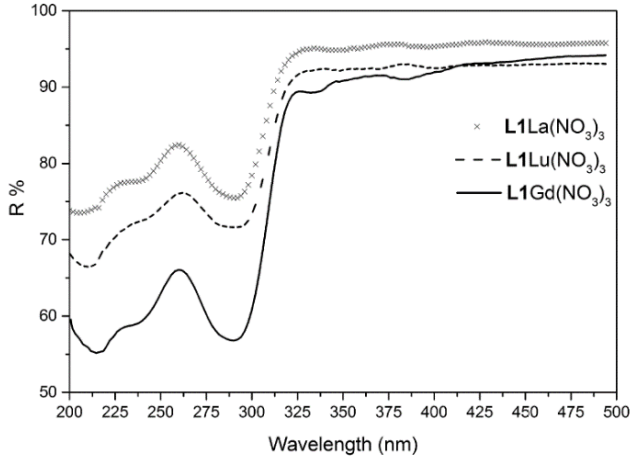

*Figure 10 Absorption spectra of the powders of **L1**$Ln(NO_3)_3$*

Very small absorption bands are also observed above 300 nm (i.e. 335 nm and 380 nm for **L1**Gd$(NO_3)_3$). As far as the absorption spectra of the amine-based complexes (**L2**La$(NO_3)_3$, **L2**Gd$(NO_3)_3$, **L2**Lu$(NO_3)_3$, Figure 11) are concerned, a main absorption band is observed at 266 nm together with a small shoulder at around 290 nm.

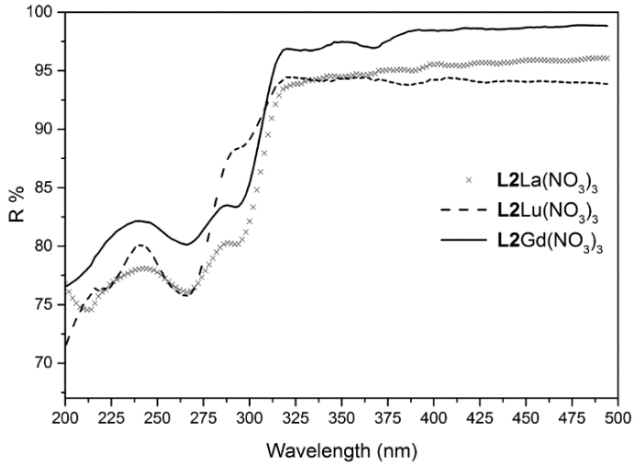

*Figure 11 Absorption spectra of the powders of **L2**Ln$(NO_3)_3$*

These absorption are ascribable to electronic transition involving the pyridine ring (i. e. . $\pi \rightarrow \pi^*$, $n \rightarrow \pi^*$). Again, several minor absorption features are observed above 300 nm. Worth to be noted is the significant red shift of the main absorption band by passing from the amine-based complexes to the imine-based ones. This is clearly due to the increased conjugation of the π-electronic system in the case of **L1**-based complexes. In fact, for these compounds the chromophore is constituted of the pyridine ring directly bound to an imine functional group.

Emission spectrum

The luminescence emission spectra upon excitation at the maximum of the main absorption band of the Ln(III) (Ln = La, Gd and Lu) complexes with the imine-based ligand **L1** are shown in Figure 12. At room temperature the ligand **L1** doesn't show any emission. Upon excitation around 290 nm (292 nm for **L1**La$(NO_3)_3$ and **L1**Lu$(NO_3)_3$, 288 nm for **L1**Gd$(NO_3)_3$) a broad emission band centered around 450 nm is observed for the La(III) and Lu(III) complexes. On the contrary, the emission spectrum of the Gd(III) complex is composed by two main features. One centered at 450 nm (weaker) and the other one (dominant) centered around 580 nm. The

emission bands located at 450 nm are ascribable to the singlet whereas the main emission band of the Gd(III) complex can be assigned to the triplet. This assignment is in agreement with several previously reported study on the remarkable metal effect in metal complexes of dibenzoylmethane[10] and methyl salicylate[17] derivatives. The authors found that, in the paramagnetic Gd(III) complexes the phosphorescence lifetime decreased significantly and fluorescence was not observable in contrast to the appreciable fluorescence intensity of the La(III) and Lu(III) diamagnetic metal complexes.

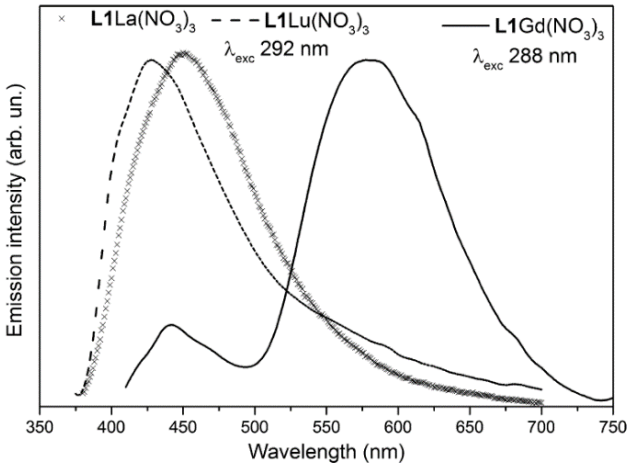

*Figure 12 Luminescence emission spectra of **L1**Eu(NO₃)₃*

This effect caused by the Gd(III) ion is the so-called ‘‘paramagnetic effect”, that is, the singlet–triplet mixing between the electronic states of a ligand is enhanced by the inhomogeneous magnetic field caused by the paramagnetic ion. As a result, the paramagnetic character of the central metal ion is found to enhance not only the $T_1 \rightarrow S_0$ radiative rate but also the $S_1 \rightarrow T_1$ intersystem crossing rate from the localized electronic states in ligands. As observed also by Crosby et al.[18] who have investigated the phosphorescence intensity and lifetime of acetylacetonato complexes with La(III), Gd(III) and Lu(III), the paramagnetic ion promotes both intersystem crossing and $T_1 \rightarrow S_0$ radiative rate far more than its closed-shell rare earth neighbors like La(III) and Lu(III). It must be also pointed out that a pure spin–orbit mixing due to the presence of a heavy metal atom does not seem to be applicable in our case. In fact, considering the simple heavy atom effect, one would expect a $T_1 \rightarrow S_0$ radiative rate (phosphorescence efficiency) of Gd(III) complex to lie between the values for the other two Ln(III) compounds. The phosphorescence

lifetime of **L1**Gd$(NO_3)_3$ measured at room temperature and at 580 nm is found to be 0.8 μs whereas the fluorescence lifetimes of the La(III) and Lu(III) are too short to be detected with our instrument. This finding is in agreement with the allowed nature of the $S_1 \rightarrow S_0$ radiative transition and, although partially relaxed, the forbidden nature of the $T_1 \rightarrow S_0$ one.

With the aim to study the impact of the electronic and coordination properties of the ligand on the luminescence of the Ln(III) complexes, the spectroscopy of the Ln(III) (Ln = La, Gd and Lu) complexes with the amine-based ligand **L2** has also been investigated. From a structural point of view, the ligand **L2** is more flexible than the ligand **L1** and, as mentioned before, the π-electronic system of **L1** is more extended than the one of **L2**, as the pyridine aromatic ring is directly bound to a C=N functional group. The luminescence emission spectra of complexes with **L2** are reported in Figure 13. At room temperature the ligand **L2** is totally not emissive upon excitation in the UV range (250–400 nm).

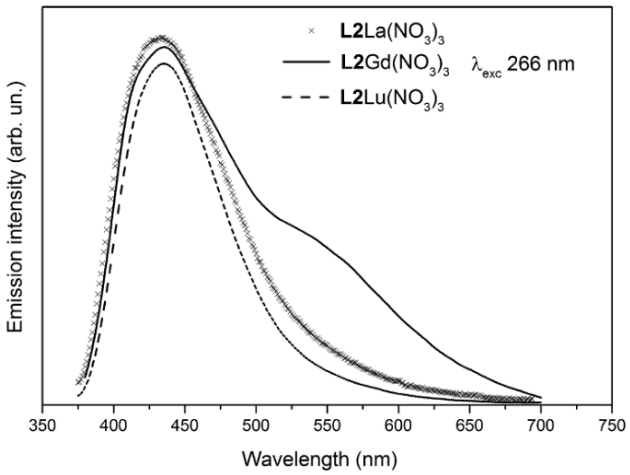

*Figure 13 Luminescence emission spectra of **L2**Eu$(NO_3)_3$*

Upon excitation in the main absorption peak (λ_{exc} = 266 nm), a broad asymmetric emission band centered around 430 nm is observed for all the Ln(III) complexes. In addition a shoulder around 550 nm is observed for the Gd(III) complex. For the same reasons discussed above the emission bands located around 430 nm are assigned to the singlet ligand fluorescence whereas the weaker additional emission feature of the Gd(III) complex can be assigned to the triplet ligand phosphorescence. Worth to be noted is the less efficient phosphorescence displayed

by the Gd(III) complex with the ligand **L2**, if compared with the phosphorescence of **L1**$Gd(NO_3)_3$. This evidence can be explained by the flexibility of the chelate structure of the **L2**$Gd(NO_3)_3$. This compound, isostructural with the Eu(III) analog (see above), shows two conformational isomers where the metal ion experiences two different coordination environments. The flexibility of this chelate structure may provide a channel for radiationless deactivation reducing the phosphorescence efficiency. The direct relationship between the rigidity of the chelate structure and phosphorescence efficiency has been already broadly documented[19].

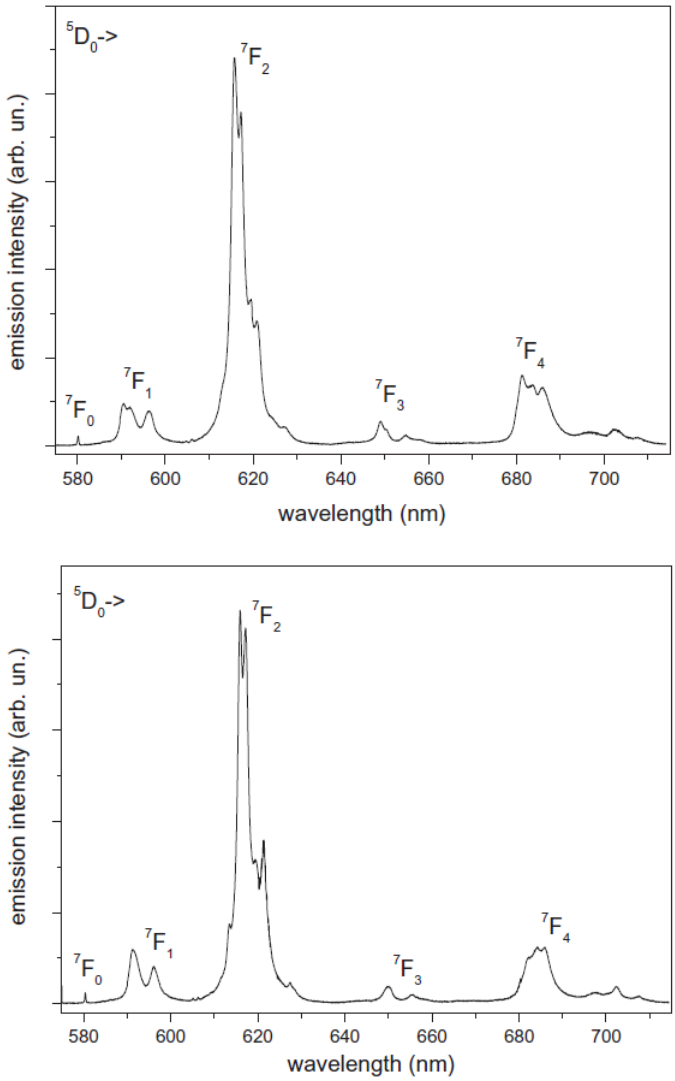

Figure 14 Emission Spectrum (upper) ***L1****Eu(NO₃)₃ and (below)* ***L3****Eu(NO₃)₃*

In addition, the different π-electronic system of the **L1** and **L2** ligands (**L1** has pyridine ring conjugated with the imine group; **L2** has only pyridine ring) could

influence the efficiency of the ‘‘paramagnetic effect” of the Gd(III) ion modifying the phosphorescence output of the complex. Further work is needed to confirm this assumption.

The emission spectra of Europium complexes containing the imine ligand are showed obtained upon excitation at 465 nm (i.e. in the $^5D_2$ level) are shown in Figure 14. The spectra are very similar and show the typical profile of the emission from the $^5D_0$ level of the Eu(III) ion in a strongly distorted environment, with a dominant $^5D_0 \rightarrow {}^7F_2$ hypersensitive band.

The Stark splittings of the terminal ^7F_J (J = 1–4) levels are not fully resolved and therefore are not informative. However, the relative intensity of the $^5D_0 \rightarrow {}^7F_0$ (briefly, 0–0) band is extremely low, indicating that the effective local symmetry at the metal ion is not strongly axial. On the other hand, the emission spectra of the complexes containing the amine ligands are characterized by different features (Figure 15). In fact, they present again a dominant hypersensitive transition, characteristic of generally low symmetry at the Eu(III) ion, but in both cases the 0–0 band is far stronger than for the complexes discussed above. This indicates that the symmetry around the metal ion is lower, and is compatible of an axial character typical of the C_n and C_{nv} point groups which have been shown to give rise to strong 0–0 transitions[20,21]. This feature seems to be detectable from the crystal structures of the compound **L2**Eu$(NO_3)_3$. The lower effective local symmetry at the Eu(III) ion, according to the luminescence spectra, for the complexes **L2**Eu$(NO_3)_3$ and **L4**Eu$(NO_3)_3$ can be explained taking into account the higher flexibility of the amine ligands com- pared to the imine ones, allowing for a possible stronger distortion of the first coordination sphere of Eu(III). We also note that for complex **L2**Eu$(NO_3)_3$ two features are present in the region of the 0–0 transition, therefore indicating the presence of two Eu(III) emitting centres (see inset of Figure 15 upper). This observation is consistent with the presence of disorder in the nitrate ligands, giving rise to two different conformational isomers in the crystal structure (see above). The room temperature decay curves of the $^5D_0$ level of Eu(III) in the various complexes are almost perfectly exponential, even in the case of complex **L2**Eu$(NO_3)_3$ where two emitting conformational isomers, characterized by different coordination environment for Eu(III) ion, are present. Presumably, these two species possess

very similar decay kinetics of the $^5D_0$ level yielding no detectable deviations from a single exponential decay.

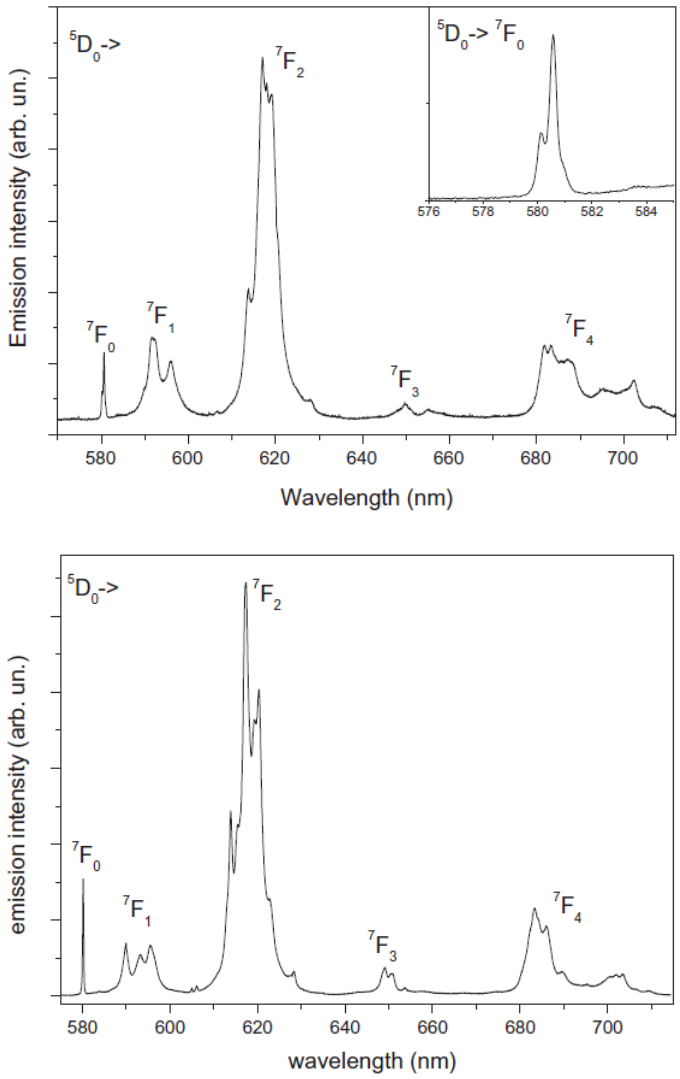

*Figure 15 Emission Spectrum **L2**Eu(NO₃)₃ (upper) and **L4**Eu(NO₃)₃ (below)*

The life-times of the emitting level extracted from the experimental curves are reported in Table 2, whose inspection clearly shows a large difference between the imine and amine complexes. In the former case, the lifetimes are close to 1 ms, therefore indicating that multiphonon relaxation due to high frequency vibrations is not operative, as expected from the absence of N–H groups in the organic ligand.

Table 2 $^5D_0$ lifetime (τ_{obs}) of the Europium complexes

Complex	$^5D_0$ excited state τ_{obs} (ms)
L1$Eu(NO_3)_3$	0.94(1)
L3$Eu(NO_3)_3$	1.07(1)
L2$Eu(NO_3)_3$	0.22(1)
L4$Eu(NO_3)_3$	0.26(1)

On the other hand, for complexes **L2**$Eu(NO_3)_3$ and **L4**$Eu(NO_3)_3$ containing an amine ligand, the presence of two N–H amino groups in close proximity to the metal ion induces the presence of a non-radiative relaxation mechanism resulting in short lifetimes just above 0.2 ms.

Synthesis and Photo-Characterization N,N'-(cyclohexane-1,2-diyl)bis(1-(quinolin-2-yl)methanimine) and N^1,N^2-bis(quinolin-2-ylmethyl)cyclohexane-1,2-diamine Lanthanide complexes

To investigate more deeply the "paramagnetic effect" of gadolinium complexes we have extended the π conjugation of the antenna system substituting the pyridine rings with a quinoline rings. The complexes have been synthesized following the scheme showed below.

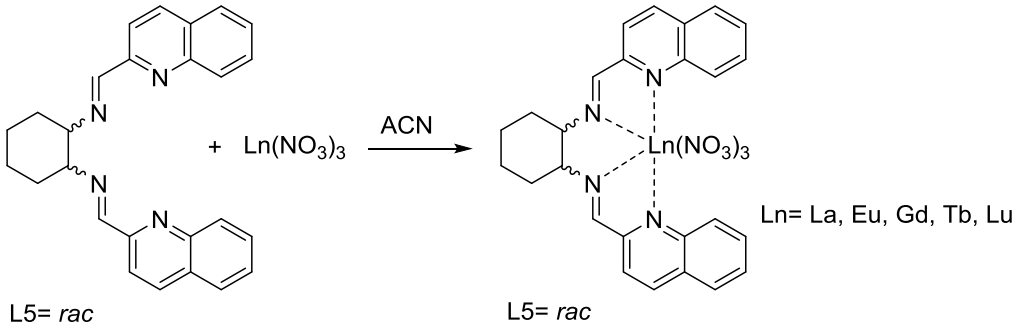

Figure 16 Synthesis of Lanthanide complexes with imine quinoline ligand

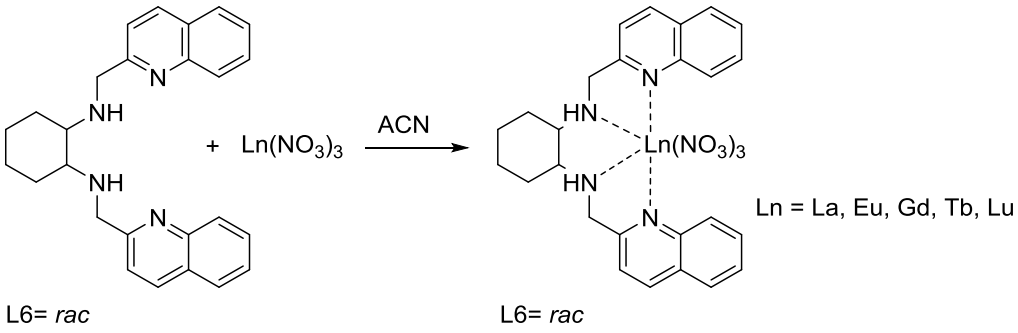

Figure 17 Synthesis of Lanthanide complexes with amine quinoline ligand

Structural studies of lanthanide complexes

The compound crystallizes in the centric triclinic space group P-1. In the asymmetric unit of the crystal one independent molecule of **L5**La$(NO_3)_3$ and one crystallization acetonitrile molecule are present. The La(III) ion exhibits a 10- fold coordination, being coordinated by one tetradentate ligand **L5** and three bidentate nitrates (Figure 18). The observed coordination polyhedron is a distorted sphenocorona and the local symmetry of La(III) ion is C_1. A chair-like

conformation of the cyclohexyl ring and an almost perfect square planar geometry of the nitrogen ligands are observed. The N atoms of the tetradentate ligand slightly deviate from the ideal square planar geometry [N(imine): +0.107(9) Å and -0.105(9) Å, N(quin): +0.052(4) Å, and -0.054(4) Å], and the distance of the La ion from the N4 least square plane of the coordinating N atoms is 0.562(8) Å.

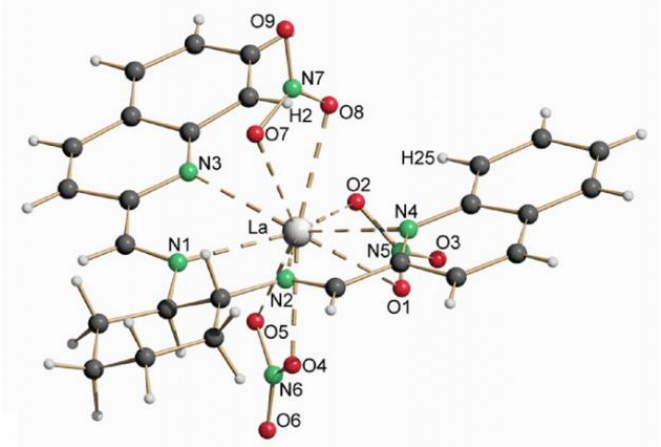

Figure 18 Perspective view of ***L5****La(NO₃)₃*

The four La-N distances show significant differences in that the two imine nitrogens form bonds at 2.58(1), 2.631(9) Å shorter than the quinoline nitrogens [2.817(9), 2.746(8) Å] (Table 5 in Appendix). This is probably due to a steric effect rather than a consequence of the different donor ability of the nitrogen atoms. In fact, the O2 and O8 atoms, belonging to the nitrate units are close to the hydrogens bound to the quinoline C atoms (H2 and H25). The observed distances are H(2)…O(8) 2.476(7) Å, H(2)…O(2) 2.409(8) Å, H(25)…O(8) 2.522(9) Å, H(25)…O(2) 2.691(8) Å. Shorter N(quin)-La distances than the observed ones would generate steric repulsion between nitrate anions and quinoline rings. It is worth noting the close similarity between the molecular structure of **L5**La$(NO_3)_3$ and the one of the Eu(III) nitrate complex of the pyridine-based analog previously investigated by us. However, while in the latter compound, the chemically equivalent Eu-Npyridine bonds (the same applies for Eu-Nimine) show similar lengths, in the case of **L5**La$(NO_3)_3$the two La-N(quinoline) distances are significantly different, as discussed above. An inspection of the crystal structure of the free ligand[22] shows that the quinoline rings are perpendicular to the cyclohexyl moiety and the trans conformation is preferred in **L5**, resulting from the electronic repulsion of the

nitrogen lone pairs. This is expected, as it is generally well known and established that the most stable conformation of polyimine ligands, in their non-coordinated form, is trans[23,24]. On the contrary, because of the coordination to the La(III) ion in **L5**La$(NO_3)_3$, the quinoline and the cyclohexyl rings lie in the same plane and the ligand shows a cis conformation. The diffraction powder pattern of **L5**La$(NO_3)_3$ is super-imposable with the one simulated from its crystal structure described above and with the powder patterns of all the investigated imine-based complexes (**L5**Ln$(NO_3)_3$;Ln = Eu, Gd, Tb and Lu, Figure 19). The close similarity of the intensities of the diffraction peaks points towards a similar molecular structures for all the complexes. As well known, the intensity of the X-ray diffraction peaks is less sensitive to the presence of weakly scattering atoms (i.e. atoms with low atomic number: C, H, O, N in the present case. For this main reason, in order to perform an accurate determination of the crystallographic position of these atoms, the intensity of each diffraction peak must be precisely measured.

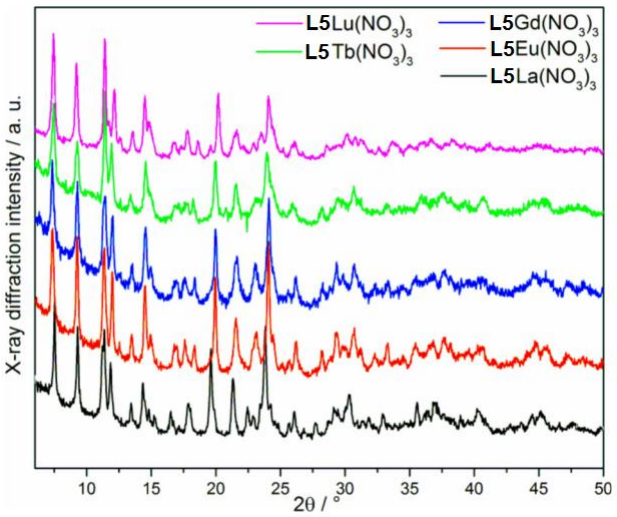

*Figure 19 Observed X-ray diffraction patterns of **L5**Ln$(NO_3)_3$ (Ln = La, Eu, Gd,Tb and Lu)*

This is possible by avoiding the spatial overlap of the peaks and this goal can be easily achieved thanks to a XRD experiment on single crystal. On the contrary, the overlap of the peaks is common in a diffraction experiment on powdered samples in a Bragg-Brentano geometry. On this basis, the calculated atomic position of light atoms by a XRPD experiment, could be affected by a not negligible degree of uncertainty. This is why, care should be taken on any reasoning regarding the coordination geometry of the metal ions in the case of **L5**Ln$(NO_3)_3$ (with Ln = Eu,

Gd, Tb and Lu) for which the crystal structure determination by XRD experiment on single crystal has not been possible, even though they are isostructural to **L5**La(NO$_3$)$_3$. By means of Rietveld refinement on the observed powder patterns, the lattice parameters of **L5**Ln(NO$_3$)$_3$ (Ln = Eu, Gd, Tb and Lu) have been calculated (Table 3). The structural molecular model employed for the calculations was the one obtained for **L5**La(NO$_3$)$_3$ by SC-XRD, upon substitution of La(III) ion with the appropriate Ln(III) ion.

*Table 3 Lattice parameters of **L5**Ln(NO$_3$)$_3$ compounds*

Ln	*a*(Å)	*b*(Å)	*c*(Å)	α(°)	β(°)	γ(°)	V(Å^3)
La	9.890(3)	12.095(4)	12.669(4)	78.40(3)	86.11(3)	86.63(4)	1480(2)
Eu	9.727(3)	12.305(4)	12.505(3)	78.57(3)	86.51(3)	87.03(3)	1463(2)
Gd	9.716(4)	12.321(5)	12.479(5)	78.56(4)	86.62(4)	87.03(5)	1461(2)
Tb	9.757(4)	12.201(6)	12.483(6)	78.10(5)	87.02(5)	87.42(5)	1451(3)
Lu	9.567(2)	12.202(3)	12.573(3)	77.70(2)	85.81(3)	87.44(3)	1430(2)

During the Rietveld calculation, the fractional atomic coordinates of the model were not refined. The contraction of the cell volume by moving from La to Lu is in line with the ion size reduction along the lanthanide series, as shown in Figure 6 in Appendix.

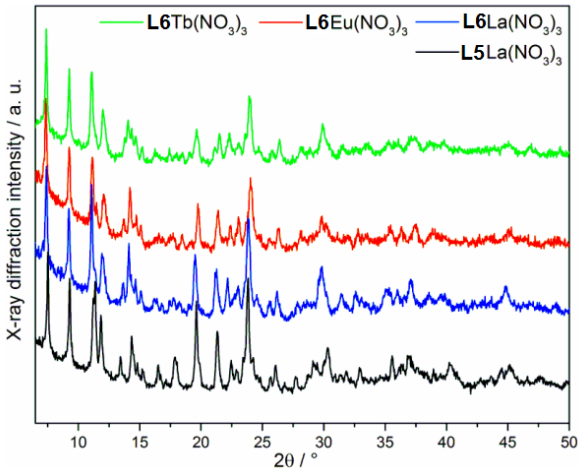

*Figure 20 Observed X-ray diffraction patterns of **L5**La(NO$_3$)$_3$ compared with **L6**Ln(NO$_3$)$_3$ (Ln = La, Eu and Tb).*

In particular, in agreement with the Vegard's law, the relationship between the cell volume and the ionic size is linear. Interestingly, the powder X-ray diffraction patterns of **L6**Ln$(NO_3)_3$ are very similar to the ones of the **L5**Ln$(NO_3)_3$ family (Figure 20), in the case of **L6**La$(NO_3)_3$, **L6**Eu$(NO_3)_3$ and **L6**Tb$(NO_3)_3$. Also for this family of compounds, a contraction of the cell volume on moving from La to Tb and a linear relationship between the cell volume and the ionic size have been observed (Table 3 and Figure 7 in Appendix). As both **L6**Gd$(NO_3)_3$ and **L6**Lu$(NO_3)_3$ present a XRD pattern typical of an amorphous material, their molecular structural details cannot be discussed.

*Table 4 Lattice parameters of **L6**Ln$(NO_3)_3$ compounds*

Ln	*a*(Å)	*b*(Å)	*c*(Å)	α(°)	β(°)	γ(°)	V(Å^3)
La	9.823(4)	12.277(5)	12.861(5)	79.02(3)	84.75(3)	85.52(4)	1513(2)
Eu	9.703(4)	12.299(5)	12.765(5)	79.17(4)	84.77(4)	86.01(4)	1488(2)
Tb	9.730(3)	12.195(4)	12.739(4)	78.62(4)	85.25(4)	86.30(4)	1475(2)

Despite the fact that molecular model employed for the Rietveld calculations was the one of the imine derivative **L5**La$(NO_3)_3$, upon refinement of the cell parameters a good fit of the diffraction intensities has been observed for all the crystalline amine-based compounds (Figure 8 in Appendix), even if the fractional atomic coordinates have not been refined. This is a clear indication of a very similar molecular structure of all the crystalline complexes investigated in this paper, regardless of the nature of the ligand (imine **L5** or amine **L6**) and the metal ion employed. This conclusion has been already drawn in the case of pyridine-based analogs containing both the imine and amine moiety. In this work, the molecular crystal structures of the Eu(III) nitrate complexes of the imine and amine ligands are pratically superimposable.

Spectroscopy in the solid state

Reflectance spectra

The diffuse reflectance spectra of the ligand **L5** and its Ln(III) complexes are shown in Figure 21. The main absorption bands of the ligand **L5** are located around 240

and 300 nm. Two other absorption features are present at around 320 and 340 nm. All these absorptions can be assigned to electronic transitions involving both the quinoline ring and the conjugated C=N group (i. e. $\pi \rightarrow \pi^*$, $n \rightarrow \pi^*$). Upon complexation with Ln(III) ions a bathochromic shift of the absorption bands is observed. In fact, for all the complexes under investigation, the absorption band around 240 nm shifts to 250 nm and the one around 300 nm shifts to 340 nm and becomes much broader.

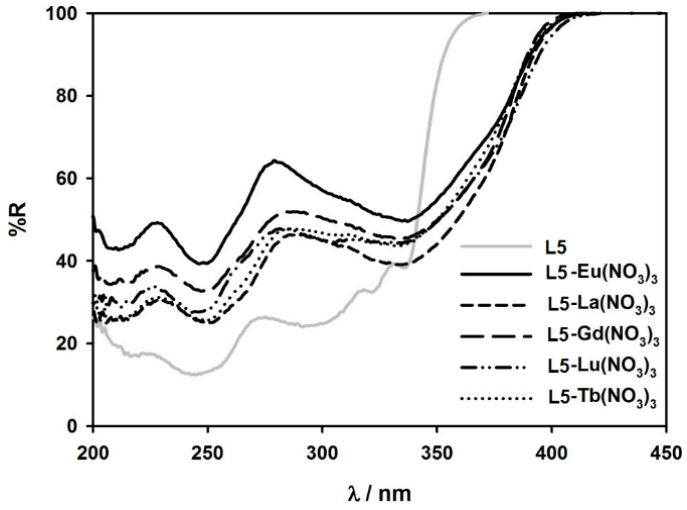

*Figure 21 Reflectance spectra of the powders of **L5** (gray line) and **L5**Ln(NO₃)₃ with Ln = La, Eu, Gd, Tb and Lu (black lines).*

A similar red shift of the absorption bands of the ligand **L6** is observed when the complexation takes place. For all the Ln(III) complexes, absorption peaks around 230 nm, 310 nm and 320 nm are observed (Figure 22).

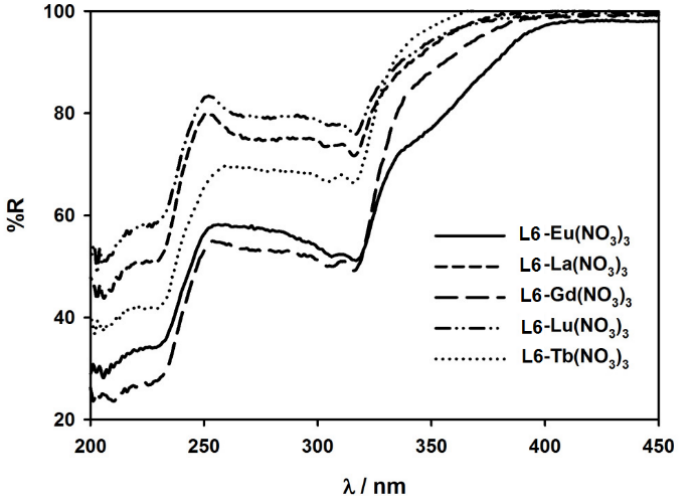

*Figure 22 diffuse reflectance spectra of the powders of **L6**Ln(NO₃)₃ with Ln = La, Eu, Gd, Tb and Lu.*

Emission spectrum

Upon excitation in one of the two main absorption maxima(λ_{exc}= 360 nm), a broad asymmetric emission band centered around 420 nm is observed for La(III), Gd(III) and Tb(III) complexes with the **L5** ligand. A small shift of the emission maximum (440 nm) with respect to the emission peaks of **L5**La$(NO_3)_3$, **L5**Gd$(NO_3)_3$ and **L5**Tb$(NO_3)_3$ (420 nm), is noticed in the case of **L5**Lu$(NO_3)_3$ (Figure 23). The observed red-shift can be related to a change of the coordination environment (i.e. a decrease of the coordination number) due to the reduced size of Lu(III). In this context, Drew et al.[25] have noticed a decrease of the coordination number from 10 to 9, when the metal cation is moved from Yb to Lu in the case of complexes of a tetradentate nitrogen ligand very similar to **L5**. In this case, the change of the coordination number is simply due to an elongation of one of the six Ln-O(NO3) bonds (Yb-O = 2.43 Å, Lu-O above 3 Å).

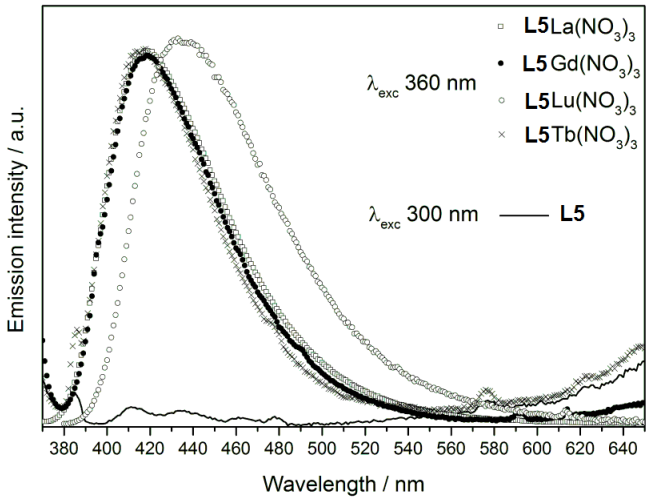

*Figure 23 Luminescence emission spectra of **L5** and **L5**Ln$(NO_3)_3$ (Ln = La, Gd, Lu and Tb).*

This elongation could also occur for **L5**Lu$(NO_3)_3$ complex and as explained before, the powder diffraction data could not be sensitive to this small structural change. The aforementioned emission bands are assigned to the ligand fluorescence, as reported in the literature for several quinoline-based systems[26,27]. Interestingly, the coordination of the metal ion to the ligand gives rise to a dramatic increase of the fluorescence intensity and this behavior can be related to a stiffening of the ligand. In particular, metal ion coordination reduces the rate of non-radiative deactivation (including E/ Z isomerization of the imine group[28,29]) of the fluorescent excited state

of the ligand and thus enhances the fluorescence quantum yield. As mentioned before, in the case of **L5**$Tb(NO_3)_3$, upon ligand excitation only ligand fluorescence has been detected and no emission in the green spectral range, typical of Tb(III) *f-f* electronic transitions, has been observed (Figure 23). Therefore, ligand **L5** is not able to sensitize Tb(III) emission. In addition, the direct excitation of Tb(III) (i.e. 488 nm) does not produce any detectable emission from the metal ion, which loses its excitation energy by non-radiative mechanisms, probably involving a metal to ligand energy transfer process. The ligand **L6** is totally not emissive upon excitation in the UV range. Analogously to the **L5**-based compounds, upon excitation in one of the main absorption peaks (λ_{exc}= 320 nm), a broad asymmetric emission band centered around 390 nm is observed for La(III) complexes with the **L6** ligand (Figure 24). This emission band is red-shifted around 420 nm in the case of **L6**$Gd(NO_3)_3$ and **L6**$Lu(NO_3)_3$.

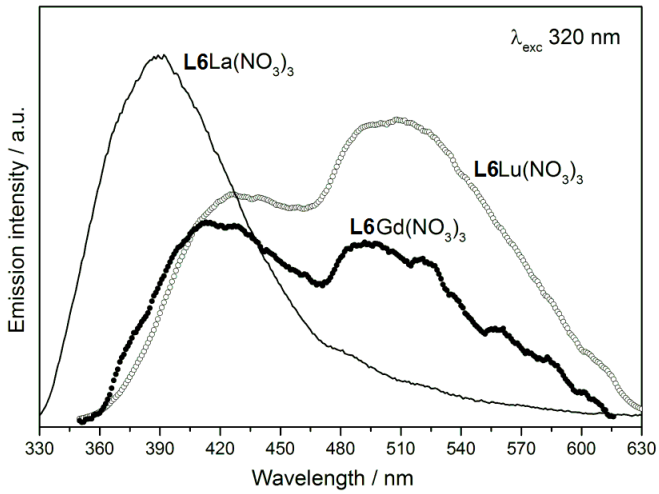

*Figure 24 luminescence emission spectra of **L6**$Ln(NO_3)_3$ (Ln = La, Gd and Lu).*

A possible explanation could be the change of the coordination environment of Gd(III) and Lu(III) if compared with La(III), for the same reasons discussed above, in the case of **L5**$Lu(NO_3)_3$. Nevertheless, due to the amorphous nature of the **L6**$Gd(NO_3)_3$ and **L6**$Lu(NO_3)_3$ powders, no structural data supporting this assumption are available. In the case of the amine-based complexes, the aforementioned emission band can be attributed to the ligand fluorescence and its enhancement upon metal coordination is likely due to the chelation enhanced fluorescence (CHEF) effect. This effect has been previously reported for quinoline-

based metal complexes of Zn(II) and Cd(II)[27,30,22] and depends on the suppression of a photoinduced electron transfer (PET) mechanism. Upon excitation of the free ligand, an electron is transferred from a donor atom, i.e. the amine nitrogens in the present case, to the quinoline ring and this process leads to the quenching of the ligand fluorescence. Involvement of the amine in metal coordination hinders the PET quenching effect. Worth to be noted is the presence of an additional emission peak in the region 500-550 nm in the case of **L6**Gd$(NO_3)_3$ and **L6**Lu$(NO_3)_3$, more defined and intense in the case of the latter compound. This peak could be attributed to the ligand phosphorescence, as suggested by several contribution concerning Gd(III)-based complex containing quinoline as chromophore[31,32]. As previously reported for Gd(III) complexes of the analogs pyridine-based ligands the paramagnetic metal effect[17] is invoked to justify the presence of phosphorescence. Also in the case of **L6**Gd$(NO_3)_3$ this effect should be involved together with the heavy atom effect, even if the contribution of each of them is difficult to determine Instead, in the case of **L6**Lu$(NO_3)_3$ it is only the heavy-atom effect that should increase the phosphorescence intensity. Finally, upon excitation at 315 nm the fluorescence emission together with the characteristic *f-f* emission of the Tb(III) ion have been observed for **L6**Tb$(NO_3)_3$ (Figure 25).

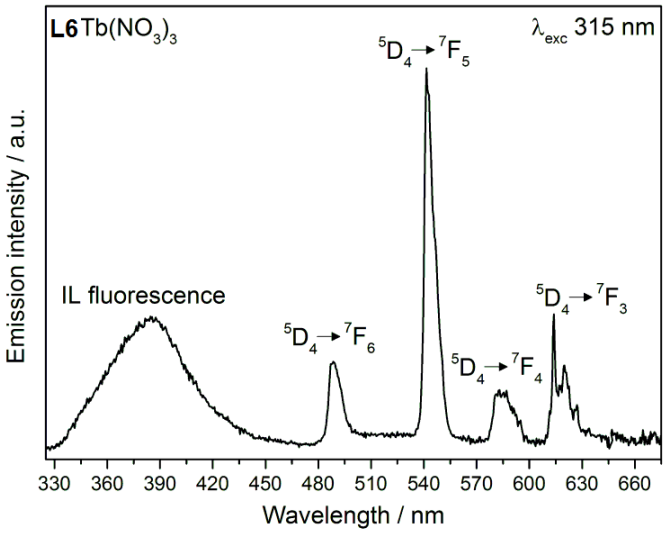

*Figure 25 Luminescence emission spectra of **L6**Tb$(NO_3)_3$ upon ligand excitation.*

Worth to be noted is the identical position of the emission peak related to the ligand fluorescence in the case of **L6**Tb$(NO_3)_3$ and **L6**La$(NO_3)_3$ complexes. This calls fora

similar Ln(III) coordination environment. This conclusion is supported by the structural data discussed above, as **L6**Tb$(NO_3)_3$ and **L6**La$(NO_3)_3$ are isostructural solids. In order to verify the involvement of a ligand to metal energy transfer mechanism, two excitation spectra have been recorded at λ_{em}=385 nm (in the IL fluorescence maximum) and 541 nm (in the $^5D_4 \rightarrow {}^7F_5$ Tb(III) transition), respectively. As they are fully superimposable (Figure 26), the involvement of intra-metal *d-f* Tb(III) excitation transitions feeding the f excited states of the metal ion, can be ruled out.

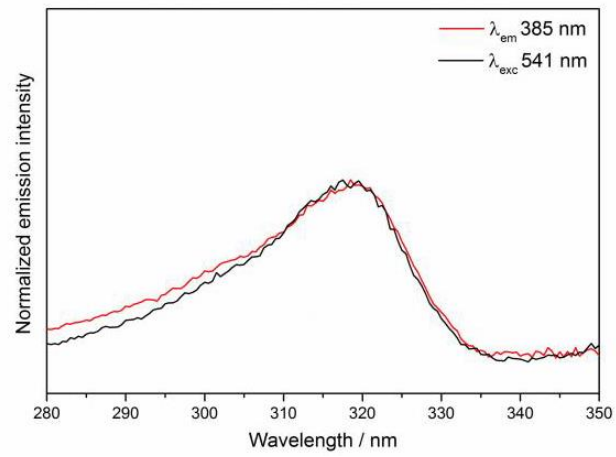

*Figure 26 Normalized excitation spectra of **L6**Tb$(NO_3)_3$ at λ_{em} 385 nm (in the IL fluorescence maximum) and 541 nm (in the $^5D_4 \rightarrow {}^7F_5$ Tb(III) transition).*

In conclusion, a ligand to metal energy transfer is active, even if not all the excitation energy is transferred, as a residual ligand fluorescence is still present. The direct excitation of Tb(III) (i.e. 377 nm or 488 nm) gives rise only to a very weak (almost undetectable) light emission from the metal ion. In order to ascertain the efficiency of the Tb(III) light emission the $^5D_4$ excited state lifetime has been measured. The analysis of the decay curves reveals that the 1/e folding time is in the range of μs (7.5 μs). As this parameter is much shorter than the expected radiative lifetimes of Tb(III) $4f^8$ excited states (in the ms range), the presence of a non-radiative mechanism is responsible of the decrease of the Tb(III) luminescence efficiency. Finally, the emission spectra of **L5**Eu$(NO_3)_3$ and **L6**Eu$(NO_3)_3$ show the typical *f-f* Eu(III) emission features upon ligand excitation (360 nm and 320 nm for **L5**Eu$(NO_3)_3$ and **L6**Eu$(NO_3)_3$, respectively; Figure 27). For both complexes a ligand to metal energy transfer effectively works. The Eu(III) emission spectra are

in practice superimposable and both compatible with a strongly distorted Eu(III) coordination environment, as the hypersensitive $^5D_0 \rightarrow {}^7F_2$ is the dominant band of the spectra. The number of emission features is compatible with a low local symmetry of Eu(III) ion. In fact, the presence of 1 and 3 components for $^5D_0 \rightarrow {}^7F_0$ and $^5D_0 \rightarrow {}^7F_1$ transitions, respectively, are in agreement with the number of crystal field levels for C_1, C_s, C_2 or C_{2v} point symmetry[33].

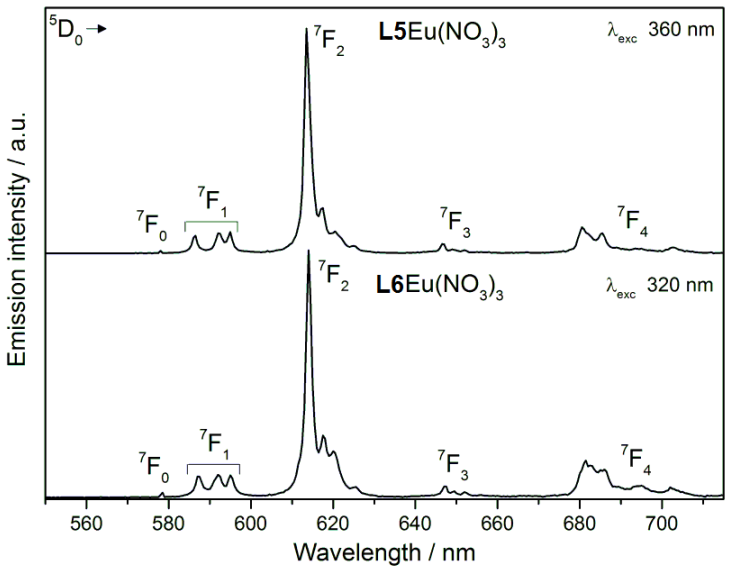

*Figure 27 luminescence emission spectra of **L5**Eu(NO₃)₃ and **L6**Eu(NO₃)₃ upon ligand excitation*

From the structural point of view, as discussed above, the two complexes are isostructural and they crystallize in the centric P-1 space group with lattice parameters only slightly different (Table 3 and 4). The metal ions, in both complexes are expected to be surrounded by a distorted and low symmetric coordination polyhedron. In fact, the actual coordination polyhedra of Eu(III) in **L5**Eu(NO₃)₃ and **L6**Eu(NO₃)₃ should be similar or should result from the distorted sphenocorona (showing C_1 point symmetry) observed for **L5**La(NO₃)₃ in the single crystal. In conclusion, the Eu(III) emission features of **L5**Eu(NO₃)₃ and **L6**Eu(NO₃)₃ are in good agreement with their structural properties. Upon excitation of the ligands, the decay curves of the $^5D_0$ excited state have been recorded. The observed life- times are 0.40 ms and 0.22 ms for **L5**Eu(NO₃)₃ and **L6**Eu(NO₃)₃, respectively. The presence, in the close proximity of Eu(III), of high energy vibrations (NH), which induce a non-radiative relaxation process, decreases the

value of the τ_{obs} for **L6**$Eu(NO_3)_3$ with respect to the one of **L5**$Eu(NO_3)_3$. The $^5D_0$ observed life-times upon direct excitation of Eu(III) (i.e. 396 nm) are the same as the ones found upon ligand excitation. Usually, for Ln(III)-based coordination compounds, due to the increased spin-orbit coupling induced by the presence of Ln(III) ions, an efficient Inter-System Crossing (ISC) from the singlet (S_1) to the triplet (T_1) excited states takes place. Moreover, the efficiency of the $T_1 \rightarrow$ f*[Ln(III)] energy transfer is determined by the energy gap between the two states. The energy of the triplet state must be slightly higher in energy than the acceptor excited state of the lanthanide ion (in particular, 20400 cm^{-1} for the $^5D_4$ of the Tb(III) ion and 17200 cm^{-1} for the $^5D_0$ of the Eu(III) ion) but with sufficiently large ΔE to minimize back-energy transfer[34].

Such thermal repopulation at room temperature of the T_1 manifold can be avoided with ΔE=1850cm^{-1} [6]For the aforementioned reasons, the energy for the triplet is 22250 cm^{-1} for the optimal energy transfer to the $^5D_4$ of the Tb(III) ion and 19050 cm^{-1} for the optimal energy transfer to $^5D_0$ of the Eu(III) ion. The energy of the T_1 level of the complexed **L5** and **L6** (approximately around 20000 cm^{-1} in the case of **L6**[1]) seems to be suitable for the sensitization of the Eu(III) f-f luminescence. On the contrary, in the case of **L5** ligand, the energy of this level is not suitable to give rise to energy transfer to the excited state of Tb(III). In this case, the energy of T_1 should be too far (too low) with respect to $^5D_4$ of the Tb(III). In the case of the ligand **L6**,T_1 level should be closer to $^5D_4$ as a dual emission (IL fluorescence and intraconfigurational *f-f* Tb(III) emission) has been recorded. Nevertheless, as far as the ligand to metal (and metal to ligand) energy transfer process is concerned, it is important to note that the relative energy of electronic states is not the only characteristic to take into account, the energy migration rates of these energy transfer processes involving both ligand singlet and triplet states are of paramount importance and should be considered in parallel to the energy.

[1] Estimated from the phosphorescence peak of **L2**$Gd(NO_3)_3$

Conclusion

In this contribution the synthesis, characterization and the luminescence spectroscopy of new Ln(III) nitrate complexes with the DACH-derivatives ligands have been presented.

Among the metal ions only Gd(III) is able to promote both $S_1 \rightarrow T_1$ intersystem crossing and $T_1 \rightarrow S_0$ radiative transition mainly in the complex with **L1**, giving rise to a strong phosphorescence emission band around 580 nm. The other La(III) and Lu(III) complexes shown only fluorescence emission peak around 430– 460 nm. This evidence clearly supports the presence of the "paramagnetic effect" of the Gd(III) ion, working on the complexes under investigation. The efficiency of this effect seems to be dependent on the flexibility of the chelate structure providing a channel for radiationless deactivation of the phosphorescence.

Metal ions as La(III), Gd(III) and Lu(III) are able to promote IL fluorescence of **L5** and **L6**, taking advantage of the stiffness of the ligand upon complexation, and the chelation enhanced fluorescence (CHEF) effect, respectively. Gd(III) and Lu(III) are also able to stimulate IL phosphorescence at room temperature from the **L6** ligand, by means of "paramagnetic effect" and/or "heavy-atom effect". Both ligands are able to sensitize the typical *f-f* Eu(III) luminescence and only **L6** the one of Tb(III) (green emission). These complexes reveal promising application in the field of luminescent devices and biomedicine since:

i) upon the same excitation wavelength, the same ligand (**L6**, in particular) can produce three different colour emissions (blue, green and red) depending on the nature of the chelated metal ion.

ii) Excitation at 360 nm, in the case of **L5**-based complexes, enable the use of glass optics and minimize interfering excitation of chromophores in biological media

Bibliography

(1) Chen, X.; Liu, Y.; Tu, D. *Lanthanide-Doped Luminescent Nanomaterials*; Nanomedicine and Nanotoxicology; Springer Berlin Heidelberg: Berlin, Heidelberg, 2014.

(2) Tanner, P. A.; Duan, C.-K. *Coord. Chem. Rev.* **2010**, *254* (23–24), 3026–3029.

(3) Bünzli, J. G. *Coord. Chem. Rev.* **2015**, *293–294*, 19–47.

(4) Lamture, J. B.; Zhou, Z. H.; Kumar, a S.; Wensel, T. G. *Inorg. Chem.* **1995**, *34* (4), 864–869.

(5) Hebbink, G. A.; Klink, S. I.; Grave, L.; Oude Alink, P. G. B.; van Veggel, F. C. J. M. *ChemPhysChem* **2002**, *3* (12), 1014–1018.

(6) Latva, M.; Takalo, H.; Mukkala, V.-M.; Matachescu, C.; Rodríguez-Ubis, J. C.; Kankare, J. *J. Lumin.* **1997**, *75* (2), 149–169.

(7) Dexter, D. L. *J. Chem. Phys.* **1953**, *21* (5), 836–850.

(8) Förster, T. *Ann. Phys.* **1948**, *437* (1–2), 55–75.

(9) Bettencourt-Dias, A. *Curr. Org. Chem.* **2007**, *11* (16), 1460–1480.

(10) Yuster, P.; Weissman, S. I. *J. Chem. Phys.* **1949**, *17* (12), 1182–1188.

(11) Horrocks, W. D.; Sudnick, D. R. *J. Am. Chem. Soc.* **1979**, *101* (2), 334–340.

(12) Freed, S.; Weissman, S. I.; Fortess, F. E.; Jacobson, H. F. *J. Chem. Phys.* **1939**, *7* (9), 824–828.

(13) Weissman, S. I. *J. Chem. Phys.* **1942**, *10* (4), 214–217.

(14) Hemmilä, I. *J. Alloys Compd.* **1995**, *225* (1–2), 480–485.

(15) Tsukube, H.; Shinoda, S. *Chem. Rev.* **2002**, *102* (6), 2389–2404.

(16) Melucci, M.; Barbarella, G.; Gazzano, M.; Cavallini, M.; Biscarini, F.; Bongini, A.; Piccinelli, F.; Monari, M.; Bandini, M.; Umani-Ronchi, A.; Biscarini, P. *Chem. - A Eur. J.* **2006**, *12* (28), 7304–7312.

(17) Tobita, S.; Arakawa, M.; Tanaka, I. *J. Phys. Chem.* **1985**, *89* (26), 5649–5654.

(18) Crosby, G. a.; Watts, R. J.; Westlake, S. J. *J. Chem. Phys.* **1971**, *55* (9), 4663–4664.

(19) Strasser, A.; Vogler, A. *Inorganica Chim. Acta* **2004**, *357* (8), 2345–2348.

(20) Piriou, B.; Fahmi, D.; Dexpert-Ghys, J.; Taitai, A.; Lacout, J. L. *J. Lumin.* **1987**, *39* (2), 97–103.

(21) Peacock, R. D. In *Rare Earths*; Springer Berlin Heidelberg: Berlin, Heidelberg, 1975; Vol. 22, pp 83–122.

(22) Ravikumar, I.; Ghosh, P. *Inorg. Chem.* **2011**, *50* (10), 4229–4231.

(23) Nakamoto, K. *J. Phys. Chem.* **1960**, *64* (10), 1420–1425.

(24) van den Ancker, T. R.; Cave, G. W. V.; Raston, C. L. *Green Chem.* **2006**, *8* (1), 50–53.

(25) Drew, M. G. B.; Foreman, M. R. S.; Hudson, M. J.; Kennedy, K. F. *Inorganica Chim. Acta* **2004**, *357* (14), 4102–4112.

(26) Masaki, M. E.; Paul, D.; Nakamura, R.; Kataoka, Y.; Shinoda, S.; Tsukube, H. *Tetrahedron* **2009**, *65* (12), 2525–2530.

(27) Williams, N. J.; Gan, W.; Reibenspies, J. H.; Hancock, R. D. *Inorg. Chem.* **2009**, *48* (4), 1407–1415.

(28) Greb, L.; Lehn, J.-M. *J. Am. Chem. Soc.* **2014**, *136* (38), 13114–13117.

(29) Pratt, a. C. *Chem. Soc. Rev.* **1977**, *6* (1), 63.

(30) Mikata, Y.; Yamashita, A.; Kawamura, A.; Konno, H.; Miyamoto, Y.; Tamotsu, S. *Dalt. Trans.* **2009**, No. 19, 3800.

(31) Quici, S.; Cavazzini, M.; Raffo, M. C.; Botta, M.; Giovenzana, G. B.; Ventura, B.; Accorsi, G.; Barigelletti, F. *Inorganica Chim. Acta* **2007**, *360* (8), 2549–2557.

(32) Lewis, D. J.; Moretta, F.; Holloway, A. T.; Pikramenou, Z. *Dalt. Trans.* **2012**, *41* (42), 13138.

(33) Binnemans, K. *Coord. Chem. Rev.* **2015**, *295*, 1–45.

(34) Bünzli, J.-C. G. *Acc. Chem. Res.* **2006**, *39* (1), 53–61.

CHAPTER TWO: Circularly Polarized Luminescence (CPL)

Introduction

The differential emission of left- and right- circularly polarized light by chiral molecules is known as Circularly Polarized Luminescence (here and after CPL). The first observation of CPL date back to 1948 when Samoilov investigated the photophysical properties of some chiral crystal of sodium uranyl acetate, $Na[UO_2(CH_3COO)_3]$[1]. Only few years later, in 1960, Professor Oosterhof et al. succeeded to record the small polarization in the emission of a solution a chiral organic compound, trans-b-hydrindanone[2], and a chiral metal complex, $[Cr(ethylenediamine)_3]^{3-}$ [2]. The extraordinary results were possible thanks to technologic progresses in optics and electronics field that increased the sensibility in the detection of polarized light. Another important milestone in the history of CPL is represented by first CPL characterization of chiral lanthanide complexes by Luk and Richardson in 1974. The study permitted to recognize that magnetic-dipole allowed *f-f* transitions of lanthanide(III) ions can easily generate light with large circular polarization[3]. The day after, the lanthanide(III) ions became the main protagonist in CPL investigations. The important results attracted the attention of the scientific community which expanded the ways to generate CP emission. Up to now, it is possible observing a CP in semiconductor materials (either chiral or doped with some chiral molecule) experienced with sufficient electric current, the first example was shown by Dekker et al. in 1997 through the use an LED having an active layer with chiral poly-phenylene venylene polymer (CP electroluminescence)[4]. The chiral excited state of a compound could be reached also through chemical reaction, phenomena observed by Dekker in 1976 using chiral dioxetane[5].

The special properties provide by CPL has allowed the building and development of smarter photonic materials for advanced technologies, such as 3D displays[6], information tecnologies[7] and chiral photoswitches[8]. However, another very important application of CPL is surely in structural investigation of chiral compounds, more precisely, of chirality of excited states[9]. Nowadays, numerous technique can be used for the structural resolution of compounds, such as ^{1}H NMR,

X-Ray diffraction, Circularly Dichroism (CD), etc., however each may have its own limitation or be appropriate for specific chiral molecule. For example, the differential absorption of right- and left- circularly polarized light (CD) give information about chiral configuration or conformation of the ground state of molecules, but sometimes it provides unambiguous data. In this context, a spectroscopy based on CPL is an attractive complementary tool that could be used to investigate the omnipresence chirality in the living world. For this reason the synthesis of CPL probes having biological target have assumed a great importance in this research field[10], a fundamental milestone for the successive implementation of a CPL-based microscopy in biology.

Theory

In CPL spectroscopy the physical quantity measured by instrument is the difference in luminescence intensity between left- circularly polarized light (I_L) and right-circularly polarized light (I_R):

$$\Delta I \equiv I_L - I_R \qquad \textbf{(1)}$$

Unfortunately, the measurement of absolute emission intensity requires long procedure, so it is preferable to express CPL grade without dimensional, dividing by the average total luminescence intensity.

$$g_{lum} = \frac{\Delta I}{\frac{1}{2}(I_L + I_R)} = \frac{I_L - I_R}{\frac{1}{2}(I_L + I_R)} \qquad \textbf{(2)}$$

where g_{lum} is called luminescence dissymmetry factor.

Such as for every theories of investigation technique (spectroscopy), the observable quantity is always correlated to some properties of compound or molecules. Also for CPL theory where the observable quantity, ΔI so g_{lum}, can be connected to molecular properties through a quantum-mechanical treatise specifying the oriental distribution of the emitting molecules respect to the direction and polarization of the excitation light and the direction of detection. Among the numerous theoretical development of circularly polarized luminescence spectroscopy, the most significant is represented by Emais and Oosterhof who evaluated the limiting case

in which the orientational distribution of emitting molecules is isotropic[11]. In this condition, for a given electronic transition ($i \leftrightarrow j$) both Δε and ΔI are proportional to a single molecular property, the rotatory strength R_{ij}, as defined in eq. (**5**):

$$\Delta I \propto R_{ij} \quad \textbf{(3)}$$

$$\Delta\varepsilon \propto R_{ij} \quad \textbf{(4)}$$

$$R_{ij} = \Im[< i|\hat{\boldsymbol{\mu}}|j >\cdot< j|\hat{\boldsymbol{m}}|i >] = \Im[\boldsymbol{\mu_{ij}} \cdot \boldsymbol{m_{ij}}] \quad \textbf{(5)}$$

where $\hat{\boldsymbol{\mu}}$ and $\hat{\boldsymbol{m}}$ are the electric and magnetic dipole transition operators and $\Im$ is the imaginary part of the following expression. In achiral compounds occur that vectors $\boldsymbol{\mu_{ij}}$ and $\boldsymbol{m_{ij}}$ are generally perpendicular each other's for symmetry reason, otherwise one of the vectors is zero. Both the conditions lead to the null value of rotatory strength and the impossibility observing CD and CPL spectrum. In chiral condition, which can be ensured by the use of chiral compound or by application of magnetic field, the rotatory strength assumed by one enantiomer is equal but with opposite sign respect to that of other enantiomer. However, a clarification should be made, the magnitude and even the sign, of R_{ij} in absorption and emission could be different since the $i >$ and $j >$ state vectors have different composition for the molecular ground state versus emitting state geometries. An elegant Emeis and Oosterhof's study highlights this last consideration. They were able to calculate the $R_{n\pi^*}$ in absorption, through CD spectra, and $R_{n\pi^*}$ in emission, through CPL spectra, of chromophore containing a ketone, and also able to deduce the geometry difference between the ground and excited state ($^1n\pi^*$)[2]. Taking in consideration all formalism described before, it's possible rewrite the dissymmetry factor in a new form:

$$g_{lum} = \frac{\Delta I}{\frac{1}{2}(I_L + I_R)} = 4\frac{R_{ij}}{|D_{ij}|} \quad \textbf{(6)}$$

where R_{ij} and D_{ij} are, respectively, the rotatory strength and dipole strength of transition and if they are explicitly express, the equation (**6**) change in following way:

$$g_{lum} = 4\frac{R_{ij}}{|D_{ij}|} = 4\frac{|\mu_{ij}| \cdot |m_{ij}|}{|\mu_{ij}|^2 + |m_{ij}|^2}\cos\theta_{\mu,m} \quad \textbf{(7)}$$

Generally, the magnitude of allowed electric dipole transition moments are bigger than that allowed magnetic dipole. This implicate that $|m_{ij}|^2$ is negligible respect to $|\mu_{ij}|^2$, so the Equation (**7**) became[12]:

$$g_{lum} \cong 4\frac{|m_{ij}|}{|\mu_{ij}|}\cos\theta_{\mu,m} \quad \textbf{(8)}$$

Lanthanide complexes as CPL emitter

The Equation (**8**) contains in itself important conclusions concerning CPL spectroscopy. High value of dissymmetry factor can be easily obtained when $|\mu_{ij}|$ is minimized and $|m_{ij}|$ is maximized, in other word when the emission came from electric dipole forbidden/magnetic dipole allowed transitions. This explains why chiral organic molecules emitting through fluorescence and phosphorescence show very low value of dissymmetry factor, generally less of 0.01[13]. Completely different is the case of *f-f* transitions, which are electric dipole forbidden for symmetry (LaPorte rule) and some of them satisfy the formal selection rules of magnetic dipole transition ($\Delta J = 0,\pm1$ except $0\leftrightarrow0$). So, the lanthanide ions, in particular the intraconfigurational *f-f* transitions, satisfy all the required condition to obtain high value of g_{lum} and they are the best candidate as CPL emitter. They can generally exhibit a dissymmetry value in the range 0.05-0.5, with some exception as the higher $|g_{lum}|$ value (1.38) obtained by champhor-base Europium complex[14].

In this field an important result was reached by Richardson, who tried to rationalize the magnitude of g_{lum} generated in lanthanide compounds. He developed quantum-mechanical treatise that takes into consideration the Spin-Orbit and Crystal field perturbation on magnetic and electric dipole of *f-f* transitions. The final result was the construction a new selection rules which labels the lanthanide transition into three different ways (DI, DII, DIII). Richardson observed that the magnitude of

dissymmetry factor decrease following the class order DI>DII>DIII. In Table 1 are shown the transition generally observed in CPL measurement and their D class[15].

Table 5 Some Ln^{3+} transition and their D class

Ion	Transition	Wavelength (nm)	Class
Sm^{3+}	$^4G_{5/2} \rightarrow {}^6H_{5/2}$	565	DII
	$^4G_{5/2} \rightarrow {}^6H_{7/2}$	595	DIII
Eu^{3+}	$^5D_0 \rightarrow {}^7F_1$	595	DI
Tb^{3+}	$^5D_4 \rightarrow {}^7F_5$	545	DII
Dy^{3+}	$^4F_{9/2} \rightarrow {}^6H_{11/2}$	670	DIII

Among all the lanthanide compounds that can be used in the CPL investigation, surely the complexes take up a privileged position in this research field. This is due to their great ability to generate a chiral environment ad to ensure high quantum yield, a capability extremely useful for the design of new CP-OLED. Alternatively, lanthanide complexes can offer good sensing properties which are used for the detection of chiral compounds through CPL investigation (CPL probe). These two main chiroptical applications of lanthanide complexes are mainly governed by macrocycles and β-diketonates-based complexes.

Macrocycle based-ligand are widely employed in the building of lanthanide probes. They are mainly based on cyclen (**1**) or its smaller version, triazacyclononane (**2**) since this macrocyclic fragment ensure great stability in water media. Moreover, these ring scaffolds can be easily functionalized at the N-atom with arms having coordinating groups such as amides, carboxylates, etc. and/or chromophore able to sensitize the lanthanide ions. These kind of ligand have been extensively used by Parker's group that has contributed to elucidate the structural conformation of the relative lanthanide complexes also by means of chiroptical spectroscopy. Achiral cyclen and triazacyclononane derivatives could give four stereoisomers, two enantiomer couples, complexes that can exist in dynamic equilibrium between each other's. The preference toward a couple of enantiomer or diastereoisomer is imposed by the presence of sterically demanding groups in the arms or in the cyclic

part. However, the chirality could be also more easily introduced by the presence of stereogenic center in the ring or, more often, on the side-arm[10] such **(S)-3** and **(S)-4** (Figure 1).

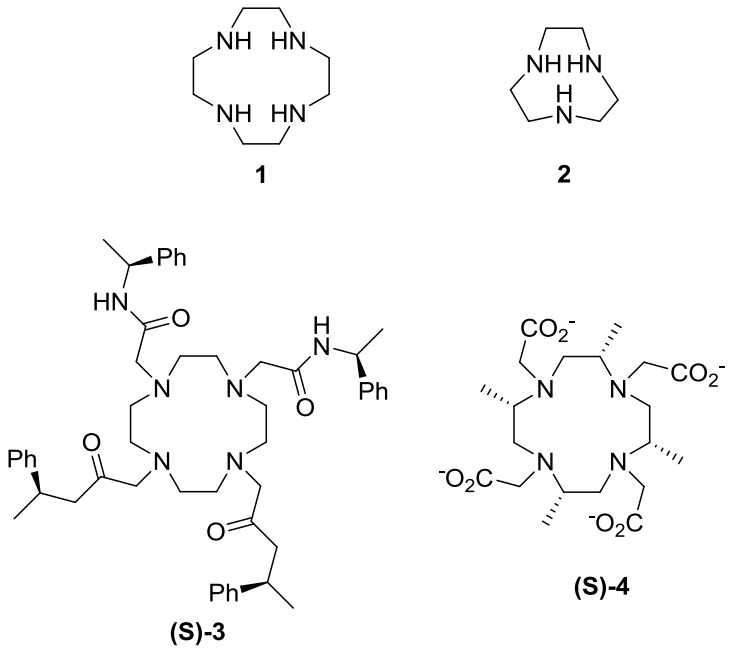

Figure 28 Cyclen and triazacyclononane derivatives

Another important class of lanthanide complexes is the β-diketonate. This bidentate monoanionic ligands guarantee a strong coordination to Ln^{3+}, thanks to oxophilicity of metal, and they permit the formation of stable *tetrakis*- and *tri*- complexes. Furthermore, by modification of substituents in 1 and 3 position, it's possible to modulate the energy of triplet state optimizing the energy transfer to different lanthanide. A common β-diketonate is HFA (1,1,1,5,5,5-Hexafluoropentane-2,4-dione) represents a good antenna either for terbium and europium and it has been utilized by Kawai[16] for synthesis an series of heteroleptic complexes, $Ln(HFA)_3L^*$. The ancillary ligands (L*) are Pybox containing one or more stereogenic center necessary to induce chirality to the complexes (Figure 2). The final europium and terbium complexes show very high quantum yield (34-41%) and also a good level of polarization with g_{lum} value reached by Eu^{3+} complexes between |0.15| and |0.46|. However, the interesting thing that Kawai et al. noticed was the signs of the $^5D_0 \rightarrow {}^7F_1$ and $^5D_0 \rightarrow {}^7F_2$ transitions are same for L* = (R)-iPr-Pybox (**(R)-5**) and

(R,R)-Me-Ph-Pybox (**(R,R)-6**), but they are inverted for bis-4R-(4-phenyl-oxazolinyl)pyridine ((R)-Ph- Pybox, **(R)-7)**.

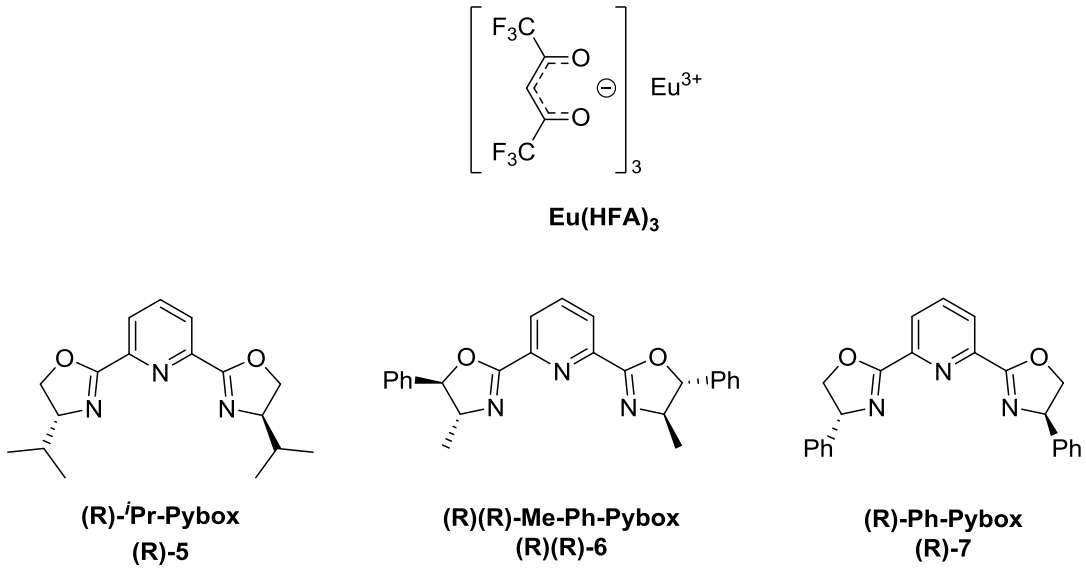

Figure 29 Diketonate-based Eu^{3+} complexes and ancillary ligand

The authors tried to explain the different signs behavior by correlating to crystal structure obtained by X-ray diffraction of single crystal, and only by this analysis it has been found that the arrangement of three β-diketonate around the lanthanide ion is dependent on the presence of ligand-ligand intramolecular interaction such as π-π,CH-π and CH-F. The use of chiral ancillary ligand is not the only one way to form chiral β-diketonate lanthanide complexes. The alternative method consist the use of chiral β-diketonate which can be easily synthetized through Claisen type reaction from cheap natural enatiopure ketone (Figure 3). Some example are **hfbc** (heptafluorobutyrylcamphorate)[14] and **hfbcv** (heptafluorobutyrylcarvone)[17] which have the ability to form *tetrakis*- Europium complexes with high value of dissymmetry factor.

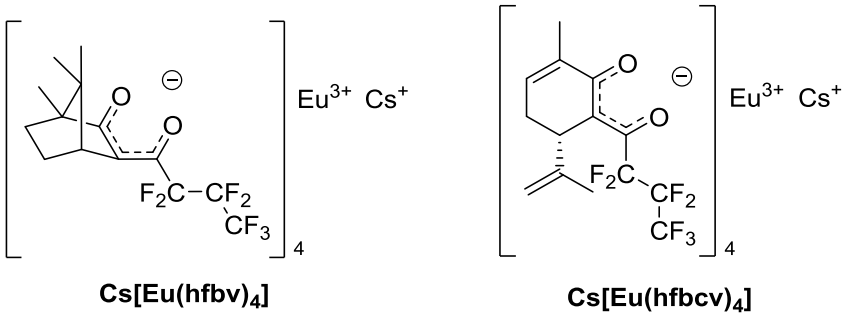

Figure 30 Europium complexes with Chiral Diketonate

Aim of study

The aim of the present study is to design and synthesize new chiral Ln(III)-based complexes with considerable CPL activity. with this in mind, we focused our attention on two possible application:

i) new materials for CP-OLED application or

ii) chiroptical probes for chiral anions or biomolecules.

Up to now, many chiral lanthanide complexes showing good CPL signal are present in literature. The introduction of chirality could occur in different ways but, surely the most used method consists in the employment of chiral ligands. Among all the chiral ligand used for synthesis of CPL lanthanide emitter, the 1,2-diamine cyclohexane derivatives has been slightly investigated. However, Raymond et al. observed that this kind of ligand can offer a good rigidity, a fundamental requisite necessary to good CPL emitter[18]. So, we have decided to increase the knowledge about the chiroptical potentiality of 1,2-diamine cyclohexane backbone by synthetizing new chiral lanthanide complexes.

Previous results have shown that N,N'-(cyclohexane-1,2-diyl)bis(1-(pyridin-2-yl)methanimine) and N^1,N^2-bis(pyridin-2-ylmethyl)cyclohexane-1,2-diamine are good ligands for the synthesis of luminescence lanthanide complexes.

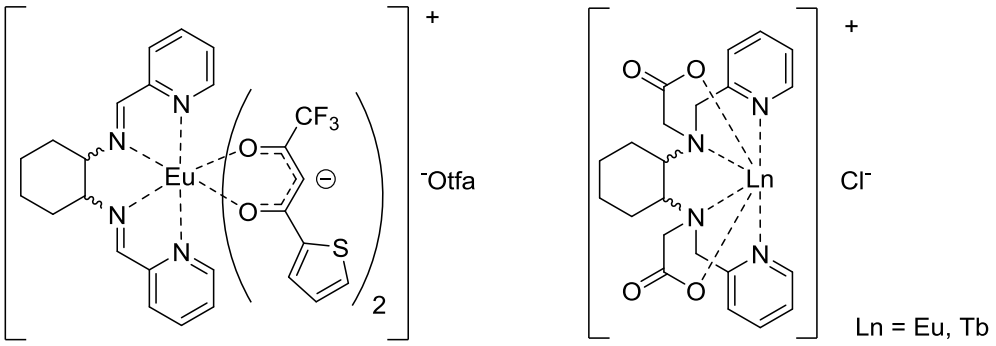

Figure 31 The investigated lanthanide complexes

For this reason, we have used the chiral N,N'-(cyclohexane-1,2-diyl)bis(1-(pyridin-2-yl)methanimine)ligand to form europium(III) complexes, tta (2-thenoyltrifluoroacetonate) to increase the Brightness of whole complexes (complex 1 Figure 4). On the other hand, in order to increase the stability and the solubility

of the complexes in water, a new ligand including two carboxylate arms has been deisgned (complex 2 Figure 4).

Results

Synthesis, Characterization and CPL spectroscopy of new N,N'-(cyclohexane-1,2-diyl)bis(1-(pyridin-2-yl)methanimine) Europium complexes

Circularly polarized (CP) organic light-emitting diodes (CP-OLEDs) are an emerging technology and recently a lanthanide-based OLEDs with remarkable CP electroluminescence have been designed[19]. These devices are based on the chiral Eu(III) complex CsEu(hfbc)4 (hfbc = 3-heptafluorobutyryl camphorate, a β-diketonate) showing the highest known CP photoluminescence[14]. In this context, a Eu(III) complex based on a new chiral diketonate (carvone) appears a promising candidate for these kind of applications[17]. To the best of our knowledge, when the chirality is introduced by the L ligand in Ln^{3+} β-diketonate systems, the CPL activity has not been neither detected or studied. Finally up to now, only one family of Ln complexes based on ternary β-diketonate, containing a tetradentate ligand as additional chromophore able to sensitize the lanthanide luminescence, has been characterized[20]. In this contribution, the synthesis of a highly luminescent heteroleptic β-diketonate complex of europium is presented. The cationic complex, characterized by two anionic tta (2-thenoyltrifluoroacetyl-acetonate) ligands and one chiral tetradentate Schiff base NNNN ligand surrounding the metal ion (Figure 5), shows a strong CPL activity (g_{lum} 0.1 around 597 nm) both in acetonitrile solution and in the solid state.

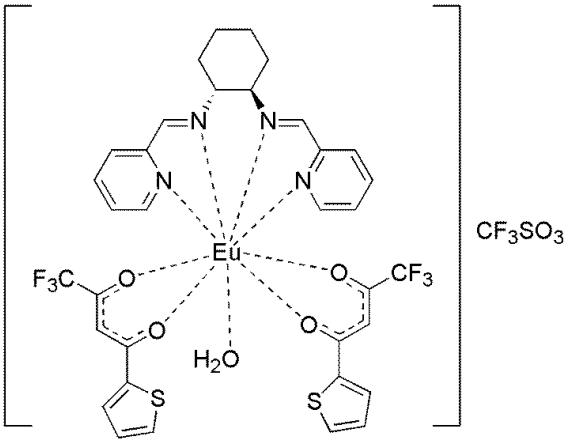

*Figure 32 Molecular structure of [Ln**L**(tta)$_2$(H$_2$O)]CF$_3$SO$_3$; **L** = N, N'-bis(2-pyridylmethylidene)- 1,2-(*R,R+S,S*)-cyclohexanediamine.*

UV-visible Absorption

The UV-visible electronic absorption spectra of [Eu**L**(tta)$_2$(H$_2$O)]CF$_3$SO$_3$ has been recorded in acetonitrile solution and compared with the ones of **L**, Eu**L**(CF$_3$SO$_3$)$_3$ and Eu(tta)$_3$ (Figure 6).

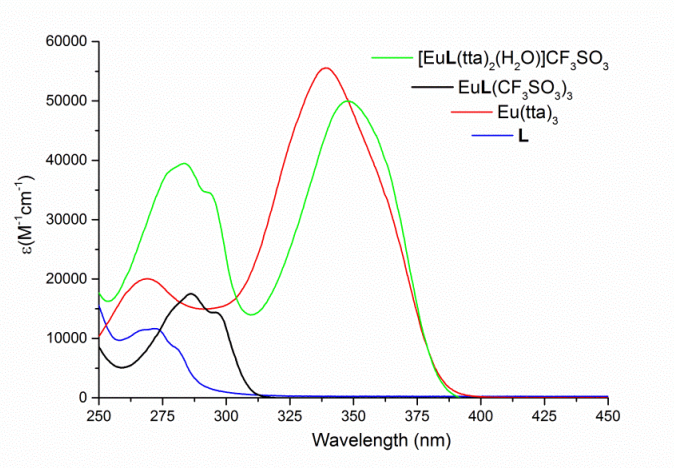

*Figure 33 Absorption spectra of **L**, Eu**L**(CF$_3$SO$_3$)$_3$, Eu(tta)$_3$ and [Eu**L**(tta)$_2$(H$_2$O)]CF$_3$SO$_3$ in acetonitrile at 298 K.*

[Eu**L**(tta)$_2$(H$_2$O)]CF$_3$SO$_3$ shows two broad absorption bands spanning the UV range from 250 to 400 nm, with two absorption maxima (280 nm with a shoulder around 290 nm and 350 nm). The Eu(tta)$_3$ complex presents one main absorption band (l_{max} = around 350 nm) which is attributed to the ligand centered singlet-singlet π-π* enolic transition[20]. The composite absorption band peaking around 260 nm observed for the ligand **L**, assigned to electronic transitions involving both the pyridine ring and the conjugated C=N group (i.e. π-π*, n-π* transitions), is red shifted to 280-285 nm upon complexation of the ligand with Eu(III) in Eu**L**(CF$_3$SO$_3$)$_3$. On the basis of this evidence, the most intense peaks for [Eu**L**(tta)$_2$(H$_2$O)]CF$_3$SO$_3$ at 285 and 350 nm are assigned to the overlapping absorption bands of **L** and tta ligands bound to Eu(III), respectively. The latter absorption band in the N-UV region is particularly attractive for obtaining absorption at lower energy, which is required in many applications. If the absorption spectrum of [Eu**L**(tta)$_2$(H$_2$O)]CF$_3$SO$_3$ is recorded in methanol solution, the same conclusion can be drawn, as long as the concentration of the complex is not decreased below 10^{-5} M. In such case, while the band of tta ligand is not significantly shifted (λ_{max} = 348 nm), the one of **L** ligand is blue-shifted (λ_{max} = 348

nm) and is superimposable with the absorption of the "free" ligand in methanol (data not shown). This suggests that in very diluted methanol solution the ligand **L** is dissociated.

Luminescence

Excitation spectra of [Eu**L**(tta)$_2$(H$_2$O)]CF$_3$SO$_3$ sample in the solid state and dissolved in acetonitrile upon monitoring the $^5D_0 \rightarrow {}^7F_2$ transition (l_{em} = 615 and 619 nm, respectively) are shown in the figure 7 (left). In both cases, the typical red luminescence of Eu(III) is effectively sensitized upon excitation of both **L** (peak around 280 nm) and the tta ligands (peak around 350 nm).

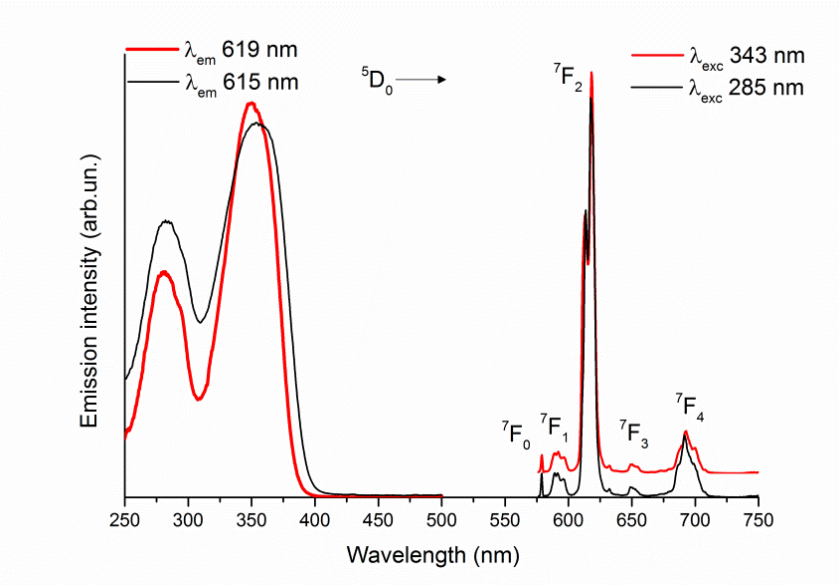

*Figure 34 Luminescence excitation spectra (left) and emission spectra (right) of [Eu**L**(tta)$_2$(H$_2$O)]CF$_3$SO$_3$ in the solid state (black lines) and dissolved in acetonitrile (red line) at 298 K. For reason of clarity, the emission spectra have been shifted on y axis.*

As for luminescence emission spectra both in the solid state and in acetonitrile (figure 7, right), the typical Eu(III) luminescence stemming from *f-f* transitions is clearly detected. Since the hypersensitive $^5D_0 \rightarrow {}^7F_2$ transition dominates in the spectrum, the point symmetry of Eu(III) deviates from the inversion symmetry[21], even in acetonitrile solution. As it is well known that the Eu(III) emission features are strongly connected to the geometry of the metal ion and the emission spectra recorded in the solid state and in acetonitrile solution are superimposable upon

several excitation conditions (i.e. l_{em} = 285 nm, 350 nm), we expect the same Eu(III) geometric environment in the solid state and in acetonitrile solution, characterized by two tta, one L ligand and one solvent molecule (water or acetonitrile) bound to the metal ion. On the contrary, the luminescence emission spectrum of the powder dissolved in methanol is similar but not superimposable to the one collected in acetonitrile. This could mean that the solvent plays a non negligible role in the definition of the geometrical environment fo Eu(III), which is slightly different in the two solvents. The most significant difference is in the region of the $^5D_0 \rightarrow {}^7F_1$ transition (Figure 8)

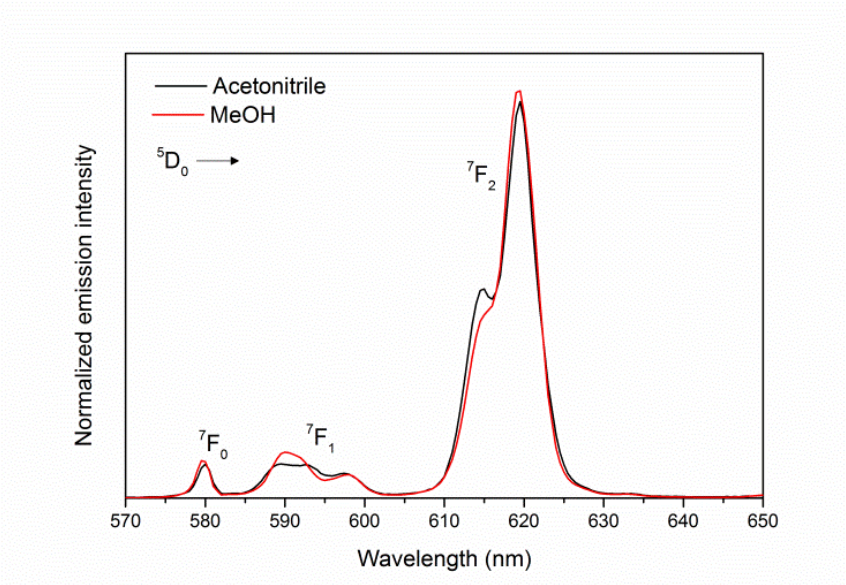

*Figure 8 Luminescence emission spectra (λ_{exc} = 280 nm) in acetonitrile and methanol solution of [Eu**L**(tta)$_2$(H$_2$O)]CF$_3$SO$_3$ at the same concentration of the CPL experiments (the spectra are normalized to the area of the $^5D_0 \rightarrow {}^7F_1$ transition and limited to the 570-650 nm range)*

The luminescence decay curves of the $^5D_0$ excited state in the solid state and in acetonitrile solution are also collected (figure 23 Appendix). In both cases, the curves are well fitted by a single exponential function and the observed lifetimes are 0.60(1) msec, 0.57(1) and 0.44(1) msec for the sample in the solid state, in methanol and in acetonitrile, respectively. By means of the equation $\phi = \tau_{obs}/\tau_R$ for the calculation of the intrinsic quantum yield, we found a value around 40% and 52% for the complex in acetonitrile and in methanol solution. The Eu(III) radiative lifetime (τ_R) is 1.1 msec in both solvents and has been determined from the analysis of the emission spectrum by using the equation reported by Werts et al.[22]. Even

though the precise estimation of the intrinsic quantum yield for the solid state sample is not possible due to the lack of knowledge of the refractive index of the powder, we expect a value at least equal to the one found in acetonitrile and methanol solution, due to the similar nature of the two complexes. The small but significant difference of the observed lifetime in methanol and acetonitrile could be connected with the slightly different Eu(III) geometrical environment observed in these two solvent (see discussion above). The excitation and emission spectrum of Eu**L**$(CF_3SO_3)_3$ in acetonitrile are presented in Figure 24 in Appendix. Also in this case, the metal-centered luminescence is effectively sensitized by the ligand **L** upon excitation around 280 nm and the emission features originate from Eu(III) located in a strongly asymmetric environment. Also for this complex, these spectra are superimposable with the ones obtained in the solid state (data not shown).

Chiroptical characterization

The CPL spectra obtained for the two enantiomers of [Eu**L**$(tta)_2(H_2O)]CF_3SO_3$ both in acetonitrile and methanol solutions are perfect mirror images. We observe several partially resolved transitions, thanks to the apparent resolution enhancement typical of spectra with nearby opposite-signed bands. This is particularly evident for the $^5D_0 \rightarrow {}^7F_2$ transition, which shows four bands in acetonitrile, two positive and two negative, and three bands in methanol (in total emission spectra only two bands are visible in both the cases). The main CPL signals are associated to the $^5D_0 \rightarrow {}^7F_1$ and $^5D_0 \rightarrow {}^7F_2$ transitions, respectively centered at 590 nm and 615 nm. The $^5D_0 \rightarrow {}^7F_3$ (655 nm) and the $^5D_0 \rightarrow {}^7F_4$ (700 nm) are less CPL active, whereas the $^5D_0 \rightarrow {}^7F_0$ (580 nm) transition does not give any CPL signal.

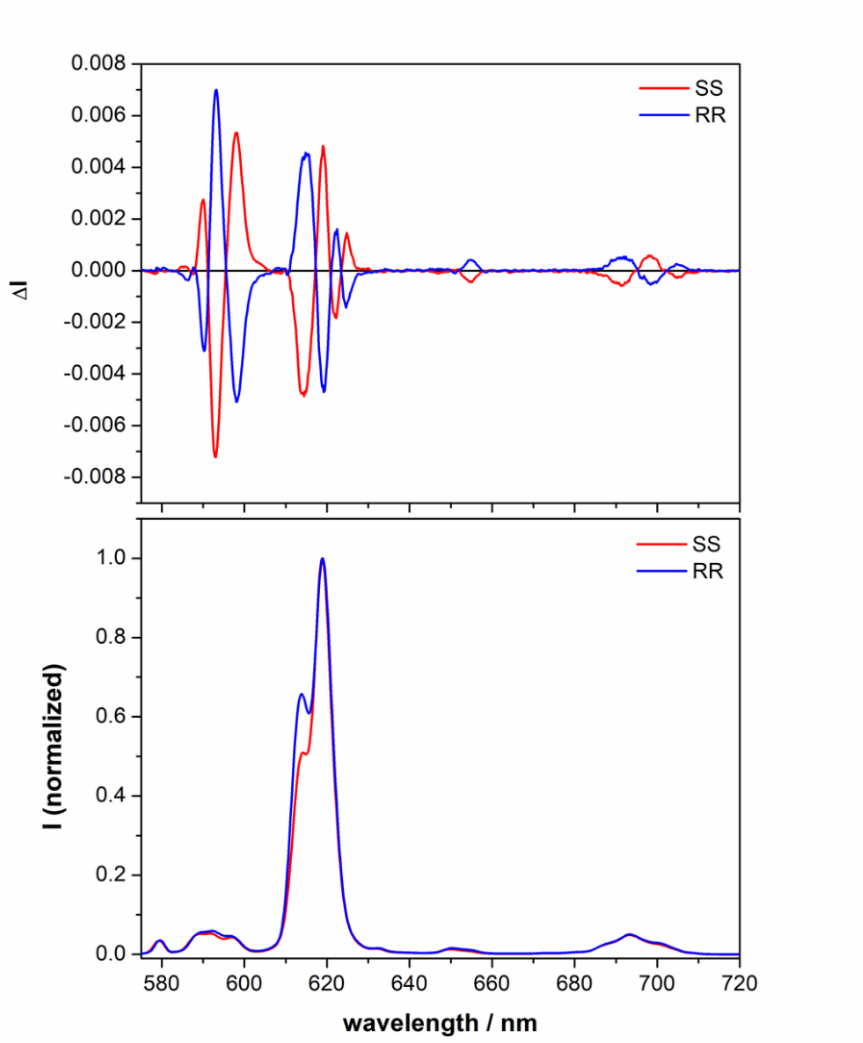

*Figure 9 Normalized CPL spectra (top) and total emission spectra (bottom) of the two enantiomers of [Eu**L**(tta)$_2$(H$_2$O)]CF$_3$SO$_3$ in CH$_3$CN. The spectra are normalized to the maximum of the $^5D_0 \rightarrow {}^7F_2$ emission band.*

The highest g_{lum} is reached for the most intense band of the $^5D_0 \rightarrow {}^7F_1$ multiplet at 592 nm: we measured a value of |0.13| in acetonitrile and |0.2| in methanol. Electronic circular dichroism (EDC) spectra in acetonitrile, methanol and in the solid state are shown in Figure 25-27 in Appendix. In all cases, they display a complex pattern, associated to both tta and **L** absorption bands. This reveals that the chiral ligand dictates a defined chiral twist in the diketonates, as well. There are several small differences between the spectra in the two solvents, which once more suggests some minor structural solven-dependent rearrangements. As for what concerns the total emission spectra in acetonitrile, some differences in the relative intensities of the two bands associated to the $^5D_0 \rightarrow {}^7F_2$ transition can be observed in

acetonitrile solution. The most blue-shifted component of the multiplet gains intensity upon time, probably indicating that the complex undergoes some modification when dissolved in CH_3CN for a few hours. Nevertheless, because the CPL spectra (normalized on the emission intensities of the red-shifted component of the transition) of the two enantiomers are mirror images, we did not investigate any further this aspect.

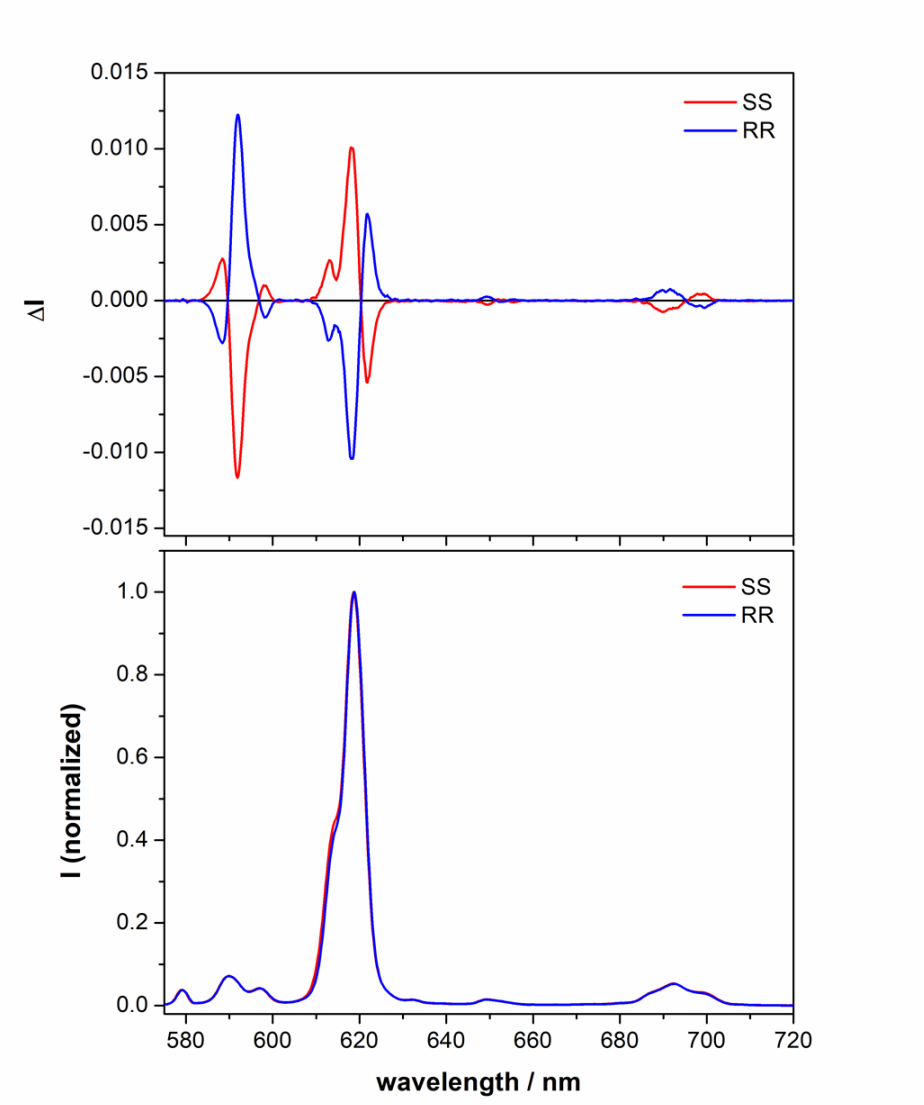

*Figure 10 Normalized CPL spectra (top) and total emission spectra (bottom) of the two enantiomers of [Eu**L**(tta)$_2$(H$_2$O)]CF$_3$SO$_3$ in MeOH. The spectra are normalized to the maximum of the $^5D_0 \rightarrow {}^7F_2$ emission band.*

The CPL spectra of the main bands were collected also for the two enantiomers at the solid-state, obtained by deposition from acetonitrile solutions on a quartz plate. The spectra display the same trend (sequence, relative intensities and signs of

bands) in comparison to the ones recorded in acetonitrile solutions. This indicates that both in solution and at the solid-state Eu(III) ion is surrounded by the same dissymmetric environment. In this case we measured a g_{lum} around |0.05| for the CPL band at 593 nm.

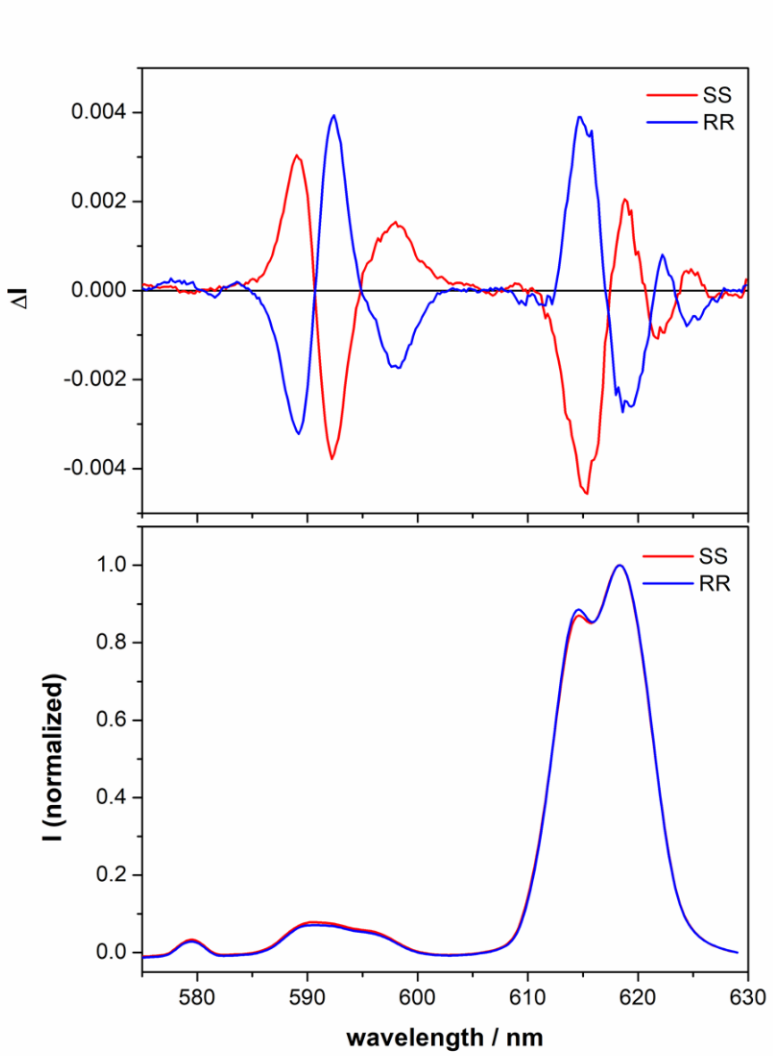

Figure 35 Normalized CPL spectra (top) and total emission spectra (bottom) of the two enantiomers of $[EuL(tta)_2(H_2O)]CF_3SO_3$ at the solid state. The spectra are normalized on the maximum of the $^5D_0 \rightarrow {}^7F_2$ emission band.

Solution structure (NMR)

We decided also to get at least some insight into the solution structure of the complex by means of paramagnetic NMR. The ^{1}H NMR spectra, both in CD_3CN

and CD_3OD, show narrow resonances, thus indicating that the complex has a static C_2 symmetry. Because the X-ray diffraction (XRD) structure lacks any symmetry, (all the atoms fall in a general position (C_1 symmetry), it does not represent neither the solid-state sample (obtained by deposition) nor the complex in solution, which is also in agreementent with the diffrences found in the CPL and ECD spectra discussed above. Moreover, because the ^{1}H-NMR signals are highly structured, due to J-couplings, and have very small half-height linewidth ($\Delta\nu_{1/2}$) one can rule out line broadening caused by chemical exchange, for example due to slowly occurring geometrical rearrangement The quantitative analysis of the paramagnetic shifts and relaxation data would require a set of other Ln analogues and it was considered not necessary for the present discussion.

Synthesis, Characterization and CPL spectroscopy of new N,N'-bis(2-pyridylmethyl)-1,2-diaminocyclohexane- N,N'-diacetic lanthanide complexes.

The introduction of chiral 1,2-diaminocyclohexane in the ligand moiety could guarantee the possibility to generate good CPL from the lanthanide. To use this special emission of lanthanide in sensing of biomolecules, the solubility of complexes in water media is strongly necessary. With this puropose, the of N,N′-bis(2-pyridylmethyl)-trans-1,2-diaminocyclohexane ligand can be easily functionalizated through the introduction of carboxylate arms which, in addiction, have the ability to strongly coordinate the lanthanide ions. We have synthetized the 2,2'-(ethane-1,2-diylbis((pyridin-2-ylmethyl)azanediyl))diacetic acid (H_2bped) and the enantiomeric form of 2,2'-((-cyclohexane-1,2-diyl)bis((pyridin-2-ylmethyl)azanediyl))diacetic acid (H_2bpcd) and the relative europium and terbium complexes (Figure 12).

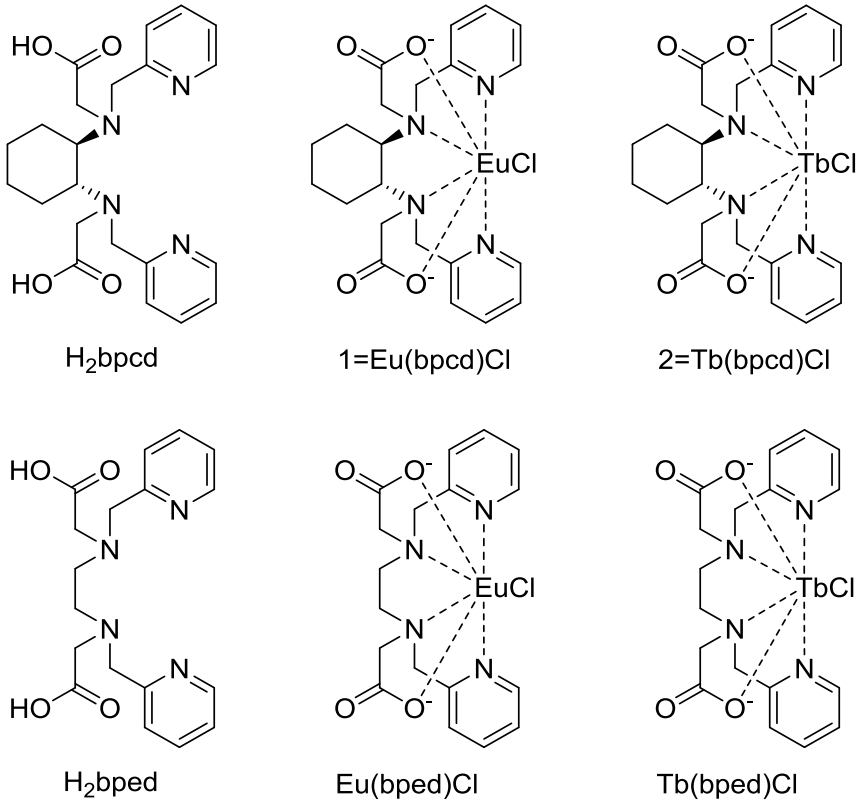

Figure 12 The ligand (H2bpcd) prepareted in R,R, S,S and Racemic forms, Eu(bpcd)Cl and Tb(bpcd)Cl preparated

Species in Solution and Structures of the Aquo Complexes

The protonation constants of H_2bpcd obtained from the best fit of the experimental emf data (Figure 13,as an example) are given in Table 2. In the same table, also the values available in the literature for the ligands in Figure 12 are reported[23].

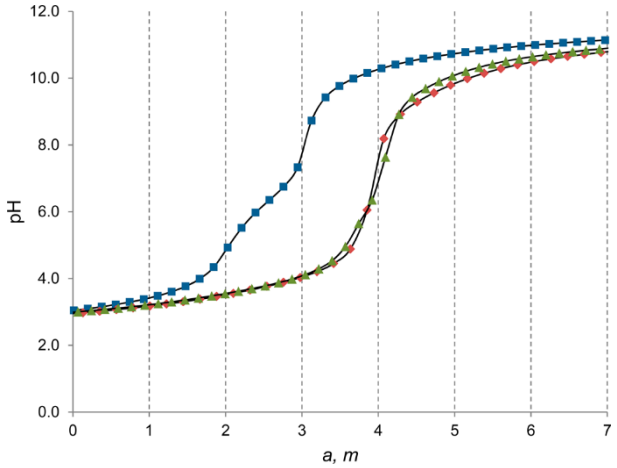

Figure 13 Titration curves for the ligand alone (blue ■, 0.95 mM) and in the presence of lanthanide ions in a 1:1 molar ratio (red ◆, Eu, 0.66 mM; green ▲, Tb, 0.64 mM): a = (mol of free NaOH)/(mol of ligand); m = (mol of free NaOH)/(mol of Ln(III) ion). Only some of the experimental points are reported in the plot. Full lines are calculated with the stability constants in Table 2.

The resulting protonation constants for H_2bpcd are indicative of two fairly strongly acidic and two weakly acidic sites. The first protonation constant (Table 2) for H_2bpcd is slightly higher than that found for the analogous H_2bped ligand. This difference in ligand basicity could be due to the structural rigidity of the cyclohexyl backbone in comparison to the more flexible ethylenic backbone and has already been observed when H_4cddadp and H_4bpeda protonations are compared (Table 2)[24]. Variable pH UV−vis titration (Figure 14) suggests that the first protonation (log K_1 = 9.72) can be assigned to an aliphatic amine group, while the second protonation (log K_2 = 5.87) is related to a pyridyl nitrogen as the absorbance at λ=260 nm increases as this species begins to form at pH ∼7. The other protonations involve an acetate and the remaining pyridyl group, as suggested by the continuous increase in the absorbance also below the pH at which the H_2bpcd species reaches its maximum concentration.

Table 6 Protonation Constants (log Kj) for the Ligand H2bpcd and Formation Constants (log β) for the Complexes with Eu(III) and Tb(III) at 25 °C. [a]Standard deviations are given in parentheses, and charges are omitted for simplicity. Protonation data for the other ligands reported in Chart 1 (and their formation constants with Gd(III)[25]) are also reported. [b]Referencef[3]; values with μ = 0.1 M ($NaNO_3$) from ref[3] are given in parentheses. [c]Reference[24]; log K_5 = 2.62. [d]Reference[26]; log K_5 = 1.66. The values of log KGdL in the last column are obtained by two different methods.

reaction	H_2bpcd (μ = 0.1 M (NaCl))	H_2bped[b] (μ = 0.15 M (NaCl))	H_4cddadp[c] (μ = 0.15 M (KCl))	H_4bpeda[d] (μ = 0.15 M (KCl))
		log K_j		
L + H ⇆ HL	9.72(1)	8.67 (8.84)	9.35	8.52
HL + H ⇆ H_2L	5.87(4)	5.53 (5.63)	5.66	5.40
H_2L + H ⇆ H_3L	2.94(7)	3.11 (3.02)	4.20	3.65
H_3L + H ⇆ H_4L	2.22(7)	<2 (2.34)	3.72	2.97
		log β		
L + Eu ⇆ EuL	11.2(2)			
L + Eu ⇆ EuL(OH) + H	2.2(3)			
L + Tb ⇆ TbL	11.35(7)			
L + Tb ⇆ TbL(OH) + H	2.1(2)			
L + Gd ⇆ GdL		12.37	20.68	20.23−20.39
L + Gd ⇆ GdL(OH) + H		2.1		

This protonation sequence is in agreement with what was suggested previously for H_2bped on the basis of a UV−vis and NMR spectroscopic study[23]. The titration curves reported for 1:1 Ln(III):ligand ratios (Figure 14) present similar profiles and show a buffering effect up to 4 equiv of hydroxide. The best fit of all the experimental data shows that only the species $[Ln(bpcd)]^+$ and [Ln(bpcd)- (OH)] are formed (Table 2) by Eu and Tb and that no additional species are present. Their formation constants, together with those related to the complexes of similar ligands with Gd(III) available in the literature, are given in Table 2[24].

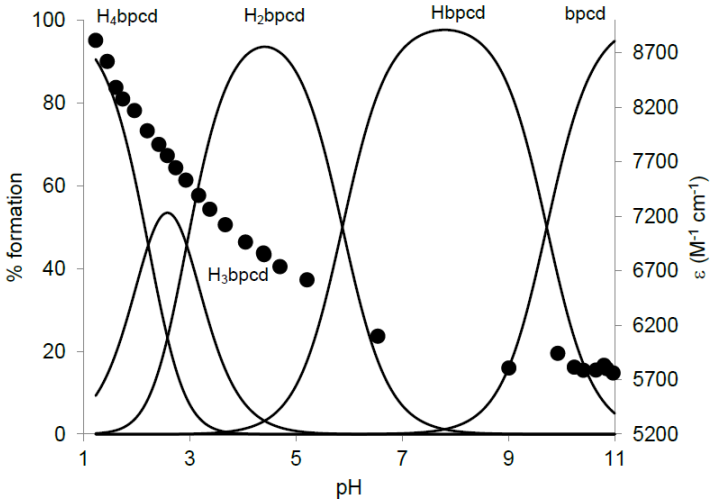

Figure 14 Molar extinction coefficient of the absorption maximum of bpcd at λ = 260 nm in function of pH along with the speciation calculated with the protonation constants reported in Table 2 and the ligand concentration employed (Cbpcd = 0.039 mM).

The stability constants for Eu(III) and Tb(III) complexation are both lower than those obtained for the complexation of Gd(III) with H_2bped. This difference could be due to the different experimental conditions (different ionic strength); however, it is indicative that the stability of the complex is not greatly affected by the replacement of the ethylenic chain with the rigid cyclohexane, as is also observed for the complexes formed with H_4bpeda and H_4cddadp with Gd(III) (Table 2). Additionally, the different ligand solvations, which are known to have an important influence on the formation thermodynamics[27], may contribute to the slightly different results in the cases of H_2bped and H_2bpcd.

DFT Calculations.

As single crystals suitable for X-ray diffraction experiments could not be obtained, in order to gain more insight into the possible structures of the complexes, DFT calculations were carried out. In principle, upon complexation, the H_2bpcd ligand could generate several isomeric complexes. Three possible coordination geometries (Figure 15), differing in the configuration of the two quaternary amine nitrogen atoms, have been already observed for its Ga(III) complex[28] and have been previously proposed for the Al(III), Ga(III), and In(III) complexes of the similar ligand H_2bped[23].

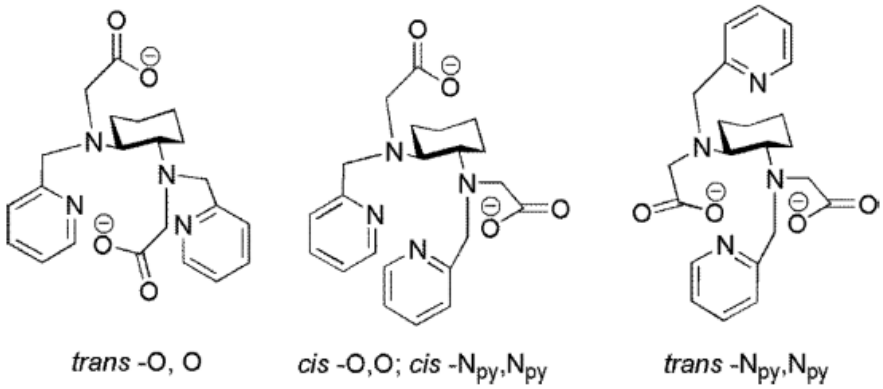

Figure 15 Possible Coordination Geometries of bpcd2−

For this reason, the DFT calculations were performed on the complexes with the three ligand coordination geometries displayed in Figure 15. In Figure 16, the

optimized structures of the isomers of the (S,S)-$[Y(bpcd)(H_2O)_5]^+$ species are shown (selected bond distances are reported in Table 3). A first result is that the complex has a final eight-coordinated geometry, suggesting that in solution only two water molecules are coordinated in the A and C isomers, while a third water replaces the pyridine nitrogen in the B isomer. The remaining water molecules are retained in the second coordination sphere, forming hydrogen bonds with the coordinated waters, the ligand carbonyl oxygens (A, C), and the pyridine nitrogen (B).

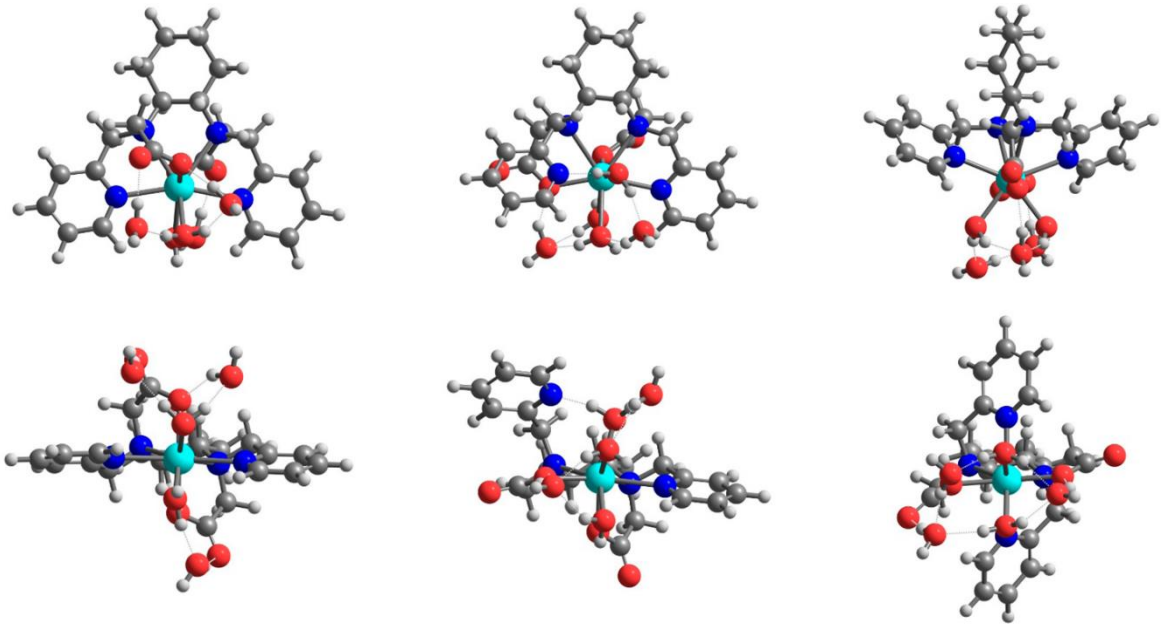

Figure 16 Optimized geometries of S,S-$[Y(bpcd)(H_2O)_5]^+$, with upper images giving axial views and lower images giving equatorial views: (A) ligand in trans-O,O geometry; (B) ligand in cis-O,O, cis-Npy,Npy geometry; (C) ligand in trans-Npy,Npy geometry.

The same calculation carried out for the (S,S)-$[La(bpcd)(H_2O)_5]^+$ analogues of the isomers A−C (Figure 17 and Table 4) produced a final geometry with two coordinated water molecules (and one interacting at a larger distance, Table 3) for the A isomer, while three coordinated waters are present in the B and C complexes.

Table 7 Selected bond distances (Å) of the minimum-energy structures of the isomers of S,S-[Y(bpcd)(H₂O)₅]⁺

	A	B	C
Y-$O_{acetate}$	2.258, 2.243	2.241, 2.199	2.258, 2.243
Y-$N_{pyridine}$	2.518, 2.566	2.549, *3.757*	2.518, 2.566
Y-N_{amine}	2.621, 2.644	2.672, 2.603	2.644, 2.621
Y-O_{water}	2.445, 2.413	2.647, 2.385, 2.504	2.413, 2.445

These results are consistent with solid- state structural data for complexes with similar ligands: a compound of Eu(III)[29] with H_4cdta (trans-1,2-cyclohexanedi-amine-N,N,N′,N′-tetraacetic acid) presents an eight-coordinated metal with two inner-sphere water molecules, while the La(III) complex with bpba (N,N′-bis(2-pyridylmethyl)-N,N′- 1,2-ethanediylbis(D-alaninate)) is nine-coordinated with three bound molecules[30].

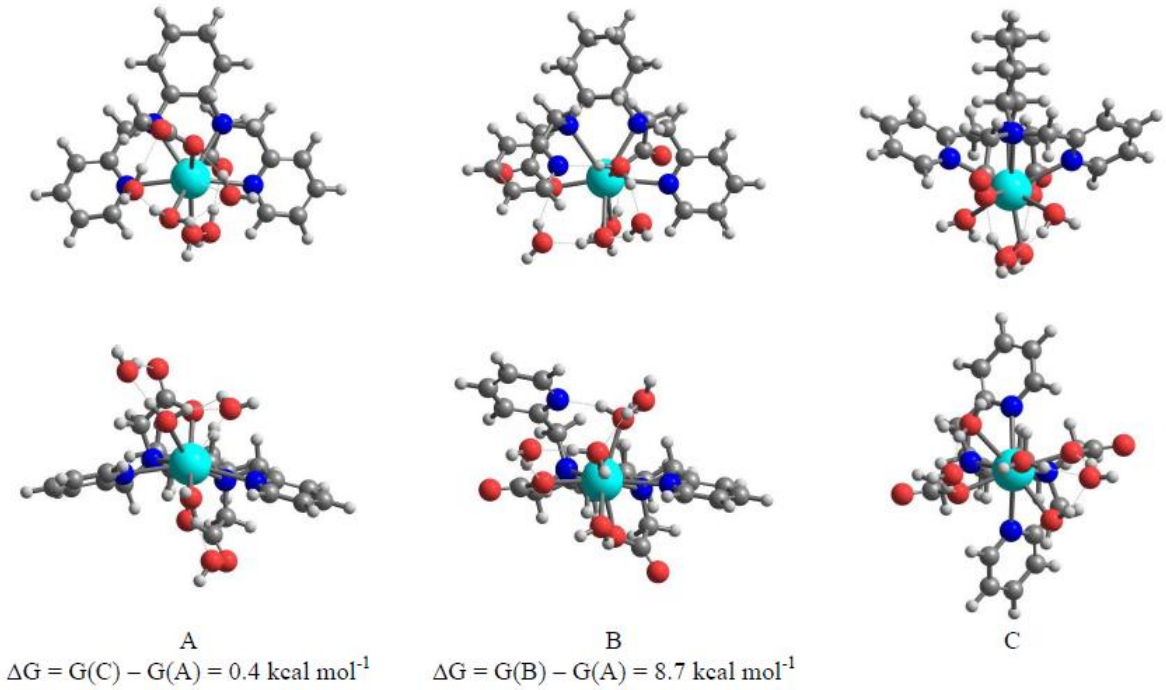

Figure 17 Optimized geometries of S,S-[La(bpcd)(H₂O)₅]⁺. Upper images: axial view. Lower images: equatorial view.

However, it should be taken into account that the Eu(III) ion is slightly larger than Y(III) and, according to EXAFS data and molecular dynamics simulations,[31] the coordination number of the aqua ion is 9 ($[Eu(H_2O)_9]^{3+}$). Possibly, the Eu(III) complexes in solution are involved in a hydration/dehydration equilibrium: $[Eu(bpcd)(H_2O)_3]^+ = [Eu(bpcd)(H_2O)_2]^+ + H_2O$. This equilibrium has been

previously suggested for the complexes with H_2bpe[32], and could explain the number of water molecules (~2.6) found in this work by luminescence lifetime measurements (see below).

Table 8 Selected bond distances (Å) of the minimum-energy structures of the isomers of S,S-[La(bpcd)(H₂O)₅]⁺

	A	B	C
La-$O_{acetate}$	2.431, 2.333	2.353, 2.323	2.409, 2.398
La-$N_{pyridine}$	2.742, 2.717	2.731, *3.652*	2.775, 2.738
La-N_{amine}	2.785, 2.816	2.815, 2.774	2.774, 2.761
La-O_{water}	2.596, 2.669, 2.896	2.747, 2.741, 2.555	2.624, 2.693, 2.744

From a thermodynamic point of view, the isomers with axial acetates (A) and pyridines (C) are equally stable ($\Delta G = G(C) - G(A) = -0.2$ kcal mol^{-1}), while isomer B is less stable by 10.7 kcal mol−1 with respect to A, indicating that a mixture of isomers should be present in solution. The same trend is obtained for the (S,S)-[La(bpcd)$(H_2O)_5]^+$ complexes with $\Delta G = G(C) - G(A) = 0.4$ kcal mol^{-1} and $\Delta G = G(B) - G(A) = 8.7$ kcal mol^{-1} (Figure 17). This result is partially in agreement with that reported for $[Ga(bpcd)]^+$, for which both the cis-O,O, cis-Npy,Npy and trans-Npy,Npy isomers are less stable than the trans-O,O isomer (ΔG calculated at the MP2 level in solution)[28]. This difference could be due to the different ionic radii and coordination numbers of the ions. In light of these calculations, we propose the presence of an equilibrium involving mainly A and C isomers, in water solution. These two species, characterized by the same point symmetry (C_1), may show very similar Eu(III) luminescence emission spectra, as they produce the same number of crystal- field levels for each $^5D_0 \rightarrow {}^7F_j$ band and the same transition energy of the $^5D_0 \rightarrow {}^7F_0$ band[33]. In fact, in this context the 0−0 transition energy is dependent on the total charge on the ligand coordinated to Eu(III), which is the same for the two isomers. In conclusion, the emission spectrum in Figure 19a can be considered compatible with the coexistence in solution of isomers A and C. We sought confirmation of these structures with paramagnetic NMR. Unfortunately the ^{1}H NMR spectra of both Eu and Tb complexes are characterized by broad resonances, which prevents any assignment. The line widths are well beyond the values one

would expect for similar complexes[34], which proves the existence of solution equilibria, possibly as those described above.

Spectroscopic Characterization.

The UV/vis absorption spectrum of the Eu(III) complex (1) in water is shown in Figure 18, together with that of the ligand (H_2bpcd). The band around 260 nm (typical of the $\pi \rightarrow \pi^*$ transition of the pyridine rings) shows a molar absorption coefficient (ε) in the range 4000−5000 M^{-1} cm^{-1} for both ligand and complex and, as expected, it is red-shifted upon Eu(III) complexation. Moreover, its vibrational progression becomes more evident. The absorption spectra of the ligand and its sodium salt (obtained by deprotonation of the carboxylic units) are identical (data not shown). As the spectrum of the Tb(III) complex is completely superimposable with that of Eu(III), it is not reported.

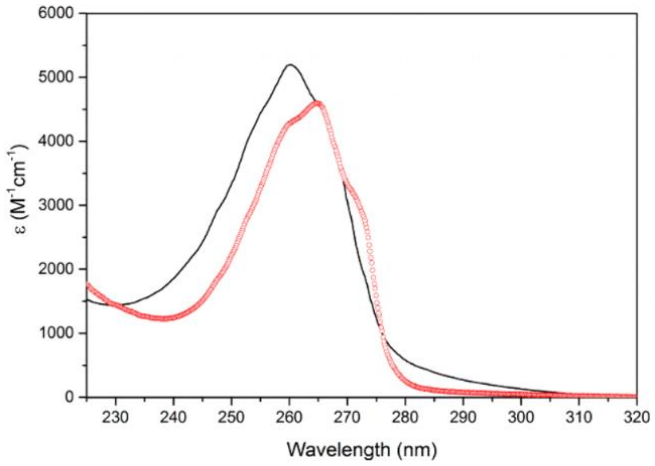

Figure 18 UV absorption spectra of the complex 1 (Eu(bpcd)Cl; red circles) and of H_2bpcd (black line) in water. [Eu(bpcd)Cl] = [H_2bpcd] = 0.1 mM.

As can be seen from inspection of the excitation and emission luminescence spectra, upon excitation of the ligand (λ_{exc} = 265 nm), the typical luminescence of both Eu(III) and Tb(III) ions, stemming from the *f*–*f* transitions, was detected (Figure 19). H_2bpcd can be considered a good sensitizer of Eu(III) and Tb(III) luminescence. Eu(III) ion is considered a valuable spectral probe, since from its luminescence emission spectrum it is usually possible to identify the number of species and the point symmetry of its environment. In detail, in the case of the $^5D_0$

→ $^7F_0$ (0−0) emission transition of Eu(III), both the ground and excited states are degenerate, which results, in principle, in a 1:1 correspondence between the number of peaks in the emission spectrum and the number of distinct Eu(III) ion environments[35,36,33]. In addition, the ligand crystal field is capable of splitting each emission band of the other terms into several components, whose number is directly connected with the point symmetry of the Eu(III) ion[21]. The spectrum of Eu(bpcd)Cl (Figure 19a), in water solution, shows the typical profile of the emission from the $^5D_0$ level of the Eu(III) ion in a strongly distorted environment, with a dominant $^5D_0 \rightarrow {}^7F_2$ hypersensitive band. In addition, the presence of one and three components in the region of $^5D_0 \rightarrow {}^7F_0$ and $^5D_0 \rightarrow {}^7F_1$ bands, respectively, calls for the existence of only one Eu(III) environment with C_1, C_s, C_2 and C_{2v} possible symmetries. As the ligand around the metal ion is chiral, C_s or C_{2v} can be ruled out and the possible point symmetry for Eu(III) in the complex will be C_1 or C_2. It is useful to remind that this luminescence emission spectrum could be also compatible with the coexistence of two isomers (as discussed above).

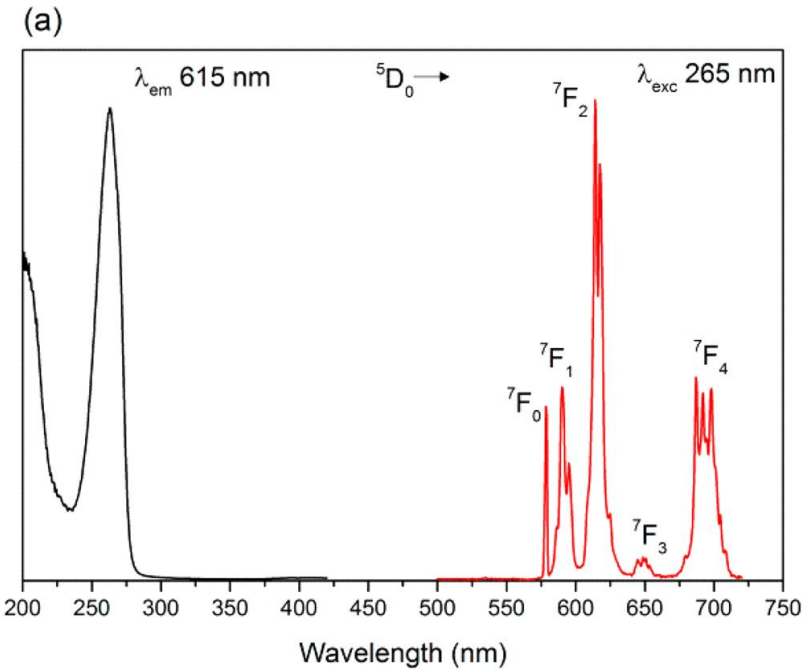

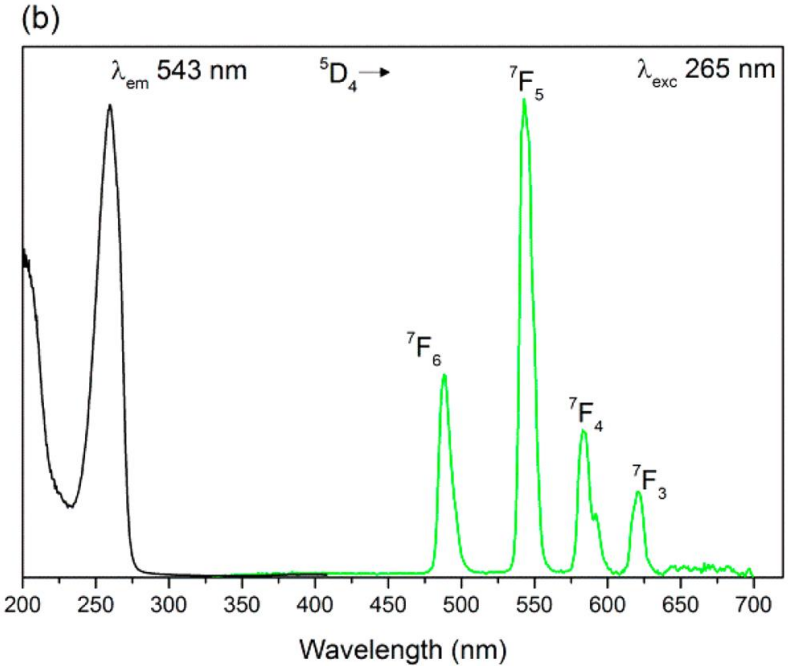

Figure 19 Steady-state luminescence excitation (left) and emission (right) spectra of (a) Eu(III) complex (1 mM Eu(bpcd)Cl in water) and (b) Tb(III) complex (1 mM Tb(bpcd)Cl in water). The same emission spectra are obtained upon direct excitation of the metal ion

The $^5D_0$ and $^5D_4$ excited state lifetimes for Eu(III) and Tb(III), respectively, have been calculated from the luminescence decay curves in H_2O and D_2O (Table 5). All of the curves were well fitted to a single exponential function, and by using Horrock's equation[37,38], it is possible to calculate the number of water molecules in the close proximity of the metal ion (hydration number). In both cases, a hydration number of 2.6−2.7 is found and, for this reason, similar coordination environments are expected for Eu(III) and Tb(III) complexes.

Table 9 Observed Excited State Lifetimes for Eu(III) and Tb(III) Complexes

	τ_{obs} (observed lifetime), ms	
complex	H_2O	D_2O
Eu(bpcd)Cl	0.30(1)	1.70(1)
Tb(bpcd)Cl	0.94(1)	2.15(1)

Chiroptical Characterization. CPL

CPL spectra of the two enantiomers of Eu(bpcd)Cl in CD_3OD show several incompletely resolved broad bands corresponding to $^5D_0 \rightarrow {}^7F_2$ and $^5D_0 \rightarrow {}^7F_1$

transitions (Figure 20). The signals are rather intense in terms of g_{lum} values, which are around |0.2| for the band with a maximum around 598 nm and |0.2| for the band around 607 nm (Figure 21).

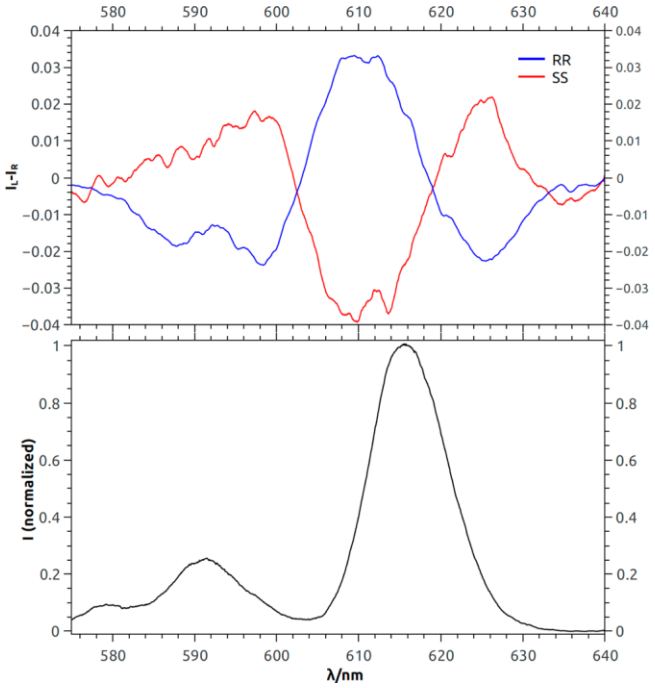

Figure 20 Normalized CPL spectra (top) and total emission (bottom) of the two enantiomers of Eu(bpcd)Cl in CD_3OD. The CPL is normalized on the maximum of the $^5D_0 \rightarrow {}^7F_2$ emission band.

The two enantiomers of Tb(bpcd)Cl in CD_3OD display rich mirror image CPL spectra (Figure 22).

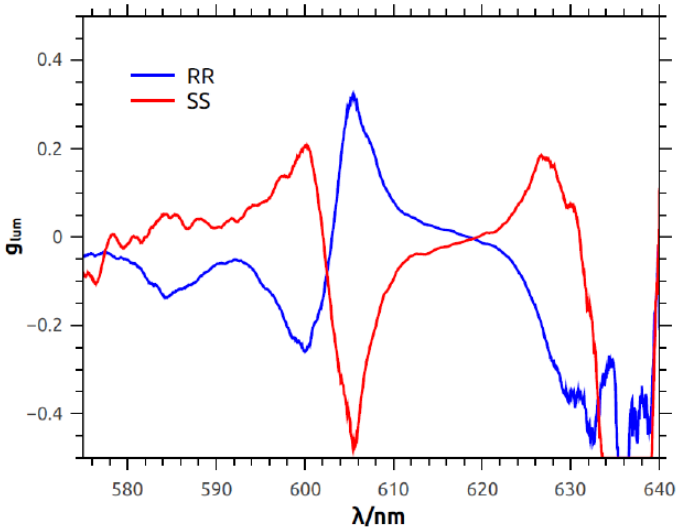

Figure 21 glum values as a function of the wavelength for the two enantiomers of Eu(bpcd)Cl in CD_3OD

The most intense band around 545 nm, associated with the $^5D_4 \rightarrow {}^7F_5$ transition, features a trisignate CPL pattern with a glum value of |0.11|, calculated on the maximum (546 nm).

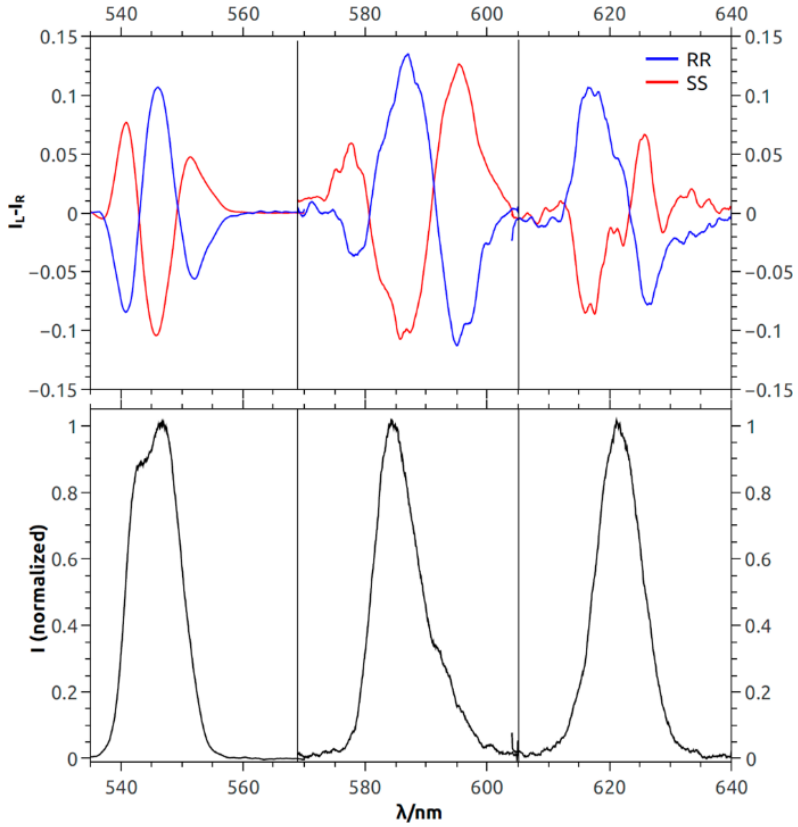

Figure 22 Normalized CPL spectra (top) and total emission spectra (bottom) of the two enantiomers of Tb(bpcd)Cl in CD_3OD. The curves in each panel are normalized on the maximum of the corresponding total emission band

The $^5D_4 \rightarrow {}^7F_4$ and $^5D_4 \rightarrow {}^7F_3$ transitions are associated with multiplets with glum values on the order of $|10^{-1}|$ (calculated on the top of each CPL band; see also Figure 23). These values are higher than those reported for chiral Tb complexes on the basis of e.g. octadentate hydroxyisophthalamide (glum = |0.048| for the $^5D_4 \rightarrow {}^7F_5$ transition)[39], aza-macrocycle compounds (|0.06|)[40], and diketonates (|0.044|−|0.082|)[16] and comparable with those measured for other cyclen-based (|0.22|)[41] or other DACH- based systems (|0.20|)[18].

In this context, we should note that the highest glum value of about 1.4 (with a maximum possible value of 2) was reported for a Eu complex[42] while Tb complexes usually display lower dissymmetry factors[12,10,15,43,44].

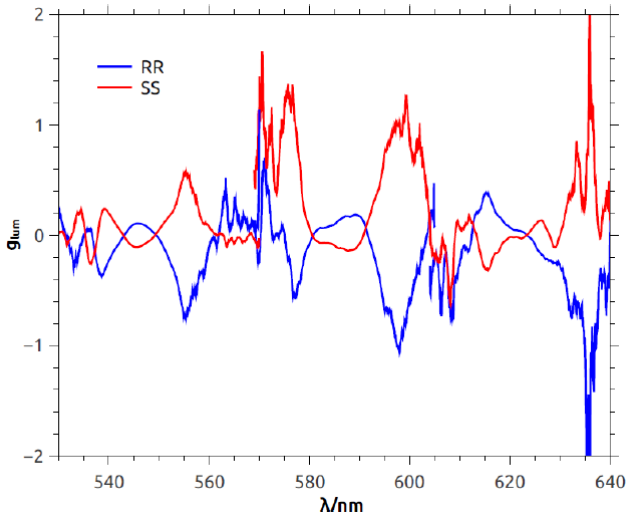

Figure 23 glum values as a function of the wavelength for the two enantiomers of Tb(bpcd)Cl in CD_3OD.

Prompted by these promising results, we recorded CPL spectra in H_2O for the main band of the two enantiomers of Tb(bpcd)Cl (Figure 24). The spectra retrace those measured in CD_3OD with a slightly lower glum value (0.07 at 546 nm; see Figure 25 and Table 6).

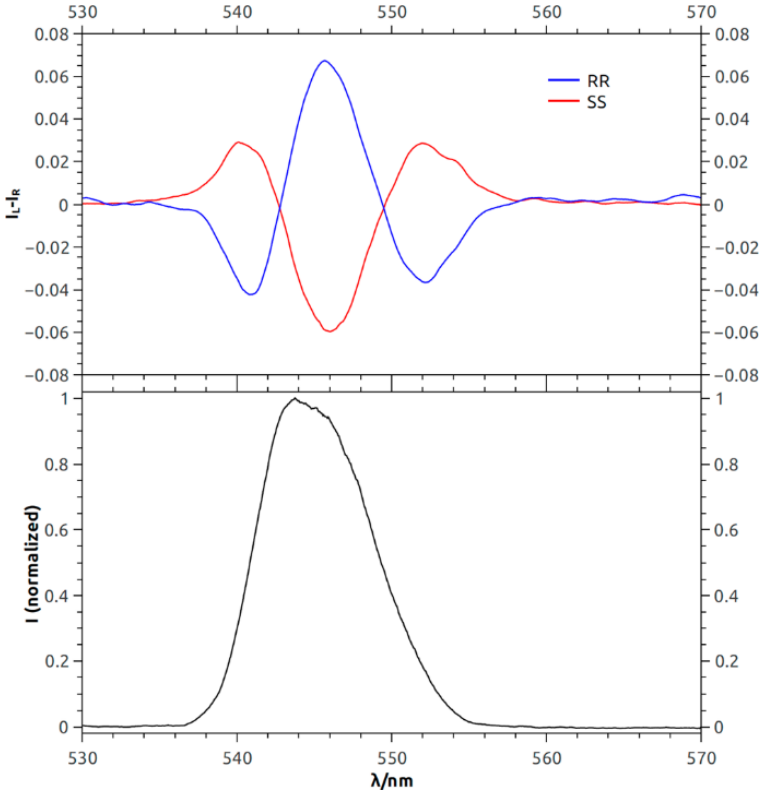

Figure 24 Normalized CPL (top) and total emission spectra (bottom) of the two enantiomers of Tb(bpcd)Cl in water. The curves are normalized on the maximum of the corresponding total emission band.

The electronic CD spectra in the UV are extremely weak (signal amplitudes below 2 mdeg), and for this reason they have not been investigated further. In order to gain insight into the mechanism at the basis of the uncommon CPL activity found for Tb(bpcd)Cl, we synthesized the analogous Yb complex (Yb(bpcd)Cl).

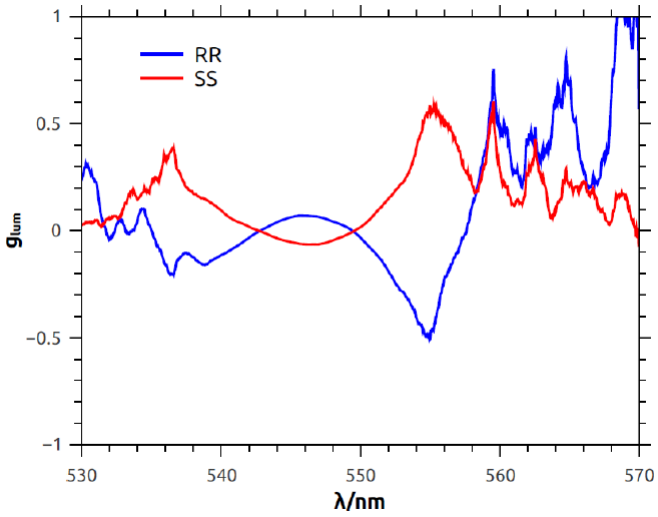

Figure 25 glum values as a function of the wavelength for the two enantiomers of Tb(bpcd)Cl in H_2O.

The only Yb *f*–*f* transition ($^2F_{7/2} \rightarrow {}^2F_{5/2}$) falls in the near-infrared (NIR) region, and thus its NIR-ECD spectrum can be recorded without significant interferences due to contributions from the chiral ligands.

Table 10 glum values calculated on the maxima (or minima) of the CPL curves for the two enantiomers of Tb(bpcd)Cl in CD_3OD

Wavelength/nm	(*R*,*R*)-Tb(bpcd)Cl	(*S*,*S*)-Tb(bpcd)Cl
546	+0.11 (+0.07)[a]	-0.11 (-0.06)[a]
586	+0.16	-0.15
594	-0.70	+0.70
616	+0.31	-0.31
625	-0.11	+0.09

[a] values measured in H_2O.

If the CPL activity in the analogous Tb and Eu complexes stems only from the dissymmetric coordination sphere around the metal center provided by the ligand, the overall integral over the ECD bands allied with the $^2F_{7/2} \rightarrow {}^2F_{5/2}$ manifold of the Yb complex is expected to vanish (static coupling limit)[12]. On the other hand, if the emission optical activity is due to coupling between metal-centered transitions and the polarizable groups provided by the ligands (even beyond the first coordination

sphere), the integral over the same manifold is expected to be nonvanishing, since such an *f*–*f* transition can no longer be considered isolated (dynamic coupling limit). The NIR-ECD spectrum of (S,S)-Yb(bpcd)Cl in CD_3OD (Figure 26) shows a multiplet featuring intense bands (gabs) associated with the $^2F_{7/2} \rightarrow {}^2F_{5/2}$ manifold (900−1000 nm).

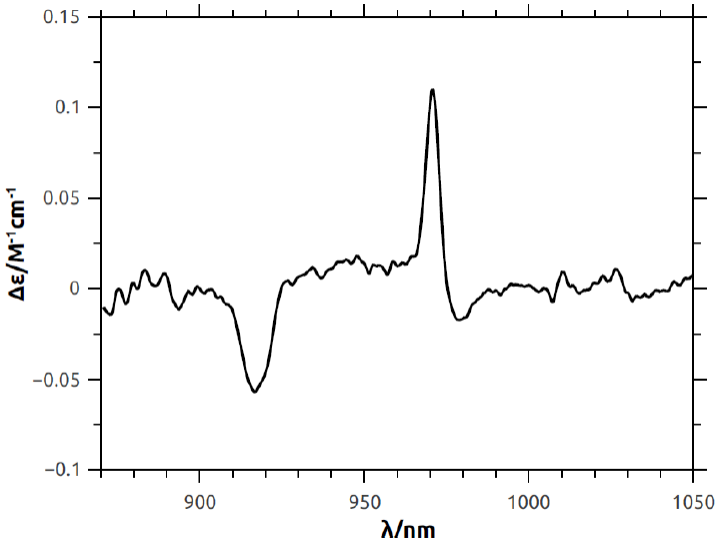

Figure 26 NIR-ECD spectra for (S,S)-Yb(bpcd)Cl in CD_3OD

The integral over such a transition indicates that around 85% of the positive area of the spectrum is canceled out by the opposite sign area, which means a positive:negative ratio of about 1.3:1. This value suggests that the CPL activity in Tb(bpcd)Cl and Eu(bpcd)Cl mostly falls in the static coupling limit. This is somewhat expected, since the pyridine moieties in the ligand are weakly chromophoric, with transitions falling in the far-UV region.

Conclusion

Our ligand H_2bpcd has been designed to tightly bind Ln(III) ions, providing a dissymmetric environment able to solicit strong chiroptical features while at the same time leaving a few coordination sites available for engaging further ancillary ligands. The complexes display a relatively good stability, in line with similar ligands studied previously (H_2bped). DFT calculations carried out on three possible isomers of (S,S)-$[Y(bpcd)(H_2O)_5]^+$ (ionic radius equivalent to those of $[Eu(bpcd)(H_2O)_5]^+$ and $[Tb(bpcd)(H_2O)_5]^+$) indicate that the two trans-O,O and trans-Npy,Npy geometries are equally stable in solution and present two coordinated water molecules. In contrast, the cis-O,O, cis-Npy,Npy isomer is less stable by ∼10 kcal mol−1 with respect to the other two forms and has a third coordinated water, which replaces one pyridine. Parallel calculations on (S,S)-$[La(bpcd)(H_2O)_5]^+$ provide final structures with three coordinated water molecules and confirm that the cis-O,O, cis-Npy,Npy isomer is the least stable. These theoretical results suggest that the Eu(III) complex in solution could be distributed among species in equilibrium with either two or three coordinated water molecules. Eu(III) and Tb(III) complexes display strong CPL activity. In particular, Tb(bpcd)Cl in both aqueous and methanol solution reaches values of the anisotropy factor g_{lum} which are smaller only than those reported for a macrocyclic Tb(III) complex. Despite the presence of different isomers, as the Eu(III) geometric environments of the two dominant trans- O,O and trans-Npy,Npy species are very similar, their $^5D_0 \rightarrow {}^7F_0$ transition energies should be similar, thus producing apparently only one 0−0 component. The hydration number of around 2.6 reveals that there are two to three sites available, which is also in agreement with the ligand denticity.

Bibliography

(1) Samoilov, B. N. *J Exp Theor Phys* **1948**, *18*, 1030–1040.

(2) Emeis, C. A.; Oosterhoff, L. J. *J. Chem. Phys.* **1971**, *54* (11), 4809–4819.

(3) Luk, C. K.; Richardson, F. S. *J. Am. Chem. Soc.* **1974**, *96* (7), 2006–2009.

(4) Peeters, E.; Christiaans, M. P. T.; Janssen, R. A. J.; Schoo, H. F. M.; Dekkers, H. P. J. M.; Meijer, E. W. *J. Am. Chem. Soc.* **1997**, *119* (41), 9909–9910.

(5) Wynberg, H.; Numan, H.; Dekkers, H. P. J. M. *J. Am. Chem. Soc.* **1977**, *99* (11), 3870–3871.

(6) Schadt, M. *Annu. Rev. Mater. Sci.* **1997**, *27* (1), 305–379.

(7) Wagenknecht, C.; Li, C.-M.; Reingruber, A.; Bao, X.-H.; Goebel, A.; Chen, Y.-A.; Zhang, Q.; Chen, K.; Pan, J.-W. *Nat. Photonics* **2010**, *4* (8), 549–552.

(8) Feringa, B. L. *Acc. Chem. Res.* **2001**, *34* (6), 504–513.

(9) Castiglioni, E.; Abbate, S.; Lebon, F.; Longhi, G. *Methods Appl. Fluoresc.* **2014**, *2* (2), 24006.

(10) Carr, R.; Evans, N. H.; Parker, D. *Chem. Soc. Rev.* **2012**, *41* (23), 7673.

(11) Emeis, C. a.; Oosterhoff, L. J. *Chem. Phys. Lett.* **1967**, *1* (4), 129–132.

(12) Zinna, F.; Di Bari, L. *Chirality* **2015**, *27* (1), 1–13.

(13) Sánchez-Carnerero, E. M.; Agarrabeitia, A. R.; Moreno, F.; Maroto, B. L.; Muller, G.; Ortiz, M. J.; de la Moya, S. *Chem. - A Eur. J.* **2015**, *21* (39), 13488–13500.

(14) Lunkley, J. L.; Shirotani, D.; Yamanari, K.; Kaizaki, S.; Muller, G. *Inorg. Chem.* **2011**, *50* (24), 12724–12732.

(15) Richardson, F. S. *Inorg. Chem.* **1980**, *19* (9), 2806–2812.

(16) Yuasa, J.; Ohno, T.; Miyata, K.; Tsumatori, H.; Hasegawa, Y.; Kawai, T. *J. Am. Chem. Soc.* **2011**, *133* (25), 9892–9902.

(17) Zinna, F.; Resta, C.; Abbate, S.; Castiglioni, E.; Longhi, G.; Mineo, P.; Di Bari, L. *Chem. Commun.* **2015**, *51* (59), 11903–11906.

(18) Samuel, A. P. S.; Lunkley, J. L.; Muller, G.; Raymond, K. N. *Eur. J. Inorg. Chem.* **2010**, *2010* (21), 3343–3347.

(19) Zinna, F.; Pasini, M.; Galeotti, F.; Botta, C.; Di Bari, L.; Giovanella, U. *Adv. Funct. Mater.* **2017**, *27* (1), 1603719.

(20) Andreiadis, E. S.; Gauthier, N.; Imbert, D.; Demadrille, R.; Pécaut, J.; Mazzanti, M. *Inorg. Chem.* **2013**, *52* (24), 14382–14390.

(21) Binnemans, K. *Coord. Chem. Rev.* **2015**, *295*, 1–45.

(22) Werts, M. H. V.; Jukes, R. T. F.; Verhoeven, J. W. *Phys. Chem. Chem. Phys.* **2002**, *4* (9), 1542–1548.

(23) Caravan, P.; Rettig, S. J.; Orvig, C. *Inorg. Chem.* **1997**, *36* (7), 1306–1315.

(24) Tircsó, G.; Regueiro-Figueroa, M.; Nagy, V.; Garda, Z.; Garai, T.; Kálmán, F. K.; Esteban-Gómez, D.; Tóth, É.; Platas-Iglesias, C. *Chem. - A Eur. J.* **2016**, *22* (3), 896–901.

(25) Lacoste, R. G.; Christoffers, G. V.; Martell, A. E. *J. Am. Chem. Soc.* **1965**, *87* (11), 2385–2388.

(26) Kálmán, F. K.; Végh, A.; Regueiro-Figueroa, M.; Tóth, É.; Platas-Iglesias, C.; Tircsó, G. *Inorg. Chem.* **2015**, *54* (5), 2345–2356.

(27) Di Bernardo, P.; Melchior, A.; Tolazzi, M.; Zanonato, P. L. *Coord. Chem. Rev.* **2012**, *256* (1–2), 328–351.

(28) Florián, J.; McLauchlan, C. C.; Kissel, D. S.; Eichman, C. C.; Herlinger, A. W. *Inorg. Chem.* **2015**, *54* (21), 10361–10370.

(29) Wang, J.; Hu, P.; Liu, B.; Xu, R.; Wang, X.; Wang, D.; Zhang, L. Q.; Zhang, X. D. *J. Struct. Chem.* **2011**, *52* (3), 568–574.

(30) Omata, K.; Hoshi, N.; Kabuto, K.; Kabuto, C.; Sasaki, Y. *Inorg. Chem.* **2006**, *45* (14), 5263–5265.

(31) D'Angelo, P.; Zitolo, A.; Migliorati, V.; Chillemi, G.; Duvail, M.; Vitorge, P.; Abadie, S.; Spezia, R. *Inorg. Chem.* **2011**, *50* (10), 4572–4579.

(32) Caravan, P.; Mehrkhodavandi, P.; Orvig, C. *Inorg. Chem.* **1997**, *36* (7), 1316–1321.

(33) Albin, M.; Whittle, R. R.; Horrocks, W. D. *Inorg. Chem.* **1985**, *24* (26), 4591–4594.

(34) Di Bari, L.; Salvadori, P. *Coord. Chem. Rev.* **2005**, *249* (24), 2854–2879.

(35) Albin, M.; Horrocks, W. D. *Inorg. Chem.* **1985**, *24* (6), 895–900.

(36) Choppin, G. R.; Peterman, D. R. *Coord. Chem. Rev.* **1998**, *174* (1), 283–299.

(37) Horrocks, W. D.; Sudnick, D. R. *J. Am. Chem. Soc.* **1979**, *101* (2), 334–340.

(38) Supkowski, R. M.; Horrocks, W. D. W. *Inorganica Chim. Acta* **2002**, *340*, 44–48.

(39) Petoud, S.; Muller, G.; Moore, E. G.; Xu, J.; Sokolnicki, J.; Riehl, J. P.; Le, U. N.; Cohen, S. M.; Raymond, K. N. *J. Am. Chem. Soc.* **2007**, *129* (1), 77–83.

(40) Gregoliński, J.; Starynowicz, P.; Hua, K. T.; Lunkley, J. L.; Muller, G.; Lisowski, J. *J. Am. Chem. Soc.* **2008**, *130* (52), 17761–17773.

(41) Dickins, R. S.; Howard, J. A. K.; Maupin, C. L.; Moloney, J. M.; Parker, D.; Riehl, J. P.; Siligardi, G.; Williams, J. A. G. *Chem. - A Eur. J.* **1999**, *5* (3), 1095–1105.

(42) Lunkley, J. L.; Shirotani, D.; Yamanari, K.; Kaizaki, S.; Muller, G. *J. Am. Chem.*

Soc. **2008**, *130* (42), 13814–13815.

(43) Montgomery, C. P.; Murray, B. S.; New, E. J.; Pal, R.; Parker, D. *Acc. Chem. Res.* **2009**, *42* (7), 925–937.

(44) Muller, G. *Dalt. Trans.* **2009**, No. 44, 9692.

Section 2: Sensing

Introduction

The possibility of investigating the structural and functional properties of living system in unperturbed conditions is key challenge in biology and medicine. In fact, the precise information about the biological events involved inside cells are powerful tools for the diagnostic and treatment of cancer or other diseases[1]. This growing interest gave rise noninvasive methodologies that are based on the use of no destroying signals, like the light. Nowadays the use of emissive probes has enormously grown due to they high sensitivity and spatial resolution in comparison with others kind of probes. Many different luminescent sensor have successfully been employed like organic fluorophores, semiconductor nanoparticle (CdSe) and metal complexes[2]. The organic fluorophores are mainly constituted by rhodamine, fluoroscein, cyanine dyes, or dipyrroylmethane (BODIPY) core structures and they are able to detect pH variation and small concentration of Ca^{2+} and Zn^{2+} [3]. However, these kind of probes are subject to photo-bleaching which reduces their application. A greater photo-stability is guarantee by semiconductor nanoparticle which have received more attention in last 10 years[4]. Nevertheless, their introduction in biology and medicine is prevented by their possible toxicity and their short circulation half-time preventing long-term imaging or cell-tracking studies[5]. In this context, the metal complexes represent a valid alterative to probe cited previously. They can be divided in two main groups, one is formed by d^6 and d^8 transition metal complexes which can easily give long-lived (10^{-7} to 10^{-4} s) LMCT and MLCT excited state allowing the use of time-gated methods reducing back-ground noise[6]. While the another important metal complexes group contains all the lanthanides whose unique magnetic[7] and luminescence[8] properties are admired for the investigation of biological events.

Lanthanide probes

The first meeting between lanthanide complexes and biology dates back to 1969 when a E. coli were stained with an alcoholic solution of $Eu(tta)_3$ (tta= thenoyltrifluoroacetonate). Surprisingly, the cells were able to bind the Europium

complexes which could be located by its intense emission by irradiating with mercury lamp[9]. From this first experiment followed many others[10] that contributed to construction of knowledge background necessary to use the extraordinary properties of lanthanide complexes in sensor field.

The trivalent lanthanides have the ability to give emission by many different transitions like MLCT, *4f-5d* and *f-f*[11] but only the latter presents unique spectroscopies properties which are extremely useful for the design of luminescent probes. In fact, the large Stokes shifts avoids the self-absorption phenomena and reduce the background signals. The long lifetime of excited state can be used in time-resolved fluorescence measurements, in this way the background fluorescence is completely suppressed[12]. Also the characteristic narrow emission can increase the sensitivity of whole probe against various analytes. However, the use of these transitions for the designing of probes doesn't present few issues but by following simple golden rules it's possible to build up an efficient sensor.

The *f-f* transitions is forbidden for symmetry, condition that increase the lifetime of excited state (fundamental for time-resolved fluorescence measurements) but it reduces enormously the molar absorptivity. This prohibition makes difficult the access to excited state then to the luminescence of lanthanides, but it can be easily bypasses by the use of light-harvesting chromophore that sensitized the Ln(III) ion luminescence. This process is called "antenna effect" and, in general, it's operated by an organic chromophore placed near to lanthanide. When the organic chromophores absorb light ($S_0 \rightarrow S_1$) the shorted-lived Singlet excited state can undergo intersystem crossing to the longer-lived Triplet excited state ($S_1 \rightarrow T_1$) whose longer lifetime permit to sensitize the lanthanide ion. The energy transfer can occur with Dexter's or Förster's mechanism, that, although in different way, are depending by the distance between lanthanide and chromophore. At the end, the more accessible excited state of lanthanide ion can relax to fundamental state by emission of photons. All these processes participate with their contribution to total emission (or Brightness) of Lanthanides complexes that can be expressed as:

$$B = \varepsilon_{Ant}\eta_{ISC}\eta_{ET}\phi_{Ln}$$

where ε_{Ant} is the molar excitation coefficient of the $S_0 \rightarrow S_1$ transition of the chromophore (antenna), η_{ISC} is the efficiency of Intersystem Crossing ($S_1 \rightarrow T_1$), η_{ET} is the efficiency of Energy Transfer between the Triplet state of Antenna and exited state of lanthanide and φ_{Ln} represents the intrinsic quantum yield of lanthanide ion which also is strongly influence by the presence of quenching groups (CH, NH, OH, etc.) closed to metal[13].

The modification of one or more of these four parameters correlated to Brightness permit to observe a luminescence variation of the lanthanide complexes, moreover, it represents the simplest operative mode for the design of efficient lanthanide-based probes. By the use of this concept, numerous luminescent lanthanide complexes have been synthetized and their sensing properties determined. They can be divided into four different types on the basis of position of chelating and antenna part of ligand (Figure 1)[14].

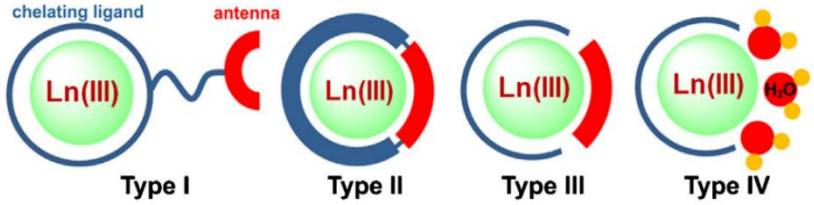

Figure 36 Different types of lanthanide probes

In the type I and II, the chelating and antenna part are linked each other's to form the whole ligand. In particular, in the type I, the lanthanide ion is completely surrounded by the chelating part of ligand and the antenna part is completely free to interact with analyte. The interaction influences the energy transfer between the antenna and the lanthanide as well as the whole luminescence of complex. In type I category, we can find complexes with polyaminopolycarboxylate and polyaza-macrocycle ligands which can be easily functionalized for the introduction of antenna part[15]. Completely different is the Type II family, in fact, in these complexes the antenna became part of the inner coordination sphere of lanthanide ion. It's also different the working methods, the analyte causes structural changing by interacting with available functional groups. The final result is a variation of absorption and luminescence spectrum[16]. The removal of the linking between the chelating and antenna parts in the Type II furnish a new typologies of probes (Type

III). In this way the antenna part can be easily removed from coordination of lanthanide by interaction with analyte turning off the luminescence of complex[17]. But away, in literature are also present opposite case, where precursor of antenna reacts with analyte to form a coordinating species which is able to give energy transfer to the lanthanide[18]. At the end, the last class of probe (Type IV) include all the complexes having a chelating part which doesn't saturate the coordination number of lanthanide ion but it leaves an open side generally occupied by the solvent molecules which reduce the intrinsic quantum yield of lanthanide. The analytes can easily displace the solvent molecules from the coordination sphere, giving rise to an increase of the luminescence intensity (turn on probes)[19].

Theoretically all the lanthanide ions showing *f-f* emission can be used in the design of probes but, for different reasons, only few are used in practice. In general, the choice is done among Sm(III), Eu(III), Tb(III), Dy(III), Nd(III) and Yb(III) due to their emissions in the Visible-NIR range, where the detection of the signal can be obtained with high sensitivity. However, Eu(III) and Tb(III) are preferred respect to others thanks to longer luminescent lifetime (millisecond range) and their less sensitive quenching by singlet oxygen and by multiphonon relaxation process. Moreover, the non-degeneracy of the $^5D_0$ emissive state of the Eu^{3+} permits to have a simple emission spectra which can be easy related to the local symmetry around the metal ion and used for the developing of responsive probe[20], like ratiometric analysis.

The narrow emission of lanthanides offers advantages into accurate determination of analytes by means of ratiometric analysis. The method is broadly used in many fluorescent analysis[21] and it consists in the use a standard, that acts like a calibrator, to increase the sensibility of probe and remove the interfering factors even at low level of absolute intensities[22]. Many different standard can be used for lanthanide complexes, but a common strategy consider the application of analogous lanthanide complexes having same chelating structure that the probe. In these way, a "cocktail" of lanthanide complexes, for example Europium(III) and Terbium(III), can be used for the determination of analyte concentration by mean of ratio of their emission intensity[23]. Another common strategy uses the particular properties of *f-f* transitions. The transitions are forbidden for symmetry but the prohibition is

partially removed by forcing of magnetic dipole (MD), transitions, electronic dipole (ED) transitions or a mixture of both (MD/ED). The *f-f* transitions induced ED transitions are defined "hypersensitive" and they undergo pronounced variation by changing of coordination environment around the lanthanides. While, the *f-f* induced MD transitions remain almost unvaried by environment changing and they can be used like standard for the ratiometric analysis. For this reason, the intensity ratio between an "hypersensitive" band and an MD-allowed band could be used for quantification of analytes that are detected by ligand exchange mechanisms[24]. The method is common accepted and it's widely used for Eu(III) complexes which have two hypersensitive bands ($\Delta J=2$ and $\Delta J=4$)[25].

Bibliography

(1) Bünzli, J. C. G. *Chem. Rev.* **2010**, *110* (5), 2729–2755.

(2) Montgomery, C. P.; Murray, B. S.; New, E. J.; Pal, R.; Parker, D. *Acc. Chem. Res.* **2009**, *42* (7), 925–937.

(3) Li, X.; Gao, X.; Shi, W.; Ma, H. *Chem. Rev.* **2014**, *114* (1), 590–659.

(4) Weng, J.; Ren, J. *Curr. Med. Chem.* **2006**, *13* (8), 897–909.

(5) Xing, Y.; Rao, J. *Cancer Biomarkers* **2008**, *4* (6), 307–319.

(6) Puckett, C. A.; Barton, J. K. *J. Am. Chem. Soc.* **2009**, *131* (25), 8738–8739.

(7) Amoroso, A. J.; Pope, S. J. A. *Chem. Soc. Rev.* **2015**, *44* (14), 4723–4742.

(8) New, E. J.; Parker, D.; Smith, D. G.; Walton, J. W. *Curr. Opin. Chem. Biol.* **2010**, *14* (2), 238–246.

(9) Scaff, W. L.; Dyer, D. L.; Mori, K. *J. Bacteriol.* **1969**, *98* (1), 246–248.

(10) Soini, E.; Hemmilä, I. *Clin. Chem.* **1979**, *25* (3), 353–361.

(11) Bünzli, J.-C. G. *Acc. Chem. Res.* **2006**, *39* (1), 53–61.

(12) Yuan, J.; Wang, G. *TrAC - Trends Anal. Chem.* **2006**, *25* (5), 490–500.

(13) Bünzli, J.-C. G. *Coord. Chem. Rev.* **2015**, *293–294*, 19–47.

(14) Wang, X.; Chang, H.; Xie, J.; Zhao, B.; Liu, B.; Xu, S.; Pei, W.; Ren, N.; Huang, L.; Huang, W. *Coord. Chem. Rev.* **2014**, *273–274*, 201–212.

(15) Smith, D. G.; McMahon, B. K.; Pal, R.; Parker, D. *Chem. Commun.* **2012**, *48* (68), 8520.

(16) Lincheneau, C.; Duke, R. M.; Gunnlaugsson, T. *Org. Biomol. Chem.* **2012**, *10* (30), 6069.

(17) Comby, S.; Tuck, S. A.; Truman, L. K.; Kotova, O.; Gunnlaugsson, T. *Inorg. Chem.* **2012**, *51* (19), 10158–10168.

(18) Peterson, K. L.; Margherio, M. J.; Doan, P.; Wilke, K. T.; Pierre, V. C. *Inorg. Chem.* **2013**, *52* (16), 9390–9398.

(19) Montalti, M.; Prodi, L.; Zaccheroni, N.; Charbonnière, L.; Douce, L.; Ziessel, R. *J. Am. Chem. Soc.* **2001**, *123* (50), 12694–12695.

(20) Heffern, M. C.; Matosziuk, L. M.; Meade, T. J. *Chem. Rev.* **2014**, *114* (8), 4496–4539.

(21) Dustin, L. B. *Clin. Appl. Immunol. Rev.* **2000**, *1* (1), 5–15.

(22) Demchenko, A. P. *J. Fluoresc.* **2010**, *20* (5), 1099–1128.

(23) Bruce, J. I.; Dickins, R. S.; Govenlock, L. J.; Gunnlaugsson, T.; Lopinski, S.; Lowe, M. P.; Parker, D.; Peacock, R. D.; Perry, J. J. B.; Aime, S.; Botta, M. *J. Am. Chem. Soc.* **2000**, *122* (40), 9674–9684.

(24) Butler, S. J.; Parker, D. *Chem. Soc. Rev.* **2013**, *42* (4), 1652–1666.

(25) Werts, M. H. V.; Jukes, R. T. F.; Verhoeven, J. W. *Phys. Chem. Chem. Phys.* **2002**, *4* (9), 1542–1548.

CHAPTER THREE: Sensing of inorganic anions

Introduction

The anions have important roles in biological systems and they can generate deleterious effects to human being[1]. A perfect example is the nitrate anion that although is not considered toxic for the humans its metabolites may be carcinogens[2]. The widespread overuse of fertilizers in agriculture has ensured that nitrate and phosphates are major pollutant in the soils and waterwaste[3]. In this way, the side-effects and the increasing of pollution have increased the attention toward critical analytical problems which has reached social and economical importance. The most the sensor used to analyze nitrate in food, fertilizers or plant tissues are based on the principle of ion exchange and they lack of sensitivity. So, the improving of the selectivity and the sensitivity of ionophores is actually a flourishing research that interest many fields of chemistry[4].

Nowadays, numerous approaches can be used for the detection of anions. For example, it can be used the alteration of photo-physical or redox properties of "reporter" placed close to groups able to interact with anions. Or the ability of anion to displace an indicator for a complex can be used. In the literature many others approaches are present and they are gathered in different reviews[56]. However, the sensors can be classified by the interaction ways used to detect the anions. They can establish:

- hydrogen bond, which is ensured by the use of pyrroles, amides and urea/thioureas groups
- electrostatic bond, by the use a metal cations or ammonium derivatives.

Although the design of probes using hydrogen bond with the anion could be very easy, their use is limited to some solvents. In fact, this interaction would be weakened in protonic solvents, like water, reducing the sensibility of sensor. Surely the electrostatic interaction guarantee a strongest bond between sensor and anion, and, in general, the use of metal cations are preferred. Although any metals have been used in the recognizing part of sensor[7], the lanthanide have had an prominent role thanks to their characteristic photo-physical properties.

Lanthanide complexes for anion sensing

Two possible methods, using by lanthanide complex to detected the anions are reported in literature. The first one is based on hydrogen bonding interaction between the binding site present in lanthanide complex and the anions. The binding sites are provided in general by thioureas, ureas, amides and amidoureas/thiousears and they are placed close to antenna that sensitize the lanthanide ions or close to the latters. In these way, a modification of energy transfer processes or changing of inner sphere of lanthanide guarantee a pronounced variation of lanthanide emission. However, this mechanism of detection is not largely used and very few example of lanthanide complexes, working with hydrogen bonding, are present in literature. The Terbium complexes with **1** and **2** (Figure 1) which show sensing properties toward acetate anions[8] is a representative example.

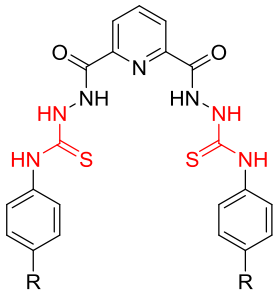

1. R=CF_3
2. R= NO_2

Figure 37 Chemical Structure of Ligands used for anion sensing

The second considers the coordination of the anion to the metal ion as a sensing action. The strong electrostatic interaction between the lanthanide and the anion and the concomitant displacing of solvent molecules are on the basis of this sensing mechanism. These kind of complexes are more preferable for sensing of anions due to the stronger sensitivity of the probe. In this field recently, the scientific community is completely focused on the sensing properties of lanthanide complexes containing derivatives of 1,4,7,10-tetraazacyclododecane (cyclen) and 1,4,7-triazacyclononane (TACN) (Figura 2). These ligands are capable to form highly stable lanthanide complexes, (an example is the clinically approved Dotarem®), and they can be easily functionalized. An example is the Cyclen ligand formed by two quinoline pendant and two acetate arms (**10**) which has the ability

to encapsulate the Europium ion with a free axial site used for the coordination of fluoride and carbonate anions[9]. DFT calculation of adducts shown the presence of C-H - - -F interaction which stabilize the whole final complex. The same interaction is also observed in pyridine analogs (**11**) and it is responsible of the increase of the binding affinity[10].

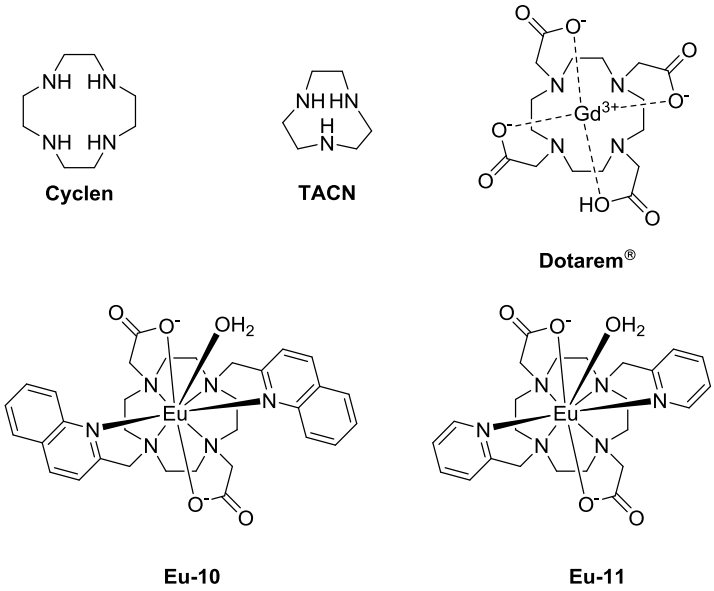

Figure 38 Cyclen ligands and Europium cyclen derivatives

Another interesting class of lanthanide complexes showing anions sensing properties are the one containing tripodes as ligands.

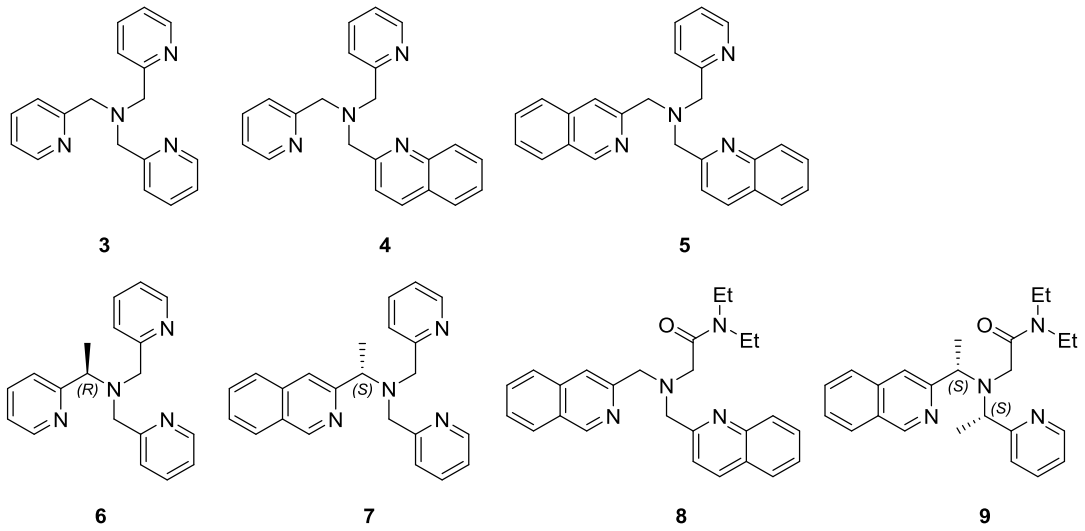

Figure 39 Tripodes used by Tsukube

They can chelate lanthanide ions leaving a coordination site available for anion sensing. Tsukube et al. investigated the sensing properties of many complexes having different neutral tripodes (figure 3), also chiral, and lanthanide ions in organic solvent (acetonitrile). In details, they evaluated the sensing properties of complexes by means of enhancement of luminescence of lanthanide emission after addiction of tetrabutylammonium salts of I^-,Br^-, Cl^-, F^-, ClO_4^-, NO_3^-, SCN^-, $CH_3CO_2^-$, HSO_4^- or $H_2PO_4^-$. The [Eu-**3**]$(CF_3SO_3)_3$ complexes show a very low emission which is slightly improved only by adding of NO_3^- (1.5 fold) and Cl^-[11]. This partial anion selectivity is preserved also upon introduction of quinoline, [Eu-**4**]$(CF_3SO_3)_3$, but the sensitivity of the complexes tremendously increases and a 20 times increase of the luminescence intensity is detected after the addiction of 3 eq. of nitrate and chloride[12]. The further substitution of pyridine with quinoline, [Eu-**5**]$(CF_3SO_3)_3$, doesn't offer any anion-responsive profile. By using the same ligands but different lanthanides, Tsukube et.al observed a good selectivity of the lanthanum complex, [La-**4**]$(CF_3SO_3)_3$, for nitrate[12], and terbium [Tb-**3**]$(CF_3SO_3)_3$ for chloride anion[11]. The introduction of one stereogenic carbon changes completely the anion responsivity. In fact, the [Eu-**6**]$(CF_3SO_3)_3$ complexes shows an enhancement of luminescence emission much more bigger (almost 5 folds) than the one observed for the achiral ligand [11]. The sensitive increasing is also increased in the case the [Eu-**7**]$(CF_3SO_3)_3$ complexes and the [La-**7**]$(CF_3SO_3)_3$ [12]. Finally, Tsukube et al. tried to improve the anion selectivity from these kind of complexes by adding one more stereocenter (molecule **9**,Figure3). The surprising results can be seen also by naked-eyes (Figure 4)[13].

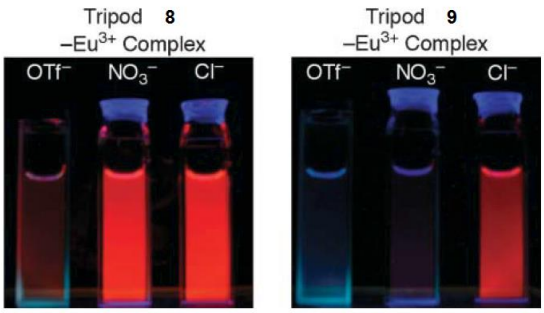

Figure 40 Naked-eye detection of NO_3^- and Cl^- anions with tripod 8 and 9–Eu^{3+} complexes

The Tsukube work's point out the importance of chirality in the anion sensing and how it can be used for increase the selectivity of a general probe[14].

Aims of the present study

To the best of our knowledge, among the factor affecting the sensing properties towards anions, the donating properties of the ligands is not properly investigated in the literature. For this reason, we have designed the new class of ligands depicted in figure 5, with the pyredine-based ligands (L1 and L3) having better donating ability than the furan-based ligand L2. As mentioned before, as chirality has a strong impact on the sensing properties of the system, we have prepared the two isomers of the pyridine-based ligands (L1 is chiral and racemic, L3 is achiral (meso isomer))

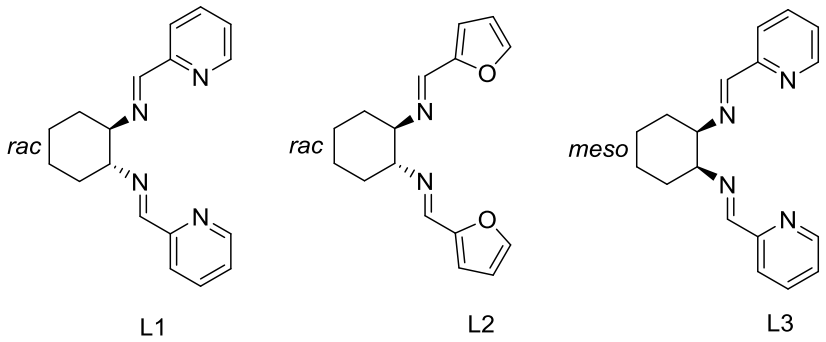

Figure 41 Ligands

The sensing properties toward several anions have been investigated in acetonitrile, an organic polar aprotic solvent.

Results

Characterization of the species in solution

The lanthanide triflates were for long considered strong electrolytes in AN, due to the low coordinating ability of the anion, since it has been demonstrated that the $Ln(SO_3CF_3)_3$ salts are completely dissociated at concentration lower than 0.05 mM in anhydrous AN. At 33 mM the lanthanide triflate in AN, is mainly present as undissociated salt and the 1:1 electrolyte ($Ln(SO_3CF_3)_2^+$). For Eu(III) triflate complexes UV–Vis spectrophotometric titrations was performed in order to investigate the nature of the species in dry AN solution and their stabilities. The absorbance changes during the titration of dry AN solution of the ligand **L1**, **L2** and **L3** with $Eu(CF_3SO_3)_3$, are shown in Figure 9,10 and 11 in appendix, respectively. The speciation models, yielding the best fit of the experimental absorbances, indicate that two highly stable mononuclear species are formed with $Eu(CF_3SO_3)_3$ (Table 1), whose stoichiometry is EuL and EuL_2. Data in Table 1 show that the pyridine-based complexes are more stable than furan-based ones: from a structural point of view, it is reasonable that all donor groups of the ligands are coordinated to the Eu^{3+} cation, as suggested by the relatively quite high values of all the stability constants. The differences in stability are likely closely related to the σ-donor ability of the aromatic donor rings (DN = 33.1 and 6 for pyridine and furan, respectively). The stability constants of the triflate complexes with the two pyridine-based isomeric ligands (**L1** and **L3**) are very similar, and higher than for the triflate complexes of the furan-based one (**L2**).

Table 11 Overall stability constants ($log\beta_j$, j = 1, 2) for the reaction Eu + jL → EuL_j (charges omitted) of the triflate complexes in AN (standard deviation in parentheses). aAN = anhydrous acetonitrile; wAN = wet acetonitrile

	L1		**L2**		**L3**	
	aAN	wAN	aAN	wAN	aAN	wAN
$Eu(OTf)_3$						
$\log \beta_1$	9.03(0.09)	5.3(0.1)	8.5(0.5)	6.19(0.05)	9.1(0.2)	5.17(0.01)
$\log \beta_2$	16.5(0.6)	10.1(0.6)	13.5(0.5)	11.4(0.1)	16.4(0.4)	10.00(0.06)

In most applications, the solvent used is not rigorously anhydrous, thus it is useful to investigate the effect of water present in AN. In the present study, the content of

water in commercial non anhydrous acetonitrile (wAN) is 23 mM and it is higher than in the anhydrous solvent (aAN 1 mM). It is expected that water dissolved in an organic solvent in significant amounts can affect the nature of the Eu^{3+} complex, due to the oxophilicity of Ln^{3+} ions[18,19] and consequently the nature of the sensing species. The absorbance changes during the titration of a wAN solution of the ligands **L1- 3** with $Eu(CF_3SO_3)_3$ are shown in Figure 12-14 in appendix. The values of the formation constants determined for **L1**, **L2** and **L3** are reported in Table 1, together with the previous ones obtained for the same ligands in anhydrous acetonitrile. The speciation models (Table 1) yielding the best fit of the experimental absorbance values show that all ligands form two 1:1 and 1:2 complexes, as found in aAN.

In all cases, the value of the stability constants relative to formation of 1:1 complexes in wAN is found to be at least three orders of magnitude lower than those detected in aAN. This drop in stability is observed also for the 1:2 species and can be explained by takin into account the ligand solvation. In our case, water molecules present in significant amount in wAN can solvate the ligands **L1**–**3** more strongly than AN by forming hydrogen bonds, thus making complex formation more difficult. The decrease of the complex stability, which results to be quite similar for **L1** and **L3** (Table 1), is bigger than for **L2** (Table 1). This lower destabilization of the complexes with **L2** can be interpreted on the basis of the weaker solvation of ether groups in water with respect to aromatic nitrogens[20].

IR spectroscopy in solution is very useful in order to study the nature of the lanthanide coordination compounds, in particular the nature of their cation/anion interactions[21] that can be influenced by concentration. In Figure 6 the region of the vibrational spectrum relative to the triflate absorption is shown for a solution of Na(OTf) (a strong electrolyte in AN; red spectra in Figure 6) and for the **L2** complexes with $Eu(OTf)_3$ in the concentration range of ∼30 mmol dm^{-3}, where the salt is not completely dissociated.

In the Na(OTf) spectra, the bands at 1270, 1220 and 1155 cm^{-1} can be assigned to the stretching modes of ionic triflate in solution. On the basis of DFT calculations for the triflate ion the experimental band at 1270 cm−1 (Figure 6 red) is assigned to the asymmetric stretching of SO_3 (calc. 1231 cm^{-1}) while that at 1155 cm^{-1} can be

assigned to the symmetric stretching mode (calc. 1008 cm^{-1}). The theoretical spectrum presents an additional band at 1176 cm^{-1} and a shoulder at 1127 cm^{-1} associated with CF_3 and CS stretching modes. Therefore, modifications in the bands related to SO_3 stretching should be diagnostic of triflate coordination. In the spectrum of a $Eu(OTf)_3$ solution (reported only in Figure 6 black) new bands appear at 1180, 1237 and 1323 cm^{-1}, which can be assigned to the coordinated triflate[15].

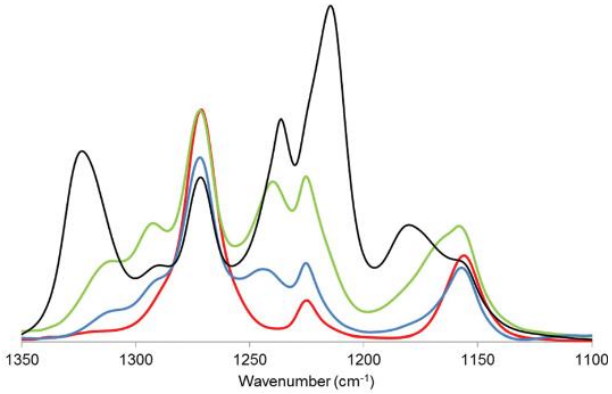

*Figure 42 IR spectra in the 1100–1350 cm^{-1} region of the solutions (all concentrations in mmol dm^{-3}): Na(OTf) 30.1 (red); $Eu(OTf)_3$ CEu = 28.1 (black); $Eu(OTf)_3$/**L2** CEu = 34.8, C**L2** = 25.3 (green); $Eu(OTf)_3$/**L2** CEu = 20.1, C**L2** = 40.5 (blue)*

In particular, the band at 1323 cm^{-1} (Figure 6 black) can be assigned to the SO_3 asymmetric stretching of the coordinated triflate where the SO_3 stretching frequency is shifted from 1231 cm^{-1} to 1310 cm^{-1}. Also the experimental band at 1155 cm^{-1} (Figure 6, black) can be assigned to the SO_3 symmetric stretching mode of the coordinated triflate. By comparing the spectra (green lines and black line in Figure 6) of solutions where only 1:1 complexes (and a small percentage of free Eu^{3+}) are present with those of $Eu(OTf)_3$, it results that triflate is still coordinated to the cation. In contrast, when only Eu(**L2**)$_2$ complex is present (Figure 6 blue lines) the band pattern of the free ionic triflate is recovered. It is thus shown that the ligands studied are able to completely displace the triflate anion from the inner coordination sphere of the Eu(III) cation when 1:2 species are formed even at high triflate concentrations. Therefore, it can be reasonably proposed that the ligands are completely coordinated to the lanthanide at the low concentrations used in the spectrophotometric titrations, where the triflate anions are dissociated. This result can be extended also to **L1** and **L3** 1:2 complex formation, ligands where furan is substituted by the more coordinating pyridine.

The IR spectra of Eu**L1** and Eu(**L1**)$_2$ complexes in AN (Figure 7) both show only the presence of dissociated triflate anion even at 1mM concentration: the strong affinity of the organic ligand, can explain the decrease of the coordinating ability of the triflate anion already at 1 mM of salt concentration. For both triflate complexes under investigation the absorption of the coordinated acetonitrile molecule was also detected (ν_3 - + $\nu_4(CH_3CN)$), at 2305 and 2307 cm^{-1} for Eu**L1** and Eu(**L1**)$_2$, respectively.

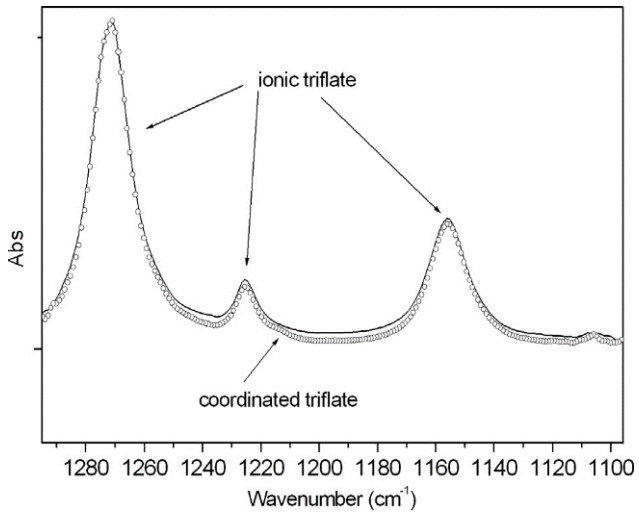

Figure 43 IR spectrum of 1mM AN solution of EuL triflate complex (straight line) and EuL$_2$ triflate complex (circles) in the region of anion absorption.

In addition the absorption at 1599 cm^{-1} (ν C=N) for both complexes, compatible with imine group bonded to the metal, reveals that, in the Eu(**L1**)$_2$ species, all imine groups are involved in the coordination of the metal, in line also with the high value of thermodynamic constants. In conclusion, the inner coordination sphere of triflate Eu**L1** and Eu(**L1**)$_2$ complexes should be constituted, by ligand molecules and solvent (AN), as proposed in Figure 8.

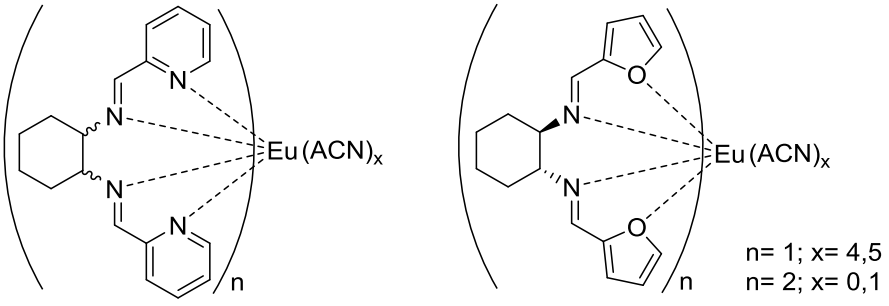

Figure 44 Proposed structural formulae for the complexes in solution. The values of x are supposed considering the more common (8 and 9) coordination number of Eu(III) ion

An efficient intramolecular energy transfer from the triplet state of the coordinated organic ligand (antenna effect) to the excited state of Ln^{3+} ions is strongly required in order to provide a high ε value and bypass the parity-forbidden nature of the *f–f* transitions, characterized by a low ε value.

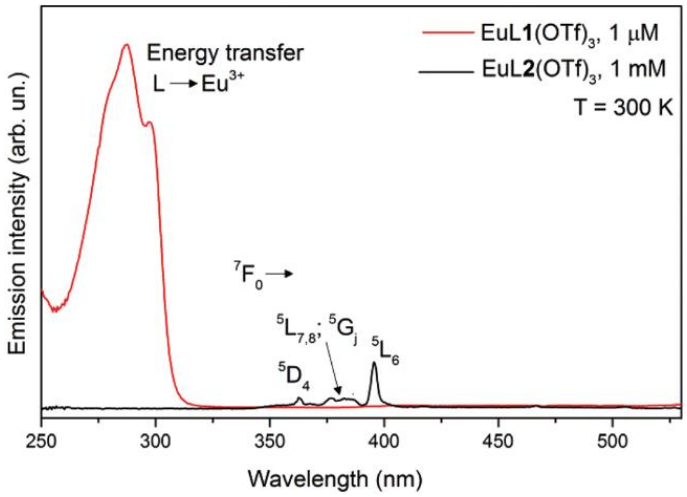

*Figure 45 Excitation spectra of Eu**L1**(OTf)3 (λem = 614 nm) and Eu**L2**(OTf)3 (λem = 615.5 nm). Slit width was adjusted to 2.5 nm for excitation and 5.0 nm for emission.*

In Figure 9 the excitation spectra of the EuL triflate complexes containing **L1** and **L2** ligands (Eu**L1**$(OTf)_3$ and Eu**L2**$(OTf)_3$, respectively) are shown. In the case of Eu**L1**$(OTf)_3$ the excitation band around 285 nm, due to a ligand to metal energy transfer process (antenna effect), effectively works, also for very low concentration of the complex (1 μmol dm^{-3}). The very strong intensity of this excitation band together with the potential displacement, in the inner coordination sphere, of the weakly bound triflate ligand or solvent molecules by a donor species, suggests this compound as an efficient sensor of anions or molecules. In contrast, the ligand **L2** is not able to induce an efficient antenna effect. For its complexes, the direct excitation of the Eu(III) ion (*f–f* transition around 395 nm) is the only efficient optical route to obtain light emission from the Eu(III) ion (Figure 9). Unfortunately, although Eu**L2**$(OTf)_3$ shows a good sensitivity toward the nitrate anion, due to the forbidden nature of the *f–f* transition the emission intensity is low and the concentration of this species in solution cannot be lowered below 1 mmol dm^{-3}; as a consequence the limit of anion detection for this sensor is not particularly low.

Characterization of the species during the sensing experiment with nitrate

UV-Vis spectrophotometric titrations have also been employed with the aim to determine the stability of the species formed by EuL_j (L = **L1**, **L2** and **L3**) complexes and the nitrate anion. In our experiments, solutions containing the ligand and the $Eu(CF_3SO_3)_3$ mixed in the desired stoichiometric ratio (1:1 or 2:1) were titrated with a solution containing the nitrate salt [$(C_2H_5)_4NNO_3$]. The electronic spectra after each addition have been collected and reported in Figure 10 a and b for the ligand **L1**.

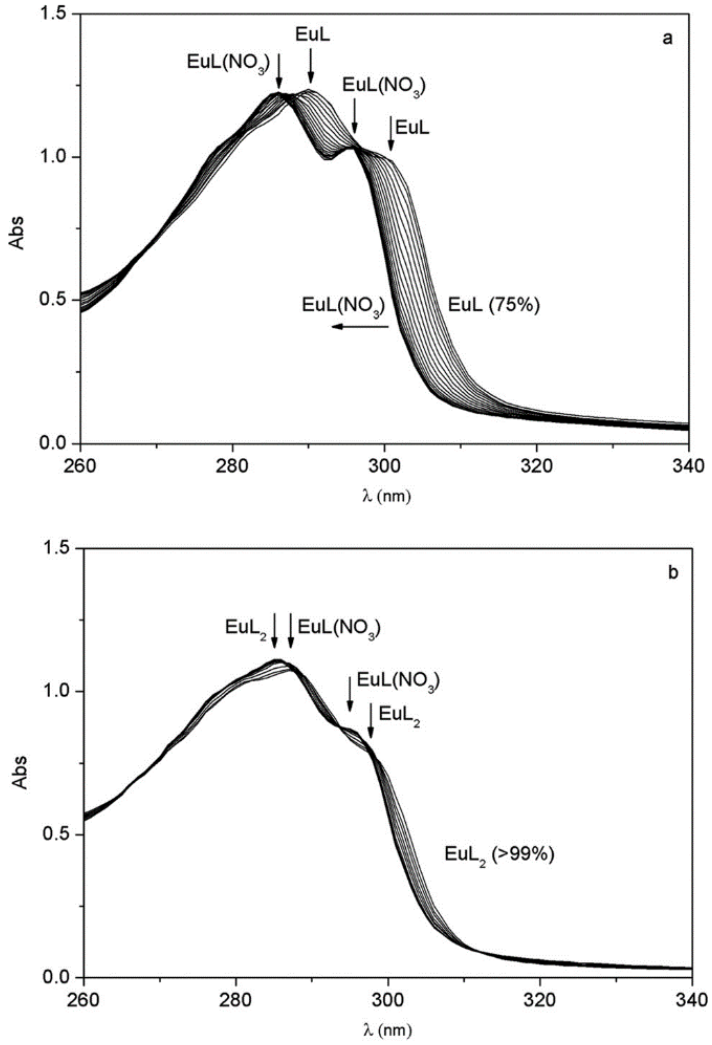

*Figure 46 Absorption spectra of: (a) solution containing 1 : 1 Eu : **L1** molar ratio (CEu = 0.053 mM, V_0 = 2.1 mL), titrated with a $(C_2H_5)_4NNO_3$ solution (2.0 mM, 18 additions of 10 μL); final CEu/CL/Cnitrate = 1/1/4. (b) Solution containing Eu : **L1** in 1 : 2 mol*

The addition of nitrate to the solution containing $Eu(CF_3SO_3)_3$: **L1** in a 1:1 ratio results in the disappearance of the maximum at λ = 290 nm and of the shoulder at

λ = 300 nm and the progressive formation of two new maxima at λ = 286 and λ = 296 nm (Figure 10a). In the case of titration of the solution containing $Eu(CF_3SO_3)_3$: **L1** in a 1:2 ratio (Figure 10 b), the starting spectral features related to the Eu(**L1**)$_2$ species (maximum at λ = 288 nm and shoulder at λ = 298 nm) disappear and two maxima at λ = 286 and 296 nm are evidenced (Figure 10 b). The speciation models yielding the best fit of the experimental data for both titrations predict the presence of only one nitrate complex. The related speciation curves upon addition of the nitrate salt to the Eu triflate complexes are shown in Figure 11.

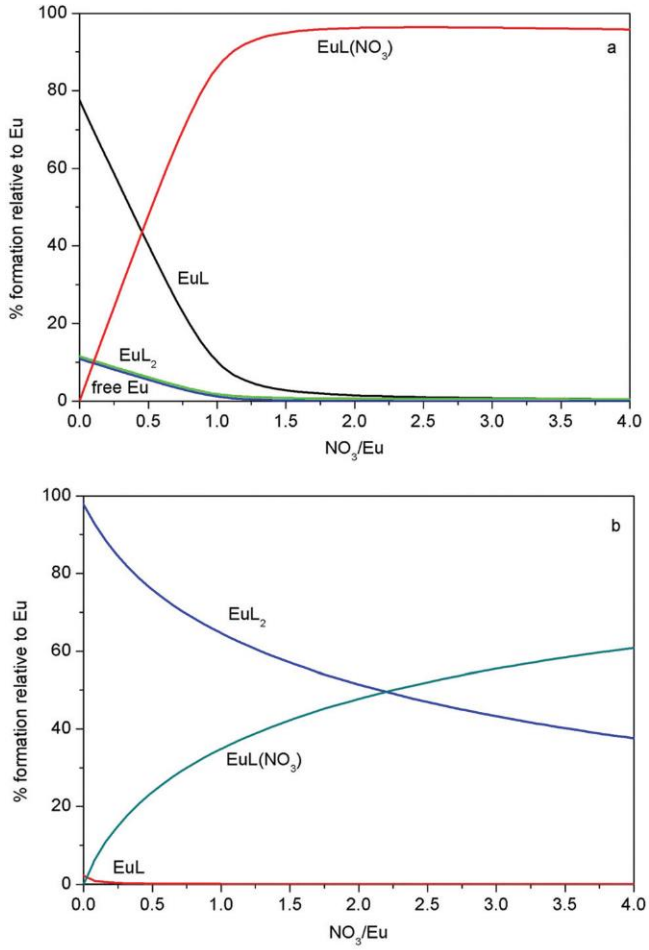

*Figure 47 Species distributions during the titrations of the $Eu(OTf)_3$: L1 solutions titrated with $(C_2H_5)_4NNO_3$ in the conditions reported in the caption of Figure 10: (a) Eu(**L1**) and (b) Eu(**L1**)$_2$.*

The ternary species formed by Eu(III), **L1** and the nitrate anion is rather stable, with a log K_1 = 7.5(0.2) for the equilibrium $Eu\mathbf{L1}^{3+} + NO_3^- \rightleftarrows [Eu\mathbf{L1}(NO_3)]^{2+}$. Complexes with two or three bound nitrate anions have not been detected under the experimental conditions of the spectrophotometric titration ([Eu(III)] ≤ 8×10^{-5} M).

Further, in the case of the titration of the Eu(**L1**)$_2$ species, the nitrate anion is also able to bind the Eu(III) ion replacing one ligand molecule, as suggested by the fact that the absorbance maxima (286 and 296 nm) at the end of the titration in Figure 10 coincide with those obtained at the end of the titration of Eu(**L1**) in Figure 10 a. In the case of the complexes with the ligand **L2**,we have not been able to clearly detect spectral changes associated with the interaction of the complex with nitrate (Figure 12).

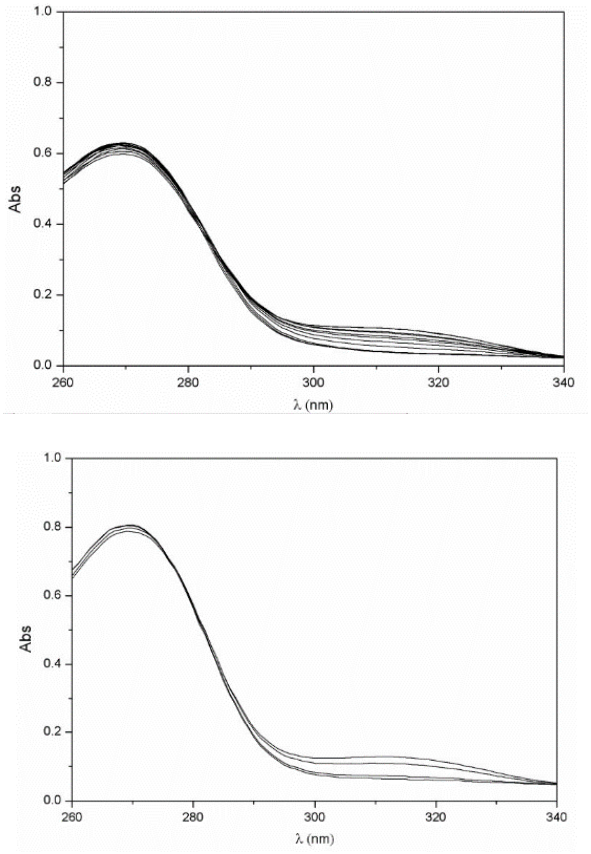

*Figure 48 Electronic spectra of: (upper) solution containing 1:1 Eu(OTf)$_3$:**L2** molar ratio (CEu= 0.019 mmol L-1,V_0 = 2.0 mL), titrated with a (C_2H_5)$_4$NNO$_3$ solution (2.4 mmol L^{-1}, 16 additions of 4 μL); final CEu/CL/Cnitrate = 1/1/4. (bottom) solution containing Eu(OTf)$_3$:**L2** in 1:2 molar ratio (CEu= 0.0096 mmol L^{-1} , V_0 = 2.0 mL) titrated with a (C_2H_5)$_4$NNO$_3$ solution (2.4 mmol L^{-1}, 8 additions of 4 μL); final CEu/CL/Cnitrate = 1/2/4.*

This suggests that either the coordination of nitrate is very weak or that the absorption spectrum of the ligand **L2** bound to the Eu(III) ion is not sensitive to the coordination of this anion.

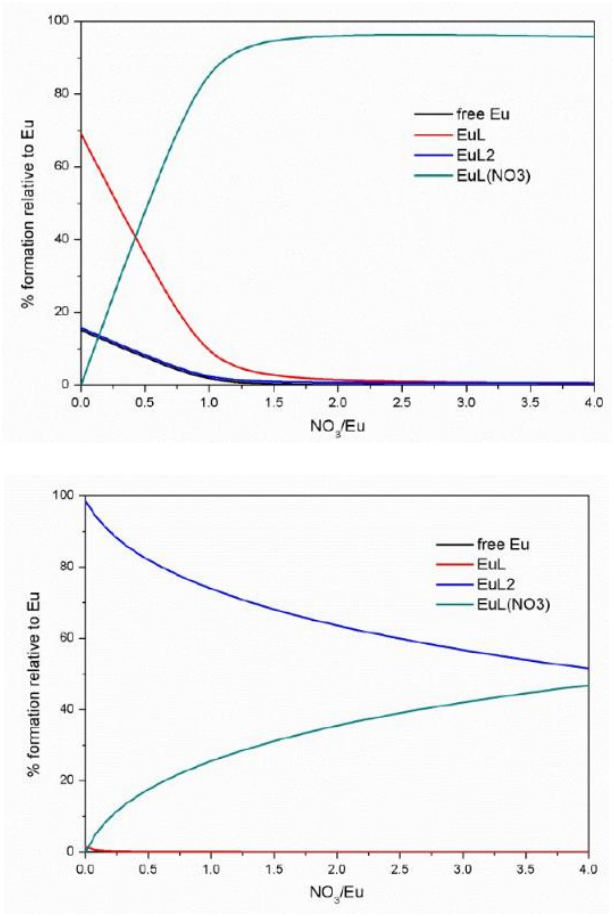

*Figure 49 Speciation during the titration of (upper) Eu**L2**(OTf)$_3$ and (bottom) Eu(**L2**)$_2$(OTf)$_3$ with $(C_2H_5)_4NNO_3$*

The addition of nitrate to the solution containing $Eu(CF_3SO_3)_3$: **L3** in a 1:1 ratio results in the disappearance of the maxima at λ = 288 and 298 nm and the progressive formation of two new maxima at λ = 286 and 297 nm (Figure 14). In the case of titration of the solution containing $Eu(CF_3SO_3)_3$: **L3** in a 1:2 ratio (Figure 14), the starting spectral features related to the Eu(**L3**)$_2$ species (maximum at λ = 289 nm and shoulder at λ = 299 nm) disappear and two maxima at λ = 282 and 297 nm are formed (Figure 14) Again, only one nitrate is able to bind the Eu(III) complex under the experimental conditions adopted, to form a ternary 1:1:1 species with a log K_1 = 8.07(0.03) relative to the equilibrium Eu**L3**$^{3+}$ +$NO3^-$ ⇄ [Eu**L3**(NO_3)]$^{2+}$. The log K_1 value is close to that found in the formation of the complex with **L1**, thus the speciation curves are very similar to those calculated previously.

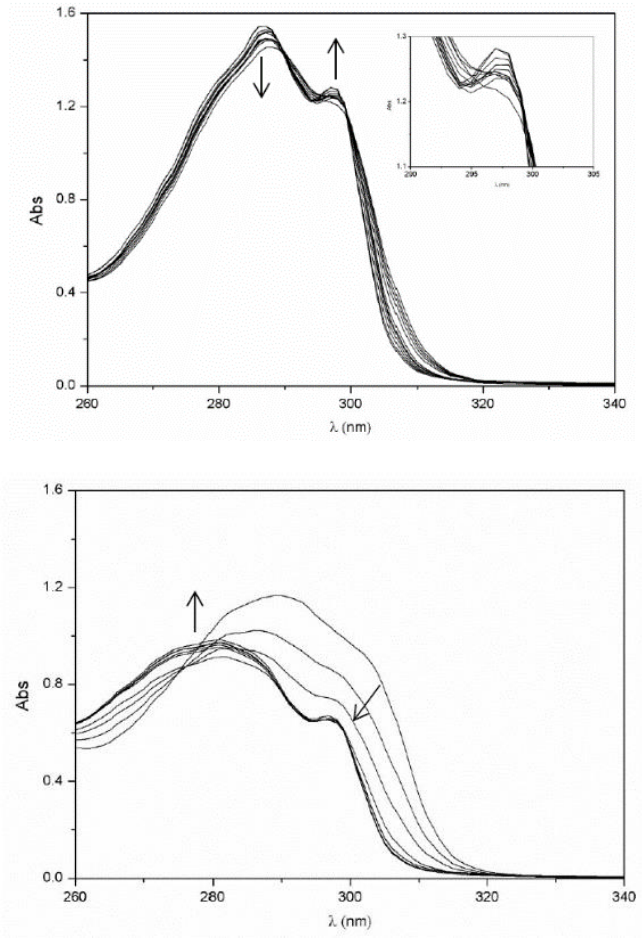

*Figure 50 Electronic spectra of: (upper) solution containing 1:1 Eu(OTf)$_3$:**L3** molar ratio (CEu= 0.0795 mmol L^{-1},V$_0$ = 2.0 mL), titrated with a (C$_2$H$_5$)$_4$NNO$_3$ solution (12.0 mmol L^{-1}, 7 additions of 3 μL + 8 additions of 3.5 μL); final CEu/CL/Cnitrate = 1/1/4. (bottom) solution containing Eu(OTf)$_3$:**L3** in 1:2 molar ratio (CEu= 0.0394 mmol L^{-1} , V$_0$ = 2.0 mL) titrated with a (C$_2$H$_5$)$_4$NNO$_3$ solution (2.4 mmol L^{-1}, 8 additions of 3.5 μL); final CEu/CL/Cnitrate = 1/2/4.*

In conclusion, Eu(III) complexes with the pyridine-imine isomers are both able to form a stable 1:1 adduct with nitrate which can be detected by absorbance changes. On the contrary, the absorbance spectra of complexes with **L2** are insensitive to the presence of the anion in the coordination sphere of the metal. The stereochemistry of the ligand [R,R (+S,S)or R,S] does not show a remarkable impact on the stability of the complex formed.

Luminescence Sensing

The impact of the ligand donor ability, the complex stoichiometry and the complex stereochemistry.

In order to evaluate the role of the ligand donor ability, the complex stoichiometry and the complex stereochemistry on the luminescence sensing response towards the nitrate anion, several luminescence emission spectra have been recorded under different conditions upon addition of the nitrate salt [$(C_2H_5)_4NNO_3$] to an anhydrous AN solution of the desired triflate complexes. In particular, two solutions of L : $Eu(CF_3SO_3)_3$ = 1:1 and L :$Eu(CF_3SO_3)_3$ = 2:1 (with L = **L1**, **L2** and **L3**) have been prepared at the same concentrations employed during the spectrophotometric titration experiments. The related luminescence emission spectra are presented in the Figure 12-17 in appendix.

The change of the Eu(III) emission features during the sensing experiments are usually strongly connected to the alterations of its inner coordination sphere, in particular to the degree of asymmetry of its geometric environment. The asymmetry ratio[22 23]:

$$R = \frac{I\left({}^5D_0 \rightarrow {}^7F_2\right)}{I\left({}^5D_0 \rightarrow {}^7F_1\right)}$$

is indicative of the degree of asymmetry of the coordination polyhedron around the Eu(III) ion and therefore is broadly exploited in the sensing experiments involving the Eu(III) ion[24]. The sensitivity of the Eu(III) luminescence response towards the nitrate anion is easily estimated by plotting R vs. the number of added nitrate equivalents. These diagrams are reported in Figure 15, respectively, for the EuL and EuL_2 (L = **L1**, **L2** and **L3**) triflate complexes. From inspection of Figure 15, several observations can be made: (*i*) the sensitivity towards the nitrate anion is strongly dependent on the ligand donor ability. The poorer donating ligand **L2** shows the best sensitivity. This is true for both triflate complexes differing by the ligand to metal stoichiometric ratio (EuL and EuL_2). (*ii*) The luminescence sensing response is affected by the nature and stoichiometry of the triflate complex. In particular, as far as the curve profile is concerned for the complexes of the **L1** and **L3** ligands, a sigmoidal trend is observed in the cases of Eu**L1** and Eu**L3** whereas

a logarithmic-like trend is observed in the case of Eu(**L1**)$_2$ and Eu(**L3**)$_2$. For the complexes of **L2** the trend is logarithmic for Eu**L2** and sigmoidal for Eu(**L2**)$_2$. (*iii*) The plot of R vs. nitrate concentration is little dependent on the stereochemistry of the pyridine-based ligand. In fact, the curves are very similar for Eu**L1** and Eu**L3** and for Eu(**L1**)$_2$ and Eu(**L3**)$_2$. In conclusion, the stereochemistry of the ligand does not seem to play a crucial role on the luminescence sensing response towards the nitrate anion. Furthermore, also the close similarity of the stability constants of the triflate and nitrate complexes discussed above and the similar coordination geometry of the **L1** and **L3** ligands observed in the solid state support the same conclusion. From a close inspection of Figure 11 and 15, for the ligand **L1** (the same applies for the ligand **L3**) the R value increases up to the addition of 1 eq. of anion for Eu(**L1**)$_2$(CF$_3$SO$_3$)$_3$ and up to the addition of 2 eq. for Eu**L1**(CF$_3$SO$_3$)$_3$ (Figure 15).

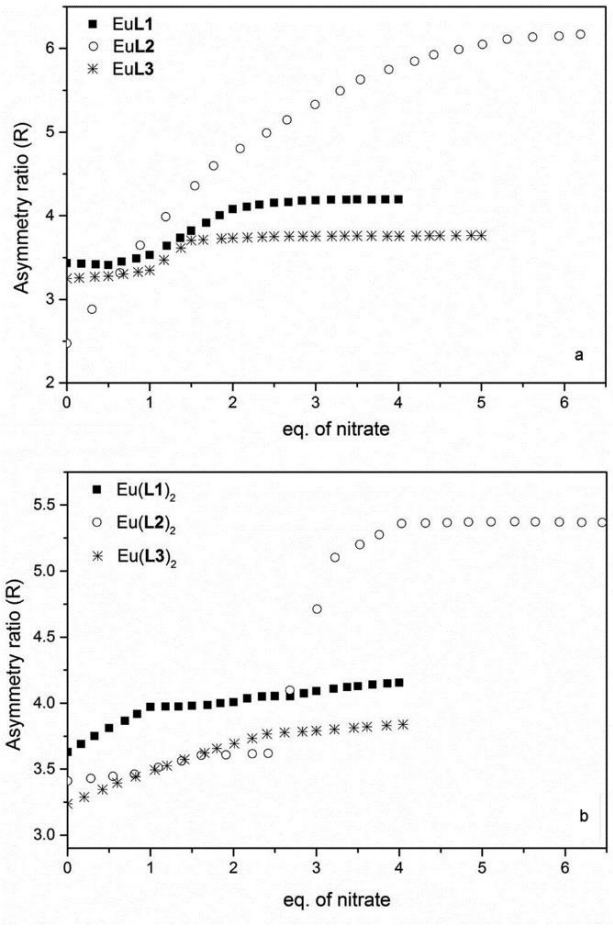

*Figure 51 Asymmetry ratio (R) vs. nitrate concentration plots for the (a) EuL and (b) EuL$_2$ triflate complexes. [Eu**L1**] = 0.04 mM, [Eu**L2**] = 0.02 mM, [Eu**L3**] = 0.08 mM, [Eu(**L1**)$_2$] = 0.04 mM, [Eu(**L2**)$_2$] = 0.02 mM and [Eu(**L3**)$_2$] = 0.04 mM*

The impact of the concentration of the complexes.

It is well known that the nitrate anion shows a high affinity for the lanthanide ions[18]. As discussed by Bünzli et al.[25], $Tb(NO_3)_3$ behaves as a non-electrolyte in anhydrous acetonitrile if its concentration is above 1 mM. On the other hand, it starts to behave as an electrolyte when the concentration is decreased to 0.2 mM. As far as the triflate anion is concerned, it shows a low affinity for Ln(III) and its lanthanide salts are completely dissociated at a concentration below 0.05 mM[17]. In order to observe an equilibrium between the undissociated $Ln(CF_3SO_3)_3$ and the 1:1 electrolyte ($[Ln(CF_3SO_3)_2]^+$) the concentration of the salt must be 33 mM[15]. In conclusion, the number of triflate or nitrate anions in the inner coordination sphere of the Ln(III) and the related value of the asymmetry ratio (R) are strongly dependent on the concentration of the complex. As far as the nitrate complex with the ligand **L1** is concerned, from infra-red absorption spectroscopy the coordination of three nitrate anions to the Eu(III) has been demonstrated when the concentration of the complex is higher than 1 mM[26]. On the other hand, as reported before, only one nitrate anion is present in the first coordination sphere of the metal ion when the concentration is decreased to 0.04–0.08 mM (Figure 11). From these data, concentration-dependent behavior of the sensing towards the nitrate anion is expected. In fact, as reported in Figure 16, the plots of R values vs. nitrate concentration are different at different Eu**L1** concentrations. In particular, at 1 mM of the complex concentration, the luminescence response is poorly sensitive towards the nitrate concentration up to the addition of 2 eq. of anion.

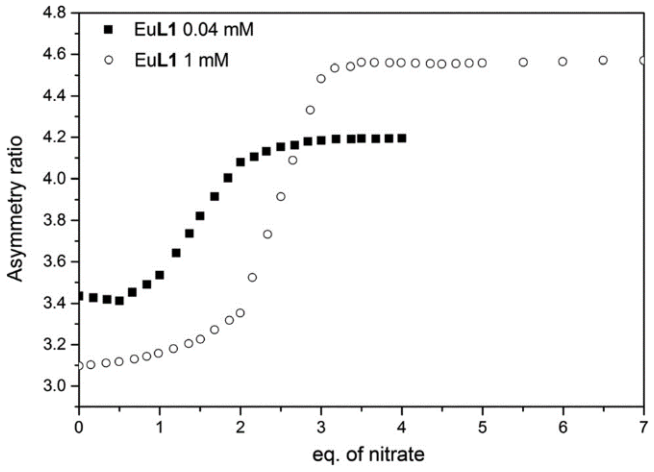

*Figure 52 Asymmetry ratio (R) vs. nitrate concentration plot for the Eu**L1** at two different concentrations (i.e. 0.04 and 1 mM) of $Eu(OTf)_3$ salt*

The addition of the third equivalent gives rise to a drastic increase of the R value. Unlike the speciation at a low concentration (0.04 mM), we can propose the presence of several nitrate complexes [Eu**L1**$(NO_3)_x$; x =1–3] during the titration with nitrate at the 1 mM concentration. In this context, it is worth pointing out that the luminescence emission spectrum of the complex upon the addition of 3,5 eq. of nitrate is completely superimposable with the one of the nitrate complex Eu**L1**$(NO_3)_3$ (Figure 17) at 1 mM, containing three anions in the inner coordination sphere, as mentioned before[26].

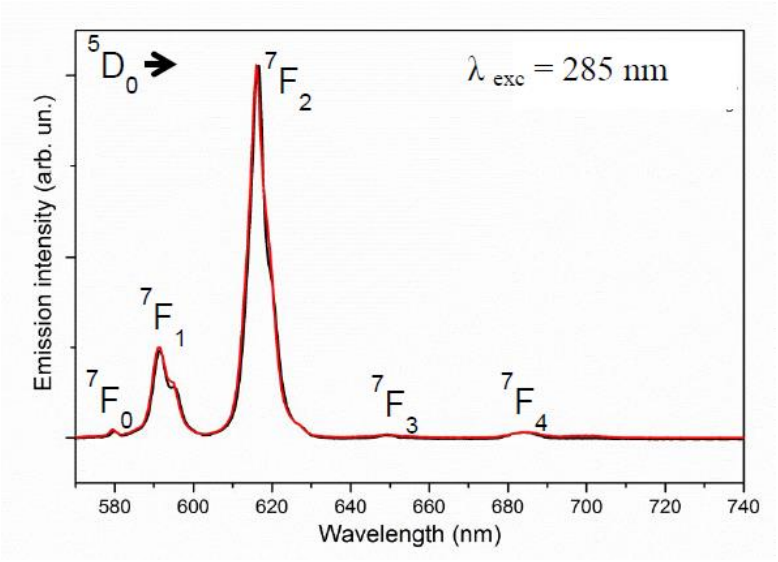

*Figure 53 Luminescence emission spectra of 1 mM AN solution of Eu**L1**$(NO_3)_3$ (black line) and Eu**L1** + 3.5 eq of nitrate (red line).*

The concentration-dependent sensing towards the nitrate anion is also observed for the **L2**-based triflate complexes (Figure 18). At 0.02 mM the logarithmic-like curve approaches an asymptote after the addition of 5 eq. of nitrate. On the other hand, at 1 mM the curve profile is almost linear and a change of the slope is observed around 2 eq. of the anion. The curve approaches an asymptote after the addition of 4 eq. of nitrate. As shown by Bünzli et al.[27] the maximum of nitrate ions bound to a Ln(III) ion [Tb(III)] is 5 ($[Tb(NO_3)_5]^{2-}$) at 2 mM. This conclusion is confirmed also for the Eu(III) ion, since upon addition of the nitrate anion to a 1 mM solution of $Eu(CF_3SO_3)_3$ the value of the asymmetry ratio increases from almost 1 to 5 up to the addition of 5 eq. of the anion.

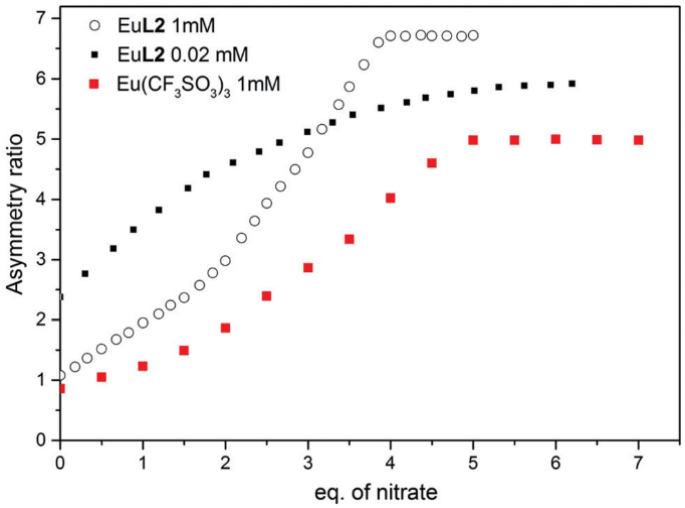

*Figure 54 Asymmetry ratio (R) vs. nitrate concentration plot for the Eu**L2** at two different concentrations (i.e. 0.02 and 1 mM)*

After 5 eq. the value of R, as well as the luminescence emission spectrum, does not change thereafter (Figure 18, red squares) and therefore the Eu(III) complex at the end of the titration should have 5 nitrate anions bound to the metal ion. With a similar reasoning, we can propose the presence of 4 nitrate anions bound to the Eu(III) at the end of the titration of the triflate complex Eu**L2** with nitrate (Figure 18, open circles). To confirm this assumption, the luminescence emission spectra of solution 1, 2 and 3 are superimposed in Figure 19 Solution (1) is composed of Eu**L2** (1 mM) +4.5 eq. of nitrate (a composition at the end of the titration, Figure 18), solution (2) of Eu**L2**$(NO_3)_3$ and solution (3) of Eu**L2**$(NO_3)_3$ upon addition of one eq. of nitrate anion.

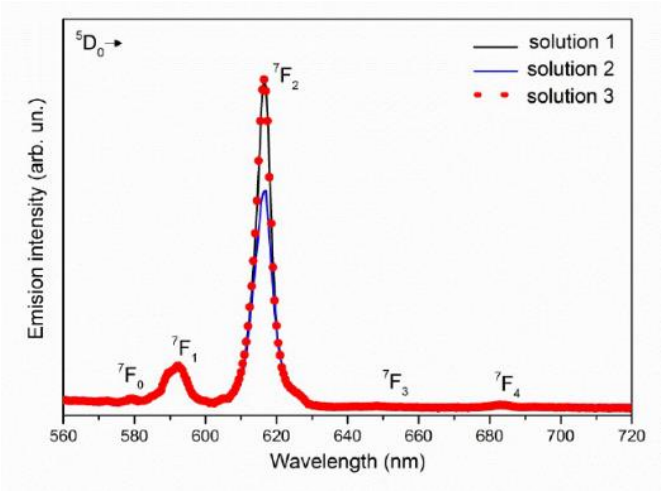

*Figure 55 Luminescence emission spectra of 1 mM AN solution of Eu**L2** + 4.5 eq of nitrate (solution 1, black line), Eu**L2**$(NO_3)_3$ (solution 2, blue line) and Eu**L2**$(NO_3)_3$ + 1 eq of nitrate (solution 3, red dotted line).*

The perfect match between the luminescence emission spectra of the solutions 1 and 3 leads us to confirm the aforementioned assumption. Also in the case of the triflate complexes with a 2 to 1 ligand to metal mole ratio (Eu**L2**) the sensing response towards nitrate is dependent on the concentration of the complex (Figure 20 and 21 for Eu(**L1**)$_2$ and Eu(**L2**)$_2$, respectively).

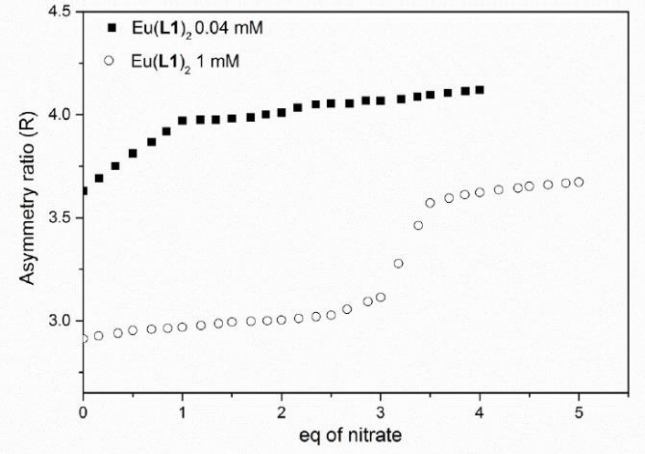

*Figure 56 Asymmetry ratio (R) vs nitrate concentration plot for Eu(**L1**)$_2$ at two different concentration (i.e. 0.04 and 1 mM).*

At 1 mM, in the case of Eu(**L1**)$_2$ the presence in solution of the luminescent Eu(**L1**)$_2$,Eu**L1**NO_3,Eu**L1**$(NO_3)_2$ and Eu**L1**$(NO_3)_3$ species is expected. Their percentage of formation is dependent on the concentration of the nitrate anion. As for the titration of the triflate complex Eu(**L1**)$_2$ with nitrate at 0.04 mM (Figure 15), a constant value of R is not reached even after the addition of 4 eq. of nitrate, also at 1mM (Figure 20).

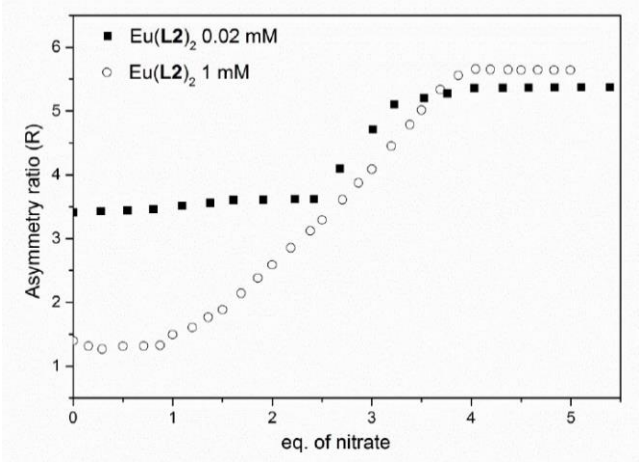

*Figure 57 Asymmetry ratio (R) vs nitrate concentration plot for Eu(**L2**)$_2$ at two different concentration (i.e. 0.02 and 1 mM)*

Finally, as far as the meso ligand **L3** is concerned, the effect of the concentration of the complex on the luminescence sensing towards nitrate is quite coincident with the one observed for the ligand **L1** (data not shown).

Sensing of other anions in non anhydrous acetonitrile

These interesting results have pushed us to investigate the sensing properties of these complexes toward different anions. In particular, we have investigated the variation of luminescence of 1:1 triflate complexes. In this condition the furan-based **L2**-Eu^{3+} complex works as the most effective anion-responsive luminescent probe towards nitrate. It offers almost a 7-fold luminescence intensity increase for this ion, while among the other anions only bromide slightly influences the Eu^{3+} luminescence intensity (Figure22).

This means that the furan-based triflate complex shows an excellent anion-sensing selectivity. The other two triflate complexes under investigation (**L1**-Eu^{3+} and **L3**-Eu^{3+}) show worse anion sensitivity, in particular the latter. For the complex with the achiral meso isomeric ligand **L3** the nitrate sensitivity is almost the same as for the chloride one (around two-fold intensity enhancement) and no other anion-responsivity was observed (Figure 23). In the case of the complex with racemic trans ligand **L1** the order of selectivity is Cl^- >Br^- >$NO3^-$ (3, 2.6 and 2.4-fold luminescence enhancement, respectively; Figure 24). Among the pyridine- based complexes (**L1**-Eu^{3+} and **L3**-Eu^{3+}) the role of the ligand stereochemistry on the bromide-responsivity is worth to be noted: only the complex with the trans isomeric ligand **L1** is sensitive to this anion (Figure 24).

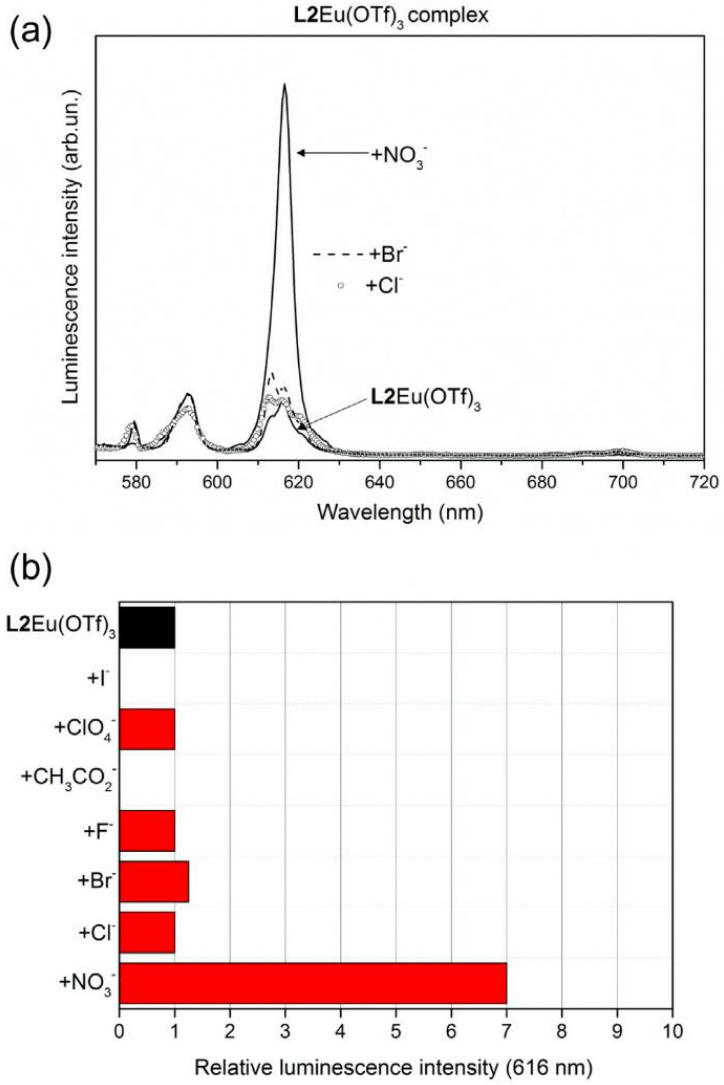

*Figure 58 a) Luminescence anion sensing with **L2**Eu(OTf)₃ complex. [**L2**] = 0.1 mM, [Eu (OTf)₃] = 0.1 mM, [n-R₄NX] = 0.6mM in wet acetonitrile. Excitation at 395 nm. Slit widths: 5 and 2.5 nm. b) Relative emission intensities at 616 nm in presence of different anions.*

The lower anion sensitivity observed for the triflate complex of the achiral **L3** ligand when compared to the one of the complex with the chiral racemic **L1** ligand is in line with previously reported results. In this context, since in the anion sensing field chirality offers higher sensitivity of the lanthanide luminescence than achirality, the proper choice of the ligand stereo-centers is required in the design of efficient anion sensing systems

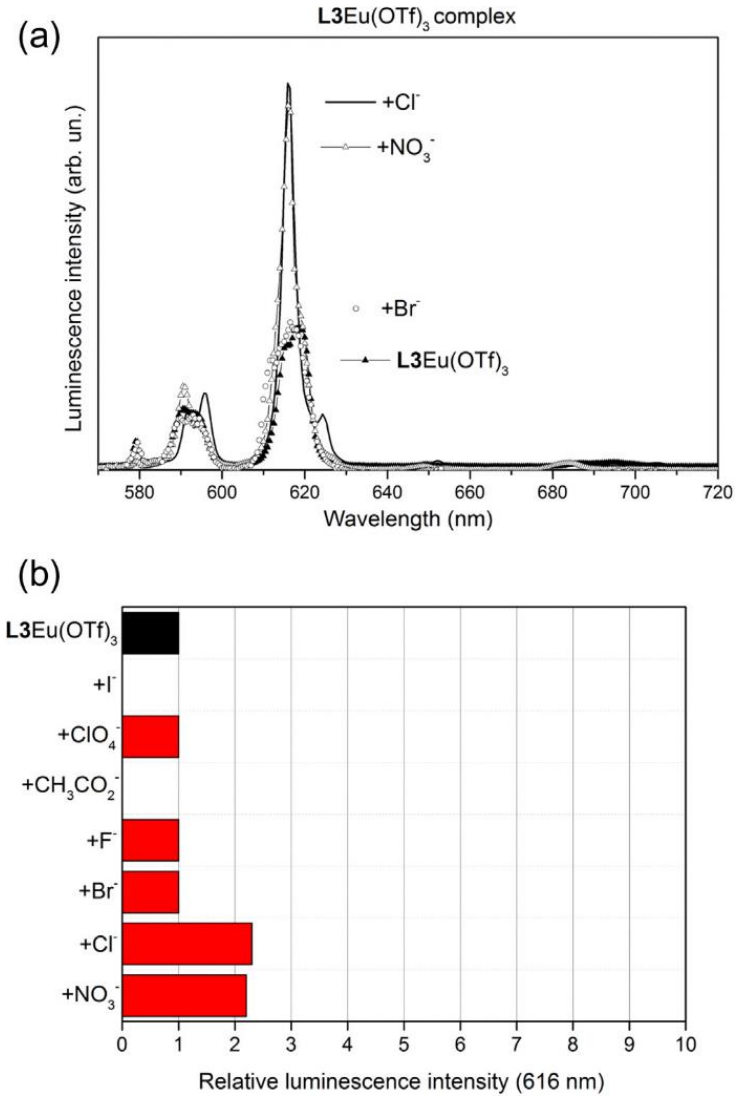

*Figure 59 a) Luminescence anion sensing with **L3**Eu(OTf)₃ complex. [**L3**] = 0.1 mM, [Eu (OTf)₃] = 0.1 mM, [n-R₄NX] = 0.6mM in wet acetonitrile. Excitation at 278 nm. Slit widths: 5 and 2.5 nm. b) Relative emission intensities at 616 nm in presence of different anions*

Due to the limited performance of the triflate complex based on the meso isomer **L3**, the similar ligand with the furan as donor ring has not been taken into account.

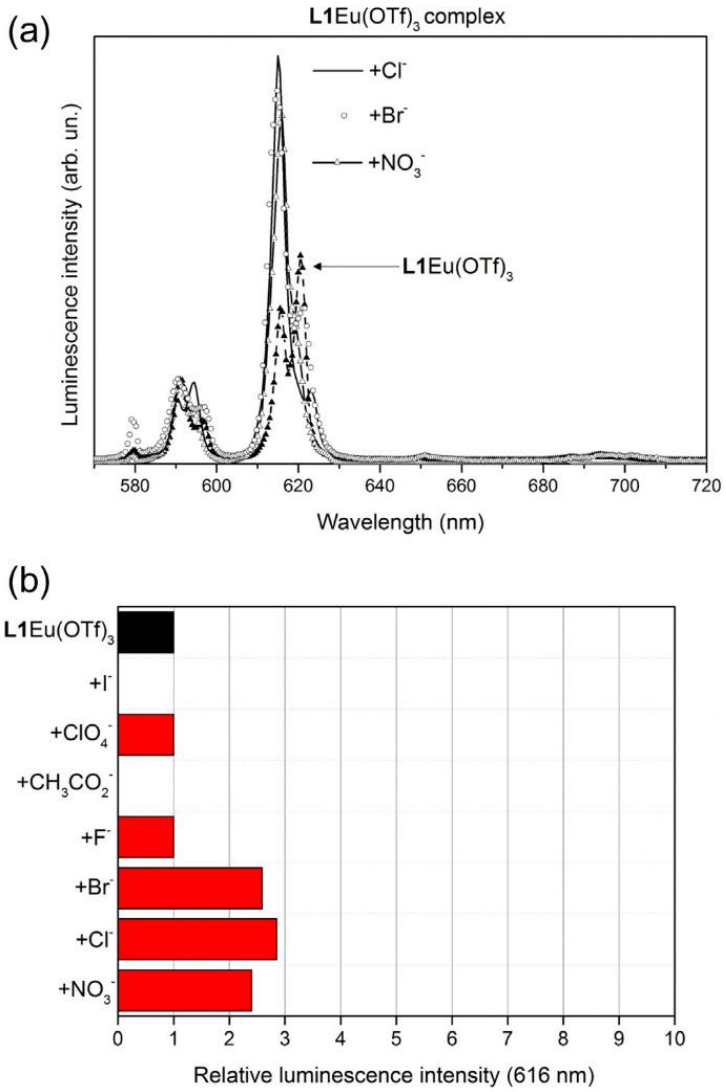

*Figure 60 a) Luminescence anion sensing with **L1**Eu(OTf)₃ complex. [**L1**] = 0.1 mM, [Eu (OTf)₃] = 0.1 mM, [n-R₄NX] = 0.6mM in acetonitrile. Excitation at 288 nm. Slit widths: 5 and 2.5 nm. b) Relative emission intensities at 616 nm in presence of different anions*

Conclusion

The luminescence sensing towards the nitrate anion in anhydrous acetonitrile solution has been studied employing their Eu(III) triflate complexes. The crucial role of the donor ability of the ligand on the sensing properties is demonstrated: when a poorly donating furan aromatic ring is present in the ligand backbone (**L2**), the best luminescence sensitivity towards the nitrate anion is obtained. On the contrary, the absorption spectrum of the ligand **L2** when bound to the Eu^{3+} ion, is not sensitive to the coordination of the nitrate. This is probably due to the weaker bond between the ligand and the metal ion reducing the sensitivity of the spectrophotometric absorption to the alterations of the inner coordination sphere. The stoichiometry of the triflate complexes (EuL or EuL_2) also plays an important role on the luminescence sensing properties. On the contrary, the stereochemistry of the ligands (*rac* or *meso*) does not strongly affect the luminescence sensing towards nitrate. Finally, the concentration of the complexes also modifies the sensing response, since during the titration of the triflate complexes with the nitrate anion, the number of the nitrate or triflate anions bound to the metal ion, which influences its luminescence, is dependent on the concentration of the species.

The presence of a higher amount of water in non-anhydrous acetonitrile decreases by several orders of magnitude the stability of the formed species, although the speciation in solution is the same as in anhydrous acetonitrile. The decrease of the stability is probably due to a higher degree of hydration of both the ligands and the Eu^{3+} ion, when non-anhydrous acetonitrile is employed for all the ligands. In the case of EuL complexes, as the Eu^{3+} inner coordination sphere shows different degree of asymmetry in wAN and aAN, also an active role of the water molecules in the Eu^{3+} coordination environment of the complexes (inner and outer coordination sphere) should be taken into account. Also in wAN the role of the ligand donor ability is crucial as the complex containing the poorly donating furan ring (**L2**) shows the best sensitivity and selectivity towards the nitrate ion. On the other hand, the stereochemistry of the ligand also plays an important role: comparing the *cis* and *trans* isomer of the pyridine-based ligand, only the latter is able to promote the Eu^{3+} luminescence sensing towards bromide ion. Furthermore, the sensitivity of the luminescence response of the *cis* isomeric complex Eu**L3**

towards chloride and nitrate is lower than the one shown by the *trans* isomer Eu**L1**. The presence of an efficient antenna effect in the case of the pyridine-based triflate complexes candidates these molecules as promising anion sensors in polar solvents able to detect the analyte in the micromolar concentration range.

Bibliography

(1) Berg, J. M. *Acc. Chem. Res.* **1995**, *28* (1), 14–19.

(2) Ellis, G.; Adatia, I.; Yazdanpanah, M.; Makela, S. K. *Clin. Biochem.* **1998**, *31* (4), 195–220.

(3) Gale, P. A.; Quesada, R. *Coord. Chem. Rev.* **2006**, *250* (23–24), 3219–3244.

(4) Suksai, C.; Tuntulani, T. *Chem. Soc. Rev.* **2003**, *32* (4), 192.

(5) Gale, P. A.; Caltagirone, C. *Chem. Soc. Rev.* **2015**, *44* (13), 4212–4227.

(6) Gunnlaugsson, T.; Glynn, M.; Tocci (née Hussey), G. M.; Kruger, P. E.; Pfeffer, F. M. *Coord. Chem. Rev.* **2006**, *250* (23–24), 3094–3117.

(7) Tetilla, M. A.; Aragoni, M. C.; Arca, M.; Caltagirone, C.; Bazzicalupi, C.; Bencini, A.; Garau, A.; Isaia, F.; Laguna, A.; Lippolis, V.; Meli, V. *Chem. Commun.* **2011**, *47* (13), 3805.

(8) Lincheneau, C.; Duke, R. M.; Gunnlaugsson, T. *Org. Biomol. Chem.* **2012**, *10* (30), 6069.

(9) Butler, S. J. *Chem. Commun.* **2015**, *51* (54), 10879–10882.

(10) Aletti, A. B.; Gillen, D. M.; Gunnlaugsson, T. *Coord. Chem. Rev.* **2017**, 1–23.

(11) Yamada, T.; Shinoda, S.; Tsukube, H. *Chem. Commun.* **2002**, No. 11, 1218–1219.

(12) Masaki, M. E.; Paul, D.; Nakamura, R.; Kataoka, Y.; Shinoda, S.; Tsukube, H. *Tetrahedron* **2009**, *65* (12), 2525–2530.

(13) Kataoka, Y.; Paul, D.; Miyake, H.; Shinoda, S.; Tsukube, H. *Dalt. Trans.* **2007**, No. 26, 2784.

(14) Shinoda, S.; Tsukube, H. *Analyst* **2011**, *136* (3), 431–435.

(15) Di Bernardo, P.; Choppin, G. R.; Portanova, R.; Zanonato, P. L. *Inorganica Chim. Acta* **1993**, *207* (1), 85–91.

(16) Cassol, A.; Di Bernardo, P.; Portanova, R.; Tolazzi, M.; Zanonato, P. L. *Inorganica Chim. Acta* **1997**, *262* (1), 1–8.

(17) De Namor*, A. F. D.; Chahine, S.; Jafou, O.; Baron, K. *J. Coord. Chem.* **2003**, *56* (14), 1245–1255.

(18) Di Bernardo, P.; Melchior, A.; Tolazzi, M.; Zanonato, P. L. *Coord. Chem. Rev.* **2012**, *256* (1–2), 328–351.

(19) Di Bernardo, P.; Zanonato, P. L.; Melchior, A.; Portanova, R.; Tolazzi, M.; Choppin, G. R.; Wang, Z. *Inorg. Chem.* **2008**, *47* (3), 1155–1164.

(20) Viswanadhan, V. N.; Ghose, A. K.; Singh, U. C.; Wendoloski, J. J. *J. Chem. Inf. Comput. Sci.* **1999**, *39* (2), 405–412.

(21) Di Bernardo, P.; Zanonato, P. L.; Benetollo, F.; Melchior, A.; Tolazzi, M.; Rao, L.

Inorg. Chem. **2012**, *51* (16), 9045–9055.

(22) Oomen, E. W. J. L.; van Dongen, A. M. A. *J. Non. Cryst. Solids* **1989**, *111* (2–3), 205–213.

(23) Reisfeld* †, R.; Zigansky, E.; Gaft, M. *Mol. Phys.* **2004**, *102* (11–12), 1319–1330.

(24) Piccinelli, F.; Bettinelli, M.; Melchior, A.; Grazioli, C.; Tolazzi, M. *Dalt. Trans.* **2015**, *44* (1), 182–192.

(25) Bünzli, J.-C. G.; Vuckovic, M. M. *Inorganica Chim. Acta* **1983**, *73* (C), 53–61.

(26) Piccinelli, F.; Melchior, A.; Speghini, A.; Monari, M.; Tolazzi, M.; Bettinelli, M. *Polyhedron* **2013**, *57*, 30–38.

(27) Buenzli, J. C. G.; Mabillard, C.; Yersin, J. R. *Inorg. Chem.* **1982**, *21* (12), 4214–4218.

CHAPTER FOUR: Sensing of Biologically relevant Anions

Introduction

The determination of metabolites and their concentration represents an important tool for the prevention and the battle against the cancer. An example is citrate, whose concentration variation has been observed in malignant prostate cancer tissue and provide the most consistent characteristic change in the onset and progression of prostate cancer[1]. Another important metabolite is the lactate due to the crucial role of this molecule in several fields such as clinical diagnostics, sports medicine, food industry and biotechnology[2]. In particular, lactate is strongly connected to several diseases. For example, when sepsis is suspected in a patient, it is recommended to measure the lactate concentration promptly[3]. Also, abnormally elevated lactate concentrations are revealed in subjects affected by Parkinson's disease[4] and high level of serum lactate are also connected to a severe liver pathology[5]. Furthermore, lactate is well known as a specific biomarker for specific types of cancers such as prostate and breast cancer[6]. Finally, the quantity of lactate in food can be used as an indicator of freshness, stability and storage quality, as high level of it can be synonymous of microbial contamination[7]. In this context, detection of the enantiomeric composition of L/D-lactate can reveal food adulterations, like the fraudulent addition of the synthetic racemate. The determination of lactate is typically based on enzymatic methods, using lactic acid dehydrogenase (LDH), coupled to absorption spectrophotometric analysis of NAD^+ or fluorimetric detection of NADH[8]. The sensitivity of methods can reach to almost 1 μM but, in each case, they require sample pre-treatment to avoid the interfering of other bio-molecules. Therefore, the constant need of low cost, simple, rapid, highly sensitive and reliable methods with enantiospecific response for quantification of lactate and other metabolites is not surprising.

Among all the possible alternative of non-enzymatic methods used for the determinations of lactate and others bio-molecules, the use of luminescent lanthanide complexes have an important role thanks to unique photo-properties of metal ions. The particular properties have been successfully used in bioassay analysis and more recently to design optical sensor for intracellular imaging[9].

Lanthanide complexes for sensing of bio-anions and bio-molecules (biological analytes)

The design of sensors based on lanthanide complexes follows the simple concept of alteration of emission properties, like luminescence intensity, excited-state lifetime and emission profile, through interaction with analytes. Different sensing strategies have been arisen from this concept and some of them are preferred for the detection of bio-anions and bio-molecules. They are:

- *Modulation of sensitization by Antenna-Ln distance.* The energy transfer occur between an acceptor and donator is always depending by the their distance. Same influence is found between Antenna and Lanthanide ion and it's used to modulate the final luminescence of complex during sensing of, for example, tartaric acid [10].
- *Modulation of the Antenna Excited State.* The strategy consists to modification of Antenna Excited State by using chemoselective reactions with the analytes which are in general small molecules, like hydrogen peroxide, nitric oxide or others[11].
- *Modulation of q (hydration number).* The approach permit to detect analytes by simply ligand exchange of water molecules coordinated to Lanthanide ion with the analyte. The substitution increase the total emission of complex due to remove of quenching vibrations of water from inner sphere of the metalion. This simple method is widely used for the detection of anions[12].
- *Modulation of CPL (Circularly Polarized Luminescence).* The Lanthanide ions have the ability to give easily Circularly Polarized Luminescence (CPL) when they are surround by a chiral environment. The CPL activity is measured by the dissymmetry factor g_{em}

$$g_{em} = \frac{2(I_L - I_R)}{I_L + I_R}$$

where I_L and I_R are the left and right circularly polarized component of the radiation emitted by the lanthanide. The g_{lum} is depended on the geometry and symmetry of the complex which can be strongly modified with by interaction of chiral analytes like, amino acids or protein[13,14].

Among all the approaches cited above, the latter, modulation of CPL, is the most sensitive and it possesses several other advantages respect to total luminescence. Parker et al. have recently demonstrate how the CPL of chiral lanthanide complex can improve the spatial resolution in bio-imaging[15] and how it can use instead of total emission for the quantification of metabolites[16]. All these promising results encouraged the scientific community to investigate more deeply the CPL properties of lanthanide complexes and how it can be used for investigation of chirality of molecules and for the detection of bio-molecules.

In the CPL sensing experiment, the g_{lum} factor is used in order to investigate the interaction between analyte and lanthanide complex. Two main examples are worth to be underlined:

- *Perturbation of a dynamically racemic complexes*. Some Ln(III) complexes with achiral ligand have the properties to exist as dynamic racemic mixture with Δ and Λ helicity at the metal in solution. The no predominance of one enantiomeric form over the other assures a perfect counterbalancing of the chiroptical properties and no CD and CPL signals are detected. At this point, a chiral analytes may interact with ground state of complexes through outer sphere interactions forming diastereoisomeric species[17]. The interaction push the ground state equilibrium out from racemic condition carrying the preferential formation of one diastereoisomeric species. This perturbation is often referred to as the "Pfeiffer effect"[18] and guarantee an enantiomeric excess in the ground state that can be detected by the measurement of CD and CPL. Most of the investigation in this field were performed on $Ln(DPA)_3$ (DPA = 2,6-pyridine-dicarboxyate, Figure 1), where the negative charge of the complex promotes electrostatic interaction with analytes such as amino acids, etc., in outer coordination sphere[19]. Despite the numerous investigation carried out on the $Ln(DPA)_3$, only few information are available about the factors that influence the perturbation of the racemic equilibrium. Muller tried to fill this vacancy, by observing the effects of the small structural changings of the chiral analytes on CPL signal. Unfortunately, he didn't find any correlation unless that the presence of an

aromatic groups on the chiral analytes may influence the magnitude of the CPL signal[20].

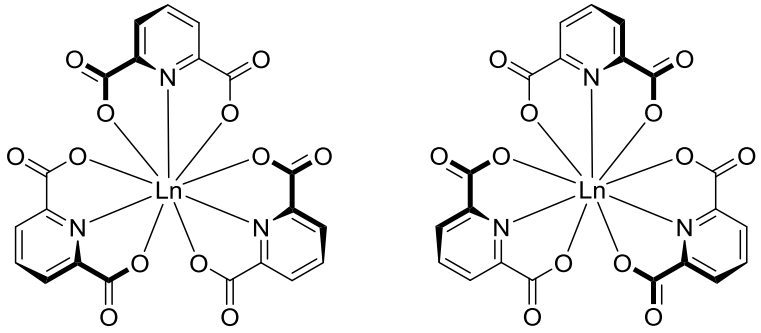

Figure 61 Structural representation of $Ln[DPA]_3^{3-}$, viewed along the trigonal symmetry axis

However, the Pfeiffer effect is not the only one possible process able to induce a chirality to a enatiomerics couple in dynamic equilibrium lanthanide complexes. the other possible process involve the excited state populations of the enantiomerc couple. More precisely, the process works through entatioselective quenching of one enatiomeric form of the complex by the use a chiral quencher. The final result is a time-dependent optically enriched excited state (in other word the excited state becomes chiral over time) and it can be analyzed using the time-resolved feature of the CPL instrumentation. Richardson was pioneer about the study of this process, and he has mainly used the $Ln(DPA)_3$[21] in his investigations.

- *Perturbation of a chiral complex based on an enantiopure ligand*. The simplest chirality insertion in lanthanide complexes is through use of enatiopure chiral ligands. This relative simple strategy has permitted to synthetize numerous chiral lanthanide complexes whose sensing properties have been deeply investigated for the development of CPL probes.

  Also in this case, the displacement of solvent molecules by analytes, (in general anions) gives rise to a change of inner coordination sphere of chiral lanthanide complex resulting in an altered CPL signature. Especially, this kind of approach furnishes more information respect to others investigation method such as NMR. An example was reported by Parker et al.[22] who studied sensing proprieties of Eu(III) complex of unsaturated chiral DOTA-

based macrocyclic (S,S,S)-**1** (Figure 2) towards a series of *O*-phosphorylated amino acid.

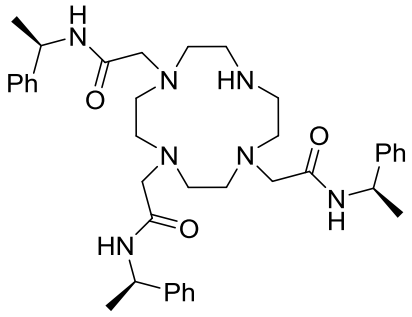

(S,S,S)-**1**

Figure 62 Chemical structure of ligand based on DOTA-macrocyclic derivatives.

The ^{1}H NMR spectra profile are the same for different amino acids. On the other hand, completely different CPL signatures have been observed for each amino acids[22]. This results demonstrate the strong sensitivity of the CPL techinique towards chirality.

Lanthanide complexes with enantiopure ligands can be used also for the detection of cations, such in the case of alkaline metal ions. The representative example is given by tretakis(+)-hfbc Europium complex. X-ray structure and chiroptical studies shown stereospecific formation of Δ configuration when cesium and sodium are used to counterbalance the negative charge of complexes. The stereospecific configuration is also preserved in solution thanks to presence of metal - - - CF_3 interaction how is show in Figure 3 that also influence chiral arrangement of four ligands by the alkaline metal size[23,24,25,26].

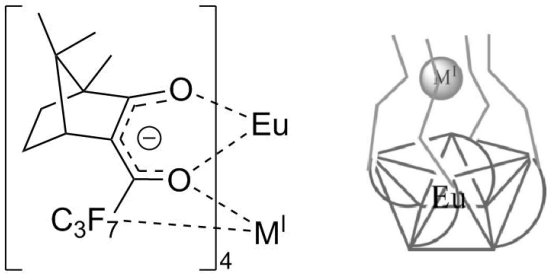

Figure 63 Chemical structure of M^{I} [Eu((+)-hfbc)$_4$] (left) and its proposed structure in solution (side view, right)

Aims of the study

The sensing of biomolecules is of great importance for diagnostic and for elucidation of possible processes occurring inside cells. In bio environment the chirality represents a common condition and can be investigated, by chiroptical methods. Among these methods the CD is widely used for the determination structural conformations of several biomolecules (like proteins) in the ground state. Chiral Lanthanide complexes are used for the sensing of chiral analytes and are mainly based on cyclen-ring in particular DOTA due to its easy functionalization and the high stability of its complexes. Their chiroptical properties have been deeply studied and their extraordinary sensing against lactate , citrate, etc. have been investigated.

In the present project, we have designed new chiral lanthanide-based complexes, alternative to DOTA-likeones, with potential application as sensors of chiral analyte or biomolecules. In this context, we rencetly studied the coordination chemistry of Eu(III) and Tb(III) ions with ligands carrying the chiral 1,2-diaminocyclohexane (DACH) backbone, which have been suitably modified to form stable complexes in water[27–30]. In particular, we obtained the water soluble Tb-complex ($[Tb(bpcd)(H_2O)_x]^+$, Figure 4) characterized by strong Tb-based CPL activity upon excitation of the ligand.[30] The chiral H_2bpcd (N,N′-bis(2-pyridylmethyl)-*trans*-1,2-diaminocyclohexane-N,N′-diacetic acid) (Figure 4), tightly binds Ln(III) ions, providing a dissymmetric environment, while at the same time leaving 2 - 3 sites available for binding to further ancillary ligands.

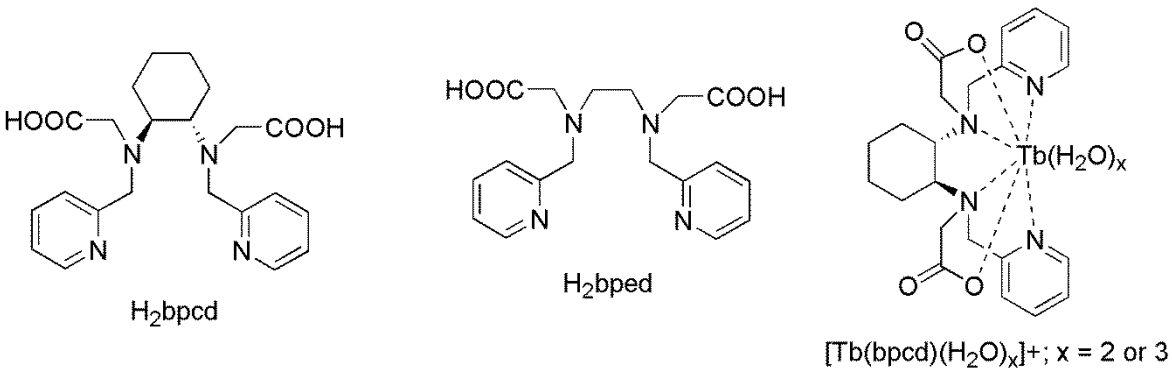

Figure 64 Ligands and complex discussed in the present work. The ligand H_2bpcd has been prepared in its (S,S), (R,R) and racemic forms. The two (or three) water molecules in the Tb(III) complex can be easily replaced by an analyte.

For all these reasons, the Tb-complex can be considered a valuable CPL probe for important analytes in aqueous media. In the present contribution we have investigated the optical and chiroptical response of the aforementioned Tb complex to L-lactate by means of TL and CPL spectroscopy. The same experiments have been also carried out on the analogous Tb complex of the achiral ligand H_2bped (Figure 4) in order to identify the role of the chiral DACH backbone on the optical and chiroptical luminescence signaling of L-lactate.

DFT calculations, which have been previously applied successfully to get structural and thermochemical data for *f*-block metal complexes,[28,31,32] are used in order to evaluate the relative stability of the 1:1 Tb(bpcd)/L-lactate adducts (CHAPTER TWO), when the ligand stereochemistry is (*S*,*S*).

Results

L-lactate sensing experiments: Total Luminescence

In figure 5, the evolution of the Total Luminescence emission spectra of the complex $[Tb(R,R\text{-bpcd})(H_2O)]^+$ upon addition of L-lactate is presented.

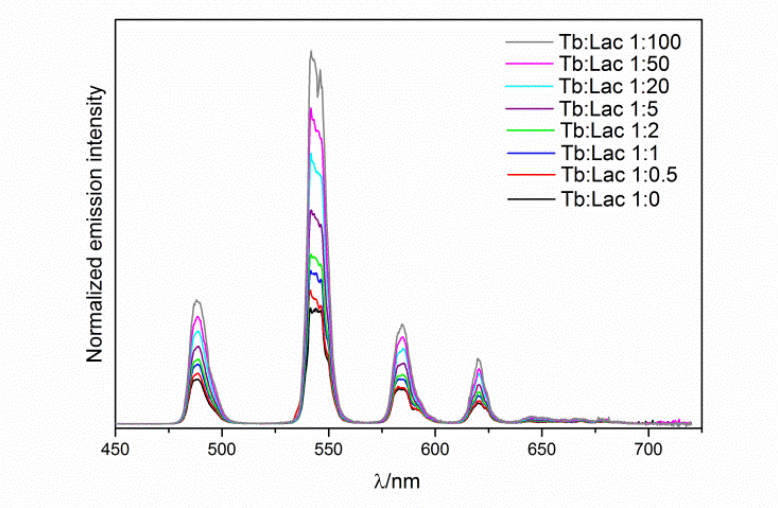

Figure 65 Evolution of the total luminescence emission spectra upon addition of the L-lactate anion, for complex $[Tb(R,R\text{-bpcd})(H_2O)_x]+$ (λ_{exc} = 270 nm).

Thanks to the excitation of the ligand around 270 nm followed by ligand to Tb(III) energy transfer, the typical visually green emission originating from the transition of the Tb(III) ion is collected (figure 5). Upon addition of L-lactate the intensity of all Tb(III) emission bands increases until reaching a plateau when the molar ratio between L-lactate and the metal is around 100. The same experiments have been carried out on the Tb(III) complexes of (S,S)-H_2bpcd and H_2bped ligands (Figure 4) and the increase of the relative emission intensity at 546 nm (the maximum of the $^5D_4 \rightarrow {}^7F_5$ band) as a function of the L-lactate molar ratio is shown in figure 6(a). In addition, the Tb(III) $^5D_4$ excited state lifetimes have been also measured after each addition of L-lactate. All the decay curves are well fitted to a single exponential function and the values of the observed lifetimes are reported as a function of the L-lactate molar ratio (Figure 6(b)). Upon interacting with the chiral anion, the two enantiomeric complexes give rise to a diastereomer pair, which we may shortly define (R,R)-L and (S,S)-L, and are characterized by potentially different photophysical properties.

(a)

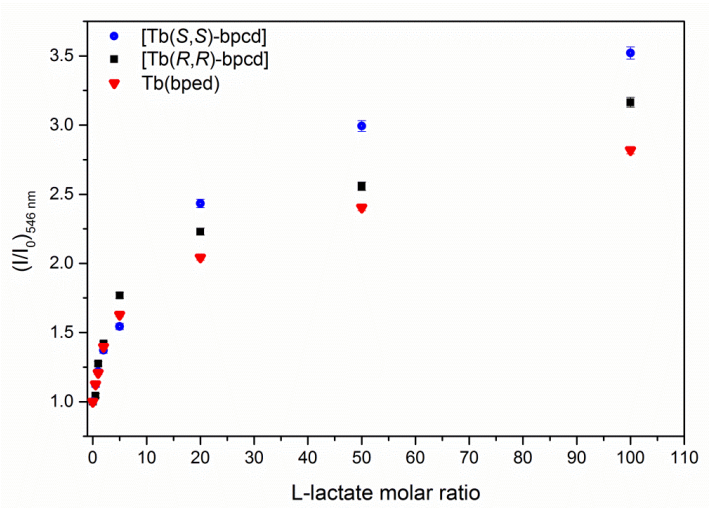

(b)

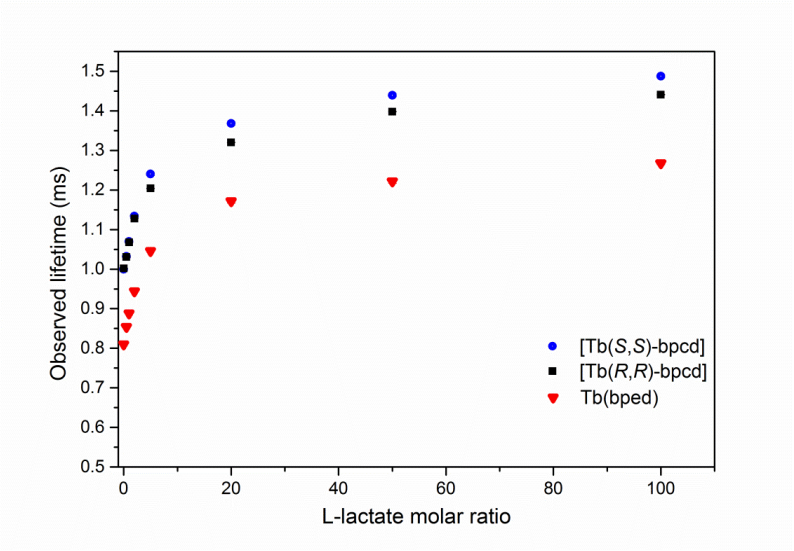

Figure 66 (a) Relative emission intensity at 546 nm and (b) Observed lifetime as a function of the L-lactate to metal molar ratio (L-lactate molar ratio) for Tb complexes with (S,S)-bpcd, (R,R)-bpcd and bped ligands (I_0 = emission intensity at 546 nm of the start

As far as the curve profile is concerned, for all the investigated complexes a logarithmic-like trend is observed both in figures 6a and 6b. As expected, the relative curves of the $[Tb(rac\text{-}bpcd)]^+$ (not reported) fall in the middle of the curves of the two enantiomers. For this reason, under this aspect the racemic complex will not be discussed further. Whilst the evolution of the lifetime values is very similar for the two enantiomeric complexes ($[Tb(S,S\text{-}bpcd)]^+$ and $[Tb(R,R\text{-}bpcd)]^+$), the increase of the relative intensity of the $^5D_4 \rightarrow {}^7F_5$ emission band (around 546 nm) is more sensitive to the presence of L-lactate in the case of the $[Tb(S,S\text{-}bpcd)]^+$

complex (Fig.6a). On the other hand, the achiral $[Tb(bped)]^+$ complex is less sensitive towards L-lactate and the observed lifetime during the titration experiment is always lower, in comparison with the lifetime values of the enantiomeric pair containing the bpcd ligand. The increase of both emission intensity and the observed lifetimes for all the complexes under investigation can be tentatively explained by assuming a replacement of the inner sphere water molecules by the target anion. This phenomenon should reduce the non-radiative quenching of the Tb(III) excited state caused by the presence in the close proximity of the metal ion of OH groups with high vibrational energy.[33] On the basis of a similar reasoning, the shorter observed lifetimes in the case of $[Tb(bped)]^+$ compound, can be ascribed to the presence of a higher number of water molecules close to the metal ion.

In order to ascertain this point, the decay curves of the Tb(III) $^5D_4$ excited state in H_2O and D_2O for $[Tb(bped)]^+$ complex, are shown in figure 7.

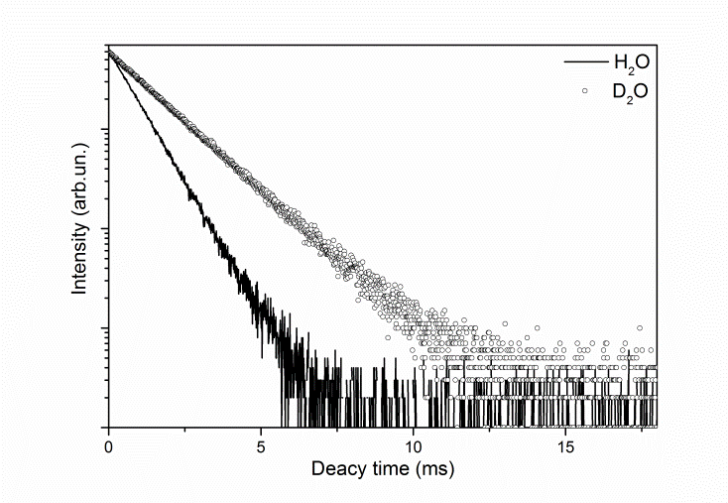

Figure 67 Luminescence decay curves from $^5D_4$ excited state of Tb(III) in $[Tb(bped)]^+$ complex in H_2O and D_2O (1mM, λ_{exc} = 270 nm, λ_{em} = 546 nm)

The curves, well fitted to a single exponential, present a decay constant of 0.81(1) ms and 1.55(1) ms in water and D_2O, respectively. The number of water molecules in the close proximity to the metal ion (hydration number) was calculated by the Horrock's equation.[34,35] As this number [2.5(5)] is the same as the one calculated previously for $[Tb(rac\text{-}bpcd)]^+$ complex (2.6(5)),[30] (CHAPTER TWO) the reason of the aforementioned discrepancy should be sought elsewhere and this point will be discussed in detail later in this contribution.

Finally, the binding constants between L-lactate and $[Tb(bpcd)]^+$ and $[Tb(bped)]^+$complexes have been calculated by the Benesi–Hildebrand method.[36] In Figure 8, the plot of $I_0/(I_0 - I)$ vs. $[L\text{-lactate}]^{-1}$ for the $[Tb(S,S\text{-bpcd})]^+$ complex, shows a good linear relationship, characteristic of 1:1 binding. The binding constant can be calculated from the ratio of intercept/slope,[37] and its value is 22.6(1) M^{-1}. The same calculation performed on the $[Tb(R,R\text{-bpcd})]^+$ and $[Tb(bped)]^+$ complexes (data not shown) provide similar binding constants [28.6(1) and 28.2(1) M^{-1}, respectively]. In the light of these results, the adduct between L-lactate and the enantiomeric pair of complexes reveals a similar stability, slightly higher in the case of the (R, R) isomer.

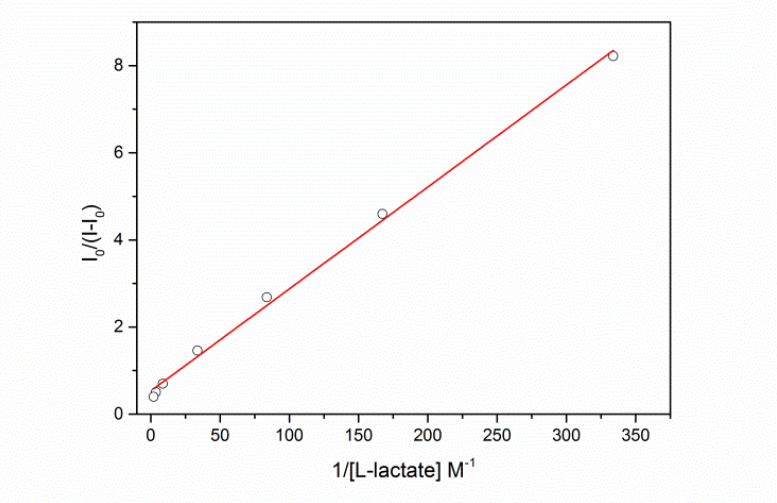

Figure 68 Benesi–Hildebrand plot against $[L\text{-lactate}]^{-1}$ for the $[Tb(S,S\text{-bpcd})]^+$ complex. I_0 is the emission intensity at 546 nm of the starting complex; I is the emission intensity at 546 nm of the L-lactate:complex adduct after each addition of the analyte.

The ITC output during the titration of a $[Tb(rac\text{-bpcd})]^+$ solution with the L-lactate solution is reported in Figure 9a (the area of the peaks corresponds to $Q_{ex,j}$). In Figure 9b the total heat evolved at the j^{th} injection[2] ($Q_{cum,j}$) is reported along with the values calculated with the logK and □H values reported in Table 1.

[2] $Q_{cum,j} = \sum_1^j Q_{obs,j}$

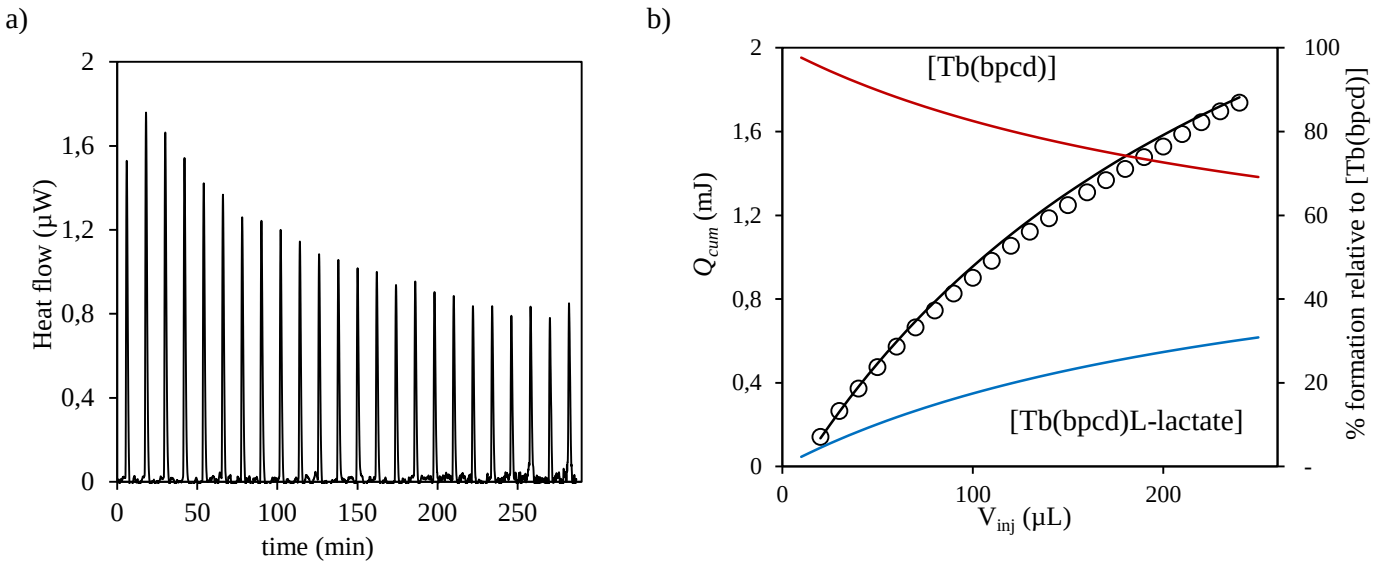

Figure 69 a) ITC titration raw output signal (positive sign here corresponds to an exothermic reaction) the obtained Qex have been subtracted by the heat obtained by the dilution experiment with a L-lactate solution at the same concentration (titration conditions in Methods section); b) experimental (circles) and calculated (solid line) cumulative heat ($Q_{cum,j} = \sum_1^j Q_{obs,j}$) vs. total added lactate volume (V_{inj}). The calculated speciation is also shown.

Both, enthalpy and entropy for the formation of [Tb(rac-bpcd)L-lactate] are positive, which is often found in charge neutralization reactions in aqueous solutions.[38,39] The obtained formation constant is in good agreement with that obtained by fluorimetric titration and very similar to the third stepwise formation constant of [Tb(L-lactate)$_3$] and [Eu(L-lactate)$_3$] complexes (Table 1).[40–42]

Table 12 Equilibrium constant and thermodynamic parameters for the formation of [Tb(rac-bpcd)L-lactate] complex (T = 298.15 K, I=0.1 M NaCl), determined through ITC. Stepwise formation constants for the reaction [Ln(Lactate)$_2$]+Lactate ⇆[Ln(Lactate)$_3$] with Ln = Eu^{3+}, Tb^{3+} (T = 298.15K, I=0.2M $NaClO_4$,[40] 0.1M NaCl).[41,42] Charges omitted for clarity

Reaction	**logK**	**ΔG (kJ mol^{-1})**	**ΔH (kJ mol^{-1})**	**ΔS (J mol^{-1}) K^{-1}**
[Tb(rac-bpcd)] + L-lactate⇆[Tb(rac-bpcd)L-lactate]	1.30(9) 1.35/1.45*	-7.0(1) -7.7 /-8.3	14.44(5) -	72.4(1) -
[Tb(lactate)$_2$] + Lactate ⇆ [Tb(lactate)$_3$]	1.18[40]	-6.7	-	-
	1.15[41]	-6.6	-	-
[Eu(lactate)$_2$] + Lactate ⇆ [Eu(lactate)$_3$]	1.3[42]	-7	-	-
***from fluorimetric titration**				

Previously we demonstrated that the complex with bpcd is present in two forms energetically equivalent (trans-O,O and trans-N$_{py}$, N$_{py}$). The formation of the

ternary complex with lactate implies the removal of two water molecules from these species to produce final complexes where the lanthanide is completely dehydrated and the lactate act as chelate, as suggested by the longer luminescence lifetimes measured when increasing the lactate/Tb molar rations. The lactate anion can chelate lanthanides either through the carboxylate group or the hydroxo/carboxylate oxygens.[43] Furthermore, it has been proposed[42] that in $[Eu(lactate)]^{2+}$ complex the anion is coordinated through carboxyl oxygen and with the deprotonated hydroxyl group (hydroxylate). On the contrary, hydroxyl group was considered protonated in the $[Eu(lactate)_2]^{+}$ and $[Eu(lactate)_3]$ species.[42,43] We calculated the minimum energy structures for the two possible chelation modes of the stable coordination isomers with the Y(III) ion (Figure 10) considering the ligand in (S,S) configuration and the hydroxyl group to be protonated. The Y-O (lactate) bond lengths reported in Table 2 show that the carboxylate group interacts more strongly with $[Y(S,S\text{-}bpcd)]^{+}$ unit when the coordination occurs both through the carboxylate and hydroxyl groups as it presents a shorter average Y-O bond distance with respect to the other coordination mode. The calculated energy difference in gas phase and PCM solvent for the a-d isomers (Table 6 in Appendix) also indicates that the carboxyl- hydroxyl coordination is more favored. The trans-O,O isomers have been also studied in presence of 4 explicit water molecules (Figure 10 e, f). The Y-O bond distance is further reduced in the e isomer, and it results that the hydroxyl group is hydrogen bonded to an outer sphere water molecule. On the contrary, the Y-O bond is slightly elongated in the f isomer with respect to b structure. The ΔE calculated is still favorable to the hydroxo- carboxy- coordination, in agreement with previous results found for the $[La(lactate)_n]^{3-n}$ complexes (Table 6 in Appendix).

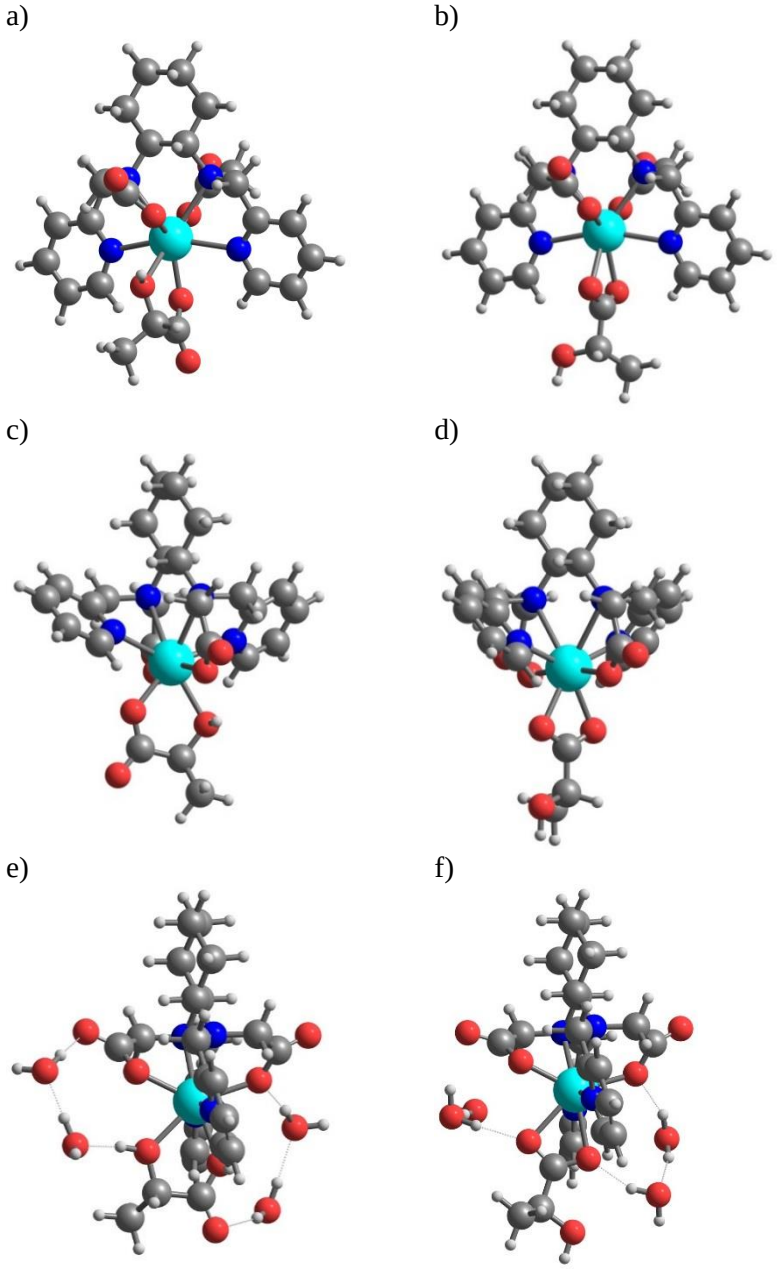

Figure 70 Minimum energy structures of the [Y(S,S-bpcd)L-lactate] complex. trans-O,O isomer: a) Ohydoxo, O carboxy chelate, b) lactate Ocarboxy chelate. trans-Npy, Npy isomer: c) lactate Ohydoxo, Ocarboxy chelate, d) lactate Ocarboxy chelate. Structures e) and and f) correspond to structures a) and b) optimized with 4 additional solvation water molecules

Table 13 Y-O distances (Å) for the structures reported in Figure 10. For the structures b, d and f the average Y-O distance is reported

Structure	Ln-$O_{carboxy}$	Ln-$O_{hydroxo}$
a	2.274	2.505
b	2.450	-
c	2.219	2.452
d	2.352	-
e	2.250	2.428
f	2.482	-

L-lactate sensing: Circularly Polarized Luminescence

As previously observed in CHAPTER TWO, the Tb(III) complex with the chiral ligand bpcd shows a strong CPL activity (value for g_{lum} around 0.07 at the peak of the 546 nm band).[30] The change of the CPL signal during the titration with L-lactate is shown in Figure 11, for both enantiomers and for the racemic complexes.

(a)

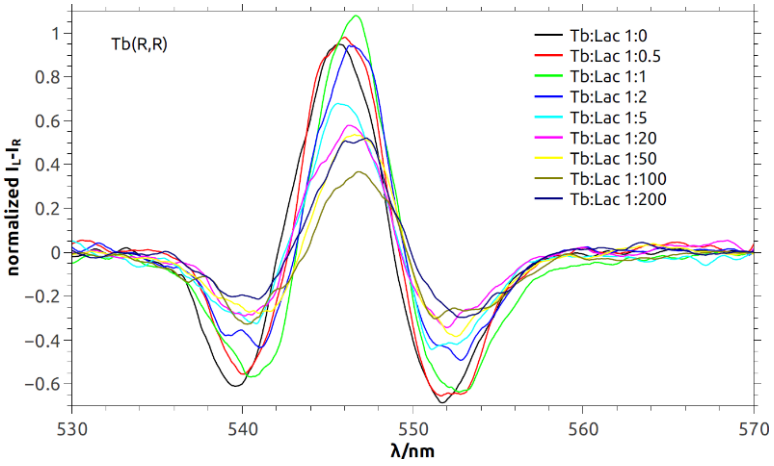

(b)

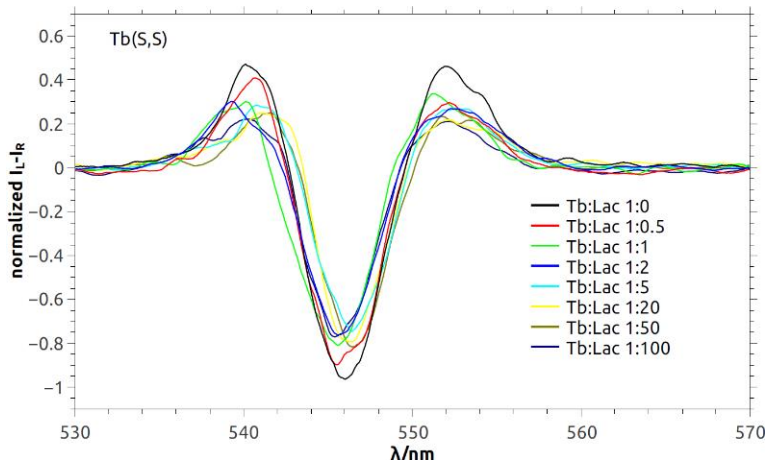

(c)

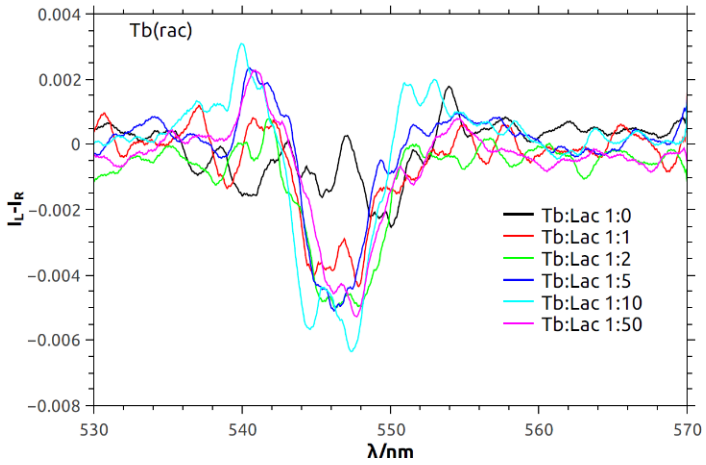

Figure 71 Normalized CPL spectra of [Tb(bpcd)]$^+$ complex upon addition of L-lactate for (a) the ligand with (R,R) stereochemistry, (b) the ligand with (S,S) stereochemistry and (c) the racemic ligand. All the CPL spectra relative to the enantiopure complexes are normalized to the first titration point (namely the 1:0 case)

Figure 11 shows a close-up relative to the $^5D_4 \rightarrow {}^7F_5$ multiplet, whose multiplicity becomes partly resolved, in contrast to the TL counterpart, thanks to some sign alternation of the dichroic signal. For both enantiomers of the complex, upon addition of the target anion, the dichroic signal decreases: this means that the adduct with lactate is at the same time more emissive (see Figure 6) but less CPL-active. This decrease is more prominent for the complex with (R,R) stereochemistry. In fact, the value of CPL at 546 nm, normalized to the total emission, shows a 50 % variation from 0 to 100 equivalents of L-lactate added, while in the case of the complex with (S,S) stereochemistry the variation is only around 17%. In addition, the g_{lum} factor reaches a constant value upon the addition addition of L-lactate in 20-50 eq. excess. During the titration of the racemic complex [Tb(rac-bpcd)]$^+$, L-lactate interacts with one enantiomer as much as it does with the other one, on account of the very similar binding constants found in the previous section. This means that free (R,R) and (S,S) yield to the bound diastereomer pair (R,R)-L and (S,S)-L to the same extent. i.e. the ratios (R,R):(S,S) and (R,R)-L:(S,S)-L remain both constantly close to unity. The CPL signals of the two enantiomers of the free complexes will perfectly balance and cancel out. On the contrary, for the diastereomeric adducts, being (S,S)-L more emissive than (R,R)-L and at the same time the latter less CPL-active than the former one, the total CPL signals do not cancel and we must expect that the signal of (S,S)-L diastereomer dominates, which

is exactly what we observed (Figure 11c). The differences in TL (including lifetimes) and CPL for pair (R,R)-L and (S,S)-L witness the significant variations in the first coordination sphere for the two diastereomers, possibly both in terms of water coordination and of geometry. As previously documented,[30] the ligands bped and bpcd show similar protonation constants and, as far as the stabilities of the respective Gd(III) and Eu(III) complexes are concerned, similar formation constants are measured. From a stereochemical point of view, both bped and rac-bpcd can generate a pair of similar enantiomeric complexes: **λ** and **δ** conformations, for the dynamically racemic $[Ln(bped)]^+$ and (R,R) + (S,S) configurations, for $[Ln(rac\text{-}bpcd)]^+$ (Figure 12). The co-presence of the **λ** and **δ** conformations in solution is supported by DFT calculations carried out for [Ln(bped)L-lactate] complex which predict a similar stability of the **λ**-L and **δ**-L adducts and the possibility of fast interconversion (Figure 21 in Appendix).

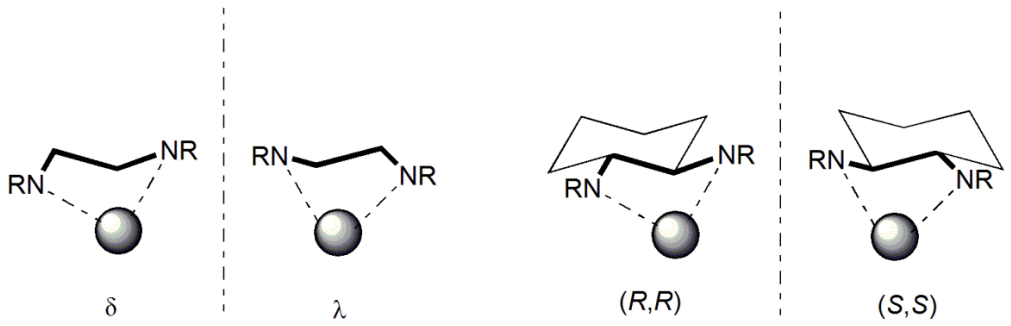

*Figure 72 **λ** and **δ** enantiomers of bped-based complexes (left) and (R,R) and (S,S) enantiomers of rac-bpcd-based complexes (right).*

All this suggests both a similar coordination chemistry of these ligands and similar optical and chiroptical response towards L-lactate. Surprisingly, the titration of $[Tb(bped)]^+$ complex with L-lactate does not produce any CPL activity (Figure 13), this could be related to the distribution of the different isomers in rapid equilibrium, as suggested by the small energy differences in Figure 21 in Appendix. In order to deepen the reasons for such different behavior, we decided to investigate in detail the coordination geometry of the metal ion bound to bped and bpcd ligands. In this context, Eu(III) is considered a valuable structural probe as its *f-f* luminescence is strongly connected with the site symmetry of the metal ion.

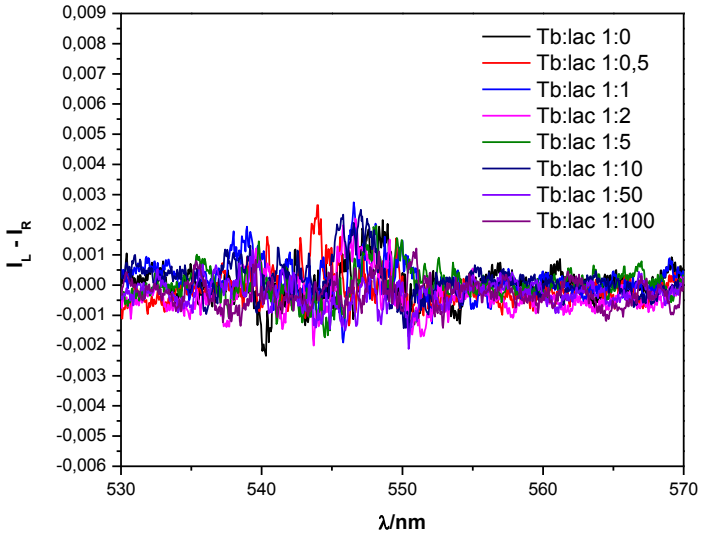

Figure 73 Normalized CPL spectrum of [Tb(bped)]$^+$ complex upon addition of L-lactate

As the ionic size of Tb(III) and Eu(III) are quite similar, all the structural conclusion arising from the Eu(III) luminescence in the bped and bpcd-based complexes can be extended to their analogues of Tb(III). In this context, the synthesis of [Eu(rac-bpcd)]$^+$ and [Eu(bped)]$^+$ complexes was performed and their luminescence emission spectra were collected in aqueous solution (Figure 14).

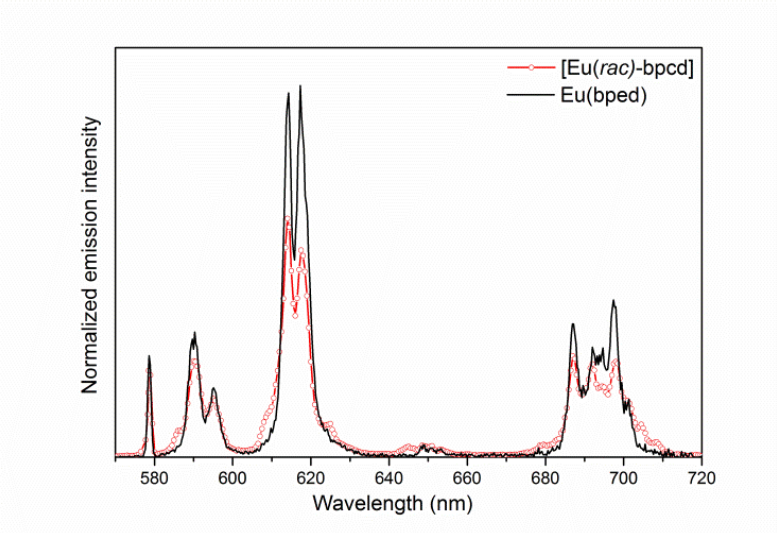

Figure 74 Luminescence emission spectra of [Eu(rac-bpcd)]$^+$ (red circles) and [Eu(bped)]$^+$ (black line) complexes, normalized to the area of the $^5D_0 \rightarrow {}^7F_1$ band, both 1mM in water upon excitation at 270 nm.

As previously reported from the inspection of the $[Eu(rac\text{-}bpcd)]^+$ luminescence emission spectrum,[30] a C_1 point symmetry of the metal ion is suggested. Since the emission spectrum of $[Eu(bped)]^+$ is similar to the one of $[Eu(rac\text{-}bpcd)]^+$, the same point symmetry of the metal ion can be assumed in both complexes. Nevertheless, the two luminescence emission spectra show one significant difference: the value of the asymmetry ratio[44,45]:

$$R = \frac{I(^5D_0 \rightarrow {}^7F_2)}{I(^5D_0 \rightarrow {}^7F_1)}$$

which is related to the degree of asymmetry of the coordination polyhedron around the Eu(III) ion. R is 2.72 for $[Eu(rac\text{-}bpcd)]^+$ and 3.48 for $Eu(bped)]^+$. We strongly believe that the different chiroptical behavior detected during the titration of $[Tb(rac\text{-}bpcd)]^+$ and $[Tb(bped)]^+$ with L-lactate could be related with the different coordination geometry connected with the degree of distortion of their metal coordination sphere. The same reasoning can be adopted in order to justify the discrepancy of the decay constants (see above) during the same titration experiments.

With a view of possible practical applications, we investigated the behavior of $[Tb(rac\text{-}bpcd)]^+$ in a complex L-lactate-based matrix. We used a commercial Ringer's lactate solution (Fresenius Kabi) used in common clinical practice to treat metabolic acidosis and to replace electrolytes and fluids after blood losses. This solution contains sodium L-lactate (28.3 mM) in water alongside with NaCl (6.0 g/L), KCl (0.40 g/L) and $CaCl_2 \cdot 2H_2O$ (0.27 g/L). By adding to this solution $[Tb(rac\text{-}bpcd)]^+$ to obtain a 5 mM solution (1:5.4/Tb(bpcd):L-lactate). As expected, this solution shows a CPL spectrum (Figure 15) in agreement with the titration curves (Figure 11c), both in terms of shape and intensity ($g_{lum} \sim 6 \cdot 10^{-3}$), thus suggesting the selectivity of $[Tb(rac\text{-}bpcd)]^+$ towards the target anion even in real complex matrices.

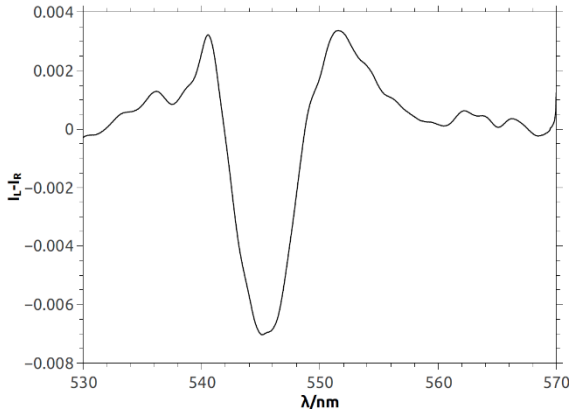

Figure 75 CPL spectrum of [Tb(rac-bpcd)]+ (5 mM) in a commercial Ringer's lactate solution

Conclusion

By means of a combination of techniques, we demonstrated that lactate reversibly binds $[Tb(bpcd)]^+$ complex, displacing the water molecules completing Tb(III) coordination sphere in the pristine complex. The$[Tb(bpcd)]^+$ complex is chiral, as it incorporates trans-1,2-diaminocyclohexane, which is commercially available and rather inexpensive in both enantiomeric forms. The two enantiomers of Tb(bpcd) bind L-lactate to a very similar extent, but the luminescence lifetimes for the two diastereomeric adducts (R,R)-L and (S,S)-L are very different, possibly on account of different geometries or different dynamics around the emitting center.

The formation constant of the ternary [Tb(rac-bpcd)L-lactate] complex has been determined both by luminescence titration and isothermal titration calorimetry. The data obtained by the two independent techniques are in good agreement and show that the L-lactate interacts weakly with the complex (logK = 1.3 - 1.45). The associated enthalpy and entropy terms, both positive, are also compatible with the complex formation between charged species in water. Theoretical calculations suggest that the most likely coordination mode is that involving the hydroxyl group.

The use of $[Tb(bped)]^+$ and $[Tb(rac\text{-}bpcd)]^+$ complexes as chiroptical luminescent probes of L-lactate underlines the peculiar role of the chiral DACH backbone: the target anion is capable to induce CPL activity from the racemic mixture of Tb complexes containing DACH-based ligand [figure 11c, $[Tb(rac\text{-}bpcd)]^+$] but not from $[Tb(bped)]^+$ complex (figure 21 in Appendix). This evidence is connected with the different CPL activity of the two diastereomeric adducts, being (R,R)-L less CPL-active than (S,S)-L.

Our findings would lend themselves to the development of an analytical assay based on Tb luminescence in the visible. Moreover, thanks to the differential quantum yield of the two diastereomeric species (R,R)-L and (S,S)-L, one can use the racemic complex to reveal L-lactate by measuring the induced CPL spectrum. Interestingly this has been demonstrated in a commercial complex solution for medical use, containing several electrolytes, namely Ringer's lactate. The results reported here are encouraging, although the light-absorption features of the ligand and consequently the excitation spectrum of the complex are not ideal for practical

uses, because they require hard UV excitation. We prospect that by manipulating the pyridine chromophore softer excitation can be obtained.

Bibliography

(1) Costello, L. C.; Franklin, R. B. *Mol. Cancer* **2006**, *5* (1), 17.

(2) Azzouzi, S.; Rotariu, L.; Benito, A. M.; Maser, W. K.; Ben Ali, M.; Bala, C. *Biosens. Bioelectron.* **2015**, *69*, 280–286.

(3) Dellinger, R. P.; Levy, M. M.; Rhodes, A.; Annane, D.; Gerlach, H.; Opal, S. M.; Sevransky, J. E.; Sprung, C. L.; Douglas, I. S.; Jaeschke, R.; Osborn, T. M.; Nunnally, M. E.; Townsend, S. R.; Reinhart, K.; Kleinpell, R. M.; Angus, D. C.; Deutschman, C. S.; Machado, F. R.; Rubenfeld, G. D.; Webb, S.; Beale, R. J.; Vincent, J.-L.; Moreno, R. *Intensive Care Med.* **2013**, *39* (2), 165–228.

(4) Henchcliffe, C.; Shungu, D. C.; Mao, X.; Huang, C.; Nirenberg, M. J.; Jenkins, B. G.; Beal, M. F. *Ann. N. Y. Acad. Sci.* **2008**, *1147* (1), 206–220.

(5) Feldman, A. G.; Sokol, R. J.; Hardison, R. M.; Alonso, E. M.; Squires, R. H.; Narkewicz, M. R. *J. Pediatr.* **2017**, *182*, 217–222.e3.

(6) Lupo, J. M.; Chen, A. P.; Zierhut, M. L.; Bok, R. A.; Cunningham, C. H.; Kurhanewicz, J.; Vigneron, D. B.; Nelson, S. J. *Magn. Reson. Imaging* **2010**, *28* (2), 153–162.

(7) Gyawali, R.; Ibrahim, S. a. *Emirates J. Food Agric.* **2012**, *24* (1), 1–11.

(8) Li, Y.-S.; Ju, X.; Gao, X.-F.; Zhao, Y.-Y.; Wu, Y.-F. *Anal. Chim. Acta* **2008**, *610* (2), 249–256.

(9) Hagan, a. K.; Zuchner, T. *Anal. Bioanal. Chem.* **2011**, *400* (9), 2847–2864.

(10) Harte, A. J.; Jensen, P.; Plush, S. E.; Kruger, P. E.; Gunnlaugsson, T. *Inorg. Chem.* **2006**, *45* (23), 9465–9474.

(11) Thibon, A.; Pierre, V. C. *J. Am. Chem. Soc.* **2009**, *131* (2), 434–435.

(12) Dickins, R. S.; Aime, S.; Batsanov, A. S.; Beeby, A.; Botta, M.; Bruce, J. I.; Howard, J. A. K.; Love, C. S.; Parker, D.; Peacock, R. D.; Puschmann, H. *J. Am. Chem. Soc.* **2002**, *124* (43), 12697–12705.

(13) Heffern, M. C.; Matosziuk, L. M.; Meade, T. J. *Chem. Rev.* **2014**, *114* (8), 4496–4539.

(14) Carr, R.; Di Bari, L.; Lo Piano, S.; Parker, D.; Peacock, R. D.; Sanderson, J. M. *Dalt. Trans.* **2012**, *41* (42), 13154.

(15) Frawley, A. T.; Pal, R.; Parker, D. *Chem. Commun.* **2016**, *52* (91), 13349–13352.

(16) Shuvaev, S.; Starck, M.; Parker, D. *Chem. - A Eur. J.* **2017**, *23* (42), 9974–9989.

(17) Brittain, H. G. *J. Coord. Chem.* **1989**, *20* (4), 331–347.

(18) Donato, H.; Martin, R. B. *J. Am. Chem. Soc.* **1972**, *94* (12), 4129–4131.

(19) Huskowska, E.; Riehl, J. P. *Inorg. Chem.* **1995**, *34* (22), 5615–5621.

(20) Muller, G.; Riehl, J. P. *J. Fluoresc.* **2005**, *15* (4), 553–558.
(21) Metcalf, D. H.; Bolender, J. P.; Driver, M. S.; Richardson, F. S. *J. Phys. Chem.* **1993**, *97* (3), 553–564.
(22) Atkinson, P.; Bretonnière, Y.; Parker, D.; Muller, G. *Helv. Chim. Acta* **2005**, *88* (3), 391–405.
(23) Lunkley, J. L.; Shirotani, D.; Yamanari, K.; Kaizaki, S.; Muller, G. *J. Am. Chem. Soc.* **2008**, *130* (42), 13814–13815.
(24) Carr, R.; Evans, N. H.; Parker, D. *Chem. Soc. Rev.* **2012**, *41* (23), 7673.
(25) Muller, G. *Dalt. Trans.* **2009**, No. 44, 9692.
(26) Tsukube, H.; Shinoda, S. *Chem. Rev.* **2002**, *102* (6), 2389–2404.
(27) Piccinelli, F.; Melchior, A.; Speghini, A.; Monari, M.; Tolazzi, M.; Bettinelli, M. *Polyhedron* **2013**, *57*, 30–38.
(28) Piccinelli, F.; Bettinelli, M.; Melchior, A.; Grazioli, C.; Tolazzi, M. *Dalt. Trans.* **2015**, *44* (1), 182–192.
(29) Piccinelli, F.; Leonzio, M.; Bettinelli, M.; Melchior, A.; Faura, G.; Tolazzi, M. *Inorg. Chim. Acta* **2016**, *453*, 751–756.
(30) Leonzio, M.; Melchior, A.; Faura, G.; Tolazzi, M.; Zinna, F.; Di Bari, L.; Piccinelli, F. *Inorg. Chem.* **2017**, *56* (8), 4413–4421.
(31) Mendonça, A. C.; Martins, A. F.; Melchior, A.; Marques, S. M.; Chaves, S.; Villette, S.; Petoud, S.; Zanonato, P. L.; Tolazzi, M.; Bonnet, C. S.; Tóth, É.; Di Bernardo, P.; Geraldes, C. F. G. C.; Santos, M. A. *Dalt. Trans.* **2013**, *42* (17), 6046.
(32) Endrizzi, F.; Melchior, A.; Tolazzi, M.; Rao, L. *Dalton Trans.* **2015**, *44* (31).
(33) Bünzli, J.-C. G.; Eliseeva, S. V. Springer, Berlin, Heidelberg, 2010; pp 1–45.
(34) Horrocks, W. D. W.; Sudnick, D. R. *J. Am. Chem. Soc.* **1979**, *101* (2), 334–340.
(35) Supkowski, R. M.; Horrocks, W. D. W. *Inorganica Chim. Acta* **2002**, *340*, 44–48.
(36) Benesi, H. A.; Hildebrand, J. H. *J. Am. Chem. Soc.* **1949**, *71* (8), 2703–2707.
(37) Arunkumar, E.; Ajayaghosh, A.; Daub, J. *J. Am. Chem. Soc.* **2005**, *127* (9), 3156–3164.
(38) Di Bernardo, P.; Melchior, A.; Tolazzi, M.; Zanonato, P. L. *Coord. Chem. Rev.* **2012**, *256* (1–2), 328–351.
(39) Bianchi, A.; Calabi, L.; Corana, F.; Fontana, S.; Losi, P.; Maiocchi, A.; Paleari, L.; Valtancoli, B. *Coord. Chem. Rev.* **2000**, *204* (1), 309–393.
(40) Deelstra, H.; Verbeek, F. *Anal. Chim. Acta* **1964**, *31*, 251–257.
(41) Nilsson, M.; Nash, K. L. *Solvent Extr. Ion Exch.* **2007**, *25* (6), 665–701.

(42) Barkleit, A.; Kretzschmar, J.; Tsushima, S.; Acker, M. *Dalton Trans.* **2014**, *43* (29), 11221–11232.

(43) Roy, L. E.; Martin, L. R. *Dalt. Trans.* **2016**, *45* (39), 15517–15522.

(44) Oomen, E. W. J. L.; van Dongen, A. M. A. *J. Non. Cryst. Solids* **1989**, *111* (2–3), 205–213.

(45) Reisfeld* †, R.; Zigansky, E.; Gaft, M. *Mol. Phys.* **2004**, *102* (11–12), 1319–1330.

Experimental Section

Synthesis of ligands

Synthesis of imine ligand

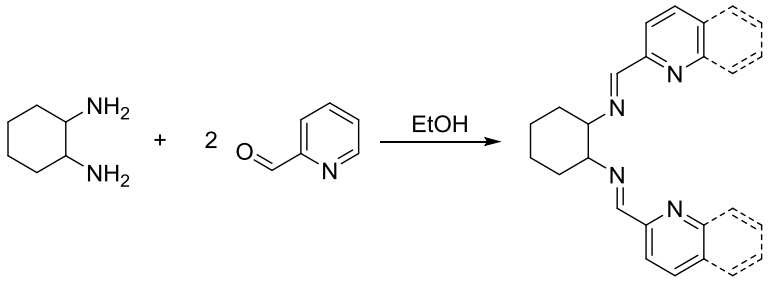

Synthesis of N,N'-(cyclohexane-1,2-diyl)bis(1-(pyridin-2-yl)methanimine). In a flask containing an ethanol solution (2mL) with 1,2-diamminocyclohexane (1.3 gr, 0.01167 mol), a ethanolic solution (2 mL) of pyridine-2-carbaldehyde (2.5 gr, 0.023 mol) has been slowly added at 0°C. After the adding, the ice-bath has been removed to establish the room temperature for over-night. The white product precipitating has been filtered and washed three time with cold ethanol (5 mL). To increase the yield the ethanol solution can be concentrated to obtain other precipitate. White solid. Yield 75%. ^{1}H NMR (600 MHz, $CDCl_3$) δ (ppm): 8.53 (d, *J* = 4.5 Hz, 2H), 8.30 (s, 2H), 7.87 (d, *J* = 7.9 Hz, 2H), 7.63 (t, *J* = 7.3 Hz, 2H), 7.20 (dd, *J* = 6.7, 5.4 Hz, 2H), 3.58 – 3.47 (m, 2H), 1.91 – 1.73 (m, 6H), 1.57 – 1.42 (m, 2H). ^{13}C (50 MHz, $CDCl_3$) δ (ppm): 161, 154, 149, 136, 124, 121, 73, 32, 24. LC-MS: m/z 293[M+1]. IR (KBr pellet): ν = 1645 (N=C imine strech), 1585 (pydine stretch), 1566 (pydine stretch), 1467 (pydine stretch), 1434 (pydine stretch), 1434 (pydine stretch), 791 (pydine stretch), 769 (pydine stretch), 993 (pyridine bend), 619 (pyridine bend).

N,N'-(cyclohexane-1,2-diyl)bis(1-(quinolin-2-yl)methanimine). White solid. Yield 85%. ^{1}H NMR (600 MHz, $CDCl_3$) δ (ppm): 8.52 (s, 2H), 8.11 – 8.04 (m, 4H), 8.03 (d, *J* = 8.5 Hz, 2H), 7.74 (d, *J* = 8.0 Hz, 2H), 7.66 (dd, *J* = 11.2, 3.9 Hz, 2H), 7.49 (t, *J* = 7.4 Hz, 2H), 3.78 – 3.56 (m, 2H), 2.00 – 1.77 (m, 6H), 1.64 – 1.46 (m, 2H). ^{13}C (50 MHz, $CDCl_3$) δ (ppm): 24.58, 32.93, 74.06, 118.76, 127.33, 127.82, 128.91, 19.67, 136.55, 147.90, 155.15, 162.07. MS (ESI): m/z 393.5 [M^+H], 415,40 [M+Na^+] . IR (KBr pellet): ν = 1642 (N=C imine strech); 1595 (N=C quinoline strech); 1365 (quinoline strech); 1427 (quinoline strech); 1460 (quinoline strech); 1500 (quinoline strech); 1558 (quinoline strech); 1615 quinoline (strech).

N,N'-(ethane-1,2-diyl)bis(1-(pyridin-2-yl)methanimine). White solid. Yield 65%. ^{1}H NMR (400 MHz, $CDCl_3$) δ (ppm): δ 8.61 (d, J = 4.1 Hz, 2H), 8.40 (s, 2H), 7.96 (d, J = 7.9 Hz, 2H), 7.71 (td, J = 7.7, 1.8 Hz, 2H), 7.28 (ddd, J = 7.5, 4.9, 1.3 Hz, 2H), 4.05 (s, 4H); ^{13}C (100 MHz, $CDCl_3$) δ (ppm): 163.6, 154.5, 149.6, 136.7, 124.9, 121.5, 61.5.

Synthesis of others imine derivatives

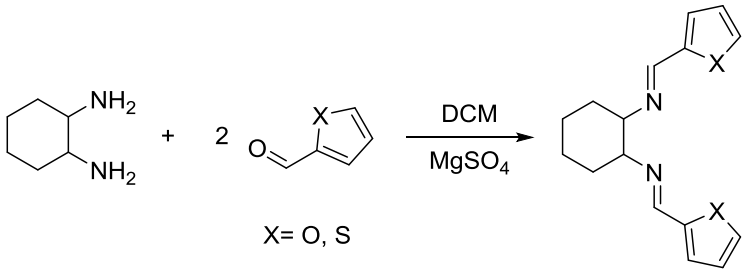

Synthesis of N,N'-(cyclohexane-1,2-diyl)bis(1-(thiophen-2-yl)methanimine). To a DCM solution with $MgSO_4$, dried agent, has been added of 1,2-diaminocyclohexane (200 mg, 1.75 mmol) . After 10 minute, thiophene-2-carbaldehyde (375 mg, 3.5 mmol) has been added at room temperature. The solution has been kept under virgosoly stirring and monitored the disappearing of thiophene-2-carboaldehyde using NMR. After almost three day, the solution has been filtered on celite and the solvent removed by using a rotar-vapor. The solid obtained has been recrystallized with hexane to give the product desiderated. White solid. Yield: 90%. ^{1}H NMR (400 MHz, CDCl3) δ (ppm): 1.44–1.50 (m, 2H), 1.78–1.85 (m, 6H), 3.30–3.33 (m, 2 H), 6.96 (dd, J=3.6, 4.8 Hz, 2 H), 7.14 (d, J=4.0 Hz, 2H), 7.29 (d, J=4.8 Hz, 2H), 8.27 ppm (s, 2H); ^{13}C (100 MHz, CDCl3) δ (ppm): 24.4,32.8, 73.4, 94.5, 127.2, 128.2, 130.2, 154.4 ppm. EI-MS: m/z (%): 112 (32), 160 (24), 193 (100), 302 (15) [M^+].

N,N'-(cyclohexane-1,2-diyl)bis(1-(furan-2-yl)methanimine). White solid. Yield:92% . ^{1}H NMR (250 MHz, CDCl3) δ (ppm): 1.37- 1.43 (m, 2H), 1.68-1.79 (m, 6H), 3.27-3.31 (m, 2H), 6.35 (dd, 2H, J=3.5, 1.7 Hz), 6.60 (dd, 2H, J=3.5, 0.6 Hz), 7.39 (d, 2H, J=1.7 Hz), 7.93 (s, 2H) . ^{13}C (62,9 MHz, $CDCl_3$) δ (ppm): 23.9, 32.6, 73.5, 111.2, 114.4, 144.4, 149.8, 150,7. MS (CI-MS/DCI), m/z (%): 270 (19)[M^+], 177 (51) [M^+ - N=CH furan], 96 (100) [N=CH furan].

Synthesis of amine ligand

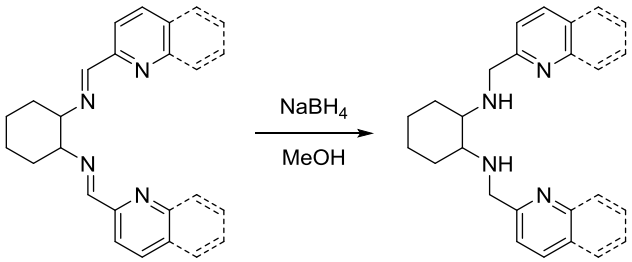

Synthesis of N1,N2-bis(pyridin-2-ylmethyl)cyclohexane-1,2-diamine. A solution of N,N'-(cyclohexane-1,2-diyl)bis(1-(pyridin-2-yl)methanimine) (2.1 gr., 0.0072 mol) in methanol (100 mL) has been cool at 0°C using an ice bath. When the temperature has been established, sodium boron hydride, $NaBH_4$ (0.8171 gr., 0,021 mol) has been slowly added to methanol solution. After the adding has been complete, the methanol solution has been (maintained) at 0°C for 30 minute and then remove the ice-bath to establish the room temperature. The reaction has been monitored by neutral alumina TLC using a mobile phase: DCM: acetonitrile 8:2 v/v. When all starting material is consumed, 10 mL of water has been added to methanol solution to remove the sodium boron hydride

excess. The methanol has been eliminated from reaction mixture under reduce pressure and the organic compounds extracted, three time with 20 mL DCM, from the aqueous solution. The organic phase has been put together, dried with $MgSO_4$.and at least filtered. The oil obtained by solvent removing, has been used without any purification. Colorless oil. Yield: 98%. ^{1}H NMR (600 MHz, $CDCl_3$) δ (ppm): 8.53 (d, *J* = 4.3 Hz, 2H), 7.63 (td, *J* = 7.7, 1.5 Hz, 2H), 7.40 (d, *J* = 7.8 Hz, 2H), 7.14 (dd, *J* = 6.9, 5.3 Hz, 2H), 4.04 (d, *J* = 14.1 Hz, 2H), 3.85 (d, *J* = 14.1 Hz, 2H), 2.38 – 2.30 (m, 1H), 2.15 (d, *J* = 13.3 Hz, 2H), 1.71 (dd, *J* = 15.6, 11.8 Hz, 2H), 1.26 – 1.18 (m, 2H), 1.13 – 1.02 (m, 2H). ^{13}C (125 MHz, $CDCl_3$) δ (ppm): 160.3, 148.9, 136.4, 122.4, 121.8, 61.2, 52.2, 31.4, 24.9; TOF-Mass (ES^+) (m/z): 297.13 ($M + H^+$).

N1,N2-bis(quinolin-2-ylmethyl)cyclohexane-1,2-diamine. Colorless oil. Yield: 96%. ^{1}H NMR (600 MHz, $CDCl_3$) δ (ppm): 8.07 (d, *J* = 8.4 Hz, 2H), 8.03 (d, *J* = 8.4 Hz, 2H), 7.78 (d, *J* = 8.0 Hz, 2H), 7.66 (t, *J* = 7.6 Hz, 2H), 7.59 (d, *J* = 8.4 Hz, 2H), 7.49 (t, *J* = 7.4 Hz, 2H), 4.25 (d, *J* = 14.5 Hz, 2H), 4.06 (d, *J* = 14.5 Hz, 2H), 2.46 – 2.39 (m, 2H), 2.21 (d, *J* = 12.6 Hz, 2H), 1.73 (d, *J* = 8.4 Hz, 2H), 1.25 (p, *J* = 10.8 Hz, 2H), 1.13 (d, *J* = 9.2 Hz, 2H). . ^{13}C (50 MHz, $CDCl_3$) δ (ppm): 23.9, 30.7, 52.1, 60.7, 119.8, 124.9, 126.5, 127.9, 128.2, 135.2, 146.7, 160.2; MS (EI) (m/z): 396 [M^+].

N1,N2-bis(furan-2-ylmethyl)cyclohexane-1,2-diamine. Colorless oil. Yield: 99%. ^{1}H NMR (300 MHz, $CDCl_3$) δ (ppm): 7.36 (s, 2H), 6.33 (d, J 4 Hz, 2H), 6.19 (d, J 4 Hz, 2H), 3.88 (d, J 16 Hz, 2H), 3.73 (d, J 16 Hz , 2H), 2.25 (m, 2H), 2.06 (m, 2H), 1.73 (m, 2H), 1.24 (m, 2H), 1.05 (m, 2H). ^{13}C (50 MHz, $CDCl_3$) δ (ppm): 25.13, 31.57, 43.72, 60.83, 106.52, 110.26, 141.66, 154.82. LC-MS: m/z 275 [M+1].

N1,N2-bis(thiophen-2-ylmethyl)cyclohexane-1,2-diamine. Colorless oil. Yield: 95%. ^{1}H NMR (600 MHz, $CDCl_3$) δ (ppm): 7.18 (dd, 2H, J 5.0 Hz, J 1.4 Hz, 5-H), 6.90-6.94 (m, 4H, 3-H, 4-H), 4.1 (d, 2H, J 14.2 Hz, CH-NH), 3.88 (d, 2H, J 14.2 Hz, CH-NH), 2.26-2.30 (m, 2H), 2.05-2.15 (m, 2H), 1.70-1.74 (m, 2H), 1.20-1.25 (m, 2H), 1.01-1.05 (m, 2H). ^{13}C (50 MHz, $CDCl_3$) δ (ppm): 145.2, 126.6, 124.5, 124.3, 60.5, 45.6, 31.6, 25.1.

N1,N2-bis(pyridin-2-ylmethyl)ethane-1,2-diamine. Colorless oil. Yield: 94%. ^{1}H NMR (250 MHz, $CDCl_3$) δ (ppm): 2.07 (s, 2H), 2.79 (s, 4H), 3.88 (s, 4H) 7.11 (t, J 6.2 Hz, 2H), 7.28 (d, J 8.2 Hz, 2H), 7.59 (t, J 8.5 Hz, 2H), 8.50 (d, J 4.8 Hz, 2H). ^{13}C (62.50 MHz, $CDCl_3$) δ (ppm): 49.10, 55.21, 121.86, 122.21, 136.40, 149.26, 159.92. ESI-MS: m/z 243.04.

Synthesis of carboxylate ligand

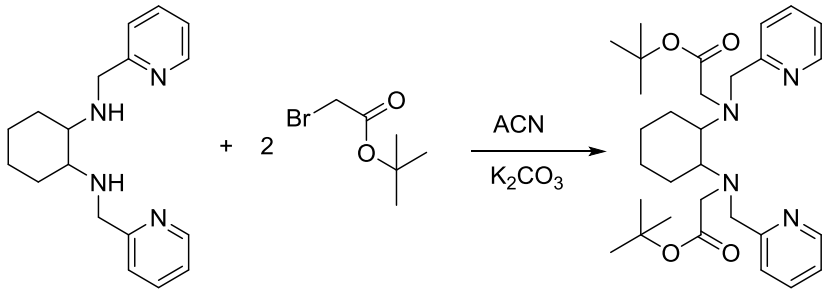

Synthesis of di-tert-butyl 2,2'-(cyclohexane-1,2-diylbis((pyridin-2-ylmethyl)azanediyl))diacetate. Under N_2 atmosphere, 3,2 eq. of K_2CO_3 (3.13 g) has been added to a dry ACN solution (40 mL) containing N1,N2-bis(pyridin-2-

ylmethyl)cyclohexane-1,2-diamine (2,1 g, 0.0071 mol). After 15 minutes, an anhydrous ACN (40 mL) solution of tert-butyl 2-bromoacetate (4.14 gr, 0.021) has been added dropwise to amine solution over 25 minute. The reaction has been left under stirring and monitored by TLC (alumina plate) using a mobile phase 90 DCM : 10 acetone :1 TEA. When all the mono-alkylate product disappear (Rf=0.21) and only the di-alkylate product is present (Rf=0.72), almost 1 day, 20 ml of water has been added to reaction mixture. The organic compounds have been extracted three times with DCM and the united organic phases has been washed two times with brine. The aqueous solutions have been put together and the remaining organic compounds extracted one time with DCM. All the organic phases have been combined and dried on Na_2SO_4 for 30 min. After this time, the CH_2Cl_2 solution has been filtrated and the solvent removed under reduce pressure. The product has been purified through flash-chromatography using an aluminum oxide column and 90 DCM : 10 acetone :1 TEA as mobile phase. White-yellow oil. Yield 30%. ^{1}H NMR (300 MHz, $CDCl_3$) δ (ppm): 8.44 (d, *J* = 4.5 Hz, 2H), 7.76 (d, *J* = 7.8 Hz, 2H), 7.50 (t, *J* = 7.1 Hz, 2H), 7.12 – 7.05 (m, 2H), 3.91 (d, *J* = 14.5 Hz, 2H), 3.69 (d, *J* = 14.5 Hz, 2H), 3.39 (d, *J* = 16.8 Hz, 2H), 3.24 (d, *J* = 16.8 Hz, 2H), 2.63 (d, *J* = 5.3 Hz, 1H), 2.10 (d, *J* = 7.4 Hz, 1H), 1.68 (d, *J* = 32.8 Hz, 1H), 1.48 – 1.37 (m, 18H), 1.09 (d, *J* = 6.7 Hz, 2H). ^{13}C (151 MHz, $CDCl_3$) δ (ppm): 171.96, 161.19, 148.60, 136.58, 124.38, 122.11, 80.60, 61.53, 56.62, 52.94, 28.47, 26.93, 26.21.

Di-tert-butyl 2,2'-(ethane-1,2-diylbis((pyridin-2-ylmethyl)azanediyl))diacetate. White-yellow oil. Yield 30%. ^{1}H NMR (600 MHz, $CDCl_3$) δ (ppm): δ 8.50 (d, *J* = 4.0 Hz, 2H), 7.60 (t, *J* = 6.7 Hz, 2H), 7.48 (d, *J* = 7.7 Hz, 2H), 7.15 – 7.09 (m, 2H), 3.91 (s, 4H), 3.32 (s, 4H), 2.82 (s, 4H), 1.44 (s, 18H).

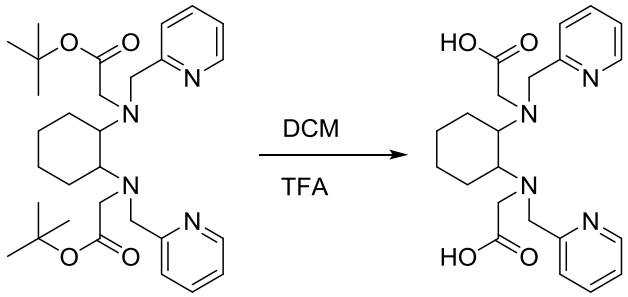

Synthesis of 2,2'-(cyclohexane-1,2-diylbis((pyridin-2-ylmethyl)azanediyl))diacetic acid. In inert atmosphere an solution of tert-butyl di acetate (700 mg, 1.33 mmol) in DCM (5 mL) has been cooled to 0°C and added slowly Trifluoroacetic acid (TFA) (6 gr, 53.36 mmol) . The solution, after the TFA adding, has been maintained to 0°C for 30 minute and then warmed to room temperature. The reaction has been left under stirring overnight. The volume of mixture has been reduce of 4/5, under reduce pressure, and the resulting solution has been added dropwise into diethyl ether (100 ml) to obtain a white-yellow precipitate. The solid has been washed several time with ether to remove TFA excess and kept under vacuum for 5 h to remove ethyl ether. White solid. The reaction is quantitative. ^{13}C (151 MHz, D_2O) δ (ppm): 172.91, 162.62, 149.35, 144.42, 127.14, 126.24, 63.02, 55.43, 51.09, 30.20, 23.82. MS (ESI): (m/z) 413.4 [MH^+] (100%), 435,30 [$M+Na^+$] (15%), 469,30 [$M+K^+$] (15%)

2,2'-(ethane-1,2-diylbis((pyridin-2-ylmethyl)azanediyl))diacetic acid. White-yellow solid. The reaction is quantitative. ^{13}C (75 MHz, [D_6] acetone) δ (ppm): 172.1, 152.3, 145.1, 142.8, 126.1, 125.3, 56.1 54.2, 51.1.

Synthesis of Lanthanide complexes

Synthesis of nitrate complexes

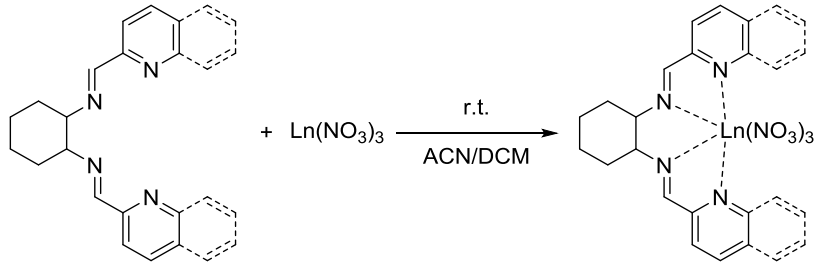

Synthesis of N,N'-(cyclohexane-1,2-diyl)bis(1-(pyridin-2-yl)methanimine) lanthanide complexes. A DCM solution (0.5 mL) containing imine lingand (50 mg , 0.17 mmol) was added to ACN solution (5 mL) containing lanthanum nitrate salts (77.18 mg , 0.17 mmol). After few minutes of the adding, a white precipitate was formed and the solution has been kept under stirring overnight. Before the work-up, the solution has been cooled at 0°C to increase the precipitate which has been collected with suction filtration and washed three time with a cooled ACN/DCM (1:1) solution. White solid.

Lanthanum nitrate complex. Yield: 77%. MS (ESI): m/z 555.20 [M-NO_3]

Europium nitrate complex. Yield: 75%. MS (ESI): m/z 569.20 [M-NO_3]

Gadolinium nitrate complex. Yield: 83%. MS (ESI): (m/z) 574.10 [M-NO_3]

Terbium nitrate complexes. Yield: 72%. MS (ESI): (m/z) 575.32 [M-NO_3]

Lutetium nitrate complex. Yield 71%. MS(ESI): m/z 591.20 [M-NO_3]

N,N'-(cyclohexane-1,2-diyl)bis(1-(quinolin-2-yl)methanimine). They have been synthetized in the same way as well as for the diimine pyridine ligand.

Lanthanum nitrate complex. Yield: 70%. Elemental Analysis Calculated: $C_{26}H_{24}LaN_7O_9$ (MW: 758.46) C, 44.34; H, 3.59; N, 14.77; O, 18.98. Founded: C, 44.48; H, 3.49; N, 14.72; O, 18.91. IR (KBr pellet): ν = 1650 (N=C imine strech); 1591 (N=C quinoline strech); 1381 (quinoline strech) ; 1432 (quinoline strech); 1474 (quinoline strech); 1504 (quinoline strech); 1563 (quinoline strech); 1619 (quinoline strech).

Europium nitrate complex. Yield: 72%. Elemental Analysis Calculated: $C_{28}H_{27}EuN_8O_9$ (MW: 771.53) C, 43.59; H, 3.53; N, 14.52; O, 18.66. Founded: C, 43.51; H, 3.47; N, 14.46; O, 18.60. IR (KBr pellet): ν = 1654 (N=C imine strech); 1593 (N=C quinoline strech); 1383 (quinoline strech); 1431 (quinoline strech); 1476 (quinoline strech); 1508 (quinoline strech); 1562 (quinoline strech); 1619 (quinoline strech).

Gadolinium nitrate complex. Yield: 60%. Elemental Analysis Calculated: $C_{28}H_{27}GdN_8O_9$ (MW: 776.81) C, 43.29; H, 3.50; N, 14.42; O, 18.54. Founded: C, 43.25; H, 3.41; N, 14.39; O, 18.46. IR (KBr pellet): ν = 1655 (N=C imine strech); 1593 (N=C quinoline strech); 1383 (quinoline strech); 1433 (quinoline strech); 1475 (quinoline strech); 1498 (quinoline strech); 1562 (quinoline strech); 1619 (quinoline strech).

Terbium nitrate complexes. Yield: 40%. Elemental Analysis Calculated: $C_{26}H_{24}TbN_7O_9$ (MW: 737.44) C, 42.35; H, 3.28; N, 13.30; O, 19.53. Founded: C, 42.29; H, 3.20; N, 13.38; O, 19.47. IR (KBr pellet): ν = 1657 (N=C imene strech); 1593 (N=C quinoline strech); 1383 (quinoline strech); 1433 (quinoline strech); 1475 (quinoline strech); 1503 (quinoline strech); 1563 (quinoline strech); 1619 (quinoline strech).

Lutetium nitrate complex. Yield: 30%. Elemental Analysis Calculated: $C_{26}H_{24}LuN_7O_9$ (MW: 753.48) C, 41.44; H, 3.21; N, 13.01; O, 19.11. Founded: C, 41.40; H, 3.14; N, 12.89; O, 19.04. IR (KBr pellet): ν = 1662 (N=C imine strech); 1593 (N=C quinoline strech); 1383 (quinoline strech); 1433 (quinoline strech); 1479 (quinoline strech); 1509 (quinoline strech); 1564 (quinoline strech); 1620 (quinoline strech).

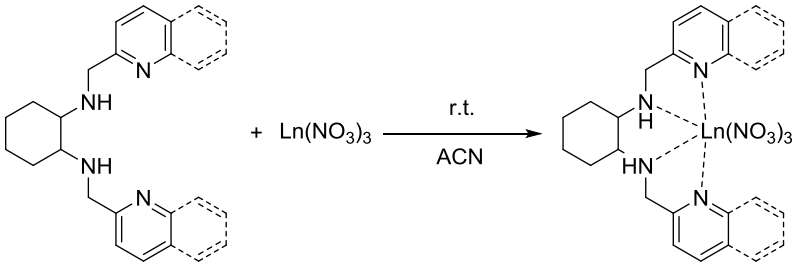

Synthesis of N1,N2-bis(pyridin-2-ylmethyl)cyclohexane-1,2-diamine lanthanide complexes. To a ACN solution (5 mL) containing the amine ligand (92 mg, 0.3103 mmol) was added the lanthanum nitrate salt (136.6 mg,0.3103 mmol). The reaction has been left under stirring overnight although a white precipitate has been formed after the adding of lanthanide salts. To increase the precipitate quantities, the solution has been cooed to 0°C and filtered using a frit. The solid separated has been washed three time with a cold ACN. White solid.

Lanthanum nitrate complex. Yield: 56%. MS (ESI): m/z 559 [M-NO_3].

Europium nitrate complex. Yield: 50%. MS (ESI): m/z 573 [M-NO_3]

Gadolinium nitrate complex. Yield: 46%. MS (ESI): m/z 578 [M-NO_3]

Terbium nitrate complexes. Yield: 48%. MS (ESI): m/z 579 [M-NO_3]

Lutetium nitrate complex. Yield: 59%. MS (ESI): m/z 595 [M-NO_3]

N,N'-(cyclohexane-1,2-diyl)bis(1-(quinolin-2-yl)methanimine). They have been synthetized in the same way as well as for the diamine pyridine ligand.

Lanthanum nitrate complex. Yield: 44%. Elemental Analysis Calculated: $C_{28}H_{28}LaN_7O_9$ (MW: 721.45) C, 43.28; H, 3.91; N, 13.59; O, 19.96. Founded: C, 43.22; H, 3.86; N, 13.63; O, 19.91.

Europium nitrate complex. Yield: 36%. Elemental Analysis Calculated: $C_{26}H_{28}EuN_7O_9$ (MW: 734.51) C, 42.52; H, 3.84; N, 13.35; O, 19.60. Founded: C, 42.45; H, 3.80; N, 13.28; O, 18.52.

Gadolinium nitrate complex. Yield: 20%. Elemental Analysis Calculated: $C_{26}H_{28}GdN_7O_9$ (MW: 739.79) C, 42.21; H, 3.81; N, 13.25; O, 19.46. Founded: C, 42.16; H, 3.77; N, 13.33; O, 19.41

Terbium nitrate complexes. Yield: 42%. Elemental Analysis Calculated: $C_{26}H_{28}TbN_7O_9$ (MW: 741.47) C, 42.12; H, 3.81; N, 13.22; O, 19.42. Founded: C, 42.07; H, 3.76; N, 13.31; O, 19.34.

Lutetium nitrate complex. Yield: 18%. Elemental Analysis Calculated: $C_{26}H_{28}LuN_7O_9$ (MW: 757.51) C, 41.22; H, 3.73; N, 12.94; O, 19.01. Founded: C, 41.18; H, 3.70; N, 13.00; O, 18.88.

Synthesis of Triflate complexes

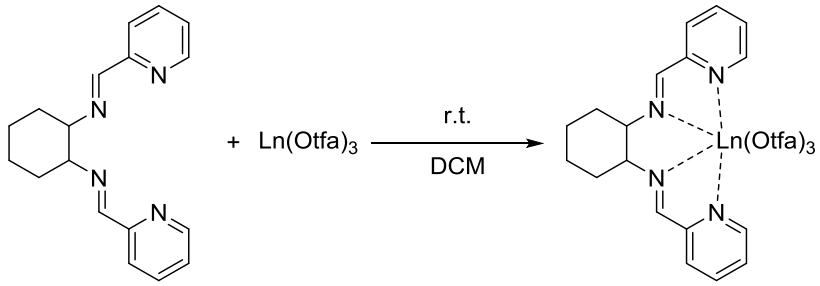

Synthesis of N,N'-(cyclohexane-1,2-diyl)bis(1-(pyridin-2-yl)methanimine) lanthanide complexes. 40 mg (0.068 mmol) of Eu(Otfa) has been added to a DCM solution (10mL) of 20 mg (0.068 mmol) N,N'-(cyclohexane-1,2-diyl)bis(1-(pyridin-2-yl)methanimine). The europium salts disappeared in few minute and a new precipitated was formed. The solution has been kept under stirring for 1 hour at room temperature and then all the solvent has been removed. The white obtained solid is the desiderated product. Yield: 95%. IR (KBr pellet): ν = 1653 (C=N stretch), 1596 (pyridine stretch), 1576 (pyridine stretch), 1467 (pyridine stretch), 1434 (pyridine stretch).

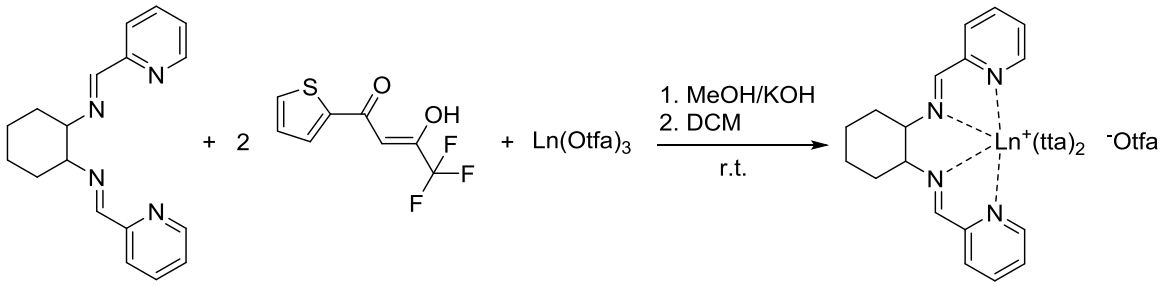

Synthesis of heteroleptic lanthanide complexes. 78 mg (0.342 mmol) of Htta has been completely dissolved in methanol (2mL) solution containing 19 mg (0.342 mmol) of KOH. The clear solution has been slowly added to methanol solution (2ml) containing 50 mg (0.171 mmol) of N,N'-(cyclohexane-1,2-diyl)bis(1-(pyridin-2-yl)methanimine) and 102 mg (0.171 mmol) of $Eu(Otfa)_3$. The final solution has been stirred for 1 hour a room temperature. After this time, the solvent has been removed under reduced pressure and the desiderated product extracted through 6 mL of DCM. Yiled: 50%. IR (KBr pellet): ν = 1645 (C=N imine stretch), 1537 (carbonyl group stretch), 1029 (pyridine bend), 638 (pyridine bend).

Synthesis of halide complexes

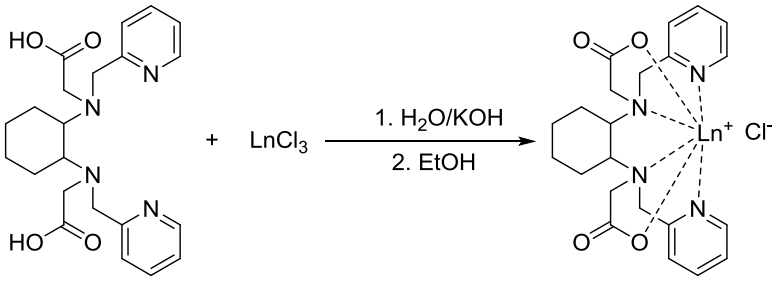

Synthesis of 2,2'-(cyclohexane-1,2-diylbis((pyridin-2-ylmethyl)azanediyl))diacetate lanthanide complexes. The chloride lanthanum salts (45 mg, 0.121 mmol) has been added to aqueous solution (2 mL) of diacetic acid (50 mg, 0.121 mmol). Under vigorously stirring, the initial acid pH has been raised to neutral pH (almost 6.5) using aqueous solution (4 mL) of KOH (27 mg, 0.484 mmol). After 8 hours all the water has been removed under reduce pressure and the resulting residue has been suspended in Ethanol (10 mL). The solution has been cooled to -18°C and kept to this temperature overnight to increase the precipitation of inorganic salts. The suspending solid has been removed by filtration and the clear ethanol solution has been concentrated to obtain the desiderated complexes. White-yellow solid.

Lanthanum Chloride complex. Yield: 56%. ^{1}H NMR (600 MHz, D_2O) δ (ppm): δ 8.55 (s, 2H), 7.85 (t, J = 7.9 Hz, 2H), 7.41 (d, J = 8.7 Hz, 4H), 4.22 (d, J = 16.8 Hz, 2H), 3.91 (d, J = 16.3 Hz, 2H), 2.95 (q, J = 16.4 Hz, 4H), 2.47 (d, J = 8.6 Hz, 2H), 1.95 (d, J = 15.1 Hz, 2H), 1.51 (d, J = 8.5 Hz, 2H), 1.01 (d, J = 10.9 Hz, 2H), 0.78 (d, J = 10.5 Hz, 2H). MS(ESI) m/z: 549.18 [M-Cl], 580.57 [M-Cl+MeOH]

Europium Chloride complex. Yield:51%. MS(ESI) m/z: 563.18 [M-Cl], 580 [M-Cl+H_2O], 594.85 [M-Cl+MeOH]

Terbium Chloride complex. Yield:53%. MS(ESI) m/z: 596.25[M-Cl], 600.92 [M-Cl+MeOH]

2,2'-(ethane-1,2-diylbis((pyridin-2-ylmethyl)azanediyl))diacetate. They have been synthetized in the same way as well as for the cycloesandiamine pyridine ligand.

Europium Chloride complex. Yield: 60%. MS(ESI) m/z: 509 [M-Cl]

Terbium Chloride complex. Yield:65%. MS(ESI) m/z: 515 [M-Cl]

Appendix

1. Crystal structures

*1.1 Rac-N,N'-(cyclohexane-1,2-diyl)bis(1-(pyridin-2-yl)methanimine) europium complex. (**L1**Eu(NO$_3$)$_3$)*

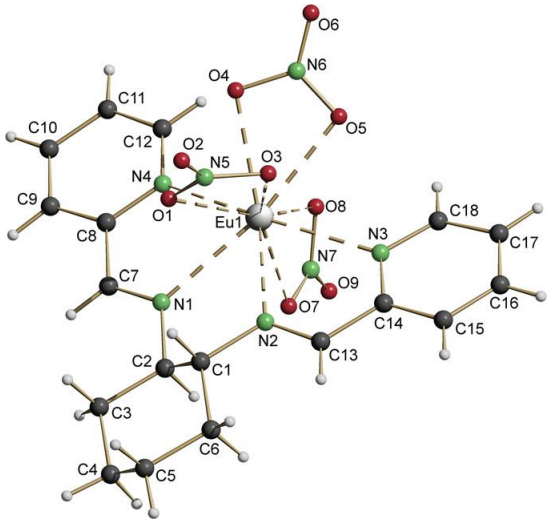

*Figure 76 Perspective view of complex **L1**Eu(NO$_3$)$_3$*

*Table 14 Crystal data and structure refinement and selected bond lengths (Å) and angles (°) for complexes for **L1**Eu(NO$_3$)$_3$*

Compound	**L1**Eu(NO$_3$)$_3$
Formula	$C_{18}H_{20}EuN_7O_9 \cdot CH_3CN$
Formula weight	671.42
T (K)	293(2)
λ (Å)	0.71073
Crystal symmetry	monoclinic
Space group	$P2_1/c$
a (Å)	9.7970(7)
b (Å)	16.2185(13)
c (Å)	16.5723(12)
α (°)	90
β (°)	102.714(4)
γ (°)	90
Cell volume (Å^3)	2568.7(3)
Z	4
D_{calc} (Mg m^{-3})	1.736
μ (Mo Kα) (mm^{-1})	2.506
F(000)	1336
Crystal size (mm)	0.10 × 0.15 × 0.20
θ limits (°)	1.78–25.00
Reflections collected	21 881
Unique observed reflections [$F_0 > 4\sigma(F_0)$]	3661 [R_{int} = 0.0912]
Goodness-of-fit (GOF) on F^2	0.979
R_1 (F)[a], wR_2 (F^2) [$I > 2\sigma(I)$][b]	0.0656, 0.1152
Largest difference in peak and hole (e Å^{-3})	1.219 and −1.215

[a] $R_1 = \Sigma||F_0| - |F_c||/\Sigma|F_0|$.

[b] $wR_2 = [\Sigma w(F_0^2 - F_c^2)^2/\Sigma w(F_0^2)^2]^{1/2}$ where $w = 1/[\sigma^2(F_0^2) + (aP)^2 + P = (F_0^2 + F_c^2)/3$.

Bond lengths for complex	L1Eu(NO
Eu(1)–N(1)	2.561(
Eu(1)–N(2)	2.53(1
Eu(1)–N(3)	2.63(1
Eu(1)–N(4)	2.622(
Eu(1)–O(1)	2.549(
Eu(1)–O(3)	2.539(
Eu(1)–O(4)	2.488(
Eu(1)–O(5)	2.496(
Eu(1)–O(7)	2.485(
Eu(1)–O(8)	2.465(

Bond angles for complex	L1Eu(NO
N(1)–Eu(1)–N(2)	63.4(3
N(1)–Eu(1)–N(3)	123.2(
N(1)–Eu(1)–N(4)	63.3(3
N(2)–Eu(1)–N(3)	64.2(3
N(2)–Eu(1)–N(4)	126.7(
N(3)–Eu(1)–N(4)	158.5(

1.2 *Meso-N,N'-(cyclohexane-1,2-diyl)bis(1-(pyridin-2-yl)methanimine) europium complex. (**L3**Eu(NO$_3$)$_3$)*

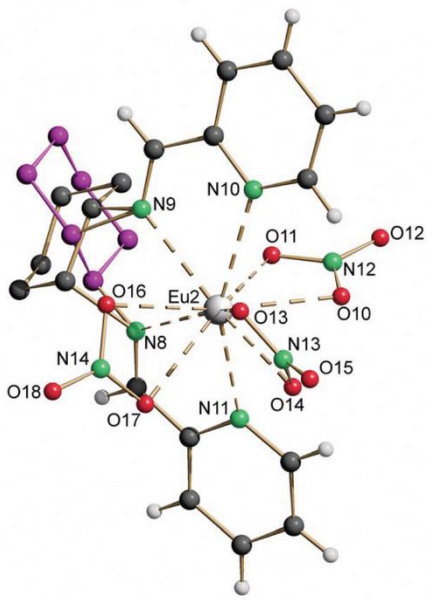

*Figure 77 Perspective view of two isomer complex **L3**Eu(NO$_3$)$_3$*

*Table 15 Crystal data and structure refinement and Selected bond lengths (Å) and angles (°) for **L3**Eu(NO$_3$)$_3$*

Compound	Eu**L3**(NO$_3$)$_3$·0.40C$_3$H$_6$O
Formula	C$_{18}$H$_{20}$EuN$_7$O$_9$.0.40C$_3$H$_6$O
Fw	653.60
T, K	293(2)
λ, Å	0.71073
Crystal symmetry	Triclinic
Space group	*P-1*
a, Å	9.7469(6)
b, Å	13.7146(8)
c, Å	20.006(1)
α	78.020(1)
β	76.941(1)
γ	86.008(1)
Cell volume, Å^3	2547.7(3)
Z	4
D$_C$, Mg m^{-3}	1.704
μ(Mo-K$_\alpha$), mm^{-1}	2.524
F(000)	1299
Crystal size/ mm	0.15 x 0.25 x 0.30
θ limits, °	1.52 – 27.00
Reflections collected	27988
Unique obs. reflections [F$_o$ > 4σ(F$_o$)]	8336 [R(int) = 0.0282]
Goodness-of-fit-on F^2	1.022
R$_1$ (F)[a], wR$_2$ (F^2) [I > 2σ(I)]	0.0346, 0.0836
Largest diff. peak and hole, e. Å^{-3}	0.0830 and -0.578

[a] $R_1 = \Sigma||F_o|-|F_c||/\Sigma|F_o|$.
[b] $wR_2 = [\Sigma w(F_o^2-F_c^2)^2/\Sigma w(F_o^2)^2]^{1/2}$ where $w = 1/[\sigma^2(F_o^2) + (aP)^2 + bP]$ where P =

Bond lengths for isomer 1		*Bond lengths for isome*	
Eu(1)-N$_{im}$ (1)	2.548(4)	Eu(2)-N$_{im}$(8)	2.54
Eu(1)-N$_{im}$ (2)	2.566(3)	Eu(2)-N$_{im}$ (9)	2.57
Eu(1)-N$_{py}$(3)	2.581(4)	Eu(2)-N$_{py}$(10)	2.59
Eu(1)-N$_{py}$(4)	2.588(4)	Eu(2)-N$_{py}$(11)	2.59
Eu(1)-O(1)	2.521(3)	Eu(2)-O(10)	2.47
Eu(1)-O(2)	2.509(3)	Eu(2)-O(11)	2.46
Eu(1)-O(4)	2.503(4)	Eu(2)-O(13)	2.52
Eu(1)-O(5)	2.603(4)	Eu(2)-O(14)	2.52
Eu(1)-O(7)	2.496(4)	Eu(2)-O(16)	2.52
Eu(1)-O(9)	2.470(3)	Eu(2)-O(17)	2.50

Bond angles for isomer 1		*Bond angles for isomer*	
N(1)-Eu(1)-N(2)	63.2(1)	N(8)-Eu(2)-N(9)	63.
N(1)-Eu(1)-N(3)	126.4(1)	N(8)-Eu(2)-N(10)	124
N(1)-Eu(1)-N(4)	64.1(1)	N(8)-Eu(2)-N(11)	63.
N(2)-Eu(1)-N(3)	63.4(1)	N(9)-Eu(2)-N(10)	63.
N(2)-Eu(1)-N(4)	121.4(1)	N(9)-Eu(2)-N(11)	122
N(3)-Eu(1)-N(4)	151.3(1)	N(10)-Eu(2)-N(11)	152

1.3 *Crystal Structure Comparison between rac-N,N'-(cyclohexane-1,2-diyl)bis(1-(pyridin-2-yl)methanimine) europium complex. (**L1**Eu(NO$_3$)$_3$) and meso-N,N'-(cyclohexane-1,2-diyl)bis(1-(pyridin-2-yl)methanimine) europium complex. (**L3**Eu(NO$_3$)$_3$)*

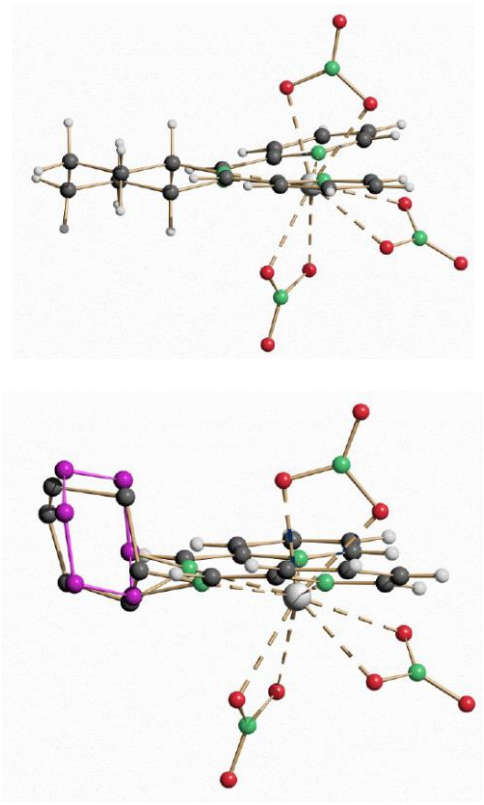

*Figure 78 Molecular crystal structure of (upper) **L1**Eu (NO$_3$)$_3$ and (below) **L3**Eu (NO$_3$)$_3$. View parallel to the N4 square plane.*

*Table 16 Comparison of Bond length and Bond angle of **L1** and **L3**Eu(NO$_3$)$_3$*

Bond lengths			
Eu**L1**(NO$_3$)$_3$		Eu**L3**(NO$_3$)$_3$	
Eu(1)–N$_{im}$(1)	2.561(9)	Eu(2)–N$_{im}$(8)	2.544(4)
Eu(1)–N$_{im}$ (2)	2.53(1)	Eu(2)–N$_{im}$ (9)	2.570(4)
Eu(1)–N$_{py}$(3)	2.63(1)	Eu(2)–N$_{py}$(10)	2.598(5)
Eu(1)–N$_{py}$(4)	2.622(9)	Eu(2)–N$_{py}$(11)	2.593(4)
Eu(1)–O(1)	2.549(8)	Eu(2)–O(10)	2.475 (4)
Eu(1)–O(3)	2.539(9)	Eu(2)–O(11)	2.460(4)
Eu(1)–O(4)	2.488(8)	Eu(2)–O(13)	2.520(4)
Eu(1)–O(5)	2.496(8)	Eu(2)–O(14)	2.523(4)
Eu(1)–O(7)	2.485(8)	Eu(2)–O(16)	2.529(4)
Eu(1)–O(8)	2.465(8)	Eu(2)–O(17)	2.504(4)
Bond angles			
N(1)–Eu(1)–N(2)	63.4(3)	N(8)–Eu(2)–N(9)	63.6(1)
N(1)–Eu(1)–N(3)	123.2(3)	N(8)–Eu(2)–N(10)	124.8(1)
N(1)–Eu(1)–N(4)	63.3(3)	N(8)–Eu(2)–N(11)	63.5(1)
N(2)–Eu(1)–N(3)	64.2(3)	N(9)–Eu(2)–N(10)	63.2(1)
N(2)–Eu(1)–N(4)	126.7(3)	N(9)–Eu(2)–N(11)	125.5(1)
N(3)–Eu(1)–N(4)	158.5(3)	N(10)–Eu(2)–N(11)	152.3(1)

1.4 *Rac-N1,N2-bis(pyridin-2-ylmethyl)cyclohexane-1,2-diamine Europium complex (**L2**Eu(NO$_3$)$_3$)*

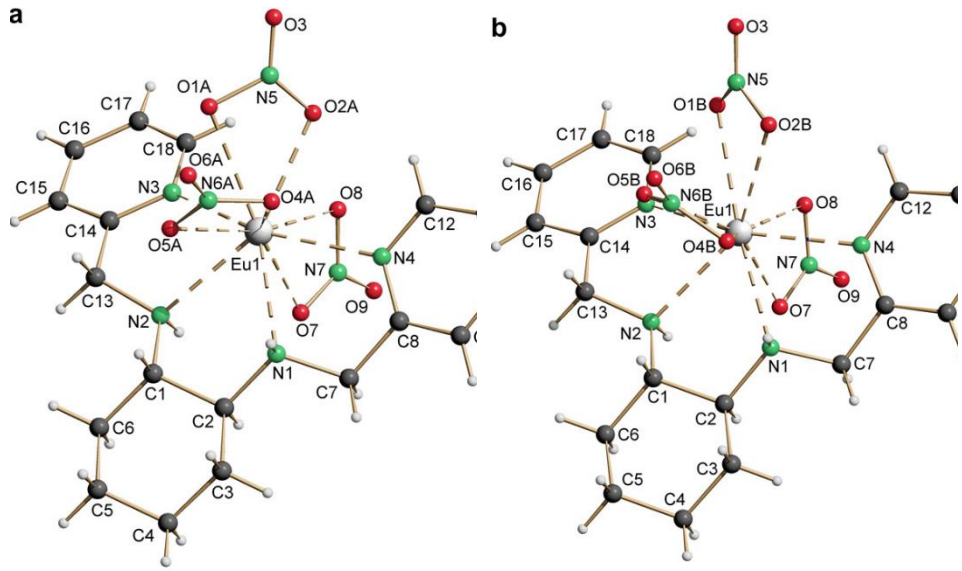

*Figure 79 Crystal Structures of **L2**Eu(NO$_3$)$_3$ (left) dominating conformation isomer and (right) minor conformation isomer*

*Table 17 Crystal data and structure refinement and selected bond lengths (Å) and angles (°) for **L2**Eu(NO$_3$)$_3$*

Compound	L2Eu(NO$_3$)$_3$
Formula	$C_{18}H_{24}EuN_7O_9$
Formula weight	634.40
T (K)	293(2)
λ (Å)	0.71073
Crystal symmetry	orthorhombic
Space group	*Pbca*
a (Å)	12.8584(17)
b (Å)	14.5569(19)
c (Å)	25.434(3)
α (°)	90
β (°)	90
γ (°)	90
Cell volume (Å^3)	4760.7(10)
Z	8
D_{calc} (Mg m^{-3})	1.770
μ (Mo Kα) (mm^{-1})	2.697
F(000)	2528
Crystal size (mm)	0.20 × 0.25 × 0.30
θ limits (°)	2.25–28.69
Reflections collected	48 669
Unique observed reflections [$F_o > 4\sigma(F_o)$]	5874 [R_{int} = 0.0682]
Goodness-of-fit (GOF) on F^2	1.035
R_1 (F)[a], wR_2 (F^2) [$I > 2\sigma(I)$][b]	0.0478, 0.1244
Largest difference in peak and hole (e Å^{-3})	1.307 and −1.742

[a] $R_1 = \Sigma||F_o| - |F_c||/\Sigma|F_o|$.

[b] $wR_2 = [\Sigma w(F_o^2 - F_c^2)^2/\Sigma w(F_o^2)^2]^{1/2}$ where $w = 1/[\sigma^2(F_o^2) + (aP)^2 + bP]$ wh $P = (F_o^2 + F_c^2)/3$.

Bond lengths for complex	L2Eu(NO$_3$)$_3$
Eu(1)–N(1)	2.575(4)
Eu(1)–N(2)	2.544(4)
Eu(1)–N(3)	2.584(5)
Eu(1)–N(4)	2.560(4)
Eu(1)–O(1A)	2.644(4)
Eu(1)–O(1B)	2.60(2)
Eu(1)–O(2A)	2.506(8)
Eu(1)–O(2B)	2.624(5)
Eu(1)–O(4A)	2.464(6)
Eu(1)–O(4B)	2.56(1)
Eu(1)–O(5A)	2.516(7)
Eu(1)–O(5B)	2.57(1)
Eu(1)–O(7)	2.470(4)
Eu(1)–O(8)	2.531(4)
Bond angles for complex	L2Eu(NO$_3$)$_3$
N(1)–Eu(1)–N(2)	66.7(1)
N(1)–Eu(1)–N(3)	128.5(1)
N(1)–Eu(1)–N(4)	64.8(1)
N(2)–Eu(1)–N(3)	63.2(2)
N(2)–Eu(1)–N(4)	129.7(1)
N(3)–Eu(1)–N(4)	152.6(2)

1.5 *Rac-N,N'-(cyclohexane-1,2-diyl)bis(1-(quinolin-2-yl)methanimine) lanthanide complex*

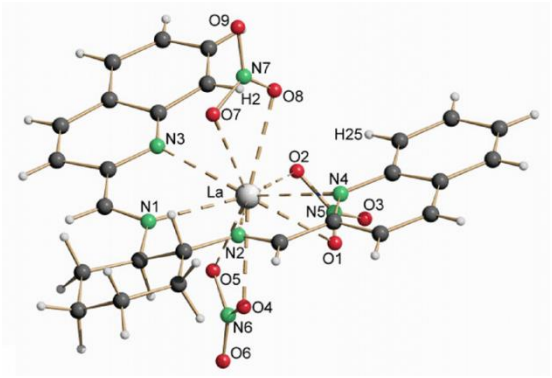

Figure 80 Perspective view of ***L5****La(NO₃)₃*

Table 18 Crystal data and structure refinement selected bond lengths (Å) and angles (°) for ***L5****La(NO₃)₃ CH₃CN*

Compound	**L5**La(NO₃)₃·CH₃CN
Formula	$C_{26}H_{24}LaN_7O_9 \cdot CH_3CN$
Fw	758.47
T, K	293(2)
λ, Å	0.71073
Crystal symmetry	Triclinic
Space group	*P-1*
a, Å	9.8319 (6)
b, Å	12.4914 (7)
c, Å	12.5719 (7)
α	78.469(4)
β	86.169 (4)
γ	87.201(4)
Cell volume, Å^3	1508.47(15)
Z	2
D_C, Mg m^{-3}	1.670
μ(Mo-K$_\alpha$), mm^{-1}	1.483
F(000)	760
Crystal size/ mm	0.20 x 0.10 x 0.05
θ limits, °	1.656 - 25.145
Reflections collected	5322
Unique obs. reflections [$F_o > 4\sigma(F_o)$]	2575 [R(int) = 0.1067]
Goodness-of-fit-on F^2	0.946
R_1 (F)[a], wR_2 (F^2) [$I > 2\sigma(I)$]	0.0703, 0.1370
Largest diff. peak and hole, e. Å^{-3}	1.219 and -1.215

[a] $R_1 = \Sigma||F_o|-|F_c||/\Sigma|F_o|$.
[b] $wR_2 = [\Sigma w(F_o^2-F_c^2)^2/\Sigma w(F_o^2)^2]^{1/2}$ where $w = 1/[\sigma^2(F_o^2) + (aP)^2 + bP]$ where $P = (F_o^2 + F_c^2)$

L5La(NO₃)₃	
Bond lengths	
La-N_{im}(1)	2.58(1)
La-N_{im} (2)	2.631(9)
La-N_{quin}(3)	2.817(9)
La-N_{quin}(4)	2.746(8)
La-O(1)	2.665(8)
La-O(2)	2.604(9)
La-O(4)	2.633(7)
La-O(5)	2.598(7)
La-O(7)	2.598(7)
La-O(8)	2.465(8)
Bond angles	
N(1)- La -N(2)	62.9(3)
N(1)- La -N(3)	63.1(3)
N(1)- La -N(4)	123.8(3)
N(2)- La -N(3)	122.5(3)
N(2)- La -N(4)	61.5(3)
N(3)- La -N(4)	153.9(3)

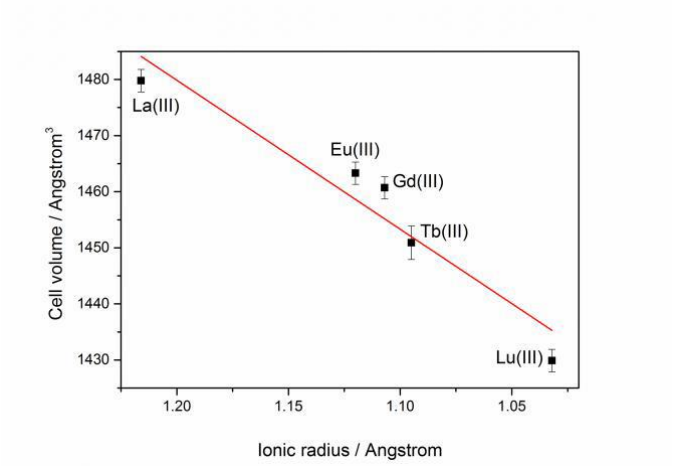

*Figure 81 Cell volume (Å^3) vs ionic radius (Å) of the Ln(III) ion in 9-fold coordination for **L5**Ln(NO$_3$)$_3$*

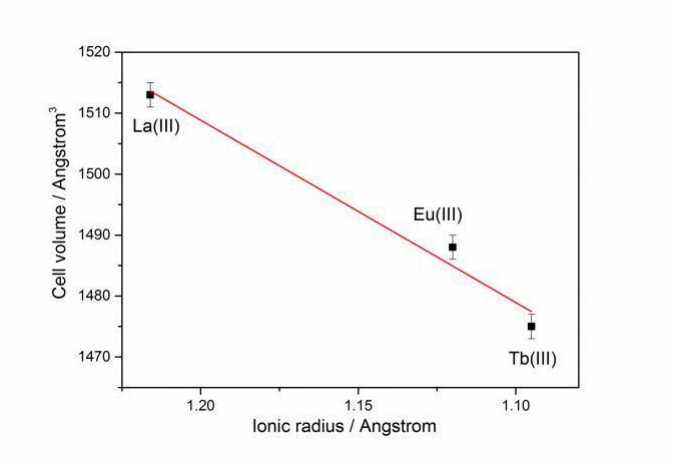

*Figure 82 Cell volume (Å^3) vs ionic radius (Å) of the Ln(III) ion in 9-fold coordination for **L6**Ln(NO$_3$)$_3$*

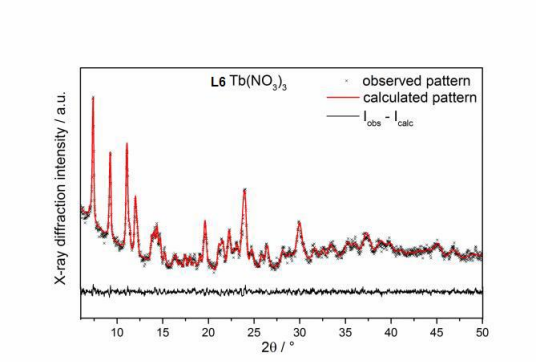

*Figure 83 Observed powder pattern (cross line), Rietveld refinement (red solid line) and line of the residual (black solid line) for **L6**Tb(NO$_3$)$_3$*

2. Titrations with inorganic anions

2.1 Titration in Dry Acetonitrile

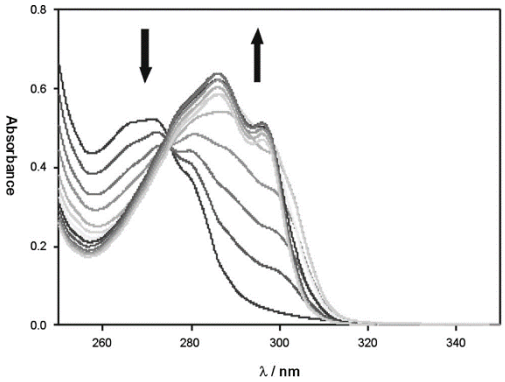

*Figure 84 UV–Vis spectroscopic titration of **L1** with $Eu(CF_3SO_3)_3$, C**L1** = 0.04mM. Arrows show the direction of the change in intensity of the adsorption bands during the titration.*

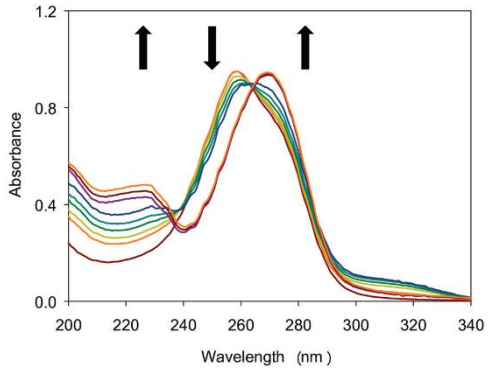

*Figure 85 Electronic spectra when **L2** (C**L2** = 0.0292 mmol dm^{-3}, spectra with $Eu(OTf)_3$ (CEu = 11.4 mmol dm^{-3})*

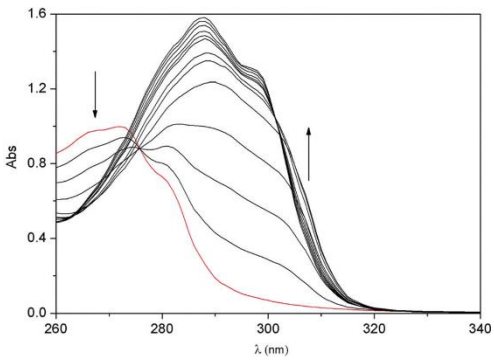

*Figure 86 Absorption spectra variations when **L3** is titrated with $Eu(OTf)_3$ (C**L3** = 0.08 mM) (CEu = 7.26 mM)*

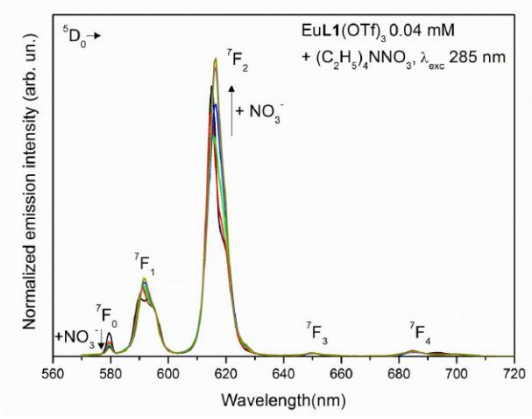

Figure 87 Evolution of the luminescence emission spectrum of 0.04 mM AN solution All the spectra are normalized to the area of the $^5D_0 \rightarrow {}^7F_1$ emission band. As the λ_{exc} = 285 nm, L→Eu^{3+} energy transfer (ET) has been exploited (antenna effect).

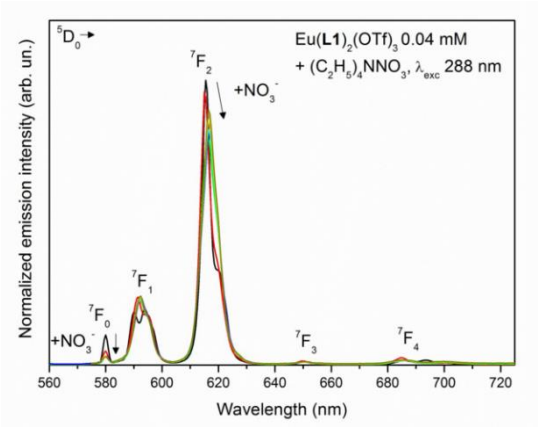

*Figure 88 Evolution of the luminescence emission spectrum of 0.04 mM AN solution of Eu(**L1**)$_2$(OTf)$_3$ upon addition of the nitrate anion. All the spectra are normalized to the area of the $^5D_0 \rightarrow {}^7F_1$ emission band. As the λ_{exc} = 288 nm, L→Eu^{3+} energy transfer (ET) has been exploited (antenna effect).*

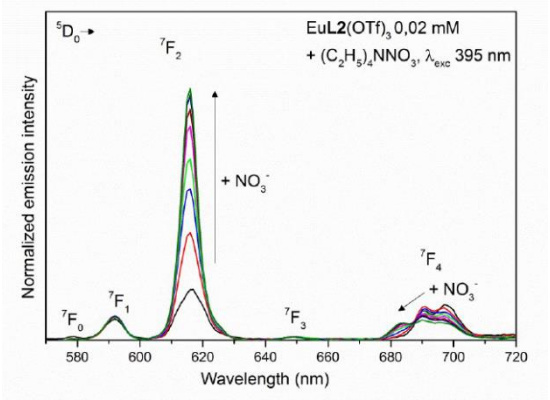

*Figure 89 Evolution of the luminescence emission spectrum of 0.02 mM AN solution of Eu**L2**(OTf)$_3$ upon addition of the nitrate anion. All the spectra are normalized to the area of the $^5D_0 \rightarrow {}^7F_1$ emission band*

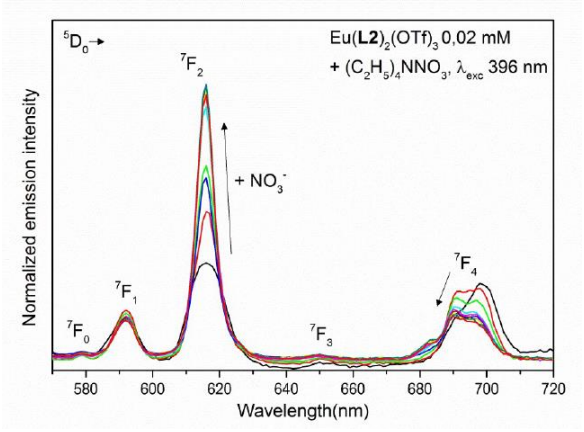

*Figure 90 Evolution of the luminescence emission spectrum of 0.02 mM AN solution of Eu(**L2**)$_2$(OTf)$_3$ upon addition of the nitrate anion. All the spectra are normalized to the area of the $^5D_0 \rightarrow {}^7F_1$ emission band.*

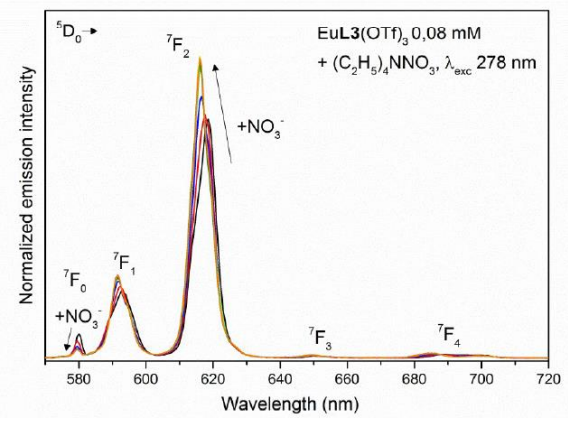

*Figure 91 Evolution of the luminescence emission spectrum of 0.08 mM AN solution of Eu**L3**(OTf)$_3$ upon addition of the nitrate anion. All the spectra are normalized to the area of the $^5D_0 \rightarrow {}^7F_1$ emission band. As the λ_{exc} = 278 nm, L→Eu^{3+} energy transfer (ET) has been exploited (antenna effect)*

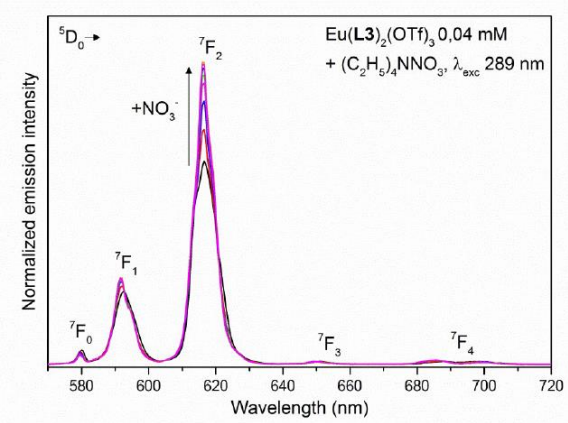

*Figure 92 Evolution of the luminescence emission spectrum of 0.04 mM AN solution of Eu(**L3**)$_2$(OTf)$_3$ upon addition of the nitrate anion. All the spectra are normalized to the area of the $^5D_0 \rightarrow {}^7F_1$ emission band. As the λ_{exc} = 289 nm, L→Eu^{3+} energy transfer (ET) has been exploited (antenna effect)*

2.2 Titration in Wet Acetonitrile

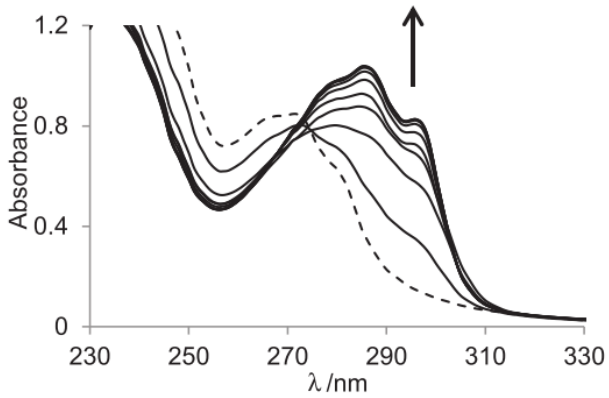

*Figure 93 Spectrophotometric titrations in non-anhydrous acetonitrile of **L1** (CL1 = 0.08 mM) titrated with Eu(OTf)$_3$ (CEu = 2.31 mM, final CEu/C**L1** = 1.5)*

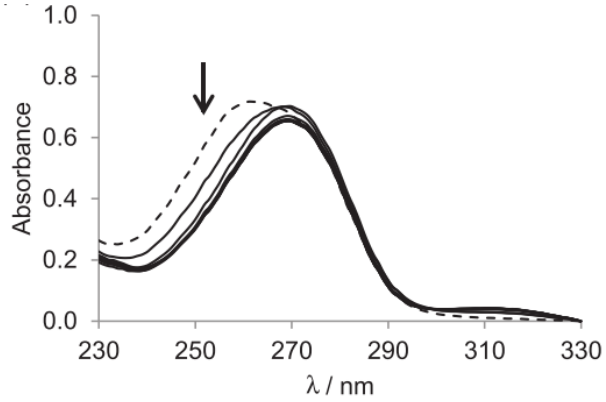

*Figure 94 Spectrophotometric titrations in non-anhydrous acetonitrile of **L2** (C**L2** = 0.03 mM) titrated with Eu(OTf)$_3$ (CEu = 2.3 mM, CEu/C**L2** = 1.8)*

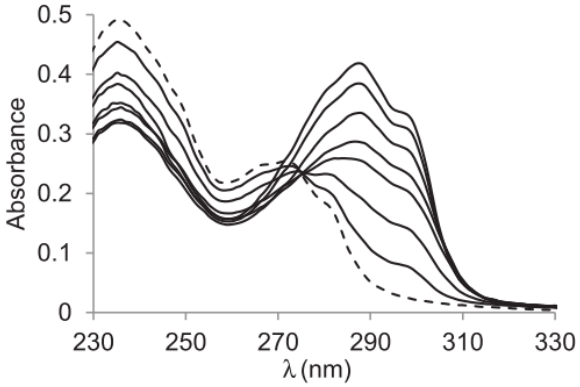

*Figure 95 Spectrophotometric titrations in non-anhydrous acetonitrile of **L3** (C**L3** = 0.02 mM) titrated with Eu(OTf)$_3$ (CEu = 1.45 mM, final CEu/CL3 = 1.6*

3. Titrations with organic anions

Table 19 Relative energies (kcal mol^{-1}) of the different isomers of the [Y(bpcd)lac]- complex in gas phase and PCM (ΔE = Eb-d - Ea). The energy difference for the solvated complex is referred to the e isomer.

Structure	$\Delta E_{gas\ phase}$	ΔE_{PCM}
a	0.0	0.0
b	4.3	4.7
c	6.3	-0.2
d	9.7	1.5
e	0.0	0.0
f	13.6	9.1

a) Isomer 1: trans-O,O Isomer 2: trans-N_{py},N_{py}

View perpendicular to the CC(ethyl) axis

View along the CC(ethyl) axis

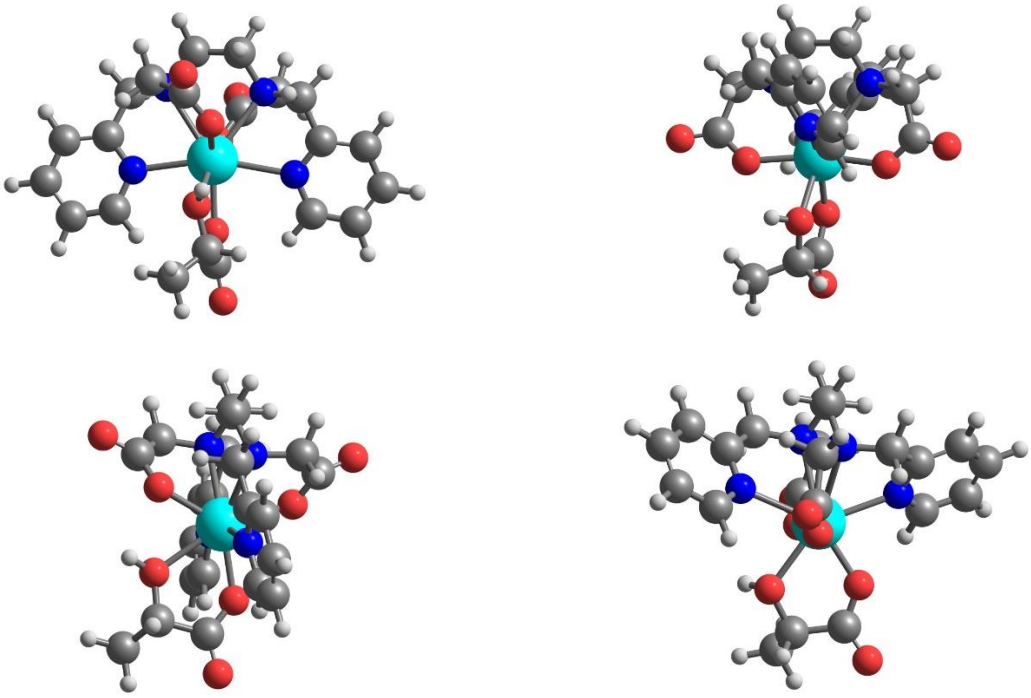

b)

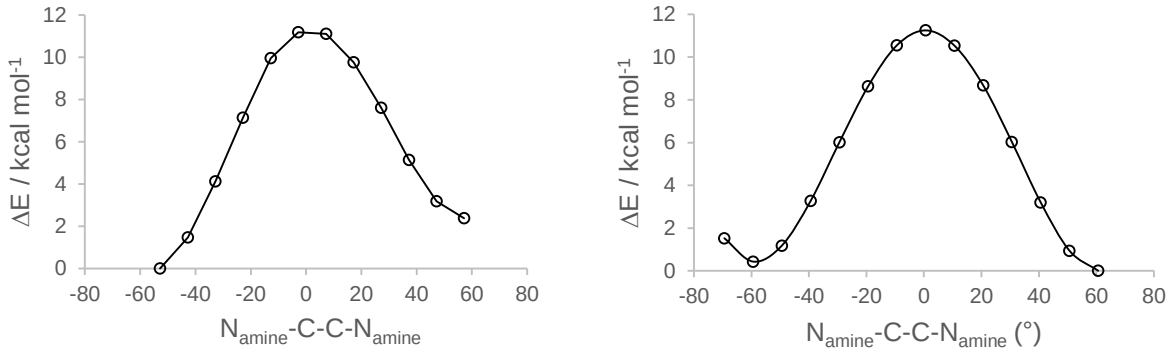

Figure 96 a) minimum energy structures of the coordination isomers of the [Y(bped)S-lactate] complex (i.e. the δ and λ forms, Figure 12); b) Energy of the [Y(bped)S-lactate] complex as a function of the Namine-C-C-Namine torsional angle calculated in PCM water. At each angle value the geometry has been left to relax. The inversion of the dihedral angle for the isomer 1 (from ~ -60° to +60°) leads to two structures of nearly slightly different energy (ΔE = 2.4 kcal mol^{-1}) with a conversion energy barrier of 11.2 kcal mol^{-1}. For the isomer 2 (dihedral from ~ 60° to -60°) two structures of nearly equal energy (ΔE = 0.4 kcal mol^{-1}) are obtained. The energy barrier is of 11.2 kcal mol^{-1} also in this case.

4. Tta complexes

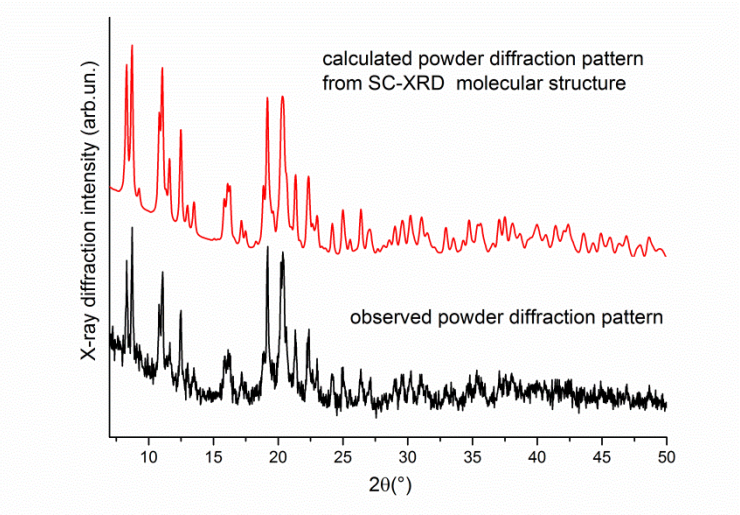

*Figure 97 X-ray diffraction patterns of [Eu**L**(tta)$_2$(H$_2$O)]CF$_3$SO$_3$ (**L** as racemate) calculated from SC-XRD structure (top) and observed from the powder (bottom)-*

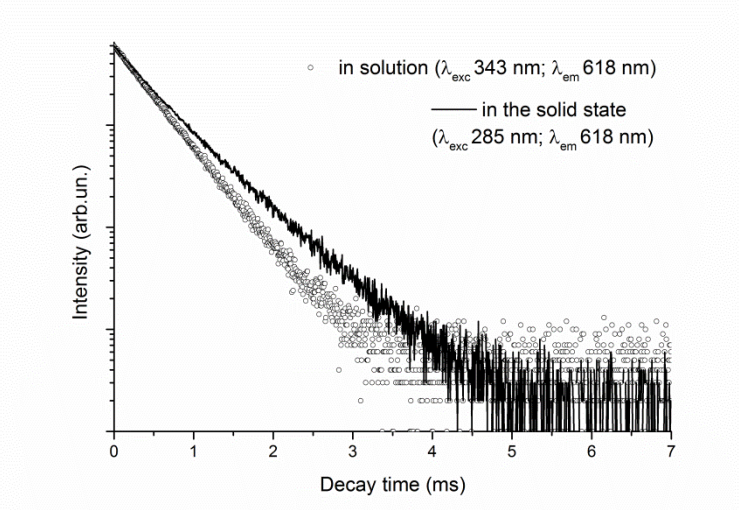

Figure 98 Room temperature decay curves of the $^5D_0$ Eu(III) emission excited at 285 nm in the solid state and at 343 nm in acetonitrile solution

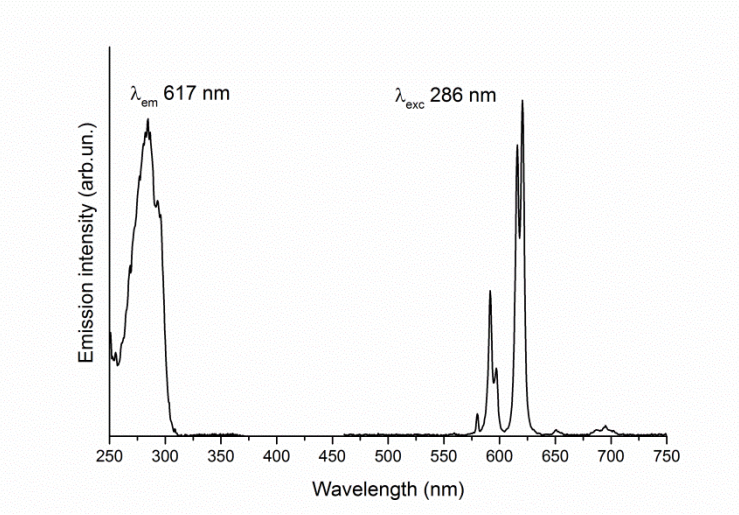

*Figure 99 Luminescence excitation spectra (left) and emission spectra (right) of Eu**L**$(CF_3SO_3)_3$ dissolved in acetonitrile at 298 K*

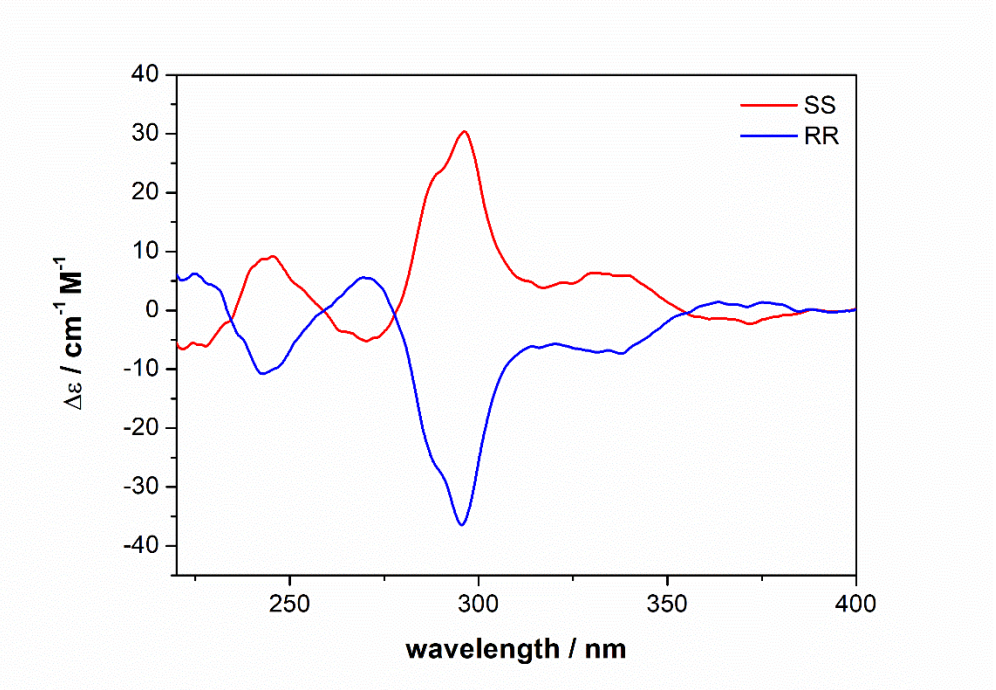

*Figure 100 ECD spectra for the two enantiomers of Eu**L**$(CF_3SO_3)_3$ in acetonitrile*

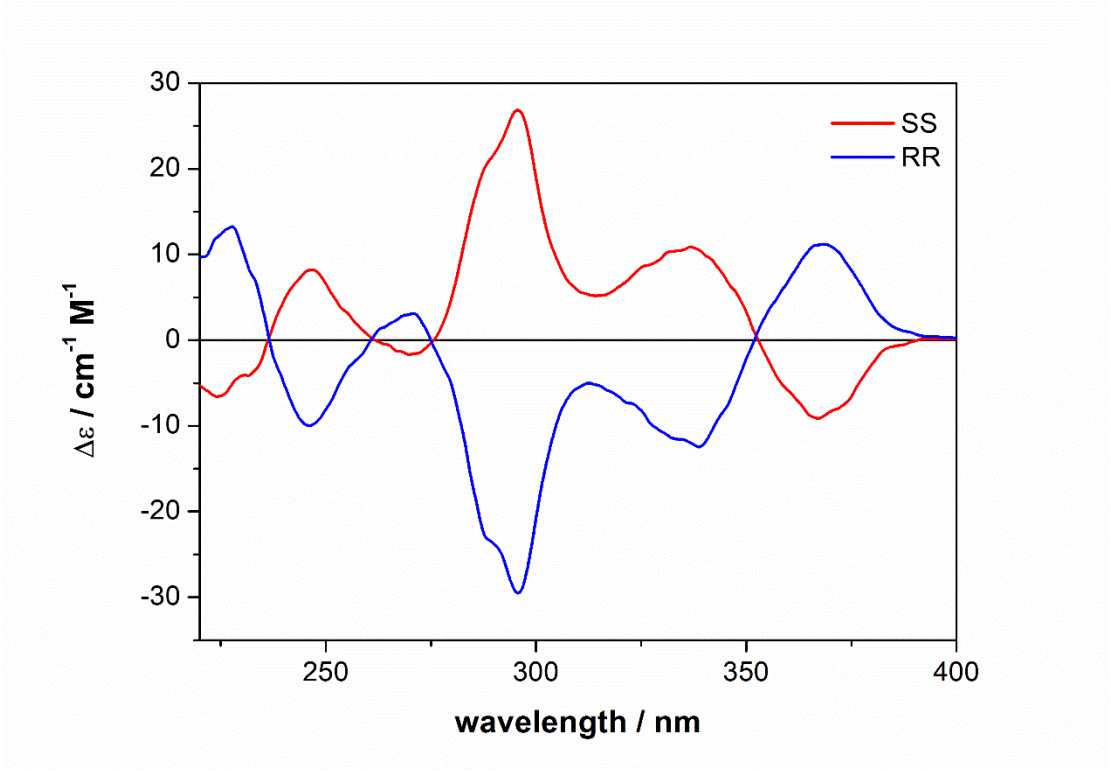

*Figure 101 ECD spectra for the two enantiomers of Eu**L**(CF3SO3)3 in methanol solution*

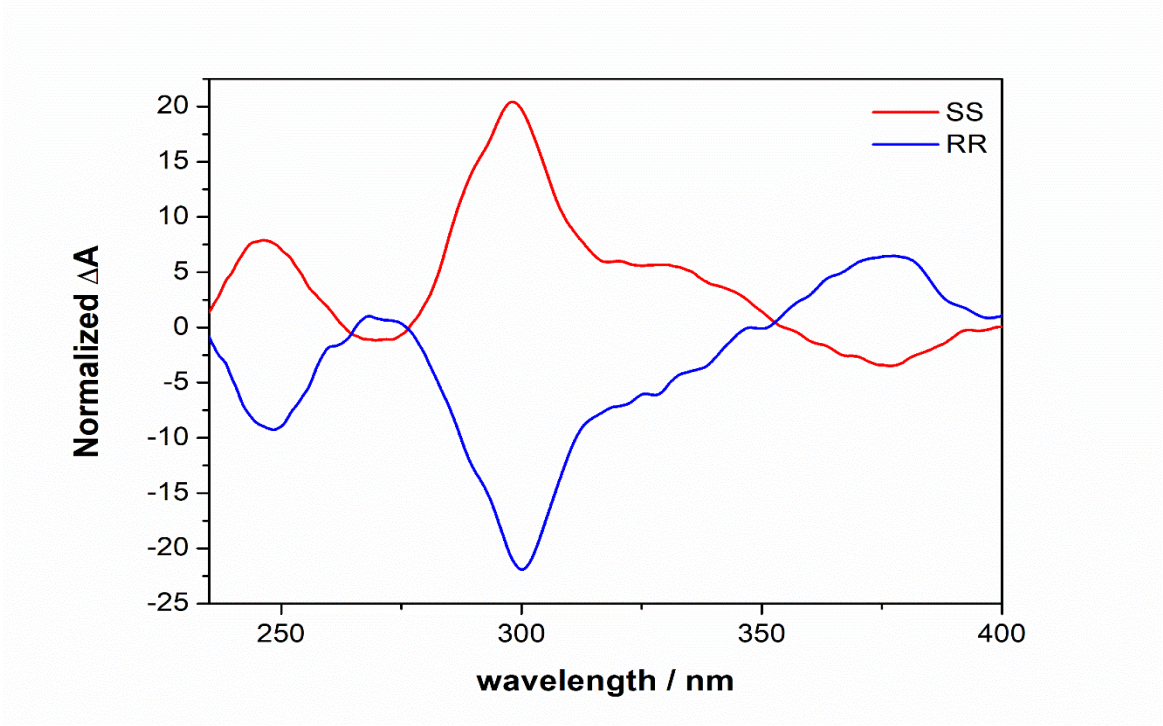

*Figure 102 Normalized ECD spectra for the two enantiomers of Eu**L**(CF3SO3)3 at solid state.*